Microwave-assisted flow processing in heterogeneously copper nano-catalyzed reactions

Microwave-assisted flow processing in heterogeneously copper nano-catalyzed reactions

PROEFSCHRIFT

ter verkrijging van de graad van doctor aan de
Technische Universiteit Eindhoven, op gezag van de
rector magnificus, prof.dr.ir. C.J. van Duijn, voor een
commissie aangewezen door het College voor
Promoties in het openbaar te verdedigen
op dinsdag 16 oktober 2012 om 16.00 uur

door

Faysal Benaskar

geboren te Berkane, Marokko

Dit proefschrift is goedgekeurd door de promotoren:

prof.dr.ir. J.C. Schouten
en
prof.dr. L.A. Hulshof

Copromotor:
prof.dr. V. Hessel

Eindhoven University of Technology, 2012
A catalogue record is available from the Eindhoven University of Technology Library
Benaskar, Faysal
Microwave-assisted flow processing in heterogeneously copper nano-catalyzed reactions
ISBN: 978-90-386-3240-7

… To my Grandparents…

…my Mother and Father…

…my Sister and Brothers…

…my Samy, Nour, Naddine…

…my Ana…

Summary

Microwave-assisted flow processing in heterogeneously copper nano-catalyzed reactions

In the last decades, micro-processing and microwave technology have been established as mature technologies, however, mainly instigated by academia. Many advances in micro-process technology have led to novel routes and/or process windows to replace batch operations by more efficient continuous processes, both at lab and at industrial scales. Especially, the fine-chemicals industry has been recognized for realistic implementation of these technologies with respect to both scale as well as cost. In this thesis, the major hurdles to combine microwave and micro-processing technology for organic syntheses have been addressed. In comparison to gas-phase reactions, metal-catalyzed liquid-phase organic synthesis requires different operational process windows to realize successful implementation of micro-processing. Major issue here is to avoid solid bases and slurry catalysts by including pre-treatment steps and depositing catalysts onto structured supports. In addition, the use of metals as catalysts under microwave irradiation is known for rapid energy absorption and, therefore, requires special attention regarding temperature control. The Ullmann-type coupling reaction and the Simmons-Smith type cyclopropanation are both intensively employed in the fine-chemicals industry and were, therefore, investigated over various novel heterogeneous Cu catalysts in this project.

The Cu-catalyzed coupling of aromatic compounds is not only an excellent example to investigate the benefits of integrated microwave and micro/milli-reactor technologies, but also for its potential applications in the production of pharmaceutically active molecules, such as antivirals and antibiotics (*e.g.* Vancomycin). This type of organic reactions provides considerable challenges to overcome, both with respect to the severe reaction conditions and, undoubtedly, the sustainability of heterogeneous catalysis which substantially contributes to the cost in flow processing. More importantly, however, was the use of heterogeneous CuZn nano-colloids which, as oxidative stable “metallic microwave-absorber”, provide an additional benefit (but also point of attention) regarding the higher temperatures at the locus of the reaction.

Therefore, monometallic and bimetallic Cu-based nanoparticles with a narrow size-distribution and a high resistance against oxidation and agglomeration were developed. The chemical and colloidal stability of these Cu-based nanoparticles, including their purity and morphology, could be significantly improved by coating the

copper nanoparticles with poly(*N*-vinylpyrrolidone). These nano-catalysts were then tested for their performance in the Ullmann-type coupling reaction and the Simmons-Smith cyclopropanation.

Subsequently, these novel nano-catalysts were immobilized onto a microwave-transparent TiO_2 support and used in a fixed-bed reactor. Novel routes for the preparation of highly active TiO_2-supported Cu and CuZn catalysts were proposed and applied in Cu-catalyzed organic reactions. The copper oxidation was significantly suppressed by using $CuZn/TiO_2$ catalytic films and a strong relation between the catalyst composition and activity was found for the Ullmann C-O coupling reaction. This novel preparation method was based on titania dip-coating onto glass beads, obtaining either structured mesoporous or non-porous titania thin films, which could be loaded with the catalyst nanoparticles by deposition onto the calcined films. These catalysts were analyzed using various characterization techniques and in-operando synchrotron X-ray absorption spectroscopy, giving a better understanding of their catalytic behavior.

Besides catalyzing a reaction, the energy supply towards the catalyst surface is obviously as important and has been also investigated in this project. This issue has been addressed separately, because in traditional reactors the energy supply is particularly governed by classical heat-transfer limitations. Furthermore, the troubleshooting of the major obstacles for continuous operations to synergize the benefits of microwave systems and micro/milli-processing in flow synthesis has been targeted. A micro fixed-bed reactor was designed, using packed spherical glass beads coated with the catalyst and support, for kg-scale flow operations in the Ullmann C-O coupling. In addition, the influence of reactor shape and dimensions for effective microwave irradiation was studied. Experimental evidence of complete microwave penetration in the radial direction was found, allowing rapid and controlled heating without significant radial temperature gradients in the flow-through reactors.

The abovementioned developments in chemistry, nano-catalysis and reactor engineering were the basis for an extended cost study, consisting of 14 process scenarios. In this way, the cost-impact of micro-processing and microwave heating for liquid-phase reactions in fine-chemicals synthesis could be envisaged. Two examples were studied, *i.e.* the Ullmann-type coupling reactions and the Aspirin synthesis. It could be concluded that the operating costs for the Ullmann-type processes compared to those for the Aspirin synthesis can be defined as either material based (*e.g.* reactant excess, pretreatment and catalyst synthesis) or downstream processing based (*e.g.* work-up, waste treatment) processes. The impact of integrating microwave heating and micro-processing systems on profitability was evaluated with respect to operational costs and chemical productivity. This techno-economic evaluation provided a route map, highlighting feasible routes to combine different technologies, chemical processes and catalyst systems.

Table of Contents

Chapter 1

Introduction

1.1 The Cu-catalyzed Ullmann C-O coupling and Simmons-Smith cyclopropanation for fine-chemicals synthesis

A centennial overview of the Ullmann reaction. In 1903, Ullmann, Sponagel and Goldberg have been the first to report the copper-assisted nucleophilic substitution reaction of aromatic reagents towards bi-aromatic products [1]. Although their chemical protocol required stoichiometric use of copper, high reaction temperatures and a reaction time of several hours, many industrial applications for pharma-intermediates, agrochemicals and high added-value chemicals have adapted this methodology [2]. Based on the current classification, the Ullmann-condensation/coupling reaction is nowadays recognized as the copper-assisted coupling between aryl halides and aryl amines or (thio)-phenols towards the synthesis of bi-aryl amines or aryl-(thio)ethers (Scheme 1a). On the other hand, the Ullmann-reaction represents the copper-assisted synthesis of bi-aryl components from two aryl halides (Scheme 1b) [3].

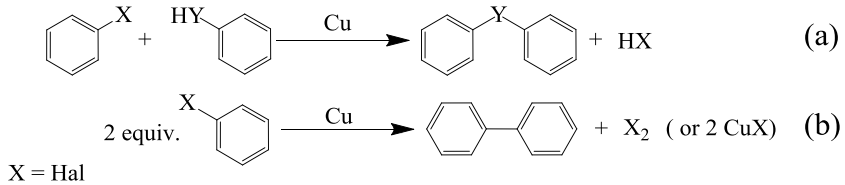

Scheme 1.1. The Ullmann reaction from a halo-aromate and either a phenol, thiol or amine (a) and from 2 equiv halo-aromates (b).

In addition, the copper-assisted Goldberg-condensation reaction is known as the coupling reaction of an aryl halide and an amide resulting in a C-N aryl-bond [4], while the copper-assisted condensation of 2-halobenzoic acids and dicarbonyls has been coined as the Hurtley-condensation reaction [5]. The successes of Pd-catalyzed cross-coupling reactions in the last three decades, *e.g.* the Hartwig-Buchwald amination reaction, have simultaneously resurrected the interests in the

original Cu-based coupling reactions [6]. Especially due to the catalyst cost and product purity, a renaissance was made in the copper-catalyzed cross-coupling reactions, which is known as the modified Ullmann-reaction. As a result, previous obstacles regarding high catalyst loadings and reaction temperatures/times have been resolved, using new procedures, and implemented in a wide spectrum of applications [7]. These improvements could mainly be attributed to the discovery of novel ligands, which improved the Cu-catalyst solubility in the reaction media. The use of chelating moieties, *e.g.* di-amines [8], amino acids [9], phenantrolines [10], diols [11] and other *N,O*-containing ligands [12], proved increased activity as a result of their positive effect on the Cu solubility in typical organic solvents. These successes of the modified Ullmann reaction led to implementation in large-scale production [13]. Undoubtedly, this methodology provided many benefits as compared to the recent successes of Pd-catalyzed coupling systems.

However, mechanistic understanding of the modified Cu-catalyzed Ullmann-reaction still remained inferior to knowledge about the mechanistic pathway of the Pd-catalyzed Hartwig-Buchwald arylation-type coupling reactions. Another major drawback of the Ullmann-type C-O, C-N and C-S coupling reactions was the necessity of a strong base, such as sodium *tert*-butoxide, which, acting simultaneously as a nucleophile, clearly limited its applications to rather straightforward and non-functionalized substrates. A novel protocol was introduced in 1997 by Buchwald and co-workers wherein the reactive base was substituted by cesium carbonate[14]. This strategy was adapted by many researchers and proved to be the optimum base in most cases, leading to a significant improvement in the synthesis of diaryl ethers [10d, 15]. In medicinal chemistry, many successes were reported in a number of syntheses of diaryl ethers, using copper triflate ($Cu[SO_3CF_3]_2$) in combination with ethyl acetate and naphthoic acid as ligands at 110 °C in toluene. In this way, also C-O couplings of many unactivated aryl halides and hindered phenols could be realized [14]. Substituting the $(CuOTf)_2$-benzene complex as copper(I) source by the more stable $Cu(CH_3CN)_4PF_6$, known as Kubas salt, demonstrated even more successes [16]. Palomo *et al.* developed in the same year a phosphorimidic triamide base (P4-Bu^t), also known as Schwesinger base**,** which showed a significant rate enhancement in almost all of their etherification examples of aryl halides with a variety of phenols. This improvement was mainly attributable to the *in-situ* formation of a naked phenoxide anion and the stoichiometric use of CuBr [17]. In our recently reported work, a similar observation was made, using similar types of naked-ion nucleophiles [18]. Gratifyingly in our case, the separate generation of potassium phenoxide and the use of 18-crown-6 as solubilizer made it possible to avoid unnecessary by-products (originating from phenoxide generation) and also to increase the solubility of potassium phenoxide and the related by-product potassium chloride.

Traditionally, the main disadvantage of copper(I) salts as homogeneous catalysts in organic solvents is their very low solubility, reducing the yields considerably due to mass-transfer limitations. A solution was proposed by Venkataraman *et al.*, who introduced the use of soluble, air-stable, bromo(triphenylphosphine) copper(I) complexes (and the related bidentate

complexes). In this way, electron-rich *para*- and *meta*-substituted phenols could be coupled to aromatic bromides in good yields [10d, 15a]. Their work in 2003 has led to many improvements of ligand-assisted arylations of phenols [12a] and an impressive number of studies on the effect of various additives and ligands besides increasing the Cu(I) solubility, such as tetramethylheptadione [15b], bis-pyridineimine [15c, d] and dimethylglycine [15e], appeared. A remarkable ligand improvement was achieved in the arylation of tyrosine derivatives without epimerization [15f], using tris(hydroxymethyl)-ethane [15g], diketone [15h] and aminophosphonate [15i] which all demonstrated better reactivity and selectivity when compared to the conventional catalysts [19]. In addition, also the unsatisfactory reactivity of aryl chlorides, classified as stable and relatively cheap reactants, was considered to be a serious limitation for a real industrial breakthrough. The combination of copper(I) bromide and a diketone ligand showed some improvement [15j] when aryl chlorides were applied. Other methods were reported to provide increased productivity for aryl chlorides, using microwaves [20] and ligand-less systems [21]. In contrast to these developments, a much more efficient combination of Cu nanoparticles and a highly soluble naked-ion phenoxide was developed in our group for substituted chloro-heterocycles [22] and will be discussed in the following chapters.

Mechanism of the Ullmann reaction. So far, the majority of the mechanistic studies, conducted for coupling reactions, are based on Pd catalysts. Nevertheless, consensus exists on two possible catalytic cycles for the copper-catalyzed etherification of nucleophiles (see Scheme 2). In mechanism A, an oxidative addition of the aryl halide occurs prior to the actual nucleophilic substitution, both leading to the coupling product and simultaneously regenerating the catalytic copper species. In mechanism B, the nucleophile forms a copper-complex, that enables the substitution of the halide to form a bi-aromatic ether [7a, 7d, e].

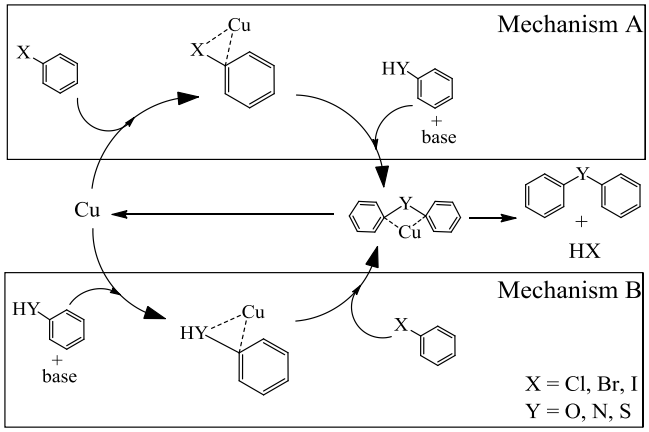

Scheme 1.2. Two most plausible mechanisms for the Cu-catalyzed Ullmann-type coupling reaction following initial Cu interaction either with the aryl halide (A) or nucleophile (B).

Most catalysts used in the Cu-based Ullmann coupling reaction are homogeneous, which allowed intrinsic research on the mechanism of the reaction. Although it is generally accepted that the catalytically active Cu species is a Cu(I)-salt [23], also Cu(II)-salts and metallic Cu(0) have shown catalytic activity [24].

Undoubtedly, the use of metallic copper promises a higher potential for efficient application as a heterogeneous catalyst, although the *in-situ* formation of the active Cu(I) species might still be the major contributor to the reactivity [25]. This conclusion is primarily based on the fact that two Cu(I) species are able to disproportionate into Cu(0) and a Cu(II) species [26]. Therefore, intrinsically, both Cu(0) and Cu(I) could act as a catalyst where, according to Lindley *et al.*, the first interaction occurs between the nucleophile and the catalyst followed by halide displacement [27]. The various copper oxidation states can be categorized for five different mechanistic pathways in the Ullmann coupling reaction [28]. The involvement of a Cu(III)-complex has only recently been accepted as an intermediate to catalyze the coupling reaction [29]. The first mechanistic pathway is initiated by the oxidative addition of an aryl halide and the formation of a Cu(III) species which ends with a reductive elimination step. The first reports on the presence and activity of organocopper(III) species were made in the early 1970s by Cohen *et al.*[30], based on an earlier observation of other organocopper species by Whitesides *et al.*[31] Later, however, Van Koten *et al.* opposed this Cu(III)-type mechanisms, based on a long-standing knowledge and acceptance of the more plausible presence of arylcopper(I)-complexes in the reaction [2a, 32]. Another mechanism is the single electron transfer (SET) by the formation of a radical anion from the aryl halide, leading to electron exchange mechanism between Cu(I) and Cu(II). The very first reports on the involvement of free radicals in the Ullmann reaction were published by Waters *et al.*, shortly before Fritz Ullmann's death, and were subject of heavy speculation at that time [33]. Only in the late 1960s, Kornblum [34] and Russell [35] independently observed the presence of free-radicals in chain (coupling) reactions, which were expanded for aromatic systems by Bunnett *et al.* [36] Their mechanistic study led to the introduction of a "$S_{RN}1$" classification, referring to a unimolecular radical-nucleophilic substitution. This mechanism does not necessarily require the use a metal (complex) as the formation of a radical could also be initiated photo or electrochemically.

Nevertheless, reports on the organometallic-assisted electron transfer[32a, 37] led to organocopper applications in the Cu-catalyzed Ullmann coupling reaction following a $S_{RN}1$ mechanism [38]. Arai and coworkers were the first to demonstrate the existence of an organometallic species with a paramagnetic character originating from an electron transfer of Cu(I) species [38-39]. Their results supported work on the Cu-catalyzed aromatic $S_{RN}1$ reaction pathway [40] by many other groups, yet at the same time provoked uncertainty to other researchers [23, 41]. The third proposed mechanistic pathway of the Cu-catalyzed Ullmann reaction is the σ-bond metathesis where the active copper species is assumed to remain at a Cu(I)-oxidation state. According to Bacon *et al.*, this mechanism involves a σ-complex formation between the Cu-electrons and the electron pair of a halogen atom, resulting in an efficient interaction with the nucleophile [42]. Conversely, Van Koten *et al.* demonstrated a deviating mechanism via "intimate-electron" transfer by means of a Cu(I)-Cu(II) redox reaction, opposing Bacon's philosophy of a σ-metathesis procedure [43]. Nonetheless, the σ-bond metathesis is currently still accepted as a way to displace the aryl halide by a strong nucleophile to form a Cu-

Nu species. As a result, copper induces a partial positive charge on the adjacent carbon to promote nucleophilic substitution and Cu(I)-retention. The final reaction mechanism has been proposed by Weingarten *et al.* and involved π-complexation between Cu(I) and the π-electrons of the aryl halide to consequently stimulate an aromatic substitution by a nucleophilic attack [44]. During the π-complexation Cu(I) acts as an electron acceptor by facilitating the halide cleavage and stabilizing the aromatic system as was observed for Cu(I)-benzene [45] complexes and chlorobenzene-chromium tricarbonyl complexes [46].

Ullmann C-O coupling in fine-chemicals synthesis. Diaryl ethers and their derivatives are found in a variety of fine chemical and pharmaceutical products, emphasizing on the importance of copper-mediated arylations of phenols as essential tool for industrial applications. However, due to the complex mechanism of the classical Ullmann diaryl ether synthesis (because of the strong reactivity dependence of aryl-substituents), the first breakthrough was made in the late 1990s by Chan, Lam, and Evans by their first applications of aryl boronic acids as arylating agents [47]. Nevertheless, with the original procedure satisfying performance could still be achieved for intermolecular coupling reactions towards pharma-active compounds, *e.g.* in the synthesis of cycloisodityrosine-derived agents (see Scheme 3 upper part), such as K-13, OF4949-III, and OF4949-IV (Boger *et al.*) [48].

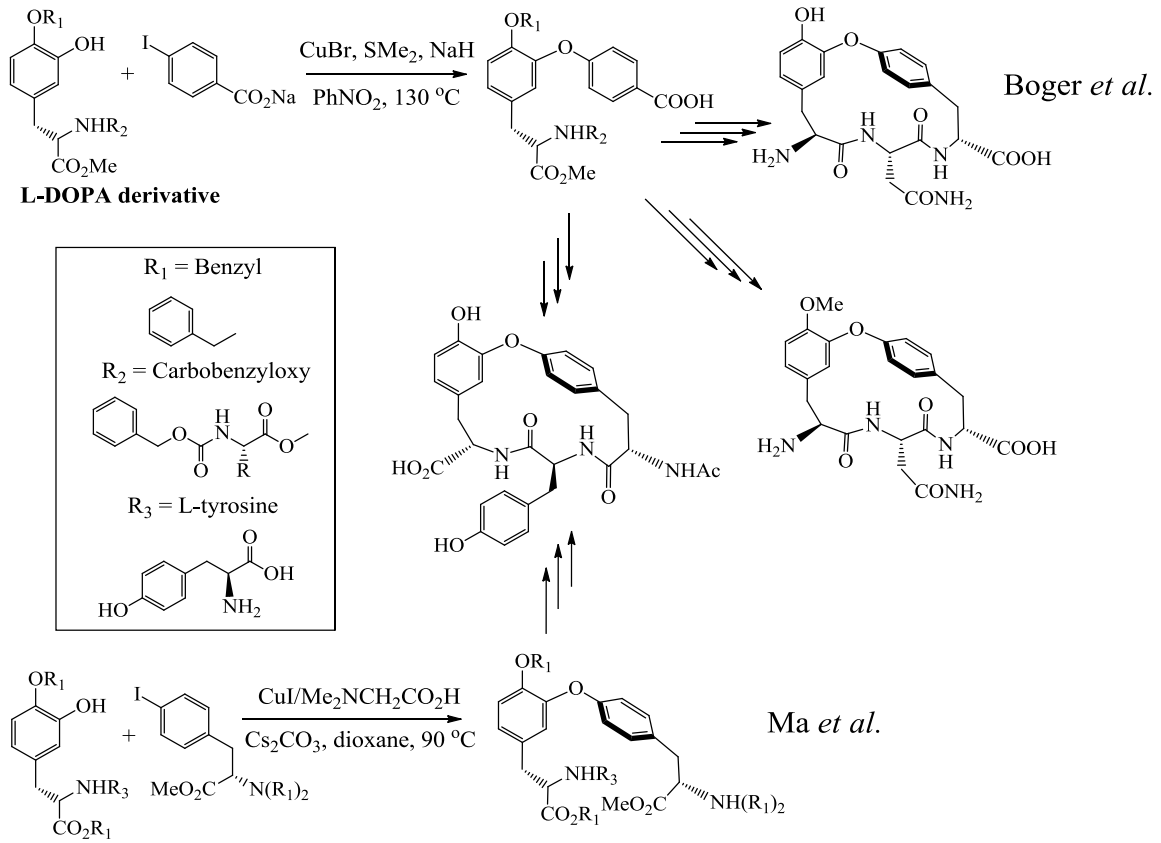

Scheme 1.3. Applications of the Cu-catalyzed Ullmann C-O coupling reaction in the synthesis of intermediates for cycloisodityrosine-derived agents, following the Boger (above) and Ma (below) protocols.

One of the intermediates was obtained rather straightforward from the coupling of a L-DOPA derivative and sodium *p*-iodobenzoate, using a mixture of sodium hydride and a copper bromide/dimethylsulfide complex in nitrobenzene. Racemized by-products could be avoided using the solvent nitrobenzene at 130 ^{o}C, which, in the case of the conventional solvent pyridine, resulted in significant epimerization [48].

This example shows a successful Ullmann coupling of an electron-rich aryl iodide with simple substrates and an unactivated phenol. However, in the case of a coupling between electron-rich aryl iodides containing *o*-alkoxy substituents with a single functionalized tyrosine derivative only limited success could be achieved. Moreover, no activity was observed in the coupling of two functionalized tyrosine with iodo-phenylalanine derivatives. In 2006, Ma *et al.* proposed an improved strategy for the synthesis of the same compound, using a more efficient CuI/*N*,*N*-dimethylglycine complex, starting from an activated L-DOPA derivative and a protected iodo-phenylalanine (Scheme 3, lower part) [15f]. Similar effects of substituents in the reactants on the reactivity were observed by Wipf *et al.* in an Ullmann-coupling step in the diepoxin-σ synthesis, which is a highly oxygenated antifungal and anticancer natural product [49]. The authors showed that the coupling of a tetralone with 1-iodo-8-methoxy-naphtalene could only be successfully carried out after reduction of the ketone in tetralone, which emphasizes the importance of the substituent type. Similar effects were also reported by Furstner *et al.* [50] in the aspercyclide C synthesis and were confirmed by Ramana *et al.* [51] in 2007, who showed both independently major benefits in preparing the diaryl ether core at the start of the synthesis. This was earlier suggested by Kametler *et al.* in the macrocyclic bis(bibenzy1) ether synthesis of Plagiochins A and B [52].

Although nowadays the use of advanced copper ligands and the use of nanoparticles demonstrate major improvements in the synthesis of diaryl ethers, the introduction of Cs_2CO_3 as base by Buchwald was the crucial step in the synthesis of verbanachalcone, a compound reported to act as a nerve growth stimulator. Cuny *et al.* assembled efficiently the diaryl ether core of verbanachalcone by a C-O coupling of a phenol and an aryl bromide in the presence of Cs_2CO_3 in pyridine [53]. Another success in the diaryl ether synthesis of pharmaceutical compounds has been the discovery of widely used boronic acids as arylating agents [47b, c]. Mainly due to their high reactivity at mild temperatures combined with $Cu(OAc)_2$, Evans *et al.* demonstrated an efficient synthetic route of thyroxine, using triethylamine as base and pyridine as solvent, which both are also believed to act as ligands in the organocopper intermediates [47a]. More examples of this mild and efficient strategy towards diaryl ethers can be found in many medicinal reports, such as the preparation of Isodityrosine [54], Pulcherosine [55], Combretastatin D2 [56], Rodgersinol [57], Puetuberosanol [58] and Tejedine [59]. Another interesting example is a precursor preparation in the synthesis of Teicoplanin Aglycon synthesis, which demonstrated an appealing epimerization-free arylation with a substituted arylglycine derivative [60]. In addition, the trace amine-associated receptor agonists [61] and ultrapotent HIV-protease inhibitors preparation are considered to be major advances in medicinal chemistry with due to improved diaryl ether syntheses [62].

Homogeneous catalysts in the Ullmann C-O coupling reactions. In 2003 Ma *et al.*, developed an efficient catalyst system for C-O coupling reactions at ambient temperature [63], based on earlier reported progress [15e]. They reported a facile method to couple various bromoanilides with L-tyrosine derivatives at 25 °C by combining the effects of *ortho*-substituents and the presence of amino acids as Cu-ligands using a copper loading of 30 mol%. In this way, the ambient-temperature conditions provided major benefits for this reaction that eventually could prevent racemization of the tyrosine derivatives. On the other hand, the use of relatively large Cu-loadings and the necessity to use complex *ortho*-amides, as directing group for the coupling, still required a more simplified system. Besides the low temperature, the main advantage in this system was postulated to be the activation of Cu(I), induced by strong *O*-coordination of the ligand (see Scheme 4).

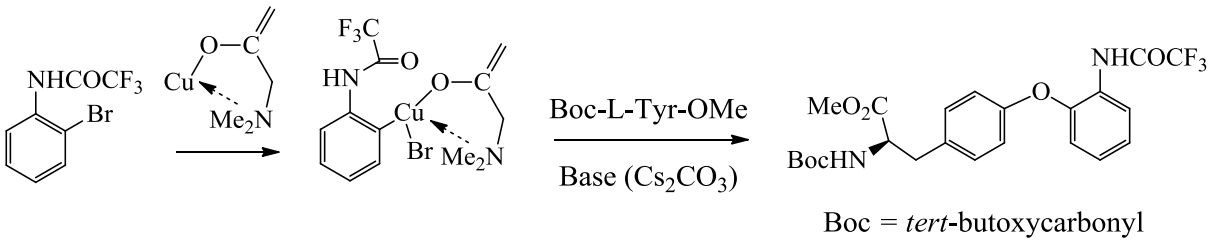

Boc = *tert*-butoxycarbonyl

Scheme 1.4. The reaction of 2-bromotrifluoroacetanilide with a L-tyrosine derivative using CuI/*N*,*N*-dimethylglycine in the presence of Cs_2CO_3 at room temperature, providing a highly selective peptide synthesis via the Ullmann C-O coupling strategy.

In another study, Bao and coworkers described a similar efficient copper-based catalyst for the arylation of phenol derivatives. The use of a β-keto ester as supporting ligand for copper afforded diaryl ethers from aryl bromides at mild temperatures and from aryl iodides even at room temperature [15h]. Taillefer *et al.* developed a novel Schiff base and oxime-types as Cu-ligands for another type of coupling reactions, which also demonstrated to be efficient in the synthesis of diaryl ethers [12c, 64]. Only 10 wt% CuI, in conjunction with these ligands, was needed to establish the coupling of a large range of aryl bromides with phenols under mild conditions using the inexpensive base K_3PO_4 [12c, 15c]. Pyrrolidine-2-phosphonic acid phenyl monoester has also been reported as a Cu ligand in the coupling of phenols with aryl iodides or bromides, though at higher temperatures [15i]. Also, the use of a 1,10-phenanthroline as ligand in association with a KF/Al_2O_3 system as the base [65] and the direct impregnation of copper onto charcoal under microwave irradiation [20b] have been reported. In another study by Xia *et al.*, significant advances were reported in the development of an efficient Cu-catalyst for the arylation of phenols with relatively inactive aryl chlorides [15j]. The authors developed one of the first catalyst systems, based on a 2,2,6,6-tetramethyl-3,5-heptadione ligand, which utilized inexpensive starting materials, albeit at relatively harsh conditions (135 °C). In the same group, examples of the arylation of phenols with aryl iodides in acetonitrile at 82 °C were demonstrated with the use of only copper precursors in the absence of any ligands [66]. Two other examples have been reported in ligand-free catalyst systems [21c, 67]. Nevertheless high reaction temperatures appeared to be necessary (150-160 °C), albeit with employment of

active aryl iodides and bromides. The use of iodides and bromides is favorable due to their high reactivity as electrophile, but regarding atom efficiency, stability and raw material cost the use of chlorides is far more beneficial.

Although the abovementioned examples are only a selected fraction of the current progress in C-O coupling reactions, many more examples can be found in the literature [68], which all have in common being based on homogeneously catalyzed processes. Still less developed, the use of heterogeneously catalyzed processes is undoubtedly much more favorable in terms of chemical process efficiency in relation to catalyst recovery.

Heterogeneous catalysts in the Ullmann C-O coupling reactions. Many reports on the development of cross-coupling reactions using heterogeneous Pd catalysts can be found in the literature [69]. Supported catalysts in the Cu-mediated Ullmann-type coupling reactions, on the other hand, have hardly been explored and, for the very few, far more in C-N coupling than in C-O and C-C coupling reactions [70]. Kidwai *et al.* developed a heterogeneous catalyst which could be applied at mild temperatures (50-60 ^{o}C) and which was used as a copper nano-slurry, consisting of Cu nanoparticles (10 mol%) with a diameter of 18 nm, for the C-O coupling of both aryl iodides and aryl bromides with phenols. This catalyst system did not require the use of ligands, making this process highly cost-competitive. However, the major drawbacks orignate from the limitations of catalyst losses after multiple catalyst recovery steps, requiring longer reaction times after each subsequent recycle [71]. In another report, Wang et al. have developed resin-supported catalysts, where a diamine ligand, attached to a SiO_2-substrate, could chelate with the copper catalyst (see Scheme 5a). This catalyst system demonstrated to be highly efficient in the coupling of aryl halogens (-I, -Br and -Cl) towards diaryl ethers at 130 ^{o}C and could even be recovered quantitatively and reused up to 10 times [72].

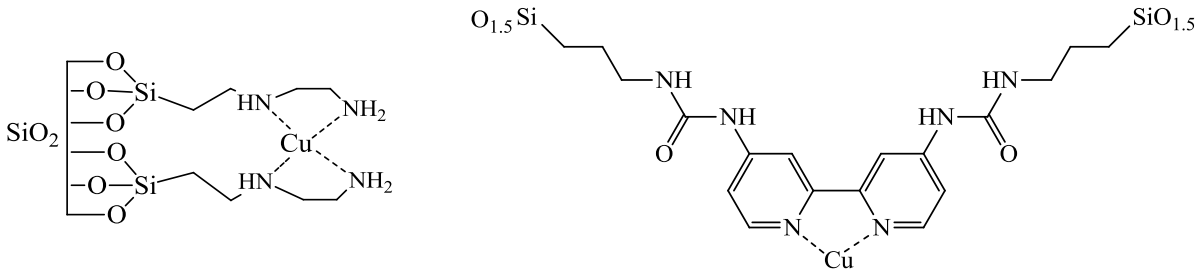

a) b)

Scheme 1.5. Resin-supported Cu-diamine/SiO_2 complex for the synthesis of diaryl ethers as developed by Wang (a) and the sol-gel based supported Cu-2,2-bipyridine/SiO_2 complex by Monnier *et al.*

Monnier *et al.* developed a sol-gel supported copper catalyst using a bidentate ligand (see Scheme 5b) for application in the C-O coupling of aryl iodides and aryl bromides with phenols, resulting in excellent yields, even after multiple recycle runs [73]. Although the aryl iodides and bromides are very reactive at trace amounts of catalyst, surprisingly, a very small amount of copper was

detected in the product stream, indicating negligible leaching from the ligand (less than 1 wt% per run).

The above-summarized systems exemplify the use of supported catalysts, but the necessity of organic ligands appeared to be indispensible. Therefore, these processes are still more expensive than conventional ceramics-based heterogeneous catalysts, *e.g.* the Cu/ZnO catalyst as used in the methanol synthesis [74]. Our group recently reported novel routes for the preparation of highly active TiO_2-supported Cu and CuZn catalysts for Ullmann-type C-O coupling reactions. Slurries of a titania precursor were dip-coated onto glass beads to obtain either structured mesoporous or non-porous titania thin films. The Cu and CuZn nanoparticles, synthesized, using a reduction-by-solvent method, were deposited onto calcined films to obtain a Cu loading of 2 wt% [75]. A study based on synchrotron X-ray absorption spectroscopy, using various Cu_xZn_y/TiO_2 catalysts, provided detailed information on the Cu-Zn interactions. The fresh and spent catalysts were analyzed after a hydrogen treatment from 25 ^oC to 375 ^oC for 12 hours followed by reoxidation in an air flow at 140 ^oC, using a microreactor cell. In this way, the role of Zn as "oxide-scavenger" and, consequently, retention of the Cu^0-oxidation state were studied [76].

The Cu-catalyzed cyclopropanations for fine-chemicals synthesis. The formation of cyclopropanes from insertion of a carbon atom in a double bond can be obtained in two mechanistically different ways, using either a methylene halogen requiring a CuZn[77] catalyst or a diazo-ester which is mainly Cu- [78], Ru- [79] or Rh-catalyzed [80] (see Scheme 6). The CuZn-catalyzed cyclopropanation, following a carbene-insertion mechanism as described by Simmons and Smith in the 1960s [77e, 81], has been the conventional tool towards the synthesis of fine-chemicals involving cyclopropanes, *e.g.* Drospirenone (Bayer) [82]. Another attractive quality of this chemical protocol is its strength in the asymmetric synthesis of optically active cyclopropane based products [83].

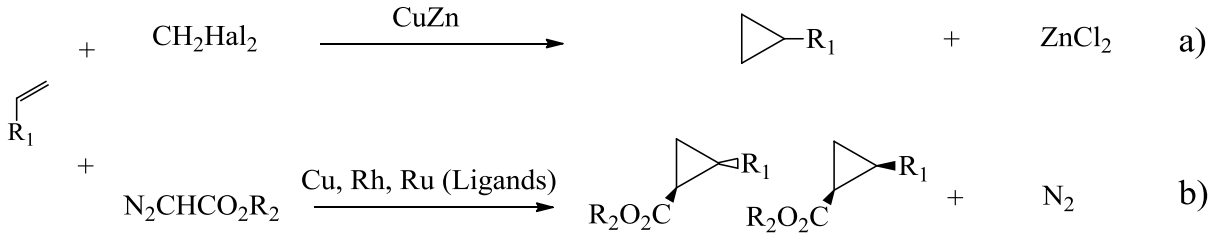

Scheme 1.6. The Cu-catalyzed original Simmons-Smith cyclopropane formation from an olefine and dihalomethanes, requiring equimolar amounts of Zn (a) and the cyclopropanation with a diazo-compound as carbon insertion moiety in the absence of Zn (b).

Cyclopropyl moieties are found in various natural and synthetic products with appealing biological properties [84], which have instigated numerous discoveries and new chemical protocols to find highly active cyclopropane derivates [85]. However, the currently obtained good to excellent yields have been reported mostly when a diazo-compound was used via either homogeneous Ru-type catalysis or expensive copper-ligand assisted catalysis [79b, 85a, 86]. In the last

decades, various effective systems have been developed and applied for the asymmetric Simmons-Smith reaction based on chiral promoters [87], pre-activated reagents [88] and various catalyst systems [89]. Although these examples are based on improvements by addition of hetero-atoms as directing groups for enhanced reactivity and stereo-chemical control, a major improvement would be the asymmetric Simmons-Smith cyclopropanation of pro-chiral olefins without the necessity of these directing groups [90]. Another example has been reported by Rodríguez-García *et al.*, where the use of transition-metal complexes provided an effective tool for the cyclopropanation of both electron-poor and electron-rich olefinic reactants with diazoalkanes [91]. Additionally, photochemical processes to activate dihalomethanes have been reported for cyclopropanes in a highly stereo-specific manner, *e.g.* the Norrish-Yang reaction [92].

Mechanistically, cyclopropanation of olefins from the decomposition of diazoalkanes, using a transition-metal catalyst, has been considered as the most important tool for efficient cyclopropane formation [93]. Therefore, many studies, more than those on the original Simmons-Smith reaction, have led to a significant understanding of the mechanism of the carbenoid cyclopropanation reaction [94]. In addition, this chemical protocol also provided a highly effective way to control the stereoselectivity of functionalized cyclopropanes, using various Cu-, Rh- and Ru-based catalysts. In scheme 7, the catalytic cycle of the carbenoid-based cyclopropane formation is depicted, where initially interaction between the diazo-moiety and the catalyst forms a metallocarbene complex as reactive intermediate compound (under release of nitrogen gas) and subsequently a carbene-transfer to the olefin occurs.

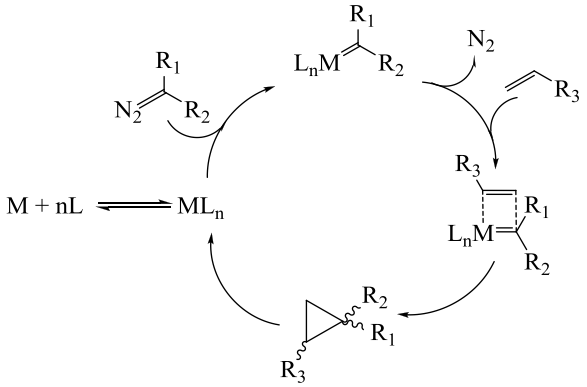

Scheme 1.7. The catalytic cycle of the metal-catalyzed cyclopropanation based on the carbenoid mechanism.

The enantioselectivity can be controlled very accurately, using a wide range of chiral ligands. As a matter of fact, the carbenoid-based reaction of ethyl diazoacetate is considered to be the most prominent test-reaction to evaluate the stereoselectivity of any novel catalyst. On the other hand, the original Simmons-Smith reaction appeared to be relatively slow and less effective in the multi-step synthesis of functional cyclopropanes and was, therefore, studied less extensively. Nevertheless, two reaction pathways have been regarded, involving either a

methylene-transfer mechanism or a carbometalation mechanism (see Scheme 8). In the latter mechanistic pathway, a highly active pseudo-trigonal methylene group of halomethylzinc halide, usually IZnCHI, attacks the olefin π-bond and, concurrently, forms a C-C and a C-Zn bond. Consequently, a 1,2-migration is believed to cleave the halide from the carbon by formation of Zn-halide. Nonetheless, this carbometalation mechanism has only been accepted in rare cases, such as using lithium carbenoids [95], and leaves many questions on the actual mechanistic addition of the metal-carbenoid to the olefin answered [96].

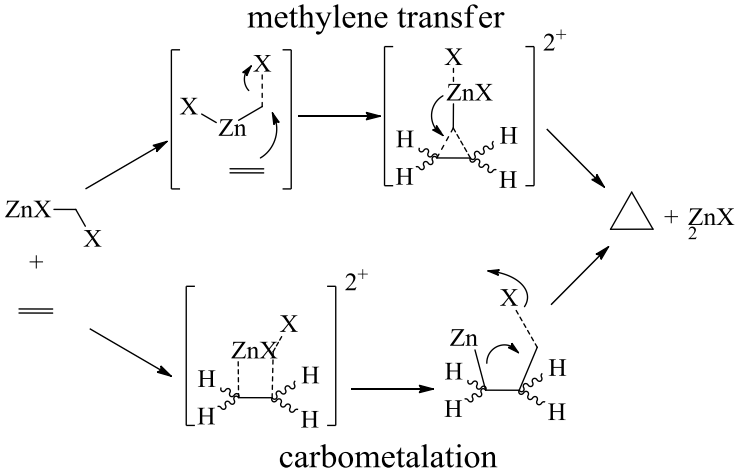

Scheme 1.8. Two proposed mechanisms of the Simmons-Smith cyclopropanation from an olefin and halomethylzinc halide, via either a f methylene-transfer or a carbometalation mechanism.

Conversely, the methylene-transfer mechanism has generally been accepted as more plausible for the Simmons-Smith cyclopropanation as confirmed by Nakamura *et al.* in 2003 using a density function theory (DFT) modelling method [97]. The reaction pathway is believed to follow two stages, a bi-molecular nucleophilic substitution attack to the carbon of the halomethylzinc halide, followed by a C-Zn bond cleavage affording the cyclopropane moiety.

Although many enhancements in stereo- and enantioselectivity were based on homogeneous catalysis, cost-efficient industrial production scales would significantly benefit from supported catalysts [78c, 79, 98], especially for continuous operations. The development of a supported catalyst is, clearly, the first and most important step in successfully performing sustainable catalysis in flow-chemistry and process intensification.

1.2 Cu nanoparticles as catalyst in organic synthesis

Cu monometallic nanoparticles. Extensive research has been reported in the field of metallic nanoparticles in the last two decades [99]. The most promising field in chemical applications of metallic nanoparticles is undoubtedly in catalytic processes [100]. Nanoparticulate copper, more specifically, has been an appealing research theme, in comparison with other nobel d-metals, since it offers low raw material and processing costs. In addition, these beneficial properties have led to extensive applications, *e.g.* in optics, electronics, sensor technology and in medical

practice [101]. The synthesis of copper nanoparticles can be done in various ways, *e.g.* thermal decomposition [102], sono-chemical reduction [103], metal vapour deposition [104], laser ablation [105], radiation methods [106], microemulsion techniques [107] and chemical reduction [108]. The most interesting, though, have been the "wet-chemical" methods by virtue of their notable synthetic simplicity and the absence of complex and demanding equipment. Simultaneously, wet chemical methods offer the ability to modulate flexibly towards product composition as well as morphology by adapting various synthetic parameters (*e.g.* source of reductant, solvent and chemical precursor) and, consequently, to control the reduction kinetics of the cationic metal precursors in solution. Typically, issues, such as the colloidal stability of the particles, narrow particle size distribution and stability against oxidation, are the major obstacles of the chemical reduction methods, especially for non-noble metal particles [109].

Currently, it is well accepted that increased surface energies in nano-dimensional particles significantly influence the rate of catalytic reactions and surface oxidation processes. Nevertheless, the proper prediction of the correlation between particle morphology and surface chemistry remains complicated. Recently, systematic investigations have been reported revealing the essential principles of nanoparticulate systems by establishing rules of nano-scalability with respect to nano-sized particles and their electronic properties [110]. Only a few publications deal with the issue of stability against oxidation in nanoparticulate copper systems. This is mainly due to lack of evidence, which originates from the intrinsic stability of zero-valent Cu surfaces of nanoparticles [111]. However, evidence exists that the formation of either a Cu-core or a CuO/Cu_2O-shell system is most probably to occur [112]. Further research on particle identification of these systems is limited to X-ray diffraction analyses, which by default does not represent sufficient sensitivity for (sub)nanometer particles [113], though, conversely, employment of nano-skin capping systems has been reported. These systems, however, considerably limit the accessibility of the reactants and, therefore, hamper the catalytic activity of the nanoparticles [114].

In our work, a systematic extension of a polyol-based reduction method [115] has been developed with the main focus on (a) the influence of the chain length of the capping agent PVP (poly[*N*-vinylpyrrolidone]), (b) the effect of varying the type of the metal precursor on the nanoparticle formation, and (c) the effect of a secondary reducing agent.

Polymetallic nano-alloys. Another very interesting field in the synthesis and application of nanoparticles is the use of bi- or tri-metallic nano-alloys because of their tunable chemical and physical properties at varying composition, atomic nano-alloy structure, and particle size of the nano-alloys. Improvement of specific nano-alloy properties, with respect to monometallic clusters due to complex (or non-lineair) synergetic effects, has proven their relevance in various fields in catalysis, materials science and electronics engineering. In general, these synergetic effects of bi-metallic nano-clusters have shown to be most dominant in catalysis due to the distinctive chemical properties as compared to the corresponding mono-

metallic nano-clusters, even though of the same size. Besides the very high specific surface area, the unique physical property of a finite-size alloy, as compared to (infinite) bulk alloys, plays an important role, *e.g.* the limited miscibility of various elements in a bulk alloy could easily be overcome by means of nano-alloying [116].

Due to the on-going demand to develop nano-based materials with well-defined and controllable structured properties (and additionally the flexibility to generate bi-, tri- and poly-metallic nano-alloys) has launched a new terminology referred to "alloy nano-clusters" (or simply "nano-alloys"). Besides the already well-accepted "magic size" phenomenon of nano-alloys, *i.e.* a most stable (against agglomeration and oxidation) alloy nano-cluster size, also an optimum atomic composition may determine a particular chemical and colloidal stability. Typically, nano-alloys exhibit certain surface structures, compositions and segregation properties [117], which are of paramount importance for their chemical reactivity, especially in catalysis[118].

CuZn bimetallic nano-alloys as chemical catalyst. A particular interest in bimetallic nano-alloys appears to be the CuZn system, which has shown to play a dominant role in catalysis. In this work, and as discussed above, the Cu-catalyzed Ullmann C-O coupling reaction has shown large rate enhancements when applying CuZn nanoparticles instead of pure Cu nanoparticles. The positive effect on catalytic activity is probably due to oxidative stability of Cu, originating from preferential oxidation by Zn [75-76]. In another example, the CuZn-catalyzed Simmons-Smith cyclopropanation exhibited much higher activities using CuZn nanoparticles as compared to CuZn micron-sized particles (see Chapter 3).

Nevertheless, Cu nanoparticles are mostly known in the heterogeneously catalyzed methanol synthesis, where often ZnO is used as support [74, 119]. For this reason, there has been a considerable interest in the interface of Cu-ZnO and the actual oxidation state of copper, instigating research on the structure of CuZn and Cu-ZnO nano-alloys. Fischer *et al.* reported on a "magic composition" of CuZn "nanobrass" colloidal nanoparticles, synthesized by thermolysis from $Cu(OCH(Me)CH_2NMe_2)_2$ and Et_2Zn. EDX-analysis demonstrated a very specific atomic composition of the nano-clusters, which deviate drastically from the starting compositions. In addition, the atomic CuZn composition strongly determined the final nanoparticles sizes, *i.e.* $Cu_{0.95}Zn_{0.05}$ particles (starting from a Cu:Zn precursor ratio of 90:10) appeared to have a diameter of 5-10 nm, whereas $Cu_{0.7}Zn_{0.3}$ and $Cu_{0.35}Zn_{0.65}$ particles (from Cu:Zn precursor ratios of 50:50 and 30:70, respectively) possess mean diameters of *ca.* 10 nm. The authors showed that the pseudo-spherical particles became more faceted at increased Zn compositions, whilst a high oxidative stability of Cu could already be obtained with only 5 wt% Zn, confirming our previous findings on the "sacrificial anode" effect of Zn on Cu. The particle morphology was strongly dependent on the composition, *i.e.* at sub-equimolar Cu-Zn compositions a Cu-core and a CuZn-shell were observed, whereas at an increased Zn-fraction the Cu and Zn atoms appeared to be more uniformly distributed. In the case of α- and β-CuZn nano-alloys, convincing

evidence was found for the preferential oxidation of the Zn atoms, affording a ZnO-shell surrounding a Zn and Cu-Zn alloy core [120].

1.3 Microwave-assisted organic flow-chemistry for large-scale synthesis

The use of microwaves as a substitute for conventional heating in performing organic reactions already received considerable attention in academic [121] and industrial research laboratories [122] during the last decades [123]. Heat transport resistances in conventionally heated systems are governing the heating process. However, microwaves, acting as volumetric heating sources, do not suffer from these heat-transfer resistances and, combined with a proper reaction medium, lead to very effective heating (Figure 1).

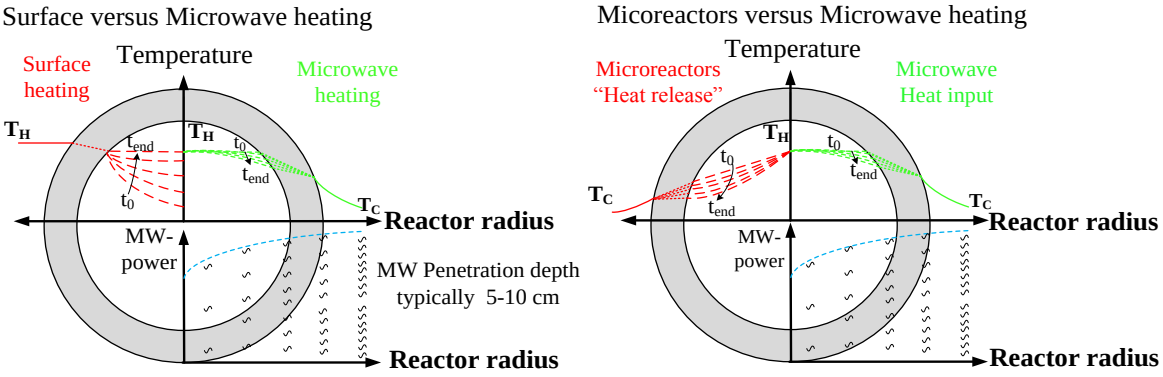

Figure 1.1. Temperature profiles of conventional and microwave heating (a) and the comparison of microreactor heat release and microwave heat input (b).

These benefits of microwave-assisted chemistry are generally applicable at lab scales. Nevertheless, in some cases these advantages can directly be translated towards larger scales, such as effective heating (under mixing), selective catalyst heating, superheating of solvents [124] and in some cases to an increased energy efficiency [125]. However, at larger scales one crucial issue severely bottlenecks scale-up, which is the limited penetration depth of microwave irradiation in larger batch reactors. For the most common microwave systems, operating at 2.45 GHz, the penetration depth of microwaves is in the order of centimeters and could slightly be increased using solvents with appropriate dielectric properties [126]. Generally, batch reactors exceeding 1-L scale have a significant non-uniform density of the electric field at the center of the reactor as compared to the outer periphery of a cylindrical reactor. Hence, thermal energy at the center of the reactor will mainly be delivered via convective (or forced convection in the case of mixing) heat-transport. This limitation is one of the major reasons to drive the change towards continuous operations in microwave-assisted processes, where, as long as the reactor dimensions do not exceed the penetration depth, a flow-through reactor could be heated with the benefits of microwaves [121c].

This change, however, requires additional efforts in fitting and optimizing the operational parameters to the reaction requirements, especially in the case of highly sensitive medicinal chemistry. Therefore, this move is still at the very beginning of its development. An example of this move was reported by Wilson *et*

al. in 2004 [127], where a glass-coiled flow-reactor was used in conjunction with microwaves in S_NAr, esterification and Suzuki cross-coupling reactions. Despite these successes, this study emphasized on the difficulties associated with combining microwave and flow processing, *i.e.* the clogging of tubes due to product crystallization. Similar failures were reported by Leadbeater *et al.* for the scale-up of various organic reactions to a hundred-grams scale, resulting in a disappointing conclusion that scale-up in a microwave flow-process could only be successfully done with homogeneous systems [128]. Recently Moseley *et al.* compared various commercial microwave systems with respect to the possibility of scaling up the Newman-Kwart rearrangement reaction in batch, stop-flow and continuous-flow reactors. Generally, also in their study it was confirmed that microwave-assisted organic flow reactors could only be carried out efficiently in homogenous reaction mixtures [129]. As an example, Hessel *et al.* demonstrated a notable improvement in the aqueous Kolbe-Schmidt reaction of a homogeneous mixture using a microwave-assisted capillary-based process [130]. Therefore, the main drawback in combining microwave heating and continuous processing is not the use and development of these technologies, but rather suiting their applications in real-life chemistry. Thus, chemistry always needs to be developed simultaneous to engineering progress.

1.4 Overview of the thesis

In this thesis, the major parts of the above-mentioned topics are covered, which undoubtedly was based on both a horizontal (*i.e.* orienting) and a vertical approach (*i.e.* focused and deep-going), seeking for realistic opportunities to establish practical methodologies for combining microwave-assisted chemistry and continuous operations. Following the above-given introduction, this investigation, to the best of my belief, follows a critical and adequate approach to conclude that the development of a "Chemistry & Engineering Quest" can certainly be proceeded with addressing the "chemistry needs" and the "engineering musts" separately, thus, simultaneously investigating suitable chemistry for a certain technology.

Therefore, in chapter 2 of this thesis the chemical reactions, selected from an intensive (literature) search based on current academic and industrial interests, are discussed. The Cu-catalyzed coupling of nucleophiles and halo-aromates appeared to be not only an excellent example of investigating the benefits of integrated microwave and micro/milli-reactor technologies, but also of its potential towards applications in the production of pharmaceutically active molecules, such as antivirals and antibiotics (*e.g.* antibiotic Vancomycin). The Ullmann-type ether synthesis (see Scheme 1), already discovered a century ago by Ullmann *et al.*, has been chosen as a key reaction in this research to exploit and improve many recent scientific endeavors in Cu-catalyzed organic reactions. This type of coupling reactions requires harsh reaction conditions, the use of activated aryl halides and excess of catalyst, which makes realistic implementation of high production volumes even more challenging.

Clearly, this type of organic reactions provides considerable challenges to overcome, both with respect to the severe reaction conditions and, undoubtedly, regarding sustainable heterogeneous catalysis which may bring considerable cost benefits in flow processing. The use of microwave energy in the Ullmann-type reactions was a first step towards the conceptual integration of both microwaves and flow-chemistry [22a]. More importantly, however, was the use of heterogeneous copper which, as a "metallic microwave-absorber", could locally heat the catalyst surface and provide an additional benefit regarding perfect reaction control by tuning the temperature at the reaction locus. Although localized metal heating is known for more than two decades, the unique combination of catalytic and heat generated functions would, in our concept of using a bi-functional metal, lead to major process advantages and novelty. To the best of our knowledge, this has not been recognized before. This start was also exploiting previous studies, where magnetic materials were shown to provide rapid microwave absorption via so-called eddy-currents and magnetic-reversal loss mechanisms, so far mostly recognized for micron-size powdered catalysts. In addition, literature reports about a strong coupling of these metals with the microwave field, providing very fast heating, but unfortunately also, dependent on their particle size, to arcing. In chapter 2, it will be concluded that it is of paramount importance, therefore, to synthesize active particles at the desired nano-size and with a high level of uniformity.

Consequently, chapter 3 deals with the development of monometallic and bimetallic Cu-based nanoparticles with a narrow size-distribution and a high resistance against oxidation and agglomeration. The chemical and colloidal stability of these Cu-based nanoparticles, including their purity and morphology, could be significantly improved, for more than three months, by coating the copper nanoparticles with poly(*N*-vinylpyrrolidone) as steric stabilizer [131]. These heterogeneous Cu-based nano-catalysts were the basis for Ullmann-type coupling reactions and the Simmons-Smith cyclopropanations as depicted in Scheme 9.

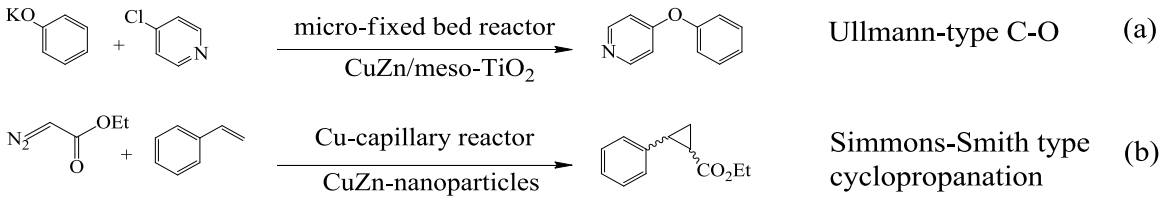

Scheme 1.9. Two types of Cu-catalyzed reactions investigated using our developed catalysts in a micro/milli flow-systems: the Ullmann-type coupling reaction (a) and the modified Simmons-Smith cyclopropanation (b).

In a subsequent step, the novel nano-catalyst, described above, was immobilized onto a microwave-transparent TiO_2 support which is highlighted in chapter 4. Novel routes for the preparation of highly active TiO_2-supported Cu and CuZn catalysts were applied in Cu-catalyzed organic reactions. The activity and stability of the catalysts were studied in the Ullmann-type coupling reaction (see Scheme 9a). It will be discussed that copper oxidation could be significantly suppressed by using $CuZn/TiO_2$ catalytic films and that a strong relation between

activity and the catalyst composition with a clear optimum in the turn-over frequency (TOF, s^{-1}) exists in the Ullmann C-O coupling reaction (see Figure 2).

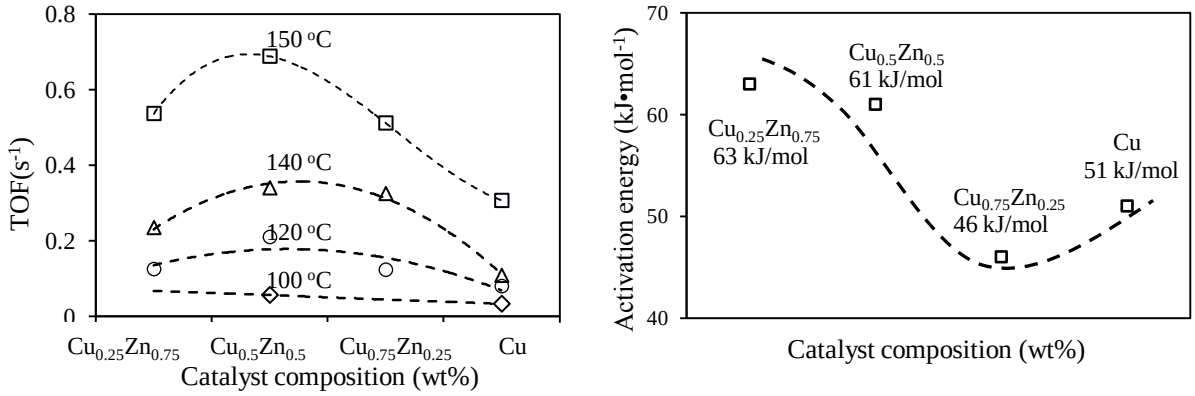

Figure 1.2. Catalyst activities and activation energies for the various developed CuZn catalysts.

To achieve this, a novel technique will be described to dip-coat a titania film onto glass beads, obtaining either structured mesoporous or non-porous titania thin films. The Cu and CuZn nanoparticles could be deposited onto calcined films (see Figure 3).

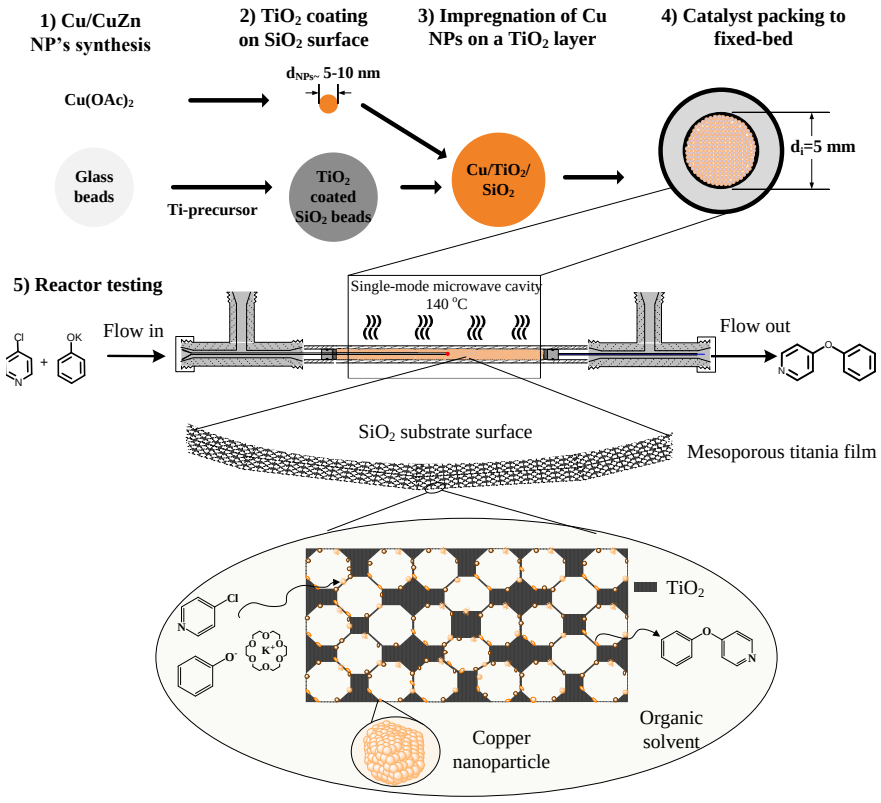

Figure 1.3. Schematic overview of the catalyst and support synthesis and the reactor design for the Ullmann-type coupling reaction.

It will be discussed how these catalysts were analyzed using various state-of-the-art characterization methods, such as inductively coupled plasma spectroscopy,

temperature programmed oxidation/ reduction techniques, ^{63}Cu nuclear magnetic resonance spectroscopy, X-ray diffraction, scanning and transmission electron microscopy, X-ray photo-electron spectroscopy and synchrotron X-ray absorption spectroscopy.

Chapter 5 deals with the issue of microwave-energy supply to heterogeneously catalyzed chemical reactions. Besides catalyzing a reaction, the energy supply towards the catalyst surface is obviously as important, especially because in traditional reactors this supply is governed by classical limitations in heat transfer. Initially, our endeavors were stimulated by exploring an adapted chemical system that could provide benefits when conventional heating is substituted by microwave irradiation and when batch processing was replaced by flow processing. Regarding the choice of the Ullmann-type coupling, it was clear that the major drawbacks in flow processing were the excess of solid bases and the metallic Cu catalysts.

It will be discussed in chapter 6 how these disadvantages were eliminated and how an experimental setup could be proposed which would synergize the benefits of microwave systems (as a novel heating technology) and micro/milli processing (as a novel reactor technology) in flow synthesis. A structured support layer was designed, where the catalyst and support were coated onto spherical glass beads, which were packed in a tubular milli-reactor (see Figure 4).

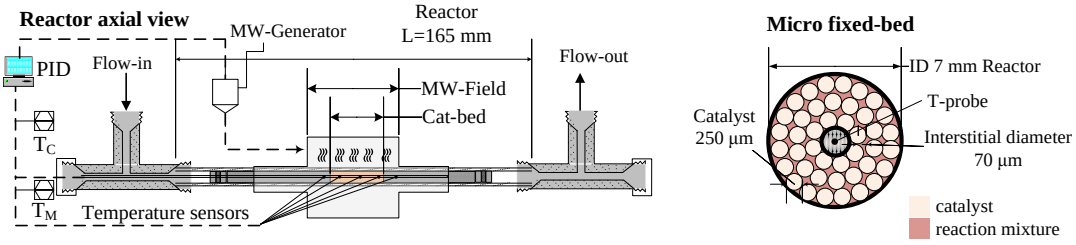

Figure 1.4. A continuously operated micro fixed-bed reactor combined with microwave heating (left), where the packing provides a highly porous micron-sized structure (right).

Simultaneously, in a separate setup, the effects of reactor shape and dimensions on effective microwave irradiation were studied. It will be revealed how experimental evidence of complete microwave penetration in the radial direction was found and how rapid and very controlled heating without significant radial temperature gradients in milli-reactors was achieved [132]. A special microwave setup with single-mode microwave cavities was designed to generate a microwave-field "hotspot" at the location of the reactor where wave cutters (stub-tuners) assure perfect control of the energy density. Figure 5 shows this microwave setup, consisting of four cavities where the electric component of the microwave field and the coupled thermal energy generation could be optimized manually.

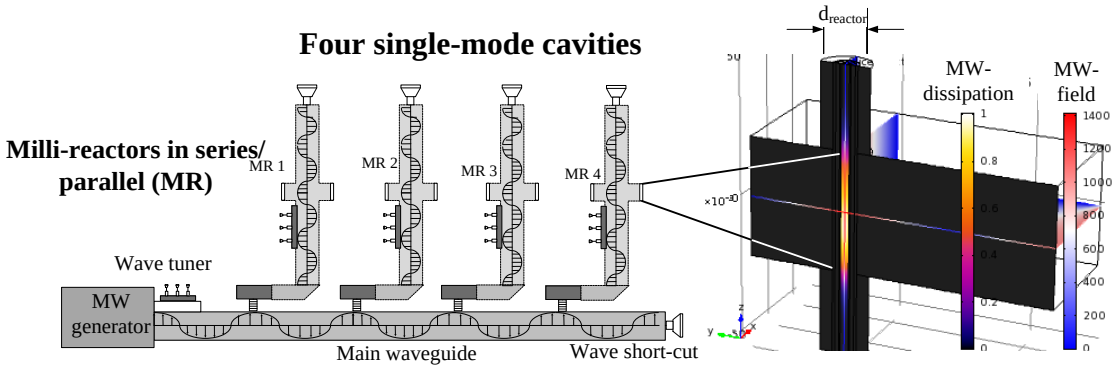

Figure 1.5. The microwave setup, where at the center of the cavity the milli-reactors (MR1-MR4) are placed, perpendicular to a resonating cavity.

In this way, it will be described how direct heating of a metal deposited onto a microwave-transparent support (TiO_2) could be used efficiently to heat the catalyst at the nano-spot, while maintaining the direct environment (*e.g.* the catalyst's support matrix) unheated. In addition it will be addressed how a high energy density in the magnetic CuZn nano-alloys, in combination with a thermal energy barrier of the support, leads to an increased catalyst activity and selectivity due to a large temperature difference between the bulk and the catalyst surface. Consequently, a multi-segmented catalyst bed (see Figure 6) was designed to utilize microwave heating more efficiently and controlled than in the case of a single catalyst bed. The temperatures in the catalyst segment (shown in brown) and at the inert segments (shown in grey) appeared much higher for the catalyst segments. The yields for the four catalyst configurations were superior to those in the conventionally heated Cu wall-coated capillary reactor (see Figure 6a) and showed an increase in yield with the number of catalyst segments, up to 75% for the four-fold segmented catalyst bed in 80 min. These high space-time-yields have so far, to the best of our knowledge, not been reported for the Ullmann-type reactions using flow processing.

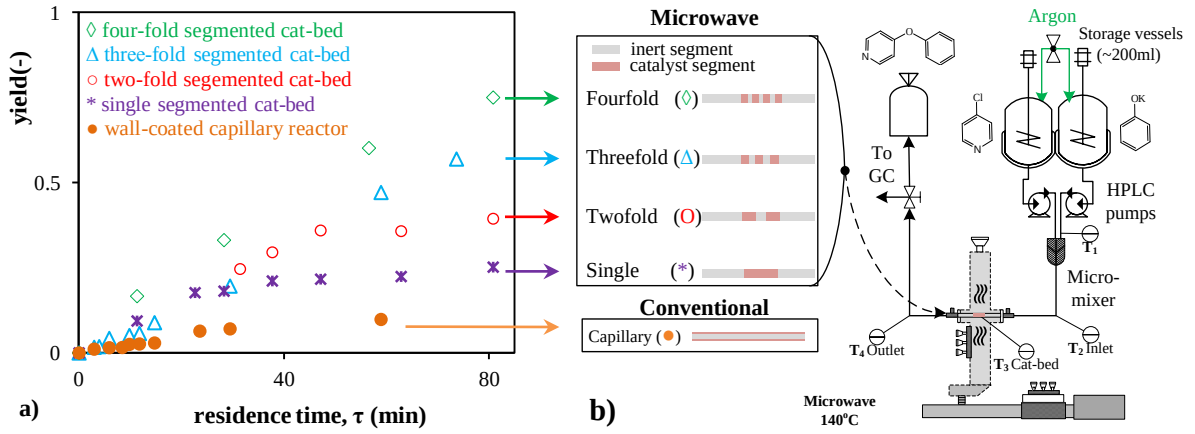

Figure 1.6. (a) Linear yield increase with catalyst segmentation using microwave heating, compared to conventional heating. (b) Setup using multi-segment catalyst beds.

Based on the chemistry, nanostructured catalysts and reactor engineering developments, an extended cost study, consisting of 14 process scenarios, was

carried out to envisage the cost-impact of microprocessing and microwaves for liquid-phase reactions in fine-chemicals synthesis. Two examples were studied, *i.e.* the Ullmann-type coupling reactions and the Aspirin synthesis [133133]. These results are presented in chapter 7. It will be revealed how the operating costs in the Ullmann-type processes compared to those of the Aspirin synthesis can be characterized as either material-based (*e.g.* reactant excess, pretreatment and catalyst synthesis) or downstream processing based (*e.g.* work-up, waste treatment) processes. The impact of integrating microwave heating and micro processing systems on profitability was demonstrated with respect to operational costs and chemical productivity.

References

[1] a) F. Ullmann, *Ber. Dtsch. Chem. Ges.* **1903**, *36*, 2382-2384; b) F. Ullmann, *Ber. Dtsch. Chem. Ges.* **1904**, *37*, 853-854; c) F. Ullmann and P. Sponagel, *Ber. Dtsch. Chem. Ges.* **1905**, *38*, 2211-2212; d) I. Goldberg, *Ber. Dtsch. Chem. Ges.* **1906**, *39*, 1691-1692.

[2] a) J. B. Buckingham, *Dictionary of Natural Products*, CRC Press, **1994**, p 1-480; b) P. N. Craig, *Comprehensive Medicinal Chemistry*, Pergamon Press, New York, **1991**, p 246; c) G. D'Aprano, M. Leclerc, G. Zotti and G. Schiavon, *Chem. Mater.* **1995**, *7*, 33-42; d) A. R. Katritzky, *Comprehensive Heterocyclic Chemistry II*, Elsevier, Oxford, **1996**, p 98.

[3] a) P. E. Fanta, *Chem. Rev.* **1946**, *38*, 139-196; b) P. E. Fanta, *Chem. Rev.* **1964**, *64*, 613-632; c) P. E. Fanta, *Synth.* **1974**, *1974*, 9,21; d) J. Hassan, M. Sévignon, C. Gozzi, E. Schulz and M. Lemaire, *Chem. Rev.* **2002**, *102*, 1359-1470.

[4] A. A. Goldberg, *J. Chem. Soc.* **1952**, 4368-4373.

[5] W. R. H. Hurtley, *J. Chem. Soc.* **1929**, 1870-1873.

[6] a) J. F. Hartwig, *Modern Amination Methods*, Wiley-VCH, Weinheim, **2000**, p 1-262; b) E. M. Beccalli, G. Broggini, M. Martinelli and S. Sottocornola, *Chem. Rev.* **2007**, *107*, 5318-5365; c) L. Jiang and S. L. Buchwald, *Metal-Catalyzed Cross-Coupling Reaction*, Wiley-VCH, Weinheim, **2004**, p 699-760; d) A. F. Littke and G. C. Fu, *Angew. Chem., Int. Ed.* **2002**, *41*, 4176-4211; e) D. S. Surry and S. L. Buchwald, *Angew. Chem., Int. Ed.* **2008**, *47*, 6338-6361.

[7] a) I. P. Beletskaya and A. V. Cheprakov, *Coord. Chem. Rev.* **2004**, *248*, 2337-2364; b) G. Evano, N. Blanchard and M. Toumi, *Chem. Rev.* **2008**, *108*, 3054-3131; c) J. P. Finet, A. Y. Fedorov, S. Combes and G. Boyer, *Curr. Org. Chem.* **2002**, *6*, 597-626; d) K. Kunz, U. Scholz and D. Ganzer, *Synlett* **2003**, *2003*, 2428-2439; e) S. V. Ley and A. W. Thomas, *Angew. Chem., Int. Ed.* **2003**, *42*, 5400-5449; f) D. Ma and Q. Cai, *Acc. Chem. Res.* **2008**, *41*, 1450-1460; g) F. Monnier and M. Taillefer, *Angew. Chem., Int. Ed.* **2008**, *47*, 3096-3099; h) F. Monnier and M. Taillefer, *Angew. Chem., Int. Ed.* **2009**, *48*, 6954-6971.

[8] a) J. C. Antilla, A. Klapars and S. L. Buchwald, *J. Am. Chem. Soc.* **2002**, *124*, 11684-11688; b) A. Klapars, X. Huang and S. L. Buchwald, *J. Am. Chem. Soc.* **2002**, *124*, 7421-7428; c) F. Y. Kwong and S. L. Buchwald, *Org. Lett.* **2003**, *5*, 793-796.

[9] a) W. Deng, Y.-F. Wang, Y. Zou, L. Liu and Q.-X. Guo, *Tetrahedron Lett.* **2004**, *45*, 2311-2315; b) D. Ma, Q. Cai and H. Zhang, *Org. Lett.* **2003**, *5*, 2453-2455.

[10] a) G. Evindar and R. A. Batey, *Org. Lett.* **2002**, *5*, 133-136; b) H. B. Goodbrand and N.-X. Hu, *J. Org. Chem.* **1998**, *64*, 670-674; c) R. Gujadhur, D. Venkataraman and J. T. Kintigh, *Tetrahedron Lett.* **2001**, *42*, 4791-4793; d) R. K. Gujadhur, C. G. Bates and D. Venkataraman, *Org. Lett.* **2001**, *3*, 4315-4317; e) C. Han, R. Shen, S. Su and J.

A. Porco, *Org. Lett.* **2003**, *6*, 27-30; f) M. Wolter, A. Klapars and S. L. Buchwald, *Org. Lett.* **2001**, *3*, 3803-3805.

[11] a) C. Enguehard, H. Allouchi, A. Gueiffier and S. L. Buchwald, *J. Org. Chem.* **2003**, *68*, 4367-4370; b) F. Y. Kwong, A. Klapars and S. L. Buchwald, *Org. Lett.* **2002**, *4*, 581-584; c) F. Lang, D. Zewge, I. N. Houpis and R. P. Volante, *Tetrahedron Lett.* **2001**, *42*, 3251-3254.

[12] a) P. J. Fagan, E. Hauptman, R. Shapiro and A. Casalnuovo, *J. Am. Chem. Soc.* **2000**, *122*, 5043-5051; b) B. d. Lange, M. H. Lambers-Verstappen, L. Schmieder-van de Vondervoort, N. Sereinig, R. de Rijk, A. H. M. de Vries and J. G. de Vries, *Synlett* **2006**, *2006*, 3105,3109; c) A. Ouali, M. Taillefer, J.-F. Spindler and A. Jutand, *Organometallics* **2006**, *26*, 65-74; d) A. Shafir and S. L. Buchwald, *J. Am. Chem. Soc.* **2006**, *128*, 8742-8743.

[13] A. H. M. de Vries, J. G. de Vries, F. B. J. v. Assema, B. de Lange, D. Mink, D. J. Hyett and P. J. D. Maas in *Vol. WO 2006/069799* (Ed. D. I. A. BV), **2006**.

[14] J.-F. Marcoux, S. Doye and S. L. Buchwald, *J. Am. Chem. Soc.* **1997**, *119*, 10539-10540.

[15] a) R. Gujadhur and D. Venkataraman, *Synth. Commun.* **2001**, *31*, 2865-2879; b) E. Buck, Z. J. Song, D. Tschaen, P. G. Dormer, R. P. Volante and P. J. Reider, *Org. Lett.* **2002**, *4*, 1623-1626; c) A. Ouali, J.-F. Spindler, H.-J. Cristau and M. Taillefer, *Adv. Synth. Catal.* **2006**, *348*, 499-505; d) H.-J. Cristau, P. P. Cellier, S. Hamada, J.-F. Spindler and M. Taillefer, *Org. Lett.* **2004**, *6*, 913-916; e) D. Ma and Q. Cai, *Org. Lett.* **2003**, *5*, 3799-3802; f) Q. Cai, G. He and D. Ma, *J. Org. Chem.* **2006**, *71*, 5268-5273; g) Y.-J. Chen and H.-H. Chen, *Org. Lett.* **2006**, *8*, 5609-5612; h) X. Lv and W. Bao, *J. Org. Chem.* **2007**, *72*, 3863-3867; i) H. Rao, Y. Jin, H. Fu, Y. Jiang and Y. Zhao, *Chem. – Eur. J.* **2006**, *12*, 3636-3646; j) N. Xia and M. Taillefer, *Chem. – Eur. J.* **2008**, *14*, 6037-6039.

[16] A. V. Kalinin, J. F. Bower, P. Riebel and V. Snieckus, *J. Org. Chem.* **1999**, *64*, 2986-2987.

[17] C. Palomo, M. Oiarbide, R. Lopez and E. Gomez-Bengoa, *Chem. Commun.* **1998**, 2091-2092.

[18] V. Engels, F. Benaskar, N. Patil, E. V. Rebrov, V. Hessel, L. A. Hulshof, D. A. Jefferson, J. A. J. M. Vekemans, S. Karwal, J. C. Schouten and A. E. H. Wheatley, *Org. Process Res. Dev.* **2010**, *14*, 644-649.

[19] a) Y. Jin, J. Liu, Y. Yin, H. Fu, Y. Jiang and Y. Zhao, *Synlett* **2006**, *2006*, 1564,1568; b) X. Liu, H. Fu, Y. Jiang and Y. Zhao, *Synlett* **2008**, *2008*, 221,224.

[20] a) Y.-J. Wu, H. He and A. L'Heureux, *Tetrahedron Lett.* **2003**, *44*, 4217-4218; b) B. H. Lipshutz, J. B. Unger and B. R. Taft, *Org. Lett.* **2007**, *9*, 1089-1092; c) N. D. D'Angelo, J. J. Peterson, S. K. Booker, I. Fellows, C. Dominguez, R. Hungate, P. J. Reider and T.-S. Kim, *Tetrahedron Lett.* **2006**, *47*, 5045-5048.

[21] a) L.-W. Xu, C.-G. Xia, J.-W. Li and X.-X. Hu, *Synlett* **2003**, *2003*, 2071,2073; b) Y. Zhao, Y. Wang, H. Sun, L. Li and H. Zhang, *Chem. Commun.* **2007**, 3186-3188; c) E. Sperotto, J. G. de Vries, G. P. M. van Klink and G. van Koten, *Tetrahedron Lett.* **2007**, *48*, 7366-7370.

[22] a) F. Benaskar, V. Engels, N. Patil, E. V. Rebrov, J. Meuldijk, V. Hessel, L. A. Hulshof, D. A. Jefferson, J. C. Schouten and A. E. H. Wheatley, *Tetrahedron Lett.* **2010**, *51*, 248-251; b) F. Benaskar, N. G. Patil, V. Engels, E. V. Rebrov, J. Meuldijk, L. A. Hulshof, V. Hessel, A. E. H. Wheatley and J. C. Schouten, *Chem. Eng. J.* **2012**, *Accepted/in press*.

[23] H. Weingarten, *J. Org. Chem.* **1964**, *29*, 3624-3626.

[24] P. E. Weston and H. Adkins, *J. Am. Chem. Soc.* **1928**, *50*, 859-866.

[25] M. Mansour, R. Giacovazzi, A. Ouali, M. Taillefer and A. Jutand, *Chem. Commun.* **2008**, 6051-6053.
[26] F. A. Cotton, G. Wilkinson, C. A. Murillo and M. Bochmann, *Advanced Inorganic Chemistry*, John Wiley & Sons, **1999**, p 854-876.
[27] a) J. Lindley, *Tetrahedron* **1984**, *40*, 1433-1456; b) C. Couture and A. J. Paine, *Can. J. Chem.* **1985**, *63*, 111-120.
[28] D. van Allen in *Methodology and mechanism: Reinvestigating the Ullmann reaction, Doctor of Philosophy* University of Massachusetts Amherst, Amherst, **2004**.
[29] a) T. V. Popova and N. V. Aksenova, *Russ. J. Coord. Chem.* **2003**, *29*, 743-765; b) L. M. Huffman and S. S. Stahl, *J. Am. Chem. Soc.* **2008**, *130*, 9196-9197; c) R. Xifra, X. Ribas, A. Llobet, A. Poater, M. Duran, M. Solà, T. D. P. Stack, J. Benet-Buchholz, B. Donnadieu, J. Mahía and T. Parella, *Chem. – Eur. J.* **2005**, *11*, 5146-5156.
[30] T. Cohen, J. Wood and A. G. Dietz, *Tetrahedron Lett.* **1974**, *15*, 3555-3558.
[31] a) G. M. Whitesides and P. E. Kendall, *J. Org. Chem.* **1972**, *37*, 3718-3725; b) G. M. Whitesides, W. F. Fischer, J. San Filippo, R. W. Bashe and H. O. House, *J. Am. Chem. Soc.* **1969**, *91*, 4871-4882.
[32] a) G. van Koten, J. T. B. H. Jastrzebski and J. G. Noltes, *Tetrahedron Lett.* **1976**, *17*, 223-226; b) G. van Koten, R. W. M. Ten Hoedt and J. G. Noltes, *J. Org. Chem.* **1977**, *42*, 2705-2711.
[33] a) D. H. Hey and W. A. Waters, *Chem. Rev.* **1937**, *21*, 169-208; b) W. A. Waters, *The Chemistry of Free Radicals*, University Press, Oxford and London, **1948**, p 171.
[34] N. Kornblum, R. E. Michel and R. C. Kerber, *J. Am. Chem. Soc.* **1966**, *88*, 5662-5663.
[35] G. A. Russell and W. C. Danen, *J. Am. Chem. Soc.* **1966**, *88*, 5663-5665.
[36] a) J. F. Bunnett and X. Creary, *J. Org. Chem.* **1974**, *39*, 3611-3612; b) J. F. Bunnett and J. K. Kim, *J. Am. Chem. Soc.* **1970**, *92*, 7464-7466; c) J. F. Bunnett and S. J. Shafer, *J. Org. Chem.* **1978**, *43*, 1877-1879.
[37] a) K. A. Bilevitch, N. N. Bubnov and O. Y. Okhlobystin, *Tetrahedron Lett.* **1968**, *9*, 3465-3468; b) R. G. R. Bacon and A. Karim, *J. Chem. Soc., Perkin Trans. 1* **1973**, 272-278; c) T. D. Tuong and M. Hida, *Chem. Lett.* **1973**, *2*, 363-366.
[38] S. Arai, M. Hida and T. Yamagishi, *Bull. Chem. Soc. Jpn.* **1978**, *51*, 277-282.
[39] a) S. Arai, M. Hida, T. Yamagishi and S. Ototake, *Bull. Chem. Soc. Jpn.* **1977**, *50*, 2982-2985; b) S. Arai, T. Yamagishi, S. Ototake and M. Hida, *Bull. Chem. Soc. Jpn.* **1977**, *50*, 547-548.
[40] a) C. L. Jenkins and J. K. Kochi, *J. Am. Chem. Soc.* **1972**, *94*, 856-865; b) J. K. Kochi, *Organometallic Mechanisms and Catalysis*, Academic Press, New York, **1978**.
[41] a) T. Cohen and I. Cristea, *J. Org. Chem.* **1975**, *40*, 3649-3651; b) W. R. Bowman, H. Heaney and P. H. G. Smith, *Tetrahedron Lett.* **1984**, *25*, 5821-5824.
[42] a) R. G. R. Bacon and H. A. O. Hill, *J. Chem. Soc.* **1964**, 1097-1107; b) R. G. R. Bacon and H. A. O. Hill, *J. Chem. Soc.* **1964**, 1108-1112; c) R. G. R. Bacon and H. A. O. Hill, *J. Chem. Soc.* **1964**, 1112-1119.
[43] H. L. Aalten, G. van Koten, D. M. Grove, T. Kuilman, O. G. Piekstra, L. A. Hulshof and R. A. Sheldon, *Tetrahedron* **1989**, *45*, 5565-5578.
[44] H. Weingarten, *J. Org. Chem.* **1964**, *29*, 977-978.
[45] R. W. Turner and E. L. Amma, *J. Am. Chem. Soc.* **1963**, *85*, 4046-4047.
[46] B. Nicholls and M. C. Whiting, *J. Chem. Soc.* **1959**, 551-556.
[47] a) D. A. Evans, J. L. Katz and T. R. West, *Tetrahedron Lett.* **1998**, *39*, 2937-2940; b) D. M. T. Chan, K. L. Monaco, R.-P. Wang and M. P. Winters, *Tetrahedron Lett.* **1998**, *39*, 2933-2936; c) P. Y. S. Lam, C. G. Clark, S. Saubern, J. Adams, M. P. Winters, D. M. T. Chan and A. Combs, *Tetrahedron Lett.* **1998**, *39*, 2941-2944.
[48] D. L. Boger and D. Yohannes, *J. Org. Chem.* **1990**, *55*, 6000-6017.
[49] P. Wipf and J.-K. Jung, *J. Org. Chem.* **2000**, *65*, 6319-6337.

[50] A. Furstner and C. Muller, *Chem. Commun.* **2005**, 5583-5585.
[51] C. V. Ramana, M. A. Mondal, V. G. Puranik and M. K. Gurjar, *Tetrahedron Lett.* **2007**, *48*, 7524-7527.
[52] L. Kametler, G. M. Keseru, M. Nógrádi, G. Mezey-Vándor, B. Vermes and M. Kajtár-Peredy, *Liebigs Ann. Chem.* **1992**, *1992*, 1239-1243.
[53] X. Xing, D. Padmanaban, L.-A. Yeh and G. D. Cuny, *Tetrahedron* **2002**, *58*, 7903-7910.
[54] M. E. Jung and T. I. Lazarova, *J. Org. Chem.* **1999**, *64*, 2976-2977.
[55] O. Skaff, K. A. Jolliffe and C. A. Hutton, *J. Org. Chem.* **2005**, *70*, 7353-7363.
[56] D. Cousin, J. Mann, M. Nieuwenhuyzen and H. van den Berg, *Org. Biomol. Chem.* **2006**, *4*, 54-62.
[57] S.-Y. Seo, J.-W. Jung, J.-K. Jung, N.-J. Kim, Y.-W. Chin, J. Kim and Y.-G. Suh, *J. Org. Chem.* **2006**, *72*, 666-668.
[58] A. Gillmore, C. Lauret and S. M. Roberts, *Tetrahedron* **2003**, *59*, 4363-4375.
[59] Y.-C. Wang and P. E. Georghiou, *Org. Lett.* **2002**, *4*, 2675-2678.
[60] D. A. Evans, J. L. Katz, G. S. Peterson and T. Hintermann, *J. Am. Chem. Soc.* **2001**, *123*, 12411-12413.
[61] M. E. Hart, K. L. Suchland, M. Miyakawa, J. R. Bunzow, D. K. Grandy and T. S. Scanlan, *J. Med. Chem.* **2006**, *49*, 1101-1112.
[62] J. F. Miller, C. W. Andrews, M. Brieger, E. S. Furfine, M. R. Hale, M. H. Hanlon, R. J. Hazen, I. Kaldor, E. W. McLean, D. Reynolds, D. M. Sammond, A. Spaltenstein, R. Tung, E. M. Turner, R. X. Xu and R. G. Sherrill, *Bioorg. Med. Chem. Lett.* **2006**, *16*, 1788-1794.
[63] Q. Cai, B. Zou and D. Ma, *Angew. Chem. Int., Ed.* **2006**, *118*, 1298-1301.
[64] M. Taillefer, H.-J. Cristau, P. P. Cellier and J.-F. Spindler in *Fr 2833947-WO 0353225 (Pr. Nb. Fr 2001 16547), Vol.* **2001**.
[65] R. Hosseinzadeh, M. Tajbakhsh, M. Mohadjerani and M. Alikarami, *Synlett* **2005**, *2005*, 1101,1104.
[66] M. Taillefer, H.-J. Cristau, P. P. Cellier and J.-F. Spindler, *(Rhodia Chimie, France), French Patent Application 2859205A1 20050304* **2005**.
[67] J. W. W. Chang, S. Chee, S. Mak, P. Buranaprasertsuk, W. Chavasiri and P. W. H. Chan, *Tetrahedron Lett.* **2008**, *49*, 2018-2022.
[68] a) R. Ghosh and A. G. Samuelson, *New J. Chem.* **2004**, *28*, 1390-1393; b) M. R. an der Heiden, G. D. Frey and H. Plenio, *Organometallics* **2004**, *23*, 3548-3551; c) F. Yang, L. Yan, K. Ma, L. Yang, J. Li, L. Chen and J. You, *Eur. J. Org. Chem.* **2006**, *2006*, 1109-1112; d) X.-H. Zhu, G. Chen, Y. Ma, H.-C. Song, Z.-L. Xu and Y.-Q. Wan, *Chin. J. Chem.* **2007**, *25*, 546-552; e) C. Tubaro, A. Biffis, E. Scattolin and M. Basato, *Tetrahedron* **2008**, *64*, 4187-4195; f) T. Schareina, A. Zapf, A. Cotté, N. Müller and M. Beller, *Tetrahedron Lett.* **2008**, *49*, 1851-1855; g) A. B. Naidu, O. R. Raghunath, D. J. C. Prasad and G. Sekar, *Tetrahedron Lett.* **2008**, *49*, 1057-1061.
[69] a) F. Alonso, I. P. Beletskaya and M. Yus, *Tetrahedron* **2008**, *64*, 3047-3101; b) Yin and J. Liebscher, *Chem. Rev.* **2006**, *107*, 133-173.
[70] U. Lüning, J. P. W. Eggert and K. Hagemann, *Eur. J. Org. Chem.* **2006**, *2006*, 2747-2752.
[71] M. Kidwai, N. K. Mishra, V. Bansal, A. Kumar and S. Mozumdar, *Tetrahedron Lett.* **2007**, *48*, 8883-8887.
[72] T. Miao and L. Wang, *Tetrahedron Lett.* **2007**, *48*, 95-99.
[73] S. Benyahya, F. Monnier, M. Taillefer, M. W. C. Man, C. Bied and F. Ouazzani, *Adv. Synth. Catal.* **2008**, *350*, 2205-2208.
[74] R. Naumann d'Alnoncourt, X. Xia, J. Strunk, E. Loffler, O. Hinrichsen and M. Muhler, *Phys. Chem. Chem. Phys.* **2006**, *8*, 1525-1538.

[75] F. Benaskar, V. Engels, E. V. Rebrov, N. G. Patil, J. Meuldijk, P. C. Thüne, P. C. M. M. Magusin, B. Mezari, V. Hessel, L. A. Hulshof, E. J. M. Hensen, A. E. H. Wheatley and J. C. Schouten, *Chem.– Eur. J.* **2012**, *18*, 1800-1810.

[76] F. Benaskar, V. Degirmenci, E. V. Rebrov, N. G. Patil, P. Abulkin, J. Meuldijk, V. Hessel, L. A. Hulshof, E. J. M. Hensen, A. E. H. Wheatley and J. C. Schouten, *unpublished results* **2012**.

[77] a) S. E. Denmark, B. L. Christenson, D. M. Coe and S. P. O'Connor, *Tetrahedron Lett.* **1995**, *36*, 2215-2218; b) A. H. Hoveyda, D. A. Evans and G. C. Fu, *Chem. Rev.* **1993**, *93*, 1307-1370; c) D. Bittler, H. Hofmeister, H. Laurent, K. Nickisch, R. Nickolson, K. Petzoldt and R. Wiechert, *Angew. Chem., Int. Ed.* **1982**, *21*, 696-697; d) J.-M. Conia and J.-C. Limasset, *Tetrahedron Lett.* **1965**, *6*, 3151-3155; e) H. E. Simmons, E. P. Blanchard and R. D. Smith, *J. Am. Chem. Soc.* **1964**, *86*, 1347-1356; f) E. LeGoff, *J. Org. Chem.* **1964**, *29*, 2048-2050; g) E. P. Blanchard and H. E. Simmons, *J. Am. Chem. Soc.* **1964**, *86*, 1337-1347.

[78] a) J. M. Fraile, J. A. Mayoral, N. Ravasio, M. Roldán, L. Sordelli and F. Zaccheria, *J. Catal.* **2011**, *281*, 273-278; b) G. A. Ardizzoia, S. Brenna, F. Castelli, S. Galli, C. Marelli and A. Maspero, *J. Organomet. Chem.* **2008**, *693*, 1870-1876; c) S. Syukri, A. K. Hijazi, A. Sakthivel, A. I. Al-Hmaideen and F. E. Kühn, *Inorg. Chim. Acta* **2007**, *360*, 197-202; d) M. Itagaki and K. Suenobu, *Org. Process Res. Dev.* **2007**, *11*, 509-518; e) J. M. Fraile, J. I. García, V. Martínez-Merino, J. A. Mayoral and L. Salvatella, *J. Am. Chem. Soc.* **2001**, *123*, 7616-7625.

[79] a) M. I. Burguete, A. Cornejo, E. García-Verdugo, M. J. Gil, S. V. Luis, J. A. Mayoral, V. Martínez-Merino and M. Sokolova, *J. Org. Chem.* **2007**, *72*, 4344-4350; b) A. Cornejo, J. M. Fraile, J. I. García, M. J. Gil, S. V. Luis, V. Martínez-Merino and J. A. Mayoral, *J. Org. Chem.* **2005**, *70*, 5536-5544.

[80] a) C. J. Welch, Q. Tu, T. Wang, C. Raab, P. Wang, X. Jia, X. Bu, D. Bykowski, B. Hohenstaufen and M. P. Doyle, *Adv. Synth. Catal.* **2006**, *348*, 821-825; b) D. Timmons and M. Doyle in *Chiral Dirhodium(II) Catalysts and Their Applications Multiple Bonds Between Metal Atoms*, *Vol.* Eds.: F. A. Cotton, C. A. Murillo and R. A. Walton), Springer US, **2005**, pp. 591-632; c) H. T. Chifotides and K. R. Dunbar in *Rhodium Compounds Multiple Bonds Between Metal Atoms*, *Vol.* Eds.: F. A. Cotton, C. A. Murillo and R. A. Walton), Springer US, **2005**, pp. 465-589; d) H. M. L. Davies and D. K. Hutcheson, *Tetrahedron Lett.* **1993**, *34*, 7243-7246; e) M. Kennedy, M. A. McKervey, A. R. Maguire and G. H. P. Roos, *J. Chem. Soc., Chem. Commun.* **1990**, 361-362; f) S.-i. Hashimoto, N. Watanabe and S. Ikegami, *Tetrahedron Lett.* **1990**, *31*, 5173-5174.

[81] H. E. Simmons and R. D. Smith, *J. Am. Chem. Soc.* **1958**, *80*, 5323-5324.

[82] M. B. Daniel J. Mack, Alexandra Plichta, Jón T. Njarðarson, *Midas World Review (TM), January 2009-December 2009, IMS Health Incorporated.* .

[83] a) H. E. Simmons, T. L. Cairns, S. A. Vladuchick and C. M. Hoiness, *Org. React.* **1973**, *20*, 1-131; b) M. Lautens, W. Klute and W. Tam, *Chem. Rev.* **1996**, *96*, 49-92; c) S. E. Denmark and G. Beutner, *Cycloaddition Reactions in Organic Synthesis*, Wiley-VCH Verlag GmbH & Co. KGaA, Weinheim, Germany, **2002**; d) H. Lebel, J.-F. Marcoux, C. Molinaro and A. B. Charette, *Chem. Rev.* **2003**, *103*, 977-1050; e) H. Pellissier, *Tetrahedron* **2008**, *64*, 7041-7095; f) Z. Wang in *Simmons-Smith Reaction*, *Vol.* John Wiley & Sons, Inc., **2010**.

[84] a) D. L. Boger, M. W. Ledeboer, M. Kume and Q. Jin, *Angew. Chem., Int. Ed.* **1999**, *38*, 2424-2426; b) A. D. Rodríguez and J.-G. Shi, *Org. Lett.* **1999**, *1*, 337-340; c) J. Salaün in *Cyclopropane Derivatives and their Diverse Biological Activities Small Ring Compounds in Organic Synthesis VI*, *Vol. 207* (Ed. A. de Meijere), Springer Berlin / Heidelberg, **2000**, pp. 1-67; d) A. Zampella, M. V. D'Auria, L. Minale, C.

Debitus and C. Roussakis, *J. Am. Chem. Soc.* **1996**, *118*, 11085-11088; e) Y. Zhao, T.-F. Yang, M. Lee, B. K. Chun, J. Du, R. F. Schinazi, D. Lee, M. G. Newton and C. K. Chu, *Tetrahedron Lett.* **1994**, *35*, 5405-5408.

[85] a) C.-M. Che, J.-S. Huang, F.-W. Lee, Y. Li, T.-S. Lai, H.-L. Kwong, P.-F. Teng, W.-S. Lee, W.-C. Lo, S.-M. Peng and Z.-Y. Zhou, *J. Am. Chem. Soc.* **2001**, *123*, 4119-4129; b) T. Fujiwara, M. Odaira and T. Takeda, *Tetrahedron Lett.* **2001**, *42*, 3369-3372; c) T. Nagashima and H. M. L. Davies, *J. Am. Chem. Soc.* **2001**, *123*, 2695-2696; d) C. J. Sanders, K. M. Gillespie and P. Scott, *Tetrahedron: Asymmetry* **2001**, *12*, 1055-1061; e) P. Wipf, C. Kendall and C. R. J. Stephenson, *J. Am. Chem. Soc.* **2001**, *123*, 5122-5123.

[86] M. P. Doyle, R. Duffy, M. Ratnikov and L. Zhou, *Chem. Rev.* **2009**, *110*, 704-724.

[87] a) I. Arai, A. Mori and H. Yamamoto, *J. Am. Chem. Soc.* **1985**, *107*, 8254-8256; b) T. Imai, H. Mineta and S. Nishida, *J. Org. Chem.* **1990**, *55*, 4986-4988; c) A. B. Charette, B. Cote and J. F. Marcoux, *J. Am. Chem. Soc.* **1991**, *113*, 8166-8167; d) A. B. Charette and B. Cote, *J. Am. Chem. Soc.* **1995**, *117*, 12721-12732; e) Z. Song, T. Lu, R. P. Hsung, Z. F. Al-Rashid, C. Ko and Y. Tang, *Angew. Chem., Int. Ed.* **2007**, *46*, 4069-4072.

[88] a) Y. Ukaji, M. Nishimura and T. Fujisawa, *Chem. Lett.* **1992**, *21*, 61-64; b) Y. Ukaji, K. Sada and K. Inomata, *Chem. Lett.* **1993**, *22*, 1227-1230; c) H. Kitajima, Y. Aoki, K. Ito and T. Katsuki, *Chem. Lett.* **1995**, *24*, 1113-1114; d) A. B. Charette and H. Juteau, *J. Am. Chem. Soc.* **1994**, *116*, 2651-2652; e) A. B. Charette, H. Juteau, H. Lebel and C. Molinaro, *J. Am. Chem. Soc.* **1998**, *120*, 11943-11952; f) S. E. Denmark and J. P. Edwards, *Synlett* **1992**, *1992*, 229,230.

[89] a) H. Takahashi, M. Yoshioka, M. Ohno and S. Kobayashi, *Tetrahedron Lett.* **1992**, *33*, 2575-2578; b) N. Imai, K. Sakamoto, M. Maeda, K. Kouge, K. Yoshizane and J. Nokami, *Tetrahedron Lett.* **1997**, *38*, 1423-1426; c) J. Balsells and P. J. Walsh, *J. Org. Chem.* **2000**, *65*, 5005-5008; d) H. Shitama and T. Katsuki, *Angew. Chem., Int. Ed.* **2008**, *47*, 2450-2453.

[90] a) S. Sawada, J. Oda and Y. Inouye, *J. Org. Chem.* **1968**, *33*, 2141-2143; b) Z. Yang, J. C. Lorenz and Y. Shi, *Tetrahedron Lett.* **1998**, *39*, 8621-8624; c) J. C. Lorenz, J. Long, Z. Yang, S. Xue, Y. Xie and Y. Shi, *J. Org. Chem.* **2003**, *69*, 327-334.

[91] C. Rodríguez-García, A. Oliva, R. M. Ortuño and V. Branchadell, *J. Am. Chem. Soc.* **2001**, *123*, 6157-6163.

[92] a) X. Zheng, W.-H. Fang and D. L. Phillips, *J. Chem. Phys.* **2000**, *113*, 10934-10946; b) X. Zheng, C. W. Lee, Y.-L. Li, W.-H. Fang and D. L. Phillips, *J. Chem. Phys.* **2001**, *114*, 8347-8356; c) P. J. Kropp, *Acc. Chem. Res.* **1984**, *17*, 131-137; d) P. Wessig and O. Mühling, *Angew. Chem., Int. Ed.* **2001**, *40*, 1064-1065.

[93] a) T. Rovis and D. A. Evans in *Structural and mechanistic investigations in asymmetric copper(I) and copper(II) catalyzed reactions*, *Vol. 50* **2001**, pp. 1-150; b) H. Nishiyama, *Enantiomer* **1999**, *4*, 569-574; c) V. K. Singh, A. DattaGupta and G. Sekar, *Synth.* **1997**, *1997*, 137,149; d) H. M. L. Davies and E. G. Antoulinakis, *Org. React.* **2001**, *57*, 1–326.

[94] a) M. P. Doyle and D. C. Forbes, *Chem. Rev.* **1998**, *98*, 911-936; b) M. P. Doyle, M. A. McKervey and T. Ye, *Modern Catalytic Methods for Organic Synthesis with Diazo Compounds*, John Wiley and Sons, New York, **1998**.

[95] H. C. Stiasny and R. W. Hoffmann, *Chem. – Eur. J.* **1995**, *1*, 619-624.

[96] G. Boche and J. C. W. Lohrenz, *Chem. Rev.* **2001**, *101*, 697-756.

[97] E. Nakamura, N. Yoshikai and M. Yamanaka, *J. Am. Chem. Soc.* **2002**, *124*, 7181-7192.

[98] a) B. M. L. Dioos, I. F. J. Vankelecom and P. A. Jacobs, *Adv. Synth. Catal.* **2006**, *348*, 1413-1446; b) S. Bräse, F. Lauterwasser and R. E. Ziegert, *Adv. Synth. Catal.* **2003**, *345*, 869-929.
[99] R. Ferrando, J. Jellinek and R. L. Johnston, *Chem. Rev.* **2008**, *108*, 845-910.
[100] G. Schmid, M. Baumle, M. Geerkens, I. Heim, C. Osemann and T. Sawitowski, *Chem. Soc. Rev.* **1999**, *28*, 179-185.
[101] R. J. White, R. Luque, V. L. Budarin, J. H. Clark and D. J. Macquarrie, *Chem. Soc. Rev.* **2009**, *38*, 481-494.
[102] a) M. Salavati-Niasari, F. Davar and N. Mir, *Polyhedron* **2008**, *27*, 3514-3518; b) Y. H. Kim, D. K. Lee, B. G. Jo, J. H. Jeong and Y. S. Kang, *Colloids Surf., A* **2006**, *284–285*, 364-368.
[103] I. Haas, S. Shanmugam and A. Gedanken, *J. Phys. Chem. B* **2006**, *110*, 16947-16952.
[104] Y. Zhang, F. Lam, X. Hu and Z. Yan, *Chin. Sci. Bull.* **2006**, *51*, 2662-2668.
[105] V. K. Pavel, V. V. Valerii, V. S. Aleksandr and A. S. Georgii, *Quantum Electron.* **2004**, *34*, 951.
[106] G. R. Dey, *Radiat. Phys. Chem.* **2005**, *74*, 172-184.
[107] a) I. Lisiecki, F. Billoudet and M. P. Pileni, *J. Mol. Liq.* **1997**, *72*, 251-261; b) M. P. Pileni and I. Lisiecki, *Colloids Surf., A* **1993**, *80*, 63-68; c) I. Lisiecki, M. Bjoerling, L. Motte, B. Ninham and M. P. Pileni, *Langmuir* **1995**, *11*, 2385-2392; d) H. Ohde, F. Hunt and C. M. Wai, *Chem. Mater.* **2001**, *13*, 4130-4135.
[108] a) W. Yu, H. Xie, L. Chen, Y. Li and C. Zhang, *Nanoscale Res. Lett.* **2009**, *4*, 465 - 470; b) Y. Kobayashi, S. Ishida, K. Ihara, Y. Yasuda, T. Morita and S. Yamada, *Colloid Polym. Sci.* **2009**, *287*, 877-880; c) H.-X. Zhang, U. Siegert, R. Liu and W.-B. Cai, *Nanoscale Res. Lett.* **2009**, *4*, 705-708; d) A. Sarkar, T. Mukherjee and S. Kapoor, *J. Phys. Chem. C* **2008**, *112*, 3334-3340.
[109] P. Kanninen, C. Johans, J. Merta and K. Kontturi, *J. Colloid Interface Sci.* **2008**, *318*, 88-95.
[110] a) G. Jones, T. Bligaard, F. Abild-Pedersen and J. K. Nørskov, *J. Phys.: Condens. Matter* **2008**, *20*, 064239; b) A. Roldán, F. Viñes, F. Illas, J. Ricart and K. Neyman, *Theor. Chem. Acc.* **2008**, *120*, 565-573; c) F. Studt, F. Abild-Pedersen, T. Bligaard, R. Z. Sørensen, C. H. Christensen and J. K. Nørskov, *Science* **2008**, *320*, 1320-1322.
[111] M. Aslam, G. Gopakumar, T. L. Shoba, I. S. Mulla, K. Vijayamohanan, S. K. Kulkarni, J. Urban and W. Vogel, *J. Colloid Interface Sci.* **2002**, *255*, 79-90.
[112] K.-H. Meiwes-Broer, *Metal clusters at surfaces: structure, quantum properties, physical chemistry*, Springer, Berlin, New York, **200**.
[113] B. Fultz and J. M. Howe, *Transmission electron microscopy and diffractometry of materials*, Springer, Berlin, New York, **2008**.
[114] a) M. Valle-Orta, D. Diaz, P. Santiago-Jacinto, A. r. Vázquez-Olmos and E. Reguera, *J. Phys. Chem. B* **2008**, *112*, 14427-14434; b) J. G. Yang, Y. L. Zhou, T. Okamoto, R. Ichino and M. Okido, *Surf. Eng.* **2007**, *23*, 448-452.
[115] N. Toshima and T. Yonezawa, *New J. Chem.* **1998**, *22*, 1179-1201.
[116] M. P. Andrews and S. C. O'Brien, *J. Phys. Chem.* **1992**, *96*, 8233-8241.
[117] a) G. Bozzolo, J. Ferrante, R. D. Noebe, B. Good, F. S. Honecy and P. Abel, *Comput. Mater. Sci.* **1999**, *15*, 169-195; b) A. V. Ruban, H. L. Skriver and J. K. Nørskov, *Phys. Rev. B* **1999**, *59*, 15990-16000.
[118] a) A. M. Molenbroek, S. Haukka and B. S. Clausen, *J. Phys. Chem. B* **1998**, *102*, 10680-10689; b) G. Schmid, *Metal Clusters in Chemistry*, Wiley-VCH, Weinheim, **1999**.
[119] a) J. M. Dominquez E, G. W. Simmons and K. Klier, *J. Mol. Catal.* **1983**, *20*, 369-385; b) F. Boccuzzi, G. Ghiotti and A. Chiorino, *Surf. Sci.* **1985**, *162*, 361-367; c) G. C. Chinchen, M. S. Spencer, K. C. Waugh and D. A. Whan, *J. Chem. Soc., Faraday*

Trans. 1 **1987**, *83*, 2193-2212; d) L. E. Y. Nonneman and V. Ponec, *Catal. Lett.* **1990**, *7*, 213-217; e) B. S. Clausen, G. Steffensen, B. Fabius, J. Villadsen, R. Feidenhans'l and H. Topsøe, *J. Catal.* **1991**, *132*, 524-535; f) T. Fujitani, M. Saito, Y. Kanai, T. Kakumoto, T. Watanabe, J. Nakamura and T. Uchijima, *Catal. Lett.* **1994**, *25*, 271-276.

[120] a) M. Cokoja, H. Parala, M. K. Schroter, A. Birkner, M. W. E. van den Berg, K. V. Klementiev, W. Grunert and R. A. Fischer, *J. Mater. Chem.* **2006**, *16*, 2420-2428; b) M. Cokoja, H. Parala, M.-K. Schröter, A. Birkner, M. W. E. van den Berg, W. Grünert and R. A. Fischer, *Chem. Mater.* **2006**, *18*, 1634-1642.

[121] a) T. Gallert, M. Hahn, M. Sellin, C. Schmöger, A. Stolle, B. Ondruschka, T. F. Keller and K. D. Jandt, *ChemSusChem* **2011**, *4*, 1654-1661; b) C. O. Kappe, *ChemSusChem* **2010**, *3*, 1085-1085; c) M. H. C. L. Dressen, B. H. P. van de Kruijs, J. Meuldijk, J. A. J. M. Vekemans and L. A. Hulshof, *Org. Process Res. Dev.* **2010**, *14*, 351-361; d) G. Shore, M. Tsimerman and M. G. Organ, *Beilstein J. Org. Chem.* **2009**, *5*, 35.

[122] a) H. Lehmann and L. LaVecchia, *Org. Process Res. Dev.* **2010**, *14*, 650-656; b) F. Bergamelli, M. Iannelli, J. A. Marafie and J. D. A. Moseley, *Org. Process Res. Dev.* **2010**, *14*, 926-930; c) H. Lehmann, *Ernst Schering Foundation Symp. Proc.* **2007**, *3*, 133-149; d) J. D. Moseley and C. O. Kappe, *Green Chem.* **2011**, *13*, 794-806; e) D. Dallinger, H. r. Lehmann, J. D. Moseley, A. Stadler and C. O. Kappe, *Org. Process Res. Dev.* **2011**, *15*, 841-854; f) J. A. Marafie and J. D. Moseley, *Org. Biomol. Chem.* **2010**, *8*, 2219-2227; g) D. R. Godwin, S. J. Lawton, J. D. Moseley, M. J. Welham and N. P. Weston, *Energy Fuels* **2010**, *24*, 5446-5453; h) J. D. Moseley and E. K. Woodman, *Energy Fuels* **2009**, *23*, 5438-5447; i) J. D. Moseley, *Chim. Oggi* **2009**, *27*, 6-10; j) J. D. Moseley, P. Lenden, M. Lockwood, K. Ruda, J.-P. Sherlock, A. D. Thomson and J. P. Gilday, *Org. Process Res. Dev.* **2007**, *12*, 30-40; k) J. D. Moseley and S. J. Lawton, *Chim. Oggi* **2007**, *25*, 16-19.

[123] C. O. Kappe and A. Stadler in *Index, Vol.* Wiley-VCH Verlag GmbH & Co. KGaA, **2006**, pp. 397-409.

[124] a) J. M. Kremsner and C. O. Kappe, *Eur. J. Org. Chem.* **2005**, *2005*, 3672-3679; b) D. Dallinger and C. O. Kappe, *Chem. Rev.* **2007**, *107*, 2563-2591.

[125] a) T. Razzaq and C. O. Kappe, *ChemSusChem* **2008**, *1*, 123-132; b) T. M. Barnard, N. E. Leadbeater, M. B. Boucher, L. M. Stencel and B. A. Wilhite, *Energy Fuels* **2007**, *21*, 1777-1781.

[126] a) H. M. Kingston and S. J. Haswell, *Microwave-Enhanced Chemistry. Fundamentals, Sample Preparation and Applications*, American Chemical Society, Washington, **1997**; b) B. A. Roberts and C. R. Strauss, *Acc. Chem. Res.* **2005**, *38*, 653-661; c) B. L. Hayes, *Aldrichimica Acta* **2004**, *37*, 66-77; d) C. O. Kappe, *Angew. Chem., Int. Ed.* **2004**, *43*, 6250-6284; e) J. Kremsner, A. Stadler and C. Kappe in *The Scale-Up of Microwave-Assisted Organic Synthesis Microwave Methods in Organic Synthesis, Vol. 266* Eds.: M. Larhed and K. Olofssonq), Springer Berlin / Heidelberg, **2006**, pp. 233-278; f) C. Strauss and R. Varma in *Microwaves in Green and Sustainable Chemistry Microwave Methods in Organic Synthesis, Vol. 266* Eds.: M. Larhed and K. Olofssonq), Springer Berlin / Heidelberg, **2006**, pp. 199-231; g) R. N. Gedye, F. E. Smith and K. C. Westaway, *Can. J. Chem.* **1988**, *66*, 17-26; h) R. Gedye, F. Smith, K. Westaway, H. Ali, L. Baldisera, L. Laberge and J. Rousell, *Tetrahedron Lett.* **1986**, *27*, 279-282; i) R. J. Giguere, T. L. Bray, S. M. Duncan and G. Majetich, *Tetrahedron Lett.* **1986**, *27*, 4945-4948.

[127] N. S. Wilson, C. R. Sarko and G. P. Roth, *Org. Process Res. Dev.* **2004**, *8*, 535-538.

[128] M. D. Bowman, J. L. Holcomb, C. M. Kormos, N. E. Leadbeater and V. A. Williams, *Org. Process Res. Dev.* **2007**, *12*, 41-57.

[129] J. D. Moseley and E. K. Woodman, *Org. Process Res. Dev.* **2008**, *12*, 967-981.

[130] F. Benaskar, V. Hessel, U. Krtschil, P. Löb and A. Stark, *Org. Process Res. Dev.* **2009**, *13*, 970-982.
[131] V. Engels, F. Benaskar, D. A. Jefferson, B. F. G. Johnson and A. E. H. Wheatley, *Dalton Trans.* **2010**, *39*, 6496-6502.
[132] N. G. Patil, A. I. G. Hermans, F. Benaskar, J. Meuldijk, L. A. Hulshof, V. Hessel, J. C. Schouten and E. V. Rebrov, *AIChE Journal* **2011**, online.
[133] F. Benaskar, A. Ben-Abdelmoumen, N. G. Patil, E. V. Rebrov, J. Meuldijk, L. A. Hulshof, V. Hessel, U. Krtschil and J. C. Schouten, *J. Flow Chem.* **2011**, *1*, 74-89.

Chapter 2

A Kinetic Study of the Cu(0)-catalyzed Ullmann $S_{Ar}N$-type C-O Coupling of Potassium Phenolate and 4-Chloropyridine

This chapter has been submitted as:
F. Benaskar, N.G. Patil, V. Engels, E.V. Rebrov, J. Meuldijk, V. Hessel, L.A. Hulshof, A.E.H. Wheatley, J.C. Schouten (2012). A kinetic study on the Cu(0)-catalyzed Ullmann $S_{Ar}N$-type C-O coupling of potassium phenolate and 4-chloropyridine. *Dalton Trans.,* Accepted/Revision. [1]

Abstract

A parametric study of the factors that influence C-O bond formation reactions has been carried out to elucidate the mechanism by which copper mediates the Ullmann-type S_NAr reaction of 4-chloropyridine with potassium phenolate. Process conditions such as temperature, reactant concentrations, catalyst type, catalyst concentration and amounts of solubilizing additives were varied to obtain the kinetic parameters. A major effect of reactant concentrations on reaction rates was found. An increased concentration of 18-crown-6 ether, used as an alkali-metal solubilizing agent for potassium phenolate, proved to be effective only for low conversions, whereas inhibited salt complexation at high product concentrations was observed. An apparent activation energy of 55.4 kJ•mol^{-1} was observed for a Cu^0 catalyst in the liquid-phase coupling reaction in a temperature range of 100-150 °C. It was demonstrated that a Langmuir-Hinshelwood kinetics model is mechanistically more likely to occur than an Eley-Rideal model for this type of surface reaction. A maximum adsorption enthalpy on Cu was found for 4-phenoxypyridine, followed by 4-chloropyridine and phenolate, respectively.

2.1 Introduction

Since the discovery of copper-catalyzed C-C, C-N and C-O coupling processes utilizing activated phenols as nucleophiles and as reported by Fritz Ullmann [2] and Irma Goldberg [3] between 1901 and 1905, progress has been achieved in obtaining higher yields under milder reaction conditions. A significant breakthrough was made when palladium-catalyzed systems were introduced by Hartwig [4]. Later developments were made by Buchwald, who developed a wide-ranging library of substituted phenolic nucleophiles and aromatic electrophiles as reagents for the synthesis of diaryl ethers [5]. Moreover, recent modifications have resulted in higher product yields whilst allowing decrease of the reaction temperature to 90-120 °C when using a range of chemically diverse catalyst substrates and promoters [6]. These improvements have mainly been achieved through the use of palladium [4a, 5, 7] and, to a lesser extent, copper catalysts [8].

Recently, we have shown enhanced yields of heterocycle-aryl ether (exceeding 90%) under modified process conditions using naked-ion phenolic derivates and cation quenchers [9]. However, whereas the role of copper in the Ullmann ether synthesis is generally defined as that of a catalyst [10], there is still limited understanding of the reaction mechanism and the role of the copper [11]. Hartwig *et al.* isolated copper-phenolate complexes which were postulated to be intermediates in the copper-catalyzed etherification of aryl halides and phenol [12]. Although uncommon, this research showed that Cu(III) species, such as alkylcopper(III) and arylcopper(III), play a role as intermediates. This was confirmed by a density functional theory (DFT) modelling study on a phenyl-ligated arylcopper(III) halide-phenolate complex which provided a free formation energy of 22.1 kcal•mol^{-1}, being consistent with experiment.

Little is known about the intrinsic kinetic parameters of Ullmann-type C-O coupling reactions. However, previous studies on the adsorption kinetics of phenolate [13] and pyridine [14] have shown a relatively fast desorption of these components from a Cu surface [15]. These results confirm the involvement of both a nucleophile and an electrophile during an adsorption process in a $S_{Ar}N$-type coupling mechanism, thus suggesting a Langmuir-Hinshelwood kinetics model. Nevertheless, for this particular type of bi-aromatic etherification, numerous publications dealing with a "renaissance of Ullmann and Goldberg reactions" [16] have still failed to provide a general and satisfactorily conclusive kinetic model. Moreover, the substrate adsorption mechanism, following either a nucleophilic (phenolate) [17] or electrophilic (halo aromate) [18] pathway, remains largely unproven. Consequently, reactions hitherto proposed to proceed via a nucleophilic aromatic substitution (S_NAr) could, in theory, also be of a more electrophilic ($S_{El}Ar$) character. Analysis of reaction kinetics promises to allow us to discriminate between an Eley-Rideal and a Langmuir-Hinshelwood kinetics mechanism.

In this study, the effect of the temperature, reactant concentration, catalyst concentration and solubilizer (cation quencher) concentration on the rate of an Ullmann C-O coupling reaction has been elucidated and a kinetic model has been

proposed. A set of experiments have been proposed based on a DoE (Design of Experiments) methodology using a fractional factorial design of experiments, where each parameter has been varied separately based on a center-point experiment. The selected experimental window of the parameters was based on our recently published study on the coupling reaction between potassium phenolate and 4-chloropyridine for kg-scale continuous processing [19].

2.2 Experimental

2.2.1 Reagents and materials

Potassium phenolate was formed from phenol (~99 wt%, Sigma-Aldrich) and potassium *tert*-butoxide (purum, ≥97.0 wt%, Aldrich). 4-Chloropyridine hydrochloride salt (99%, Aldrich) was used to obtain 4-chloropyridine in liquid form upon neutralization. *N*,*N*-dimethylacetamide (DMA, CHROMASOLV® HPLC, >99.9 wt%) was used as reaction solvent. Copper powder (99 wt%, Aldrich) was used as the catalyst and 18-crown-6 ether (99 wt%, Sigma-Aldrich) as a potassium ion scavenger. Component concentrations were determined using tetradecane (puriss. p.a., ≥99.5 wt% (GC), Fluka) as an internal standard for ^{1}H-NMR spectroscopy.

Potassium phenolate was synthesized by dissolving potassium *tert*-butoxide (0.19 mol) in THF (150 mL) and slowly adding phenol (0.20 mol) under reflux, leading to an exothermic reaction. After 1 h of stirring, THF and *tert*-butanol were slowly removed using a rotary evaporator (300 mbar, 40 ºC). Subsequently, the remaining phenol was removed in a vacuum oven (10 mbar, 100 ºC). Potassium phenolate was obtained quantitatively as a white-yellowish powder.

4-Chloropyrdine was formed from an aqueous solution of K_2CO_3 (2.5 M in 100 mL demineralised water) by slow addition of 4-chloropyridine·HCl salt (0.22 mol). After 1 h of stirring, the clear orange organic layer was extracted using diethyl ether, dried with anhydrous Na_2SO_4, filtered and concentrated by evaporation (800 mbar, 40 ºC).

2.2.2 Analytical methods

During each kinetic experiment, samples were taken at fixed time intervals and subjected to ^{1}H-NMR spectroscopy (400-MR Varian NMR spectrometer; 400 MHz, d^6-DMSO), using tetradecane as an internal standard. Spectral results were compared with literature data. Component concentrations were then calculated from the ^{1}H-NMR spectra based on an internal standard (tetradecane). Additionally, GC-MS analyses (Shimadzu QP 5000, zebron column ZB35) were applied to verify and cross-check the conversions and product yield. From these data, concentration-time histories were obtained for each experiment and subjected to mass balance verification.

2.2.3 Catalyst characterization

The crystallographic structure of the catalyst surfaces was characterized by powder X-ray diffraction (Bruker D4 Endeavour Roentgen PW3040/60 XPert

PRO powder x-ray diffractometer) using a high resolution PW3373/00 Cu LFF (unmonochromated) tube at λ = 1.5404 Å (Cu Kα) in the 2Θ range of 10-80° and a scanning rate of 0.48 °/min. Scanning electron microscopy (SEM) with an accelerating voltage of 5 keV and magnifications of 100-20,000x were used to determine particle morphology (FEI Quanta series FEG 3D G2 SEM).

2.2.4 Catalytic activity study

For each separate experiment appropriate amounts of 4-chloropyridine, potassium phenolate and 18-crown-6 ether (*ca*. 0.01 equiv with respect to phenolate) were stirred in a 75-mL baffled glass reactor loaded with DMA (15-25 mL) at 45 °C until complete dissolution occurred. Using phenol as nucleophile would require an *in situ* deprotonation step with the need for an additional solid base. Therefore, potassium phenolate was used as a naked-ion nucleophile. The potassium phenolate was completely dissolved in the solvent by the addition of 18-crown-6 ether and pre-heated to 50 °C. For the center-point experiment a mixture of 0.5 M (10 mmol, 1.14 g) of 4-chloropyridine, 0.75 M (15 mmol, 1.14 g) potassium phenolate and 0.008 M (0.15 mmol, 0.040 g) of 18-crown-6 ether (*ca*. 0.01 equiv with respect to phenolate) was stirred in a baffled glass reactor loaded with solvent DMA (20 mL). After heating the mixture to the desired reaction temperature, the solution was treated with an appropriate amount (variable mol% with respect to 4-chloropyridine) of 99 wt% metallic copper catalyst (for center-point experiment 0.05 M (1 mmol, 0.064 g)) and the resulting slurry was mechanically stirred in a jacketed reactor using a circulating oil-bath. Bulk temperatures during the reaction were measured using a thermocouple probe. All reactions were carried in an argon atmosphere. The yield of 4-phenoxypyridine was determined by comparing the aromatic regions of the ^{1}H-NMR spectra (δ = 6.5-8.6 ppm) of reaction aliquots against unreacted material. The yield (Y_t in Equation 1a) was based on the amount of 4-chloropyridine converted (X_t in Equation 1b) and the selectivity towards formation of 4-phenoxypyridine (S_t in Equation 1c) at various reaction times. The initial reaction rates (r_{init} in Equation 1d) were deduced from concentration-time histories (see Supporting Information in reference [1]).

$$Y_t(\%) = 100 \times (S_t \times X_t) \qquad \textbf{Equation 2.1a}$$

$$X_t = \frac{C^0_E - C^t_E}{C^0_E} \qquad \textbf{Equation 2.1b}$$

$$S_t = \frac{C^t_P}{C^0_E - C^t_E} \qquad \textbf{Equation 2.1c}$$

$$r_{init} = \frac{C^{\Delta t}_P \times V_L}{\Delta t \times w_{cat}} \qquad \textbf{Equation 2.1d}$$

C^0_E represents the initial electrophile (4-chloropyridine) concentration (in mol•L^{-1}) and C^t_E and C^t_P indicate the electrophile and product concentrations (in mol•L^{-1}) after a certain reaction time, respectively. The initial reaction rate (in

mol•g^{-1}•s^{-1}) is determined for normalized amounts of catalyst (as w_{cat} in g_{cat}) and reaction mixture volume V_L (in L). The $C^{\Delta t}{}_P$ (in mol•L^{-1}) indicates the amount of product formed over a defined time span Δt (given in s).

2.2.5 Catalyst deactivation study

Catalyst deactivation kinetics were obtained over the spent catalysts from the previous run. In these experiments, the catalyst was separated from the product mixture and reused in a subsequent run under identical reaction conditions. Catalyst separation was carried out by centrifugation, decantation, filtration and drying, followed by measurement of the residual catalyst weight. A catalyst recovery of above 96 wt% was achieved.

2.2.6 Design of experiments

The experimental part was designed using a "One Variable At Time-strategy" (OVAT-strategy) where separately each parameter was subjected to experiments, while leaving other parameters unchanged. Although this strategy requires an extended number of experiments, it provides much more detailed information which can be analyzed separately for each parameter. Other methods exist to conduct efficiently kinetic analyses using multi-parametric fitting models. These fractional factorial designs of experiments are mostly applied when two (or maximal three) parameters are suspected to be correlated and provide a quick insight into the severity of interrelation, such as in our case temperature and concentration. This type of design of experiments allowed to trace the cross-terms and provide operational conditions for optimum output (*e.g.* rate, conversion and selectivity), most reliably at the given experimental domain. However, the objective of this OVAT-based study was more focused on determining the intrinsic parameters and to distinguish the interrelated input variables, using the conversion data at different reaction times. The developed model was fitted by means of a multi-parameter linear regression model, where conversion was described as a function of the reaction conditions. The conversion output was divided in two parts, *i.e.* the conversion slope (as function of time) at the start of the reaction and at the conversion completion.

2.3 Results and discussion

2.3.1 Catalyst characterization

Scanning electron microscopy (SEM). SEM images demonstrated a platelet-like non-porous structure (Figure 1a) with a mean particle size of 40 ± 5 μm (Figure 1b). The active catalyst surface was calculated based on high-magnification SEM-images (see Supporting Information in reference [1]). Energy dispersive X-ray (EDX) analysis confirmed a Cu purity greater than 99.5 wt%. Selected images and the corresponding size distribution histogram are shown in Figures 1a-1d.

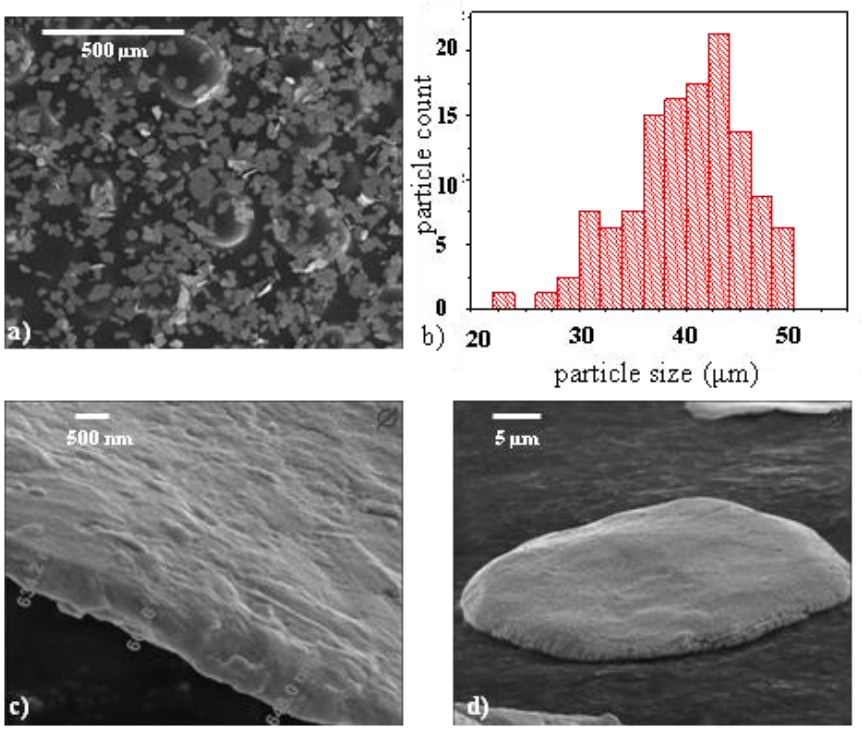

Figure 2.1. SEM-images of the commercial Cu-powder used as a catalyst (a-c) and grain-size distribution (d) as calculated from the low-magnification images.

Powder X-Ray Diffraction analysis (P-XRD). The crystallographic structure of the Cu powder was analyzed as shown in Figure 2. Characteristic diffraction peaks at 42.4, 50.5 and 73.0 degrees 2Θ correspond to the face-centered cubic (FCC) copper metal structure. Albeit negligible, a trace impurity was observed at 2Θ = 61.9° due the presence of a small amount of CuO.

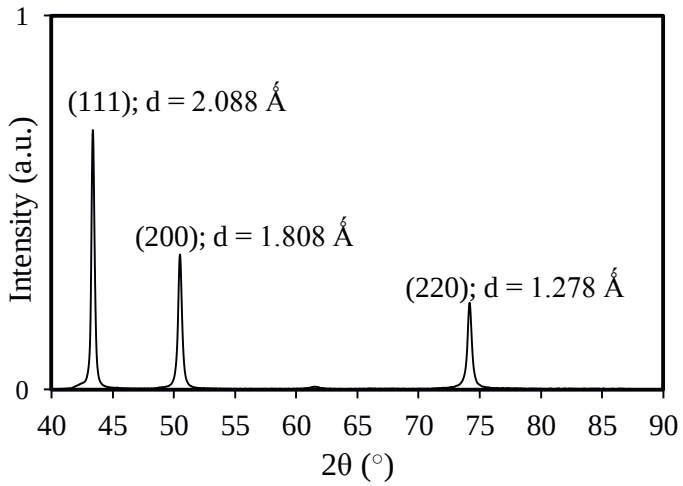

Figure 2.2. Powder-XRD spectrum of commercial, micron-sized Cu-powder as obtained from Sigma-Aldrich.

2.3.2 Catalyst deactivation study

Experiments designed to study the catalyst deactivation at low conversions were performed at 115 ºC. Figure 3 demonstrates the yield after two consecutive reaction runs of 30 min. No catalyst deactivation can be seen in these runs. The

slight yield drop after 30 min in the second run was attributed to catalyst losses during regeneration.

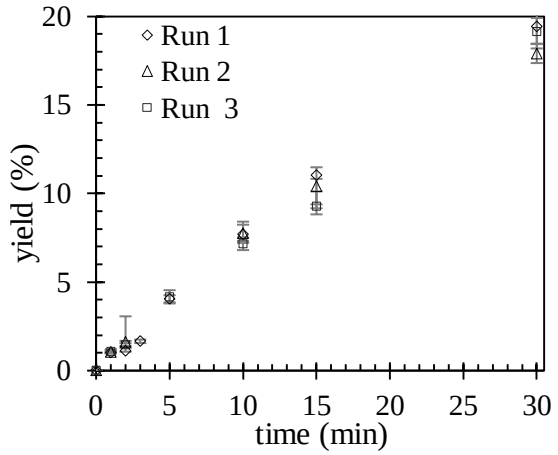

Figure 2.3. The product yield as a function of reaction time for two consecutive runs with the same catalyst and otherwise similar reaction conditions, proving negligible catalyst deactivation. Reaction conditions: T = 115 ºC, $C_{pyridine}$ = 0.2 M, $C_{phenolate}$ = 0.2 M, C_{cat} = 20 mM and $C_{solubilizer}$ = 2 mM.

2.3.3 Effect of Cu-loading

The dependence of the reaction rate on the catalyst concentration was studied at 130 ºC at concentrations of 0.05 and 0.1 M while the other reaction conditions were kept constant. The yield as a function of time is shown in Figure 4a.

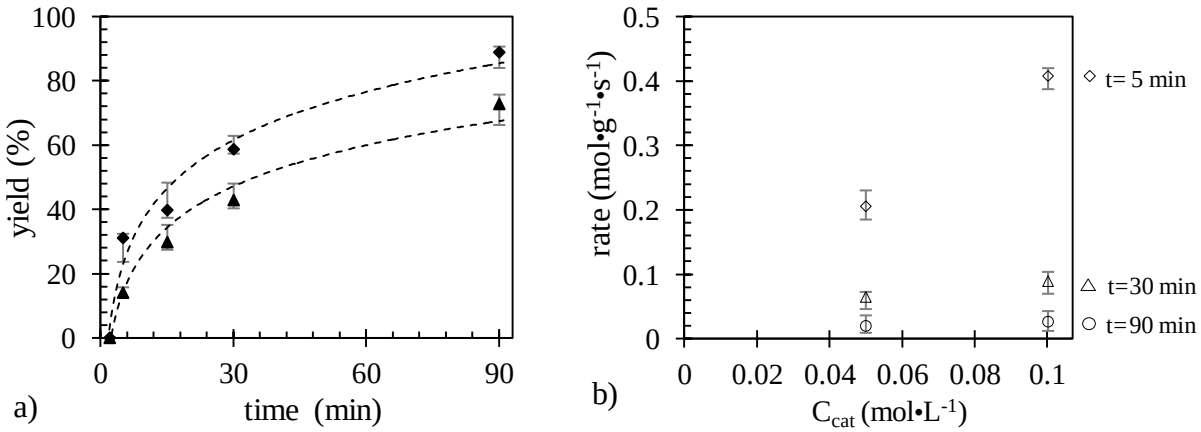

Figure 2.4. Yield profiles at 130 ºC as a function of time (a) and catalyst concentrations (b), establishing the influence of catalyst loading (▲ = 0.05 M, ♦ = 0.1 M) on the product yield. The rate as a function of catalyst loading for various reaction times shows a linear dependence. Reaction conditions: T = 130 ºC, $C_{phenolate}$ = 0.75 M, $C_{pyridine}$ = 0.5 M and $C_{18\text{-}crown\text{-}6}$ = 5 mM.

At a reaction time of 5 min, the rate doubled when using a two-fold catalyst concentration, clearly indicating the absence of mass-transfer limitations. Figure 4a confirms higher yields at a catalyst concentration of 0.1 mol•L^{-1} after 5 min. In Figure 4b the reaction rate is plotted as a function of Cu catalyst concentration at various reaction times. At longer reaction times, the reaction rate decreases, indicating a possible product inhibition effect.

2.3.4 Reaction mechanism

Assuming a strong adsorption of either the phenoxide species or of the pyridine reactant, two reaction pathways can be proposed following the Eley-Rideal (ER) mechanism. These are shown as pathway 1 and pathway 2 in Scheme 1. In contrast, if both reactants are adsorbed onto the catalyst, the Langmuir-Hinshelwood (LH) mechanism applies, where two active species are involved and electron transfer is assumed to take place as described in pathway 3 in Scheme 1. The surface reaction (step 3 in the ER or step 4 in the LH mechanism) is the rate-limiting step.

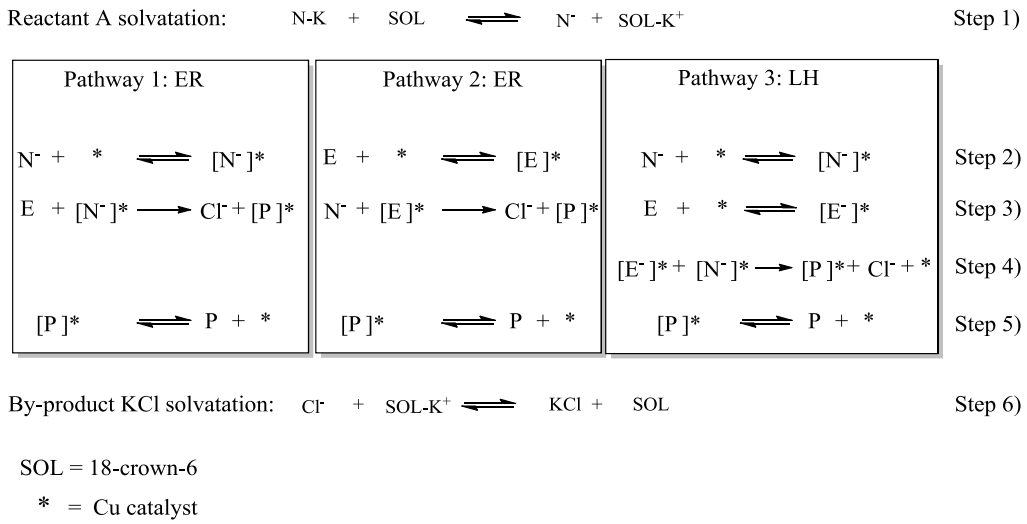

Scheme 2.1. Possible reaction mechanisms for the Ullmann C-O coupling reaction. Pathway 1: ER-mechanism with strong adsorption of the phenolate species and formation of PhOCu(I). Pathway 2: ER-mechanism with strong pyridine adsorption. Pathway 3: LH-mechanism with adsorption of both phenoxy and 4-chloropyridine species. A, B, P and * denote phenolate, 4-chloropyridine, 4-phenoxypyridine and Cu active site, respectively. Potassium phenolate dissociation towards a naked-ion nucleophile and potassium chloride formation are given in steps 1 and 6, respectively.

2.3.5 Kinetics study

Effect of reactant molar ratio on reaction rate. The initial concentration of potassium phenolate was varied while other reaction conditions, such as temperature and the concentration of 4-chloropyridine (0.5 M), catalyst and solubilizer were kept constant. After 5 min, the reaction yield was found to increase from 12 to 25 % as the nucleophile/electrophile (N/E) molar ratio was raised from 0.5 to 1.2 (Figure 5a). The highest yields, based on the limiting reactant, were obtained at a slight nucleophile excess of 0.2 M. The yield remained rather constant at a higher (1.5 times) nucleophile excess and was significantly reduced at a two-fold excess of electrophile, thus indicating a strong influence of the phenolate concentration. There exists an optimum nucleophile-electrophile molar ratio of about 1.2, indicating that a slight excess of nucleophile is required to achieve the highest product yield (see Figure 5b). Although at longer reaction times this trend appears to be less significant, initial reaction rates are considered to have a larger influence on the overall yield.

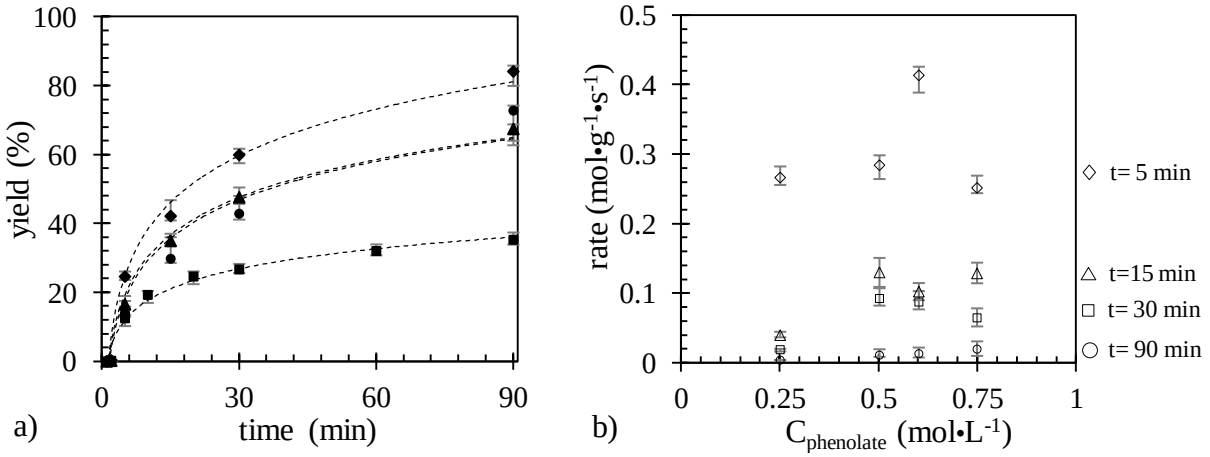

Figure 2.5. Reaction yields as a function of time (a) for different nucleophile initial concentrations (■ = 0.25 M, ▲ = 0.5 M, ● = 0.75 M and ♦ = 0.6 M) and as a function of potassium phenolate concentration (b) for various reaction times. Reaction conditions: T = 130 ºC, $C_{electrophile}$ = 0.5 M, $C_{solubilizer}$ = 5 mM and C_{cat} = 50 mM.

Effect of the overall reactant concentration. In the present study, DMA was used as solvent. It has a high solubility for both polar and apolar organic compounds, a moderate boiling point and, importantly, a promotional effect on the activation of amide bond-formation to the copper surface in catalysis. However, whilst the positive effects of using DMA are significant, work-up of the reaction mixture involves an energy demanding solvent separation step. In addition, envisaging process intensification as a means of increasing the operational concentration of the conversion, experiments were carried out in which the amount of reactants was increased while the same amount of solvent was used (see Figure 6). Three different reactant concentrations were tested at a constant N/E molar ratio of 1.5. Figure 6a shows the product yield as function of time at three overall reactant concentrations (0.25, 1.25 and 2.5 mol•L^{-1}). After 90 min, the highest yield (86%) was obtained for a total reactant concentration of 2.5 M, while yields of 78 and 73% were observed at 0.25 and 1.25 M, respectively.

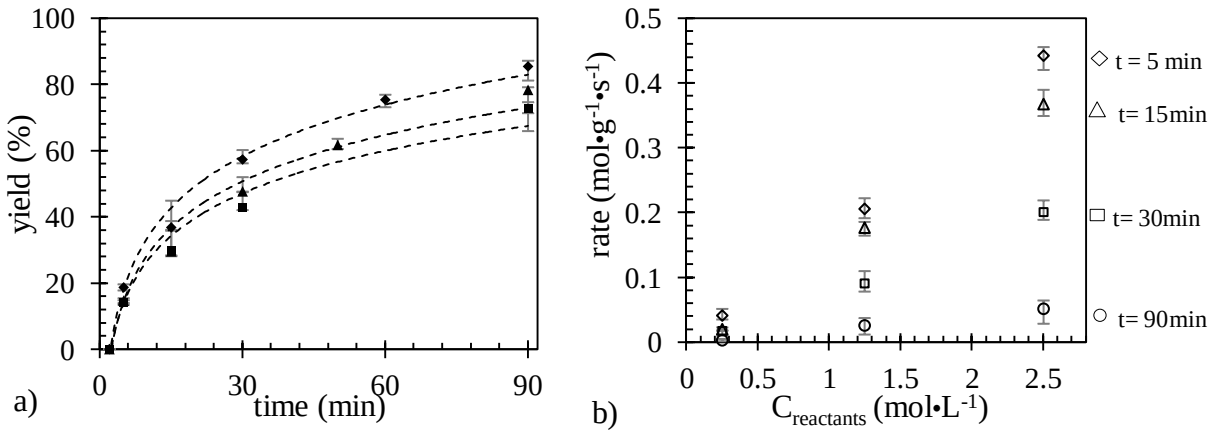

Figure 2.6. Product yield as a function of time (a) for overall reactant concentrations of 0.25 (▲), 1.25 (■) and 2.5 (♦) mol•L^{-1} and (b) at various reaction times. Reaction conditions: T = 130 ºC, $C_{phenolate}$:$C_{pyridine}$ = 1.5, C_{cat} = 10 mol% of $C_{pyridine}$ and $C_{solubilizer}$ = 1 mol% of $C_{phenolate}$.

The amount of product obtained per unit of reaction volume increased by a factor of 10 from 22.3 to 246.7 $kg \cdot m^{-3} \cdot h^{-1}$ upon increasing the reactant concentration by 10 times. A first order dependence of the reaction rate on the electrophile concentration was observed when a 1.5 excess of electrophile was used (see Figure 6b). A yield of 80% was obtained after 90 min. Interestingly, the influence of excess phenolate vanishes at this saturation conversion plateau although the phenolate to 4-chloropyridine fraction increases exponentially.

Effect of potassium phenolate solubility. The potassium phenolate solubility and reactivity were increased by adding 18-crown-6 ether in order to form a complex with cations of a size similar to the crown diameter, resulting in a dynamic equilibrium between cation coordination and dissociation. Following our previous results [9], 18-crown-6 ether was used as cation quencher to encourage the formation of a naked phenolate anion of enhanced nucleophilic character (see Scheme 2). Data suggests that trace amounts of crown ether in the tested concentration window here are sufficient to increase the reaction performance, as shown in Figure 7.

Scheme 2.2. The formation of a naked-ion phenolate nucleophile using potassium phenolate and 18-crown-6 ether as cation scavenger in DMA.

Figure 7a shows the product yield as a function of time for three 18-crown-6 ether concentrations (5, 10 and 50 mM). Figure 7b demonstrates that there are no major effects on rates for higher 18-crown-6 ether concentrations. At longer reaction times a negligible effect of the 18-crown-6 ether concentration on the productivity was observed, which was in line with literature [20]. As the reaction proceeded, potassium chloride, which is formed as a by-product, underwent competition with potassium phenolate for 18-crown-6 ether coordination, resulting in a decreased nucleophilicity and reactivity of potassium phenolate.

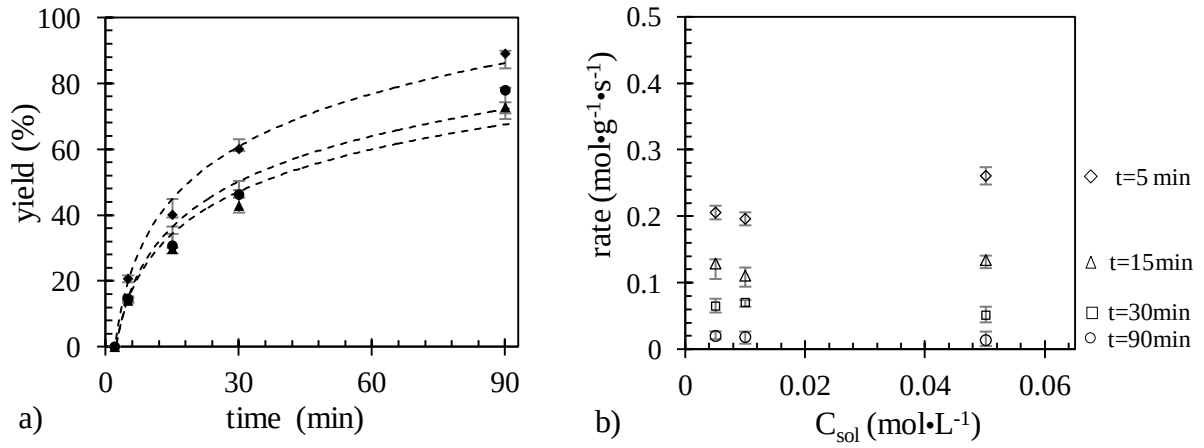

Figure 2.7. Reaction rates (a) as a function of time for different concentrations of 18-crown-6 ether (▲ = 0.005 M, ● = 0.01 M and ♦ = 0.05 M) and (b) at different reaction times. Reaction conditions: T = 130 ºC, $C_{pyridine}$ = 0.5 M, $C_{phenolate}$ = 0.75 M and C_{cat} = 0.05 M.

In addition, the relatively small chloride ion is sterically favoured over phenolate as a counter-ion for the potassium-crown ether complex. Since the crown ether is recognised to be a cation scavenger that participates in metal complexation-dissociation equilibria, it can be considered to represent a homogeneous catalyst promoter that affords one free site per conversion turn-over [21].

Effect of product inhibition. To investigate the effect of product, a series of experiments was carried out in the presence of 10, 50 and 90 mM 4-phenoxypyridine (Figure 8). The product yield decreased by 13% in the presence of 90 mM product after 5 min and by 30% after 90 min, revealing a major product influence on yield (Figure 8a). Figure 8b shows the reaction rates as a function of the initial product concentrations at various reaction times, demonstrating that the presence of product mostly influenced the initial product formation rates. This observation confirms that the reaction rate is much more affected by the presence of the product rather than any of the reactants, which is to be expected as both oxygen and nitrogen are present in the product.

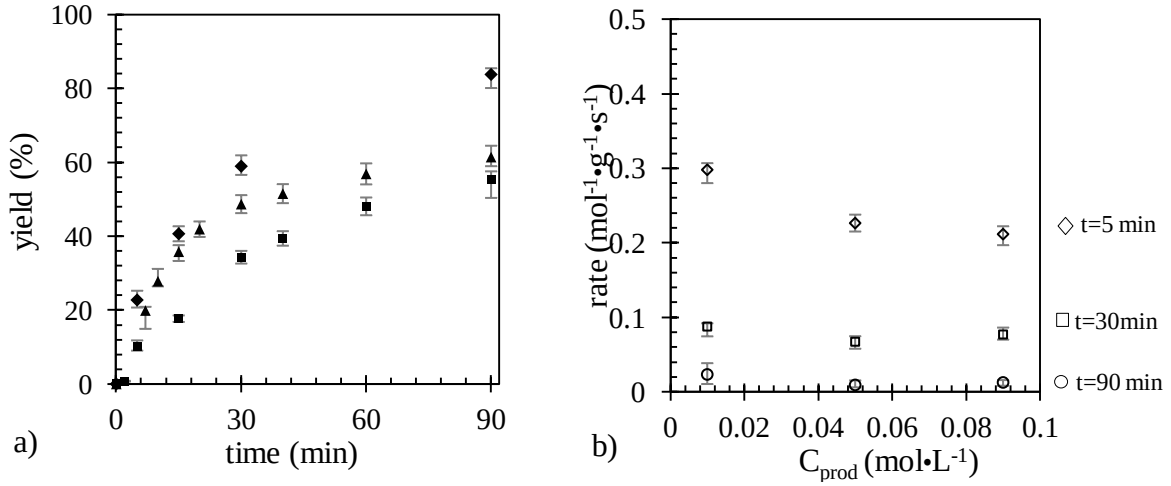

Figure 2.8. Product yields (a) as a function of time for different initial product concentrations (♦ = 0.01 M, ▲ = 0.05 M and ■ = 0.09 M) and (b) at different reaction times. Reaction conditions: T = 130 ºC, $C_{pyridine}$ = 0.5 M, $C_{phenolate}$ = 0.75 M and C_{cat} = 0.05 M.

Effect of temperature. The apparent activation energy (E_A^{App}) for the reaction of 55.4 kJ•mol^{-1} and the pre-exponential factor (A_0) of 3756.5 mol•L^{-1}•s^{-1} were obtained from experiments in the range 110-140 ºC (Figure 9). Manifar *et al.* studied the kinetic details of Ullmann-type C-N reactions between substituted aryl iodides and toluidine components, which proceed by a substitution mechanism comparable to that of the Ullmann ether coupling [22]. These authors found an apparent activation energy of 54.0 kJ•mol^{-1}. The pre-exponential factor varied from 1774.4 to 5657.8 mol•L^{-1}•s^{-1} for mono- and disubstitution reactions, thus demonstrating results comparable to those obtained in the present study for the Ullmann C-O coupling.

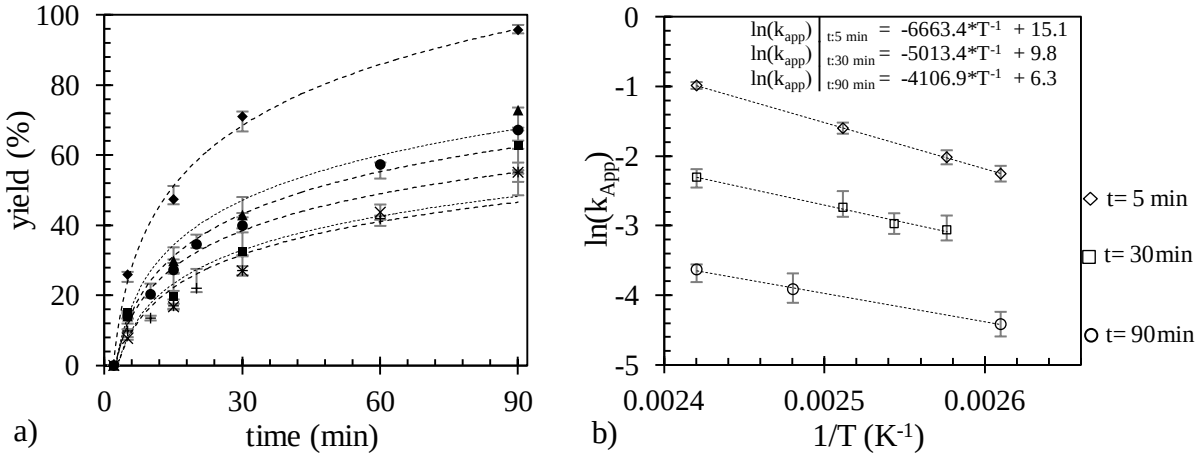

Figure 2.9. Product yields (a) as a function of time for different temperatures: ♦ = 140, ▲ = 130, ● = 125, ■ = 120, + = 115 and × = 110 in ^oC. The Arrhenius plot (b) deduced from typical reaction temperatures (in K) providing apparent activation energies for ◊ = 5 min, □ = 30 min and ○ = 90 min.

Figure 9b and Table 1 show the Arrhenius plots and parameters for the temperature operation window, respectively, demonstrating a linear relationship between the logarithmic rate constant and the reciprocal temperature at all reaction times.

Table 2.1. Logarithmic decrease of E_A^{App} and A_0 during reaction.

Time (min)	E_A^{App} (kJ•mol^{-1})	A_0 (mol•L^{-1}•s^{-1})
5	55.4	3756.5
30	41.2	2282.3
90	34.1	1840.5

Table 2 summarizes the obtained yields at 5 and 90 min for all reaction conditions, reflecting the effect of the initial rate performance and the yields at the conversion plateau.

Table 2.2. Yields obtained for all varied reaction parameters at t=5 min and t=90 min.

	Yield (%)	
Parameters	5 min	90 min
Initial catalyst loading, C_{cat} (mol•L^{-1})		
0.05	14.1	78.2
0.1	31.1	88.9
Initial molar reactant ratio: C_N:C_E		
1:2	12.5	35.3
1:1	16.5	67.5
1.2:1	24.6	84.2
1.5:1	14.1	72.8
Initial reactant concentrations, C_E (mol•L^{-1})		
0.25	14.6	78.3
1.25	14.1	72.8
2.5	18.7	85.3

Initial 18-crown-6 ether loading, C_{sol} (mol•L^{-1})		
0.005	14.1	72.8
0.01	14.6	77.9
0.05	20.6	89.0
Initial product loading, C_{prod} (mol•L^{-1})		
0.01	24.6	84.2
0.05	27.8	65.1
0.09	26.5	62.9
Temperature (°C)		
110	7.7	55.1
115	9.8	55.2
120	15.1	62.8
125	14.1	67.1
130	14.2	72.8
140	25.9	95.6

2.4 Reaction rate model development

The concentration-time histories from each experiment were used to study the Langmuir-Hinshelwood and the Eley-Rideal rate models (see Supporting Information in reference [1]). Mostly bimolecular reaction mechanisms have been proposed in recent literature [23], based on either a Cu(I) or Cu(II) homogeneous catalyst. Firstly, a copper activation step is induced where copper-nucleophile species are formed. Then, reaction with the electrophile occurs following various postulated mechanisms. Oxidative addition of ArX (followed by reductive elimination), sigma-bond metathesis, single-electron transfer (SET), iodine atom transfer (IAT) and π-complexation of ArX are the most frequently referred mechanisms for aryl halide complexation. On the other hand, a heterogeneous metallic copper catalyst requires both phenolate (N) and 4-chloropyridine (E) to adsorb and react simultaneously on the same site undergoing, albeit with different adsorption strengths, a C-O coupling. For this reason, a Cu(0)-catalyzed mechanism must be approached differently when compared to proposed mechanisms based on a two-step homogeneously catalyzed process. The obtained results following reactant adsorption, C-O bond formation and product desorption have thus led to a Langmuir-Hinshelwood mechanism where the production rate could be described using Equation 2a (see also section 4.3.3).

$$r = \frac{k \quad w \quad C_E \quad C_N}{(1 + \quad K_E C_E + \quad K_N C_N + \quad K_P C_P)^2} \qquad \textbf{Equation 2.2a}$$

W = mass of catalyst (g), k = 2.87 × 10^{-3} L^2•g^{-1}•mol^{-1}•s^{-1}, K_E = 7.33 × 10^{-1} L•mol^{-1}, K_N = 1.26 L•mol^{-1}, K_P = 9.57 L•mol^{-1}, C_E is the concentration of electrophile (4-chloropyridine), C_N is that of the nucleophile (potassium phenolate), and C_P is that of the product (4-phenoxypyridine).

Also the Eley-Rideal mechanism has been considered for the strongly adsorbing 4-chloropyridine with the copper as shown in Equation 2b [14b].

$$r = \frac{k \quad w \quad C_E \quad C_N}{(1 + \quad K_E C_E \quad + \quad K_P C_P)^2}$$ **Equation 2.2b**

W = mass of catalyst (g), k = 1.50 × 10^{-3} $L^2 \bullet g^{-1} \bullet mol^{-1} \bullet s^{-1}$, K_E = 8.01 × 10^{-1} $L \bullet mol^{-1}$, K_P = 6.95 $L \bullet mol^{-1}$, C_E is the concentration of electrophile (4-chloropyridine), and C_P is that of the product (4-phenoxypyridine).

Comparison of the parity plots of both models, shown in Figure 10, demonstrates much larger prediction accuracy for the Langmuir-Hinshelwood mechanism than for the Eley-Rideal mechanism.

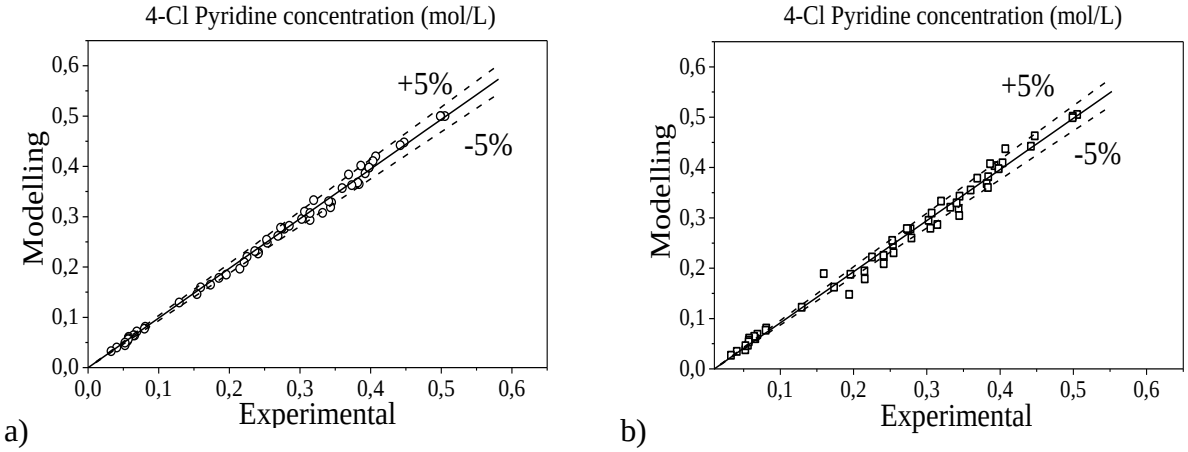

Figure 2.10. Parity plot of the fitted rate model describing a Langmuir-Hinshelwood mechanism (a) and an Eley-Rideal (b) mechanism. The lowest relative residuals value was found to be ± 9.23 x 10^{-4} and ± 2.53 x 10^{-1} for the Langmuir-Hinshelwood and Eley-Rideal mechanism, respectively.

From the adsorption constants (see Equations 2a and 2b), it can be seen that the product adsorbs almost a factor of 10 times stronger onto the catalyst surface than the reactants. In turn, the adsorption strength of the phenolate is almost double that of 4-chloropyridine. Therefore, the reaction rate decreases as the surface coverage with 4-chloropyridine decreases at longer reaction times. In contrast to low levels of accuracy found for modelling the two ER mechanisms (Figure 10b), the LH mechanism model describes the data with a higher accuracy (Figure 10a).

2.5 Discussion and conclusions

During this investigation five parameters have been varied in typical experimental ranges in order to examine their influence on product yield and reaction rate. A reaction mechanism based on a Langmuir-Hinshelwood kinetics model was previously proposed for this surface reaction [23-24], which is shown in Scheme 3. According to this mechanism, the initial formation of the phenolate species, which is substituted by smaller Cl^- ions produced during complexation of K^+ by a crown ether (18-crown-6), is followed by adsorption of the dissolved phenolate on the copper surface. The latter step involves the interaction of oxygen lone-pair electrons with the metal d-orbitals (adsorption step 1), prior to the formation of an

π^6-like interaction involving the phenyl π-system. This results in an adlayer coverage of the substrate (adsorption step 2) [25], which leads to a stabilizing negative charge on oxygen due to a changed inter-atomic distance between oxygen and the Cu species. In a simultaneous step, the pyridine approaches the copper surface via the lone-pairs of the nitrogen (adsorption step 1) before adopting a flat-laying position stabilized by the π-electrons (adsorption step 2) [26].

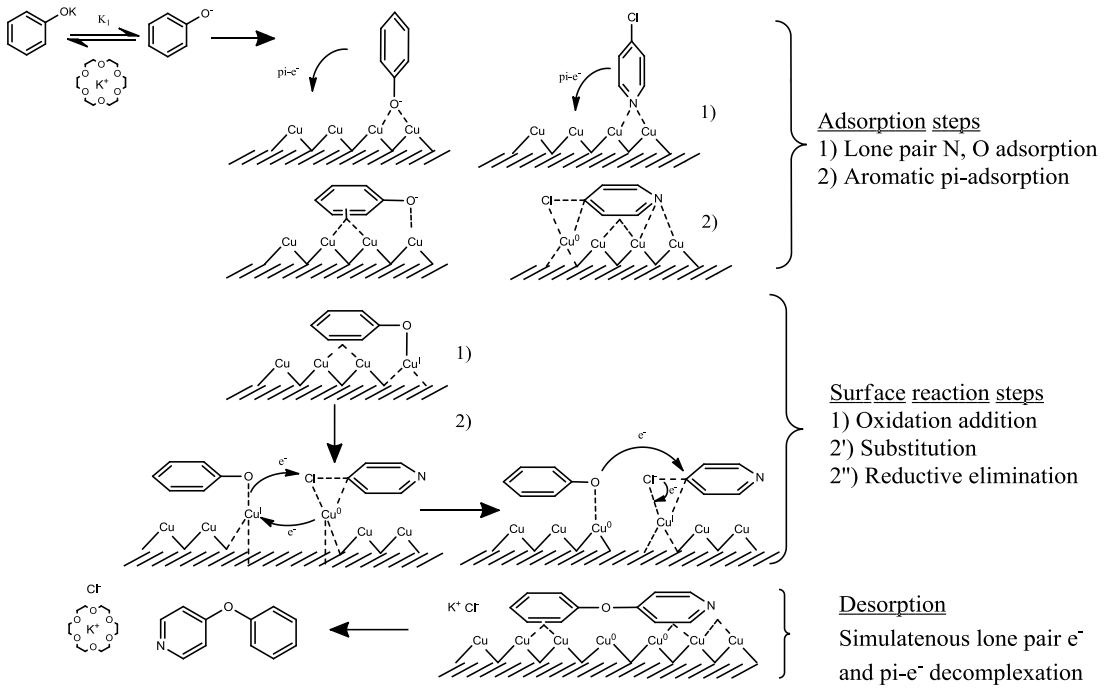

Scheme 2.3. Adsorption, reaction and desorption mechanisms of phenolate and 4-chloropyridine species leading to the formation of 4-phenoxypyridine on a Cu (III) surface.

However, in contrast to phenolate adsorption, this step is not accompanied by oxidation of the surface active sites. As both the adsorption steps end with adlayer-flipping steps, these steps might very well be equally fast. However, as the lone-pair electrons in the pyridine are slightly different positioned as compared to those in the phenolate species, it is possible that the overall coverage of both reactants results in unequal coverage fractions. Multi-layer adsorption of the reactants is assumed not to have occurred. In the second step, the surface reaction takes place involving two simultaneous processes. Initially, two electron transfer steps occur, *i.e.* from the Cu-O bond to the Cl-C bond and from a Cu-Cl bond back to form Cu^I. In this step, electrons are donated to facilitate the C-Cl bond cleavage and to reduce Cu^I to Cu^0. Immediately, the C-O bond-forming nucleophilic attack proceeds from the oxygen, inducing electron transfer to the Cu^I-Cl bond and thus reducing the second Cu^I to Cu^0 [27]. In the last step of the proposed mechanism desorption of the product occurs simultaneously with chloride inclusion in the potassium-crown ether complex. Since the bond formation has led to a planar molecule a one-step desorption can be assumed.

In this chapter, an extended parametric study of the kinetics of the Ullmann ether synthesis has been described. In particular, the role of copper as a catalyst has

formed the basis for a long-standing and as yet unresolved topic of discussion with regard to its surface chemistry. While earlier reports on the Ullmann reactions focused more on C-C and C-N coupling reactions [22], little has been done on C-O coupling. The conclusions drawn from the present study are based on well-established mechanistic processes, *i.e.* the Langmuir-Hinshelwood (and Hugson-Watson adapted) model for the liquid-liquid type Ullmann C-O coupling reaction.

Nomenclature

Symbol	Definition	Unit
C^t_i	Concentration of species i in the liquid phase at time t	$mol \cdot L^{-1}$
C_E	Concentration of electrophile	$mol \cdot L^{-1}$
C_N	Concentration of nucleophile	$mol \cdot L^{-1}$
C_P	Concentration of product	$mol \cdot L^{-1}$
X^t_i	Conversion of species i at time t	-
Y^t_i	Product yield obtained from species i at time t	-
w_{cat}	Catalyst loading in the reactor	g
d_p	Catalyst particle diameter	µm
E_A^{App}	Apparent activation energy of reaction	$J \cdot mol^{-1}$
A_0	Pre-exponential factor	$mol \cdot L^{-1} \cdot s^{-1}$
n	Reaction order	
N	Total number of measurements taken in all experiments	
r	Observed rate of 4-chloropyridine conversion	$mol \cdot g^{-1} \cdot s^{-1}$
R	Universal gas constant	$J \cdot mol^{-1} \cdot K^{-1}$
T	Liquid phase temperature	K

References

[1] F. Benaskar, N. G. Patil, V. Engels, E. V. Rebrov, J. Meuldijk, V. Hessel, L. A. Hulshof, A. E. H. Wheatley and J. C. Schouten, *Dalton Trans.* **2012**, *Revision/Accepted*.

[2] a) F. Ullmann and P. Sponagel, *Ber. Dtsch. Chem. Ges.* **1905**, *38*, 2211-2212; b) F. Ullmann and J. Bielecki, *Ber. Dtsch. Chem. Ges.* **1901**, *34*, 2174-2185; c) F. Ullmann, *Ber. Dtsch. Chem. Ges.* **1904**, *37*, 853-854; d) F. Ullmann, *Ber. Dtsch. Chem. Ges.* **1903**, *36*, 2382-2384.

[3] I. Goldberg, *Ber. Dtsch. Chem. Ges.* **1906**, *39*, 1691-1692.

[4] a) G. Mann and J. F. Hartwig, *Tetrahedron Lett.* **1997**, *38*, 8005-8008; b) G. Mann, C. Incarvito, A. L. Rheingold and J. F. Hartwig, *J. Am. Chem. Soc.* **1999**, *121*, 3224-3225.

[5] A. Aranyos, D. W. Old, A. Kiyomori, J. P. Wolfe, J. P. Sadighi and S. L. Buchwald, *J. Am. Chem. Soc.* **1999**, *121*, 4369-4378.

[6] a) S. V. Ley and A. W. Thomas, *Angew. Chem., Int. Ed.* **2003**, *42*, 5400-5449; b) F. Monnier and M. Taillefer, *Angew. Chem., Int. Ed.* **2009**, *48*, 6954-6971.

[7] a) S. Ding, N. S. Gray, Q. Ding and P. G. Schultz, *Tetrahedron Lett.* **2001**, *42*, 8751-8755; b) N. Kataoka, Q. Shelby, J. P. Stambuli and J. F. Hartwig, *J. Org. Chem.* **2002**, *67*, 5553-5566.

[8] a) E. Buck, Z. J. Song, D. Tschaen, P. G. Dormer, R. P. Volante and P. J. Reider, *Org. Lett.* **2002**, *4*, 1623-1626; b) D. M. T. Chan, K. L. Monaco, R.-P. Wang and M. P. Winters, *Tetrahedron Lett.* **1998**, *39*, 2933-2936; c) H.-J. Cristau, P. P. Cellier, S. Hamada, J.-F. Spindler and M. Taillefer, *Org. Lett.* **2004**, *6*, 913-916; d) D. A. Evans, J. L. Katz and T. R. West, *Tetrahedron Lett.* **1998**, *39*, 2937-2940; e) H. B. Goodbrand

and N.-X. Hu, *J. Org. Chem.* **1998**, *64*, 670-674; f) R. K. Gujadhur, C. G. Bates and D. Venkataraman, *Org. Lett.* **2001**, *3*, 4315-4317; g) P. Y. S. Lam, C. G. Clark, S. Saubern, J. Adams, M. P. Winters, D. M. T. Chan and A. Combs, *Tetrahedron Lett.* **1998**, *39*, 2941-2944; h) Z. Lu, R. J. Twieg and S. D. Huang, *Tetrahedron Lett.* **2003**, *44*, 6289-6292; i) D. Ma and Q. Cai, *Org. Lett.* **2003**, *5*, 3799-3802; j) D. Ma and C. Xia, *Org. Lett.* **2001**, *3*, 2583-2586; k) J.-F. Marcoux, S. Doye and S. L. Buchwald, *J. Am. Chem. Soc.* **1997**, *119*, 10539-10540; l) C. Palomo, M. Oiarbide, R. Lopez and E. Gomez-Bengoa, *Chem. Commun.* **1998**, 2091-2092.

[9] V. Engels, F. Benaskar, N. G. Patil, E. V. Rebrov, V. Hessel, L. A. Hulshof, D. A. Jefferson, J. A. J. M. Vekemans, S. Karwal, J. C. Schouten and A. E. H. Wheatley, *Org. Process Res. Dev.* **2010**, *14*, 644-649.

[10] F. Monnier and M. Taillefer, *Angew. Chem., Int. Ed.* **2008**, *47*, 3096-3099.

[11] A. M. Egorov, S. A. Matyukhova and A. V. Anisimov, *J. Phys. Org. Chem.* **2005**, *18*, 1023-1031.

[12] J. W. Tye, Z. Weng, R. Giri and J. F. Hartwig, *Angew. Chem., Int. Ed.* **2010**, *49*, 2185-2189.

[13] N. V. Richardson and P. Hofmann, *Vacuum* **1983**, *33*, 793-796.

[14] a) T. E. Jones, C. Zuo, P. W. Jagodzinski and M. E. Eberhart, *J. Phys. Chem. C* **2007**, *111*, 5493-5496; b) D. Wang, Q.-M. Xu, L.-J. Wan, C. Wang and C.-L. Bai, *Langmuir* **2002**, *18*, 5133-5138.

[15] N. Atodiresei, V. Caciuc, P. Lazić and S. Blügel, *Phys. Rev. Lett.* **2009**, *102*, 136809.

[16] K. Kunz, U. Scholz and D. Ganzer, *Synlett* **2003**, *2003*, 2428,2439.

[17] M. Xi, M. X. Yang, S. K. Jo, B. E. Bent and P. Stevens, *J. Chem. Phys.* **1994**, *101*, 9122-9131.

[18] P. R. Davies and N. Shukla, *Surf. Sci.* **1995**, *322*, 8-20.

[19] a) F. Benaskar, V. Engels, E. V. Rebrov, N. G. Patil, J. Meuldijk, P. C. Thüne, P. C. M. M. Magusin, B. Mezari, V. Hessel, L. A. Hulshof, E. J. M. Hensen, A. E. H. Wheatley and J. C. Schouten, *Chem.– Eur. J.* **2012**, *18*, 1800-1810; b) F. Benaskar, A. Ben-Abdelmoumen, N. G. Patil, E. V. Rebrov, J. Meuldijk, L. A. Hulshof, V. Hessel, U. Krtschil and J. C. Schouten, *J. Flow Chem.* **2011**, *1*, 74-89.

[20] S. A. Ba-Saif, A. B. Maude and A. Williams, *J. Chem. Soc., Perkin Trans. 2* **1994**, 2395-2400.

[21] M. Hatano, S. Suzuki, E. Takagi and K. Ishihara, *Tetrahedron Lett.* **2009**, *50*, 3171-3174.

[22] a) T. Manifar, S. Rohani, T. P. Bender, H. B. Goodbrand, R. Gaynor and M. Saban, *Ind. Eng. Chem. Res.* **2005**, *44*, 789-798; b) A. J. Paine, *J. Am. Chem. Soc.* **1987**, *109*, 1496-1502.

[23] E. Sperotto, G. P. M. van Klink, G. van Koten and J. G. de Vries, *Dalton Trans.* **2010**, *39*, 10338-10351.

[24] a) A. Casitas, N. Ioannidis, G. Mitrikas, M. Costas and X. Ribas, *Dalton Trans.* **2011**, *40*, 8796-8799; b) A. Lei, W. Liu, C. Liu and M. Chen, *Dalton Trans.* **2010**, *39*, 10352-10361.

[25] M. Saphier, A. Burg, S. Sheps, H. Cohen and D. Meyerstein, *J. Chem. Soc., Dalton Trans.* **1999**, 1845-1850.

[26] M. Saphier, A. Masarwa, H. Cohen and D. Meyerstein, *Eur. J. Inorg. Chem.* **2002**, *2002*, 1226-1234.

[27] W. A. Waters in *The Chemistry of Free Radicals*, *Vol.* University Press, Oxford and London, **1948**, p. 171.

Chapter 3

Bimetallic copper nano-catalysts in the Ullmann heterocycle-aryl etherification and the modified Simmons-Smith cyclopropanation

This chapter has been submitted as:
F. Benaskar, V. Engels, N.G. Patil, E.V. Rebrov, J. Meuldijk, V. Hessel, L.A. Hulshof, D.A. Jefferson, J.C. Schouten, A.E.H. Wheatley (2010). Copper(0) in the Ullmann heterocycle-aryl ether synthesis of 4-phenoxypyridine using multimode microwave heating. *Tetrahedron Lett.*, *51*(2), 248-251.[1]

F. Benaskar, V. Engels, N.G. Patil, E.V. Rebrov, V. Hessel, L.A. Hulshof, D.A. Jefferson, J.A.J.M. Vekemans, S. Karwal, J.C. Schouten, A.E.H. Wheatley (2010). Cu-based nano-alloys in the base-free Ullmann heterocyle-aryl ether synthesis. *Org. Process Res. Dev.*, *14*(3), 644-649. [2]

V. Engels, F. Benaskar, D.A. Jefferson, B.F.G. Johnson, A.E.H. Wheatley (2010). Cu-based nanoalloys in the base-free Ullmann heterocyle-aryl ether synthesis. *Dalton Trans.*, *39*, 6496-6502. [3]

Abstract

The action of nanoparticulate copper catalysts with a mean particle size of *ca.* 10 nm is reported in the Ullmann ether synthesis using multimode microwave heating and employing stable chloropyridine salts and phenol. The stabilized copper nanoparticles clearly demonstrated outstanding stability and reusability with respect to other copper catalysts. The Cu nano-catalyst synthesis was based on a modified polyol-based reduction method, utilizing poly(*N*-vinylpyrrolidone) (PVP, M_{av} = 40, 000) as polymeric anti-agglomerant. Various reducing agents were

investigated as means to optimize synthetic parameters for the purity, morphology and stability of a series of polymer-coated copper nanoparticles. Although it was demonstrated that ethylene glycol could act as a soft reductant in this system, the use of hypophosphite as co-reductant in conjunction with the presence of PVP has afforded nanoparticles with a mean size distribution of 9.6 ± 1.0 nm. These Cu nanoparticles appeared to be stable against oxidation for more than three months as a nano-slurry. Following these results, the first liquid-type Ullmann etherification process mediated by oxidative stable Cu, CuZn and CuSn nanoparticle catalysts in conjunction with microwave heating was further developed, avoiding the use of solid and expensive bases. This chemical process, using potassium phenolate and HCl-neutralized 4-chloropyridine, led to improved turnovers and excellent yields in the heteroaromatic Ullmann-type coupling reaction. Further enhancement could be achieved upon the addition of 18-crown-6 as a cation scavenger. Finally, the same optimized nano-catalyst was also employed in the Cu-catalyzed cyclopropanation of styrene using ethyl diazoacetate and affording ethyl-2-phenylcyclopropane-1-carboxylate. This reaction is an essential tool towards the synthesis of fine-chemicals involving cyclopropanes. In this chapter, the first results on the use of Cu- and CuZn nanoparticles are presented, which already show a significant yield enhancement as compared to current literature achievements of cyclopropane syntheses for fine-chemicals production.

3.1 Introduction

Despite being introduced more than 100 years ago [4], Ullmann and Goldberg-type aryl ether syntheses remain an essential tool for industrial-scale fine-chemicals synthesis [5] and have recently been the subject of review [6]. Commensurate with their importance, research efforts have been directed towards tailoring homogeneous catalysts of copper [7] and palladium [8] and, in this context, a better understanding of the ligand effects has been achieved to improve the catalyst performance. Moreover, Cherng *et al.* have intensively investigated the effect of solvents on yield employed in these reactions and, typified by strong polar moments, their added value when combined with microwave heating [9]. Later, also Ley and coworkers provided many examples of microwave-assisted coupling reactions where amide-containing solvents demonstrated a beneficial effect in conjunction with microwaves [10]. In particular, earlier work of Raner *et al.* [11] has already shown that the industrially important solvent *N,N*-dimethylacetamide (DMA) provides many advantages by virtue of its ability to enhance yields through improved catalyst solubility and effective microwave heating. Such types of solvents possess strong polar moments and so are rapidly heated when microwaves are applied, thus suggesting green chemistry through enhanced yields and decreased energy consumption by selective heating. Hence, for example, the single-mode microwave-assisted synthesis of phenoxypyridines using chloroheterocycles has resulted in higher yields than could be achieved with conventional heating [1, 12].

Nevertheless, in common with other applications of batch-type single-mode microwave-assisted reactions, this setup suffered from the drawback that reactions could only be conducted on a small scale [12]. These heating effects, however, can

still be used beneficially, allowing less harsh bulk temperatures, when microwave heating is applied in conjunction with the catalyst through hotspot formation at the solid surface [13]. More recently, efforts have been made to circumvent these limitations of scale in batch-type reactions, and also to avoid difficulties associated with the reliable monitoring of reaction temperatures under single-mode microwave irradiation, by deploying multimode microwave apparatus to synthesize 4-phenoxypyridine [1].

Whilst the deployment of copper-based nano-catalysis in organic synthesis is not new, the employment of nanoparticulate copper, however, undergoes currently a much more recent research trend with respect to process intensification [3, 14]. Exploitable methods for the fabrication of Cu(0) [15], CuO and Cu_2O nanomaterials [16] exist and also their applications in "click-chemistry" (in both slurry batch reactors and supported modes) [17], Stephens–Castro [18] and Sonogashira [19] coupling reactions have been reported. More examples can be found in fine-chemicals syntheses, including C-H (N-H) activation reactions in the quantitative preparation of propargylamines, bis-(4-hydroxy-2-oxothiazolyl)-methanes in ionic liquids and the selective aza-Michael reaction of *N*-alkyl- and *N*-arylpiperazines in the presence of aromatic amino or aliphatic hydroxy groups [20]. Other applications exist in fine-chemicals synthesis, *e.g.* in the field of Cu^0-catalyzed arene-sulfur bond formation towards the synthesis of thiophenols and the asymmetric hydrosilylation of ketones [7c, 21]. Alonso *et al.* have demonstrated the potential of Cu nanoparticles in the reduction of carbonyl compounds and imines, where they achieved yields comparable to those noted using more toxic nickel catalysts [15d]. According to Ranu *et al.* the main effect of reaction enhancement for nano-sized catalysts can be found in the increased Fermi-potential, inducing radical pathways (*e.g.* coupling of aryl halides with thiophenols) [21]. Moreover, the use of nanoparticulates in the Cu_2O-catalyzed Ullmann-type amination [22] and Cu^0-catalyzed Ullmann-type etherification [23] has been reported. However, in both reaction systems the use of highly expensive aryl iodides and relatively long reaction times limited the process. Furthermore, the use of heterogeneous nano-catalysts might offer new opportunities in terms of sustainable processing. Still, these same nano-catalysts suffer from major drawbacks, such as complex catalyst recovery, product contamination and copper oxidation.

The potential for synergic effects between metals has led to investigation of the activity of bimetallic nanoparticles in catalysis [24]. Hence, ZnO-supported copper has already established itself as a catalyst system in the Haldor-Topsøe process for industrial methanol syntheses. As a result, considerable efforts have been directed towards the elucidation of cooperative effects between the active metal and its support [25], where especially the formation of CuZn nano-alloy phases appeared to increase the catalytic activity [26]. In spite of the potential of these systems, bottom-up approaches for the synthesis of CuZn nano-catalysts remain little explored [27]. Hambrock *et al.* reported. in 2003 one example of CuZn nanoparticles synthesis using a wet-chemical process for colloidal CuZn nanoparticles [26]. In this work, however, the thermodynamic instability of organozinc reagents has presented obstacles to the precise control of stoichiometry

in CuZn-systems. In a similar vein, few reports exist detailing preparations of CuSn nanoparticles via chemical reduction [28]. While Calò *et al.* have demonstrated the efficiency of bronze alloys as catalysts in the Heck reaction of aryl iodides and activated aryl bromides [29], Saito and Koizumi reported the use of CuSn in the Ullmann-type synthesis of aromatic nitro compounds [30]. In this latter case, yields of up to 91% were achieved in 3 h. However, as with CuZn, CuSn alloy phases have previously exhibited a chemical instability, and this phenomenon was hold responsible for the leaching of Cu during catalytic tests. Recently, also examples of Cu nano-catalysts in diaryl ether synthesis appeared, though this required the use of expensive and chemically unstable aryl iodide substrates [23]. Moreover, practical limitations associated with the oxidative instability of Cu nanoparticles [31] have been overcome by utilizing the stabilizing properties of anti-agglomerants used during the reduction-by-solvent of $CuSO_4$ and $Cu(OAc)_2$ to Cu(0) [3].

Similar Cu nano-catalysts exhibited long-term oxidative stability and were employed in the microwave-assisted Ullmann ether synthesis of 4-phenoxypyridine from stable 4-chloropyridine salts and unactivated phenol [1]. This work is the first report on the combined use of nanoparticulate Cu and selective microwave heating in the Ullmann ether synthesis. In addition, the metal oxidation state and particle sizes were varied to envisage the most efficient catalyst under multimode microwave irradiation in the synthesis of 4-phenoxypyridine (Scheme 1).

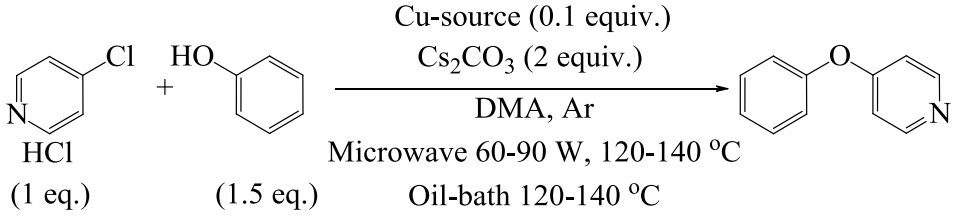

Scheme 3.1. The microwave-assisted Ullmann ether synthesis of 4-phenoxypyridine.

The use of microwave methods provided nearly a 20-fold increase in heating rate relative to that achievable using an oil-bath, which consequently led to a comparison study of the yields obtained for various catalysts using both microwave and oil-bath heating. For this type of Ullmann reaction, oxidatively stable nano-Cu has shown to be more efficient than homogeneous Cu(I) and Cu(II) catalysts, giving superior yields in significantly less time than was previously required for comparable systems [22]. Moreover, the extension of this study towards the application of bimetallic copper-based nanoparticle systems, *i.e.* CuZn and CuSn, demonstrated the potential of stable bimetallic nano-catalysts for further significant increases in turnover frequency.

The aim in these achievements was ultimately the design of a continuously operated heterogeneous catalytic reactor as a means to perform intensified processing leading to a green and cost-competitive system. Continuous processing is a convenient method for scaling processes, albeit thus far mainly applied in bulk chemical synthesis and far less in fine-chemicals production. Nevertheless, upon scale-up, continuously operated systems are economically favorable if by-product

formation and reaction times are minimized through chemistry optimization. Therefore, a new chemical route was developed to prevent the presence of cesium carbonate base for phenol activation [32] by making use of a naked-ion nucleophile and a cation scavenger to, kinetically, promoting the etherification (see Scheme 2).

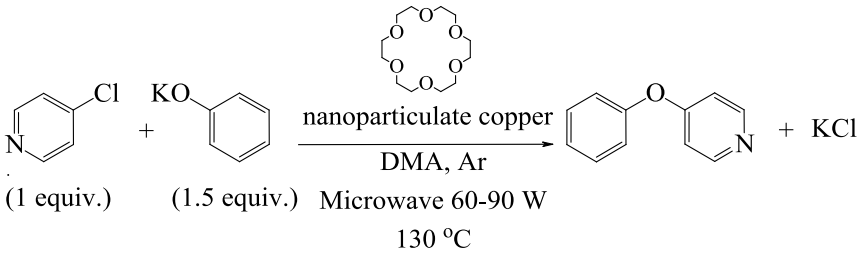

Scheme 3.2. The liquid-type Ullmann ether synthesis of 4-phenoxypyridine using potassium phenolate as naked-ion nucleophile in conjunction with 18-crown-6 as cation scavenger.

This chapter is based on a report, demonstrating, to the best of our knowledge, the first example of a liquid-type Ullmann etherification using copper-based bimetallic nanoparticle catalysts and highly nucleophilic potassium phenolate [2]. Profiting largely from the catalysis achievements as introduced for the Ullmann coupling reaction, the application of CuZn nanoparticle catalysts was also proposed for the preparation of high added-value cyclopropanes in another study. The CuZn-catalyzed cyclopropanation reaction, following a carbene-insertion mechanism as described by Simmons and Smith in the late 1950s [33], is the essential tool towards the synthesis of fine-chemicals involving cyclopropanes, where *e.g.* Drospirenone or Yaz® (Bayer) possessed a market share of *ca.* 700 M€/annum sales in 2009 [34]. The currently obtained good to excellent yields have been reported only when either homogenous Ru-type catalysts or expensive copper ligands were applied [14c, 35].

Our study shows an improvement of the state-of-art in the synthesis of cyclopropanes, by the use of cheaper and reusable heterogeneous copper catalysts for the fine-chemicals industry. To explore reaction kinetics, the cyclopropanation starting from styrene and ethyl diazoacetate to give *cis*- and *trans*-ethyl-2-phenylcyclopropane-1-carboxylate was carried out as a model reaction for the Drospirenone synthesis (see Scheme 3) [36].

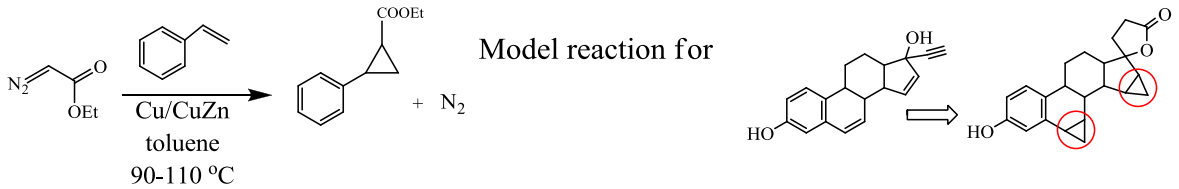

Scheme 3.3. Cyclopropanation as a model reaction in the synthesis of pharmaceutically active substances, such as Drospirenone.

The formation of cyclopropanes from the insertion of a carbon in an olefin can be obtained in two different ways, either using a methylene halogen[37] or a diazo-ester [14c, 14g, 38]. The first strategy was found and developed by Simmons and

Smith using various olefins and methylene iodine, whereas the use of diazo-compounds is a more recent discovery and has become the standard in the formation of cyclopropanes [39]. In this part of our work, the use of CuZn nano-catalysts in heterogeneously catalyzed processes was successfully demonstrated in another important class of chemical reactions. The development of a supported catalyst proved to be, clearly, the first and most important (see chapter 7) step in performing sustainable catalysis in flow chemistry and process intensification. Only in this way, an efficient process could be realistically developed where combined microwave heating and continuously operations afforded a safe (with respect to hazardous and expensive diazo-moieties) and reliable process using a cheap Cu-based catalyst as a replacement of the conventional Rh catalysts [40].

3.2 Experimental

3.2.1 The Cu-catalyzed Ullmann-type C-O coupling towards 4-phenoxypyridine

Reagents and materials. *N,N*-dimethylacetamide (DMA, anhydrous), 4-chloropyridine hydrochloride, phenol, and Cs_2CO_3 were purchased from Aldrich and used as received without further purification. Micron-sized metallic copper was purchased from Sigma Aldrich and Acros Organics. Cu wire was fabricated mechanically by specialized equipment providing and accuracy of 3%. Uniform size distribution according to the supplier's specifications was subsequently confirmed by optical microscopy.

Activity study for the solid-liquid Ullmann etherification. A mixture of 4-chloropyridine (6 mmol), phenol (9 mmol), Cs_2CO_3 (18 mmol) and DMA (15 mL) in a baffled glass reactor was treated with an appropriate amount of catalyst and the resulting slurry was heated in either a circulating oil-bath (Lauda Ecoline staredition 012, type E312, 2.3 kW) or a microwave oven (Milestones Multimode Microwave, type ETHOS 2450 MHz, 2.5 kW) (120-140 ºC for 40-240 min). Bulk temperatures during the reaction were measured using a fiber-optic probe and an infrared sensor. The yield of 4-phenoxypyridine was determined by measuring the ^{1}H-NMR spectra of reaction aliquots against unreacted material. The ^{1}H-NMR data was compared with the literature [12] and additional qualitative GC-MS measurements.

Activity study for the liquid-type Ullmann etherification. 4-Chloropyridine in liquid form was obtained by reaction of 4-chloropyridine hydrochloride with aqueous potassium carbonate (K_2CO_3 ≥99.5%, Sigma-Aldrich). Potassium phenolate was obtained by reaction of phenol with potassium *tert*-butoxide (Aldrich, reagent grade, 95%) in THF (Sigma-Aldrich, anhydrous, ≥99.9%, inhibitor-free). A baffled glass reactor was loaded with DMA (15 mL), potassium phenolate (9 mmol), and 18-crown-6 (*ca.* 0.01 equiv. with respect to phenolate) as appropriate. The mixture was stirred at 45 °C until complete dissolution occurred, where after 4-chloropyridine (6 mmol) was added. The solution was treated with an appropriate amount of catalyst (10 mol% with respect to 4-chloropyridine). The resulting slurry was heated in a microwave device (Milestones Multimode Microwave, type

ETHOS 2450 MHz, 2.5 kW) (130-140 ºC for 120 min). Bulk temperatures during the reaction were measured using a fiber-optic probe and an infrared sensor. All reactions were carried out under argon. The yield of 4-phenoxypyridine was determined by measuring the ^{1}H-NMR spectra of reaction aliquots against unreacted material. The ^{1}H-NMR spectroscopic data were compared with the literature, as were additional qualitative GC-MS measurements.

Analytical methods. ^{1}H-NMR data were collected on a Varian 400 Magnet NMR spectrometer (400 MHz). Spectra were obtained at 27 ºC and chemical shifts were internally referenced to tetradecane ($C_{14}H_{30}$) and calculated relative to TMS. Chemical shifts are expressed in δ ppm. GC-MS measurements were carried out in a Shimadzu QP 5000, zebron column ZB35 (all the obtained ^{1}H-NMR spectra and GC-MS analysis can be found in the Supporting Information part of references [1-2]). The ^{1}H-NMR assignments for 4-phenoxypyridine are: δ 8.48 (d, 2H), 7.44 (t, 2H), 7.29–7.25 (m, 1H), 7.11 (d, 2H) and 6.85 (d, 2H). The ^{1}H-NMR assignments for 4-chloropyridine are: δ 8.59 (d, 2H) and 7.34 (d, 2H). The ^{1}H-NMR assignments for potassium phenolate are: δ 7.18 (t, 2H), 6.88 (d, 2H) and 6.79 (t, 1H). The ^{1}H-NMR assignments for phenol (in $CDCl_3$) are: δ 7.24 (t, 2H), 6.93 (t, 1H), 6.84 (t, 2H) and 5.34 (s, 1H).

3.2.2 The Cu-catalyzed cyclopropanation towards ethyl-2-phenylcyclopropane-1-carboxylate

Reagents and materials. Toluene (anhydrous, 99.8%, Sigma-Aldrich), styrene (> 99%, Aldrich), ethyl diazoacetate (EDA, <10% dichloromethane, Fluka) were purchased and used as received without any further purification. Copper nanoparticles were synthesized as described above. In addition, also commercial CuZn (60/40) nanopowder (nanopowder, 70 ± 39 nm particle size (in-house TEM analysis), 56-60% Cu basis, 37-41% Zn basis, Aldrich) and micron-size copper (powder, 3 ± 1.7 μm particle size (in-house SEM analysis), 99.999% trace metals basis, Aldrich) were used as a reference case study.

Activity study for the Cu-catalyzed cyclopropanation reaction. A suspension containing the corresponding Cu catalyst (5 mol% with respect to EDA) was added to a solution of styrene (1041 mg, 0.33 mol/L) and tetradecane (*ca.* 40 mg, 0.007 mol/L) in anhydrous degassed toluene (25 mL). This reaction mixture was heated (with an oil-bath) to reaction temperature. EDA (114 mg, 0.033 mol/L) was diluted with 5 mL toluene and drop-wise injected in the reaction mixture during one minute. During the first ten minutes of the reaction, each single minute a sample was taken. Afterwards, the sampling was done every five min. The reaction was monitored by gas chromatography (GC-MS and GC-FID) and liquid-chromatography (HPLC UV-Vis). After the reaction had finished the catalyst was recovered by multiple centrifugations and washing steps in methanol.

Analytical methods. Conversion and chemo and regioselectivity were determined using a Varian 430-GC in a CP-sil 8 CB (film thinkness 1 micron) column: 60 m ×

0.25 mm × 0.93 μm (L x ID x OD). Oven temperature program: 100 °C (4 min), 10 °C/min to 120 °C (2 min), 30 °C/min to 240 °C (4 min) and for 5 min at 240 °C. Prior to the GC-FID analysis, GC-MS (Shimadzu, QP2010) with a similar column was used to identify the peaks. Retention times: ethyl diazoacetate, 4.08 min; styrene, 4.48 min; *n*-tetradecane, 10.08 min; diethyl fumarate, 8.51 min; diethyl maleate, 8.36 min; *trans*-ethyl-2-phenylcyclopropane-1-carboxylic acid, 10.51 min; *cis*-ethyl-2-phenylcyclopropane-1-carboxylic acid, 10.79 min.

3.2.3 Preparation of the nanoparticulate catalysts

Monometallic copper nanoparticles. Cu-nanoparticles were synthesized by dissolving 1 mmol of Cu(II)X (X = OAc^-, SO_4^{2-}, Cl^-) in 120 mL of anhydrous ethylene glycol to which varying amounts of PVP (M_{av} = 10,000; 40,000; 55, 000) had been added. The resulting mixture was heated to 80 °C and stirred for 2 h. The solution was cooled to 0 °C and the pH adjusted to 9–11 (5 mL 1 M NaOH solution). After the addition of either 0.40 mL (2 mmol) of a 25% aqueous solution of hydrazine hydrate, 212.0 mg (2 mmol) of sodium hypophosphite monohydrate in 0.40 mL water or 378.3 mg (10 mmol) of sodium borohydride in 1 mL water, the reaction was stirred for 1 h at 100 °C ($N_2H_4 \cdot H_2O$, $NaBH_4$, $NaH_2PO_2 \cdot H_2O$) or 140 °C ($NaH_2PO_2 \cdot H_2O$) to yield a colloidal suspension. Aliquots of nanoparticle product were purified for analysis by extracting 50 mL of the suspension using excess acetone. After sedimentation, *ca.* 90% of the supernatant was decanted and the remaining suspension was centrifuged for 5 min. The acetone layer was removed and the colloidal precipitate re-suspended in DMA (50 mL) for reaction.

Bimetallic copper nanoparticles. Copper(II) sulfate pentahydrate (0.250 g, 1 mmol) and 0.8 g poly(*N*-vinylpyrrolidone) (PVP, M(average) = 24,000) were added to 120 mL anhydrous ethylene glycol in a two-necked round bottom flask. The resulting mixture was heated to 80 ºC and stirred for 2 h. The resulting blue solution was cooled to 0 ºC. Solutions of zinc(II) chloride (0.136 g, 1 mmol) or tin(II) chloride (0.261 g, 1 mmol) in 2 mL water (LC-MS grade, resistivity 18.2 MΩ·cm at 25 °C; purified by a Millipore® purification system with a combined Jetpore® ion-exchange resin, activated carbon and UV irradiation at 185 and 254 nm) and a solution of sodium hypophosphite monohydrate (0.213 g, 2 mmol) in 5 mL water (LC-MS grade) were added promptly. After adjusting the pH value to 9-11 by adding 5 mL of 1 M NaOH solution (LC-MS grade), the reaction was stirred for 1 h at 120 ºC to yield a yellowish-red colloidal suspension. Aliquots were purified by extracting 50 mL suspensions using excess acetone (*ca.* 250 mL). After sedimentation of the particles overnight, *ca.* 90% of the supernatant was decanted and the remaining suspension centrifuged for 5 min. Upon removal of the acetone layer, the colloidal precipitate was resuspended in 50 mL DMA.

3.2.4 Catalytic nanoparticles characterization

Transmission electron microscopy (TEM). Microscopic samples were prepared by droplet coating of methanol suspensions on Ni grids (Agar Scientific, holey carbon

film, 300 mesh) and examined using a JEOL JEM-3011 high-resolution transmission electron microscope at nominal magnifications between 10 000 and 800 000. The electron optical parameters were C_S = 0.6 mm, C_C = 1.2 mm, electron energy spread = 1.5 eV and beam divergence semi-angle = 1 mrad. From these images, first indications of particle structure were obtained. Particle size distributions were calculated by counting the diameters of 100 particles in the lower magnification images, defining size intervals of 0.2 nm between $d_{min} \leq d \leq d_{max}$ and counting the number of particles falling into these intervals. The exact magnification was previously established using images of lattice fringes in large (>10 nm) particles of colloidal gold. The mean particle size was calculated to be 9.6 ± 1.0 nm by counting the diameters of 100 particles in the lower magnification images. Data processing/calculation of standard deviation used Origin Pro. 8.0.

Energy dispersive X-ray spectroscopy (EDX). Elemental compositions were qualitatively elucidated by EDX spectroscopy (nominal beam width = 4 nm) using a PGT prism Si/Li detector and an Avalon 2000 analytical system. Spectra revealed substantial Ni Kα and Kβ emission lines, these arising from scattered electrons impinging on the bars of the nickel support grid. Some spectra also showed Fe Kα and Co Kα emission lines due to parasitic scattering from the lens pole-piece, but a previous study [41] had established that no appreciable Cu Kα emission could be generated in this way if a nickel support grid was used.

Powder X-ray diffraction (PXRD). PXRD data were collected on a Röntgen PW3040/60 XPert PRO powder X-ray diffractometer with a high resolution PW3373/00 Cu LFF (unmonochromated) tube at λ = 1.5404 Å (Cu Kα). The powder sample was prepared by solvent evaporation from the colloidal suspensions deposited on the 0.5 mm deep ground area of a glass flatplate sample holder using a microscope slide so that the powder sample was smooth, flat and flush with the sample holder surface. The sample holder was inserted onto the sample stage (PW3071/60 Bracket) such that the sample material was just free of the reference plane of the sample stage.

3.3 Results and discussion

3.3.1 The original Cu-catalyzed slurry-type Ullmann etherification using microwaves and Cu nanoparticles

Microwave heating in the Ullmann etherification. Rapid microwave heating is attributed to the uniform volumetric heating effect, which cannot be attained by surface heating in conventional heating methods. Consequently, microwave heating offers much higher efficiencies with respect to energy consumption. Comparison of the microwave and oil-bath heating profiles resulted in heating rates which corresponded to an energy consumption of 14.1 kJ in 60 seconds using microwave heating, while for an oil-bath setup this consumption was 1.4 MJ in 20 min both to attain the reaction temperature in the Ullmann etherification. Figure 1a shows the batch-setup used in the chemical reaction and Figure 1b the obtained heating profiles.

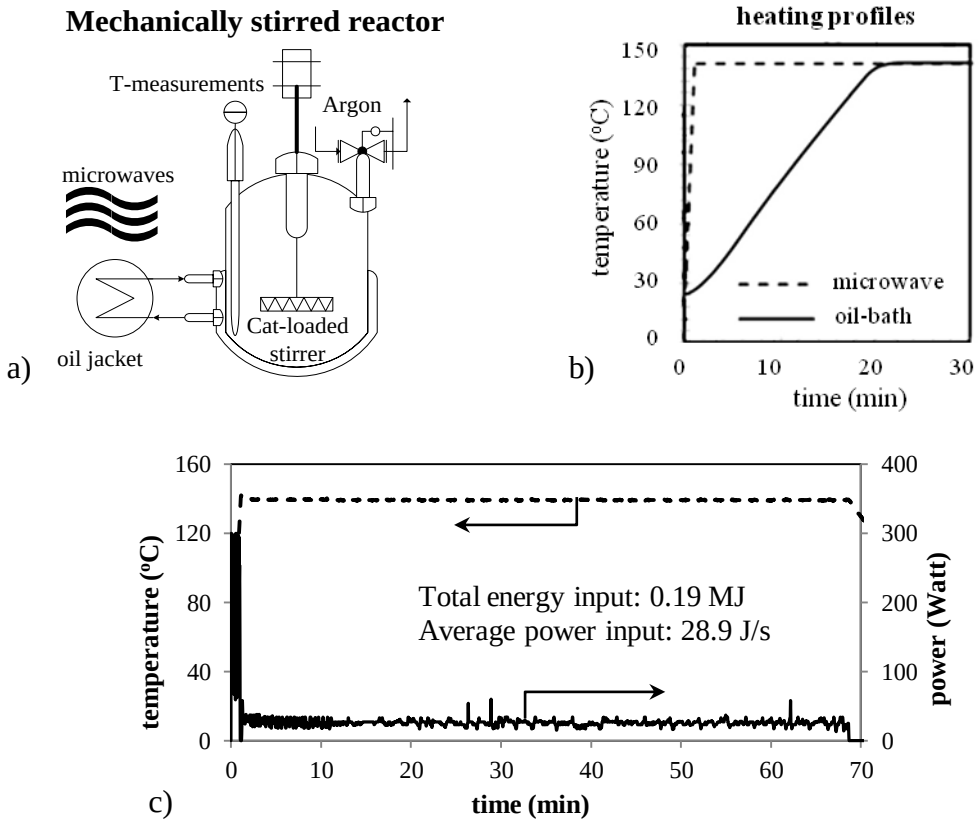

Figure 3.1. Batch setup (a) used to determine the heating profiles of microwave and oil-bath heating (b). Temperature and power plot of the microwave experiment (b).

In the initial heating period, a maximum microwave power was applied until 140 ºC was reached. The time needed in the case of microwave heating was 60 seconds at an average power of 221 Watt. Throughout the complete heating period (70 min) 119 kJ was consumed at a much lower average power of only 27 Watt. Thus, the energy consumed after the initial heating period counts for only 12% of the total microwave energy supplied (see Figure 1c). In the case of oil-bath heating the time needed to reach 140 ºC was 1200 seconds at a maximum power of 2300 W, consuming 2.8 MJ. It should be mentioned that both devices have a certain grid-to-applicator efficiency (around 50%), which is not exactly comparable for each device. Calculations are based on a volume of 15 mL DMA heated in either a multimode microwave apparatus or in a circulating oil bath. The very fast heating resulting from microwaves is directly related to the medium-free volumetric heating, while an oil-bath only heats the reactor wall. The internal heating profiles are expected to be much more uniform in the case of microwave heating, while for oil-bath heating these profiles are typically accompanied by temperature gradients from the wall to the center of the reactor. However, it should be noted that the use of multimode microwave cavities are also characterized by a highly non-uniform microwave distribution.

Catalyst activity using various Cu catalysts. As explained in the experimental section, 4-phenoxypyridine was synthesized from a solution of 4-chloropyridine hydrochloride (1 equiv.), phenol (1.5 equiv.) and Cs_2CO_3 (3 equiv.) in DMA (15

mL) which was treated with the corresponding amounts of catalyst using a baffled glass reactor in either an oil-bath or microwave apparatus. The obtained product yield and reactants conversion were determined by proton signals of 4-chloropyridine and 4-phenoxypyridine in the ^{1}H-NMR spectrum of the reaction mixture sample (see Figures 2a and 2b). Due to the ^{1}H-NMR signal overlap of the reactants and product at chemical shift from 6.5 to 7.5 ppm, the yield was determined based on the *ortho*-proton of 4-chloropyridine at 8.4-8.6 ppm (signal D in Figure 2a).

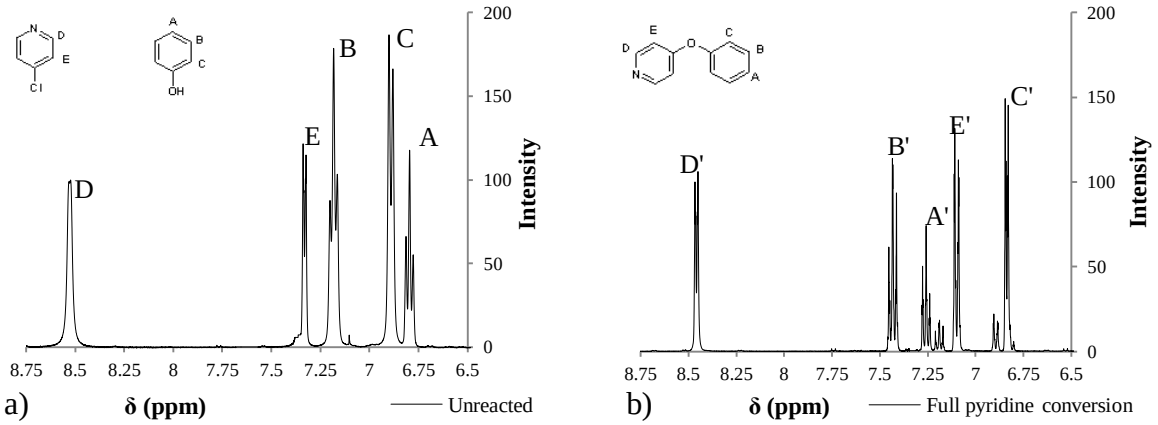

Figure 3.2. ^{1}H-NMR spectra (400 MHz, $CDCl_3$; 8.4-8.6 ppm) of the reactants (a) and product (b) at the start and end of the reaction. Assignments of the product peaks: δ 8.48 (d, *J* = 4.0 Hz, 2H), 7.44 (t, *J* = 8.0 Hz, 2H), 7.29–7.25 (m, 1H), 7.11 (d, *J* = 8.0 Hz, 2H), 6.85 (d, *J* = 8.0 Hz, 2H).

Metallic Cu and Cu(I) and Cu(II) chlorides used in these experiments were obtained commercially, while the Cu wires and the Cu nanoparticles were prepared. The Cu nanoparticles were synthesized (following the optimal synthesis route as described in our work [3]), using poly(*N*-vinylpyrrolidone) polymer [40.000 M_{av}] in ethylene glycol as capping agent, Cu(II) sulfate as catalyst precursor and sodium hypophosphite as co-reductant. This procedure resulted, after purification of the crude suspension, in particles with a mean diameter of 9.6 ± 1.0 nm as concluded from high-resolution transmission electron miscroscopy (HRTEM) and zero-valent Cu nanoparticles as concluded from energy dispersive X-ray spectroscopy (EDX) and powder X-ray diffractometry (PXRD) as shown in Figure 3.

The use of copper nanoparticles as catalyst in the Ullmann C-O coupling reaction could only be done efficiently by developing stable, zero-valent copper nanoparticles that exhibit long-term oxidation stability (*vide infra*). The results indicate a feasible and reproducible route to the large-scale application of Ullmann-type chemistry with previously unachievable yields and excellent selectivity. Only after reaction times of more than 5 h, 1-(pyridin-4-yl)pyridin-4(1*H*)-one as a by-product upon neutralization of the product solution could be detected by mass spectrometry. The results also suggest large-scale reusability of the catalyst in a multimode microwave setup.

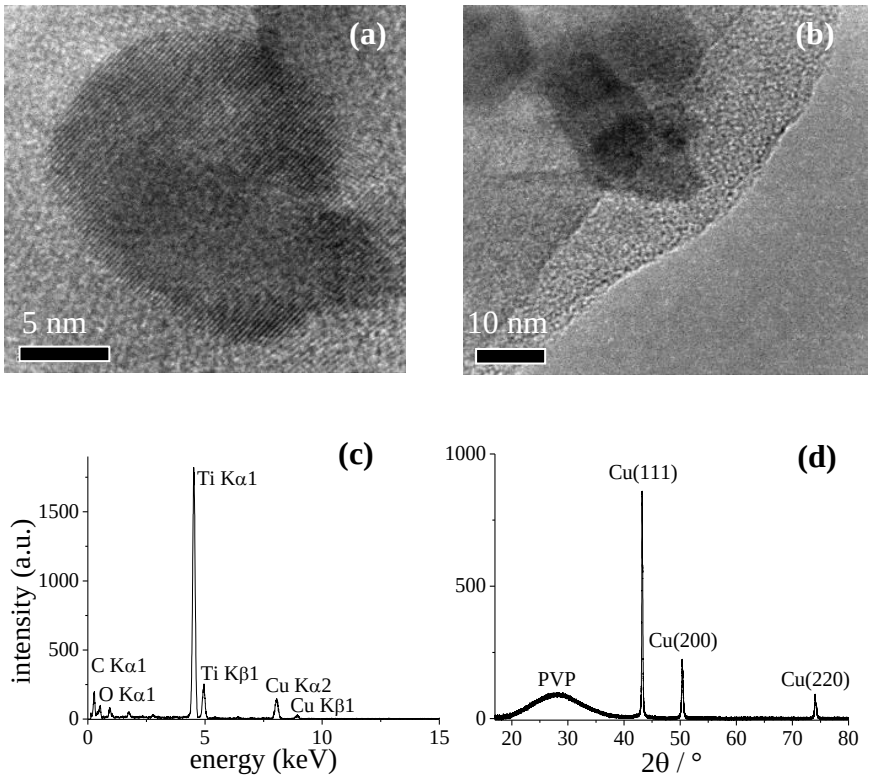

Figure 3.3. Cu nanoparticles: representative HRTEM images (a, b), EDX data (4 nm beam width; C, O and Ti lines from carrier grid material) (c), PXRD data (d). (See also Supporting Information in reference [3])

The obtained yields using various Cu-based catalysts are summarized in Table 1 (for detailed information see Supporting Information in reference [1]).

Table 3.1. Cu-catalyzed formation of 4-phenoxypyridine using various Cu-based catalysts

Entry	Cu-source[a]	Particle size (μm)	T (°C)	Heating method[b]	Time (min)	Yield (%)
1	Metallic Cu	75	120	MW	90	trace
2	Metallic Cu	45	120	MW	90	3
3	Metallic Cu	3	120	MW	90	20
4	Nano-Cu[c]	$9.6 \cdot 10^{-3}$	140	MW	120	63
5	Nano-Cu[c]	$9.6 \cdot 10^{-3}$	140	MW	240	80
6	Cu(I)Cl	-	120	MW	40	5
7	$Cu(II)Cl_2$	-	120	MW	40	4
8	Cu(I)Cl	-	120	O.B.	90	11
9	$Cu(II)Cl_2$	-	120	O.B.	90	trace
10	Cu-wire	50	140	MW	90	trace
11	Cu-wire	20	140	MW	90	trace
12	Cu-wire	50	140	O.B.	90	55
13	Cu-wire	20	140	O.B.	90	90

[a]10 mol%
[b]Microwave (MW) or oil-bath (O.B.)
[c]Protected by poly(*N*-vinylpyrrolidone).

Entries 1-3 (Table 1) reveal that, for metallic Cu, decreasing the particle size (by a factor of 25) enhances the yield of 4-phenoxypyridine, underlining surface

area/turnover relationships for the heterogeneous copper catalysts in solid-liquid type reactions. However, although experiments were performed under an argon atmosphere, the observation that the solid catalyst changed color from brown to green suggested copper oxidation to $CuCl_2$ in the case of micron-sized catalysts (entries 1-3). Further, a trial to recover copper by filtration and washing resulted in only *ca.* 30% recovery, confirming dissolution of the Cu catalyst in the form of $CuCl_2$ salts.

In contrast, nanoparticles, sterically protected by PVP as a coordinative capping agent, proved very stable to oxidation (entries 4-5), giving excellent yields of 4-phenoxypyridine after 240 min, with 72% catalyst recovery. Importantly, the PVP-coating on the surface provided long-term stability, not only against nanoparticle agglomeration, but also against oxidation *(vide infra)*. It is noteworthy that, after 30 days, EDS and HRTEM confirmed no change in either particle size or oxidation state [3]. It has been previously noted that the use of N,O-chelating ligands, such as amides, exhibit a "promotional effect" on Cu(I) catalysts by inhibiting oxidation to Cu(II) [42]. However, similar effects also were also reported in studies on the stabilization of nanoparticulate Cu(0) against cuprite formation [43]. Therefore, complex formation between heterogeneous Cu^0 nanoparticles and the keto-functions in this poly(*N*-vinylpyrrolidone) polymer apparently stabilizes the nano-catalysts with respect to oxidation. More evidence is reported by Gedanken *et al.*, who in the case of unprotected 50-70 nm particles, noted rapid oxidation to Cu(I) in the Ullmann coupling reaction of iodobenzene [31].

Furthermore, the synthesis of Cu_2O-coated Cu nanoparticles for Ullmann-type chloroheterocyclic aromatic substitutions revealed excellent catalytic performance of the uncapped particles, with the protecting oxide layer apparently preventing further oxidation [22]. Of course, the same protecting property of both Cu_2O and PVP has the drawback that it limits the accessibility of the catalyst surface for the reagents, incurring a diffusion limited reaction rate. Nevertheless, whereas for Cu_2O-coated catalysts, reaction times of 18 h were necessary for completed Ullmann-type substitutions, the currently presented PVP-coated nano-catalysts delivered good-to-excellent yields in only 4 h. The necessity of using zerovalent Cu as catalyst is shown in Table 1, where data clearly reveals that for this type of Ullmann coupling, the least active copper species were Cu(I) and Cu(II) (entries 6-9) for both oil-bath and microwave-heated systems. In addition, the work presented here also shows that the Ullmann C-O coupling reaction can be performed rather efficiently using relatively inexpensive Cu(0), which has been reported [44], mainly, with the use of catalytic amounts of noble metals.

Catalyst leaching. Loss of copper over time was examined using copper wires fixed to the mechanical stirrer (Figure 1a). The mass of the wire was determined for each run after washing and drying. Interestingly, oil-bath experiments gave good-to-excellent yields (entries 12-13) with weight losses of <20%. Moreover, the impact of increased surface area on the yield was clearly demonstrated by using 20 micron wire (entry 13). These data are consistent with earlier observations using Cu-particles (entries 1-3). However, the same procedure was ineffective in microwave

experiments, with the wires being undetectable as copper. Instead, black foams were noted, which, based on previous work with Zn and Mg wires and Fe particles [45], were attributed to Cu-carbide or carbonaceous species [46]. The origin of their formation will be further highlighted in chapter 5, though it seems probable that the wires act as antennae in the microwave field, carrying high electric loads. When discharges occur, plasma temperatures destroy the wire surface, giving carbide (carbonaceous) coated copper due to solvent combustion. This process is similar to the concept of electric discharge machining (EDM), by which method metals can be etched using electric discharges [13b, 47].

Oxidative stability of Cu nanoparticles. When $CuSO_4 \cdot 5H_2O$ was employed in conjunction with $NaH_2PO_2 \cdot H_2O$ and PVP (M_{av} 40 000), it proved possible to form a nano-sol that showed no traces of particle surface oxidation, even after three months. This was initially revealed by PXRD measurements (Figure 4a), with confirmation coming from XPS analysis (Figure 4b).

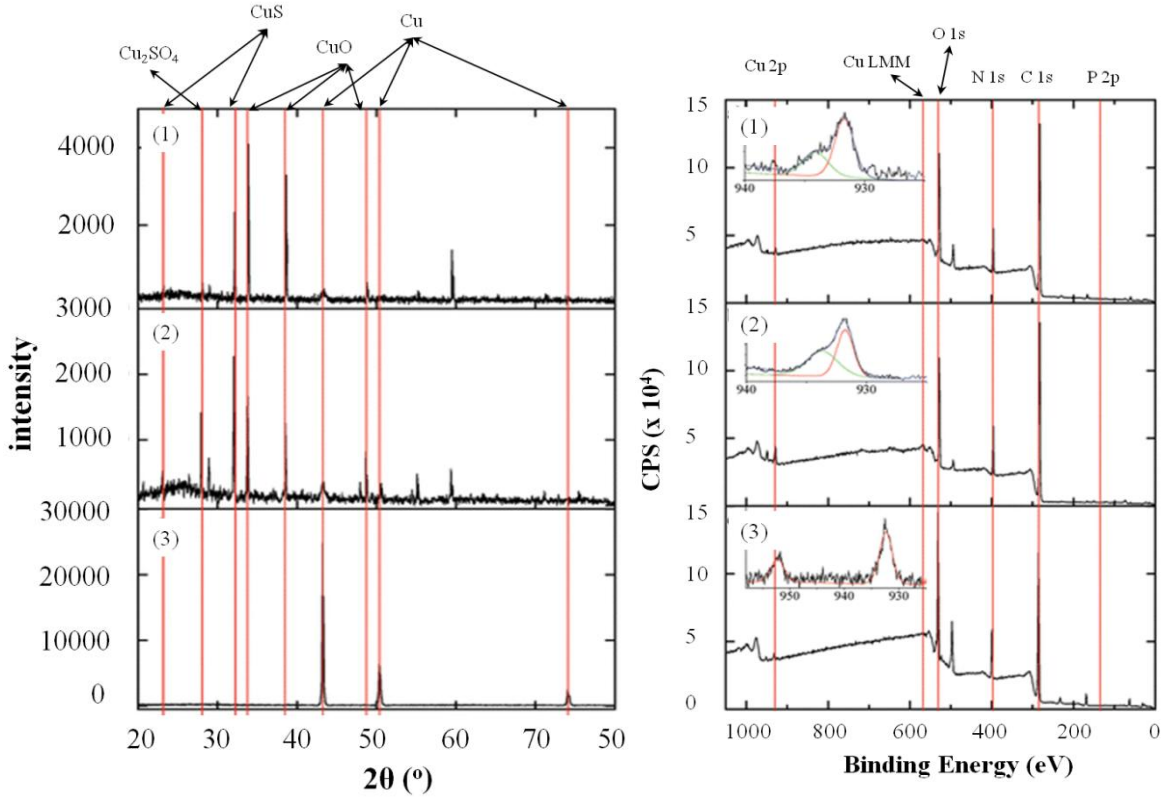

a) b)

Figure 3.4. PXRD (a) and XPS (b) spectra of samples of $CuSO_4 \cdot 5H_2O$ using (1) $NaBH_4$ (2) $N_2H_4 \cdot H_2O$ and (3) $NaH_2PO_2 \cdot H_2O$ (3 months after preparation). (XPS: Cu $2p_{1/2}$ (1–3) and $2p_{3/2}$ (3) peaks with envelope curves (Cu(0) red, Cu(I) green)).

Hence, PXRD measurements on samples that were prepared using $NaBH_4$ (1) and $N_2H_4 \cdot H_2O$ (2), respectively, revealed significant levels of CuO and other contaminants (including CuS and Cu_2SO_4). In contrast, the deployment of sodium hypophosphite as a co-reducing additive was successful, revealing both an excellent level of purity and an fcc (face-centered cubic) copper phase

with PXRD analysis (sample (3) in Figure 4a). After a period of three months, the PXRD signals demonstrated the long-term oxidative stability of the colloids prepared with sodium hypophosphite as a co-reducing agent.

In addition, XPS analyses confirmed that the use of either $NaBH_4$ or N_2H_4 to reduce $CuSO_4 \cdot 5H_2O$ also afforded contaminated (mainly CuS and Cu_2SO_4) nano-colloids that contained traces of Cu(I), which are primarily found at the particle surface [48]. Moreover, reducing the copper substrate by $NaH_2PO_2 \cdot H_2O$ and using PVP (M_{av} 40 000) demonstrated peaks in the XPS spectrum (Cu $2p_{1/2}$ at 952.2 eV and $2p_{3/2}$ at 932.0 eV in spectrum (3) of Figure 4b) confirming Cu(0) at the surface and, consequently, demonstrating significant oxidative stability.

During the nanoparticles synthesis, the rapid formation of black colloids was observed when the stronger reducing agents hydrazine or sodium borohydride were deployed. In contrast, the use of hypophosphite reductant resulted in the formation of a dark-blue solution of $Cu(OH)_2$ that changed to yellow at around 100 °C. Most probably this color change is due to the formation of intermediate Cu–PVP complexes [49]. Consequently, a green colloid developed and, at 140 °C, finally the formation of a dark-red nano-sol was observed. Accordingly, the slow reduction kinetics accompanied with the hypophosphite reductant (instead of hydrazine or borohydride) initiated the formation of specific copper oxide intermediates through re-oxidation by water (see Scheme 4). These specific oxides might well determine the subsequent formation of a surface crystallographic structure that avoids further particle oxidation after reduction with hypophosphite (due to the formation of dihydrogen phosphate product) [50].

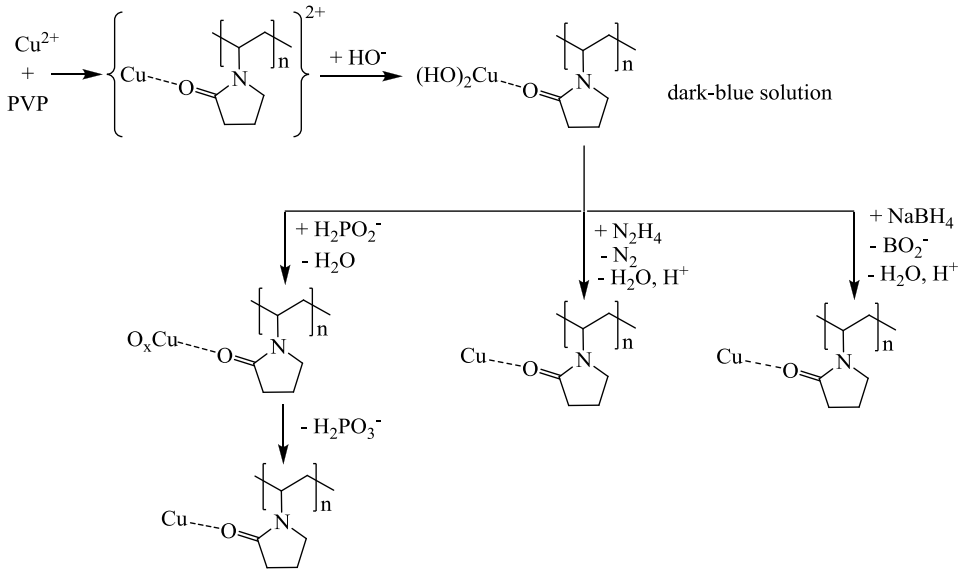

Scheme 3.4. Schematic overview of proposed reaction mechanisms for the formation of PVP-protected Cu nanoparticles.

Additionally, the steric density with which PVP covers the particle surface can also be considered to inhibit surface oxidation processes, because samples showed the formation of oxide shells dependent on the PVP chain lengths [51]. The use of hypophosphite as reductant, however, also revealed traces of phosphorus in the

EDX spectra of the nanoparticles after work-up, indicating still the presence of impurities from the reduction-step.

This investigation on the oxidative stability of PVP-protected Cu nanoparticles provides an additional powerful tool to the currently developed synthetic procedures via modulated nanoparticle synthesis in order to stepwise manipulate particle formation (*e.g.* injection rate of reducing agent or metal precursor solution, injection sequence and pH value). In contrast, previously reported syntheses have used the stepwise injection of metal precursor without the addition of NaOH [52]. In such cases, cation concentrations are likely to remain below the critical super-saturation level, which is necessary during the particle growth step. Hence, polydisperse particle distributions and often reported oxide coverage of synthesized Cu-nanoparticles are observed. The present addition of NaOH should provide a metal ion concentration that is supercritical until the particle precursor is fully reacted.

Mechanistically, the use of hypophosphite offers the advantage to control the reduction kinetics directly through the adjustment of pH. Thus, in an alkaline medium the reaction of the copper cations with hypophosphite demonstrated clearly acceleration in the reduction process and decrease in the particle mean size. Moreover, the particle mean sizes appeared to be severely influenced by the PVP : metal mass ratios. A decrease from a PVP : metal mass ratios of 12.6 to 1.6 revealed a drastic increase in mean particle sizes and, in addition, the formation cuboctahedral, instead of spherical, particles (see Figure 5). This, again, confirms the role of the polymer not only in the oxidative stability, but also in the overall particle growth.

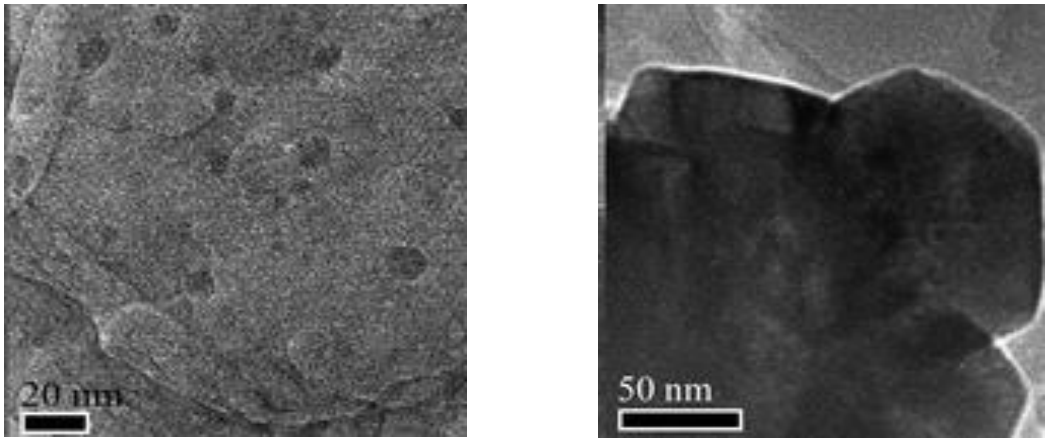

a) b)

Figure 3.5. Cu nanoparticles obtained from a PVP : metal mass ratio of 12.6 (a) and 1.6 (b).

The small nanoparticles displayed mainly a spherical shape with both (111) and (100) facets, where for larger nanoparticles also a cubic morphology was observed. This could indicate a preferential coordination of the polymer to the (100) face of the fcc metal, leading to accelerated growth on the (111) facets and their consequent disappearance. Previously, it was found that the oxidative stability of copper depends on the surface stress exhibited by (111) lattice planes

[53], suggesting that increased compression in the particle may stabilize the nanoparticles again oxidation. Indeed, in some cases HRTEM images demonstrated considerable lattice compression as compared to the corresponding value of 3.61 Å for bulk copper [3, 54]. However, (111) spacings appeared to be lower when less PVP was used (Figure 5b). In comparing the different PVP : metal ratios, therefore, the remarkable stability at an increased PVP fraction must partially be contributed to the additional protective effect of PVP, likely through electron donation from N,O lone pairs into Cu sp-hybrid orbitals [51].

3.3.2 Activity measurements of the Cu-catalyzed liquid-type Ullmann etherification

The preparation of oxidative stable PVP-capped Cu nanoparticles from $Cu^{II}SO_4$ has been introduced in the previous section, where similar method has also been applied for bimetallic CuM nano-colloids. Accordingly, a mixture of copper(II) sulfate pentahydrate and PVP in ethylene glycol was treated with either zinc(II) chloride or tin(II) chloride and, thereafter, with sodium hypophosphite monohydrate at 0 ºC and the pH adjusted to 9-11. A colloidal suspension resulted after 1 h at 120 ºC confirming the reproducibility of the aforementioned synthethic strategy. Figure 6 shows the obtained transmission electron microscopic graphs for Cu, CuSn and CuZn nanoparticles, which reveal crystalline particles with similar particle sizes as reported in section 2.3.1.

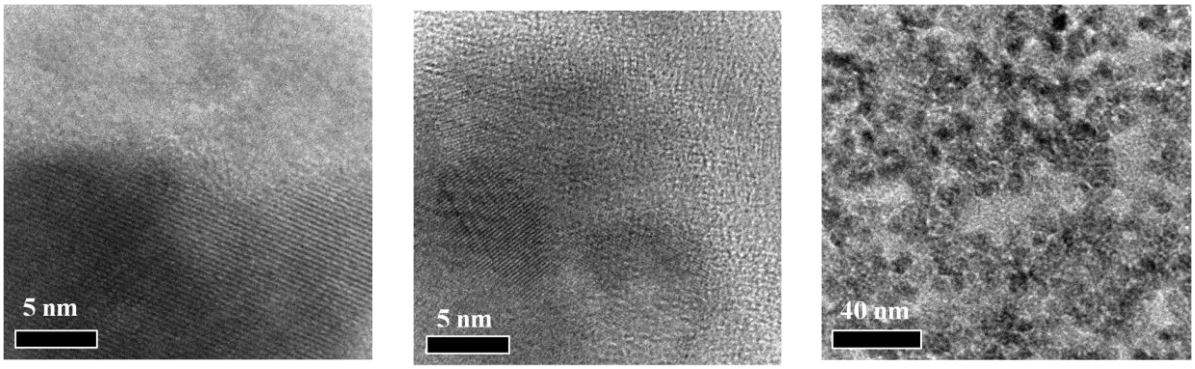

a) b) c)

Figure 3.6. HRTEM images of the nanoparticles (magnification in brackets). (a) Cu (800.000), (b) CuSn (800.000), (c) CuZn (100.000).

The energy dispersive X-ray spectroscopy on the monometallic and bimetallic nanoparticles (taken from the TEM-regions in Figure 6) confirm the presence of the Cu, Zn and Sn elements (see Figure 7).

As mentioned in the experimental part, the "liquid-type" Ullmann C-O coupling makes the use of solid bases (in this reaction Cs_2CO_3) unnecessary by the use of a potassium phenolate (as naked ion nucleophile) and a 4-chloropyridine hydrogen chloride pre-treatment step. Moreover, the use of trace amounts of 18-crown-6 increases the solubility of potassium phenolate by scavenging the potassium ion, hence affording a dissolved reaction mixture at these reactants concentrations.

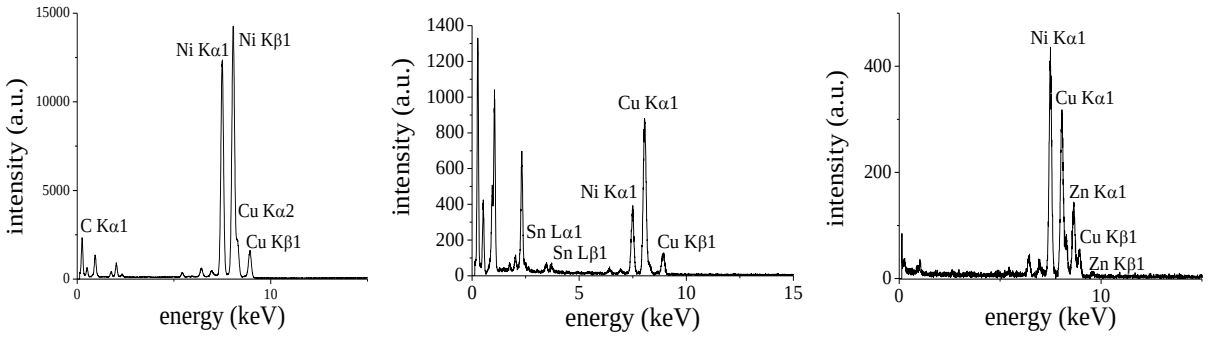

Figure 3.7. EDX analyses: Cu (a), CuZn (b), CuSn (c). Line assignment (energies in keV): C Kα_1: 0.28, O Kα_1: 0.52, Ti Kα_1: 4.51, Kβ_1: 4.93, Ni Kα_1: 7.48, Kβ_1: 8.26, Cu Kα_2: 8.03, Kβ_1: 8.91, Zn Kα_1: 8.64, Kβ_1: 9.57, Sn Lα_1: 3.44, Lβ_1: 3.66.

Using nano-structured Cu(0) and CuM (M = Zn, Sn) in the absence or presence of a crown ether (*vide infra*), the etherification temperature can be lowered from 140 °C to 130 °C (Scheme 2), whilst recording yields of up to 90% after 2 h. At temperatures below 115 °C, the yields decreased considerably, leading to 130 °C as the optimum operational temperature for these nano-alloys (see Table 2). The yields were determined based on ^{1}H-NMR signals of the *ortho*-protons of the electrophile 4-chloropyridine and monitored over time (see Figure 8).

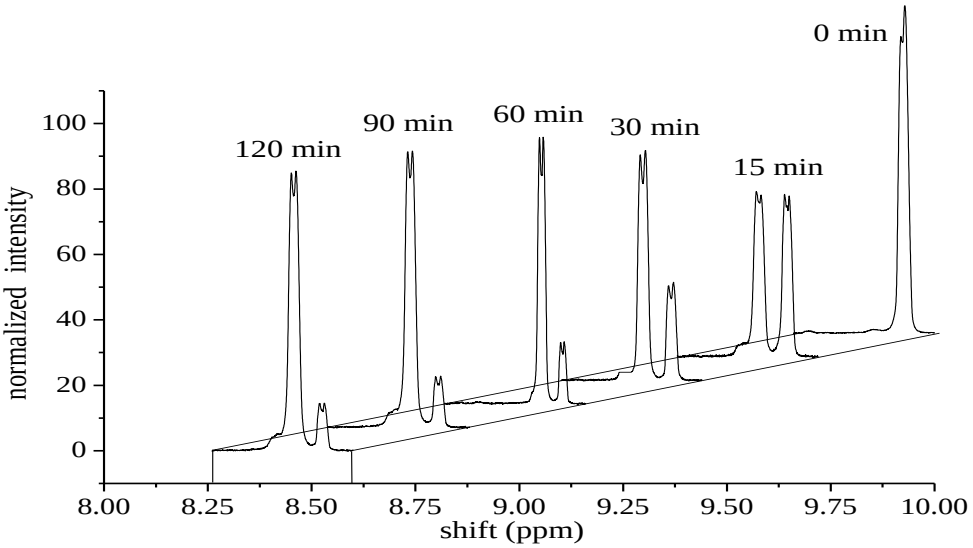

Figure 3.8. ^{1}H-NMR spectra of pyridine (8.59 ppm) and 4-phenoxypyridine (8.48 ppm) *ortho*-protons using nano-CuSn catalyst and 18-crown-6 as potassium phenolate solubilizer at various times. Total peak areas have been normalized to calculate the yield.

Entries 1 and 2 (in Table 2) reveal that, in spite of the reduced reaction temperatures, the use of nano-Cu in conjunction with phenol/Cs_2CO_3 gives an inferior turnover in comparison to that obtained when instead potassium phenolate was used as nucleophile. Taken together with the need to avoid the generation of solid deposits (controlling solubility, mass-transfer and ion-exchange mechanisms), this observation indicated the superior performance using base-free conditions.

Table 3.2. Cu(M)-catalyzed formation of 4-phenoxypyridine

Entry	Cu-source[a]	Particle size (nm)	Additive	T (ºC)	Time (min)	Yield (%)[c]	TOF (s^{-1})
1[b]	Nano-Cu	9.6	Cs_2CO_3	140	120	63	0.02
2[d]	Nano-Cu	9.6	-	130	120	75	0.04
3[d]	Nano-Cu	9.6	18-crown-6	130	120	85	0.05
4[d]	Nano-CuSn	8.2	-	130	120	82	0.11
5[d]	Nano-CuSn	8.2	18-crown-6	130	120	87	0.12
6[d]	Nano-CuZn	9.3	-	130	120	87	0.10
7[d]	Nano-CuZn	9.3	18-crown-6	130	120	90	0.06

[a] 0.015 equiv. w.r.t. 4-chloropyridine
[b] phenol used as nucleophile, see reference [1]
[c] by ^{1}H-NMR spectroscopy
[d] potassium phenolate used as nucleophile, see reference [2].

Since the role of Cs_2CO_3 was to deprotonate the phenol, affording a naked ion as a nucleophilic substituent in the subsequent SN_{Ar} reaction, it follows that omission of the base requires the deployment of an activated phenol. In this context, the use of potassium phenolate led to an improvement in yield from 63% (reached after 2 h, entry 1) to 75% (entry 2 in Table 2 and Figure 9a) at reduced temperature. Under the same conditions, hetero-bimetallic nano-catalysts showed higher conversions. Hence, 4-phenoxypyridine was formed in 82% yield using nano-CuSn and in 87% yield using nano-CuZn (entries 4 and 6 in Table 2).

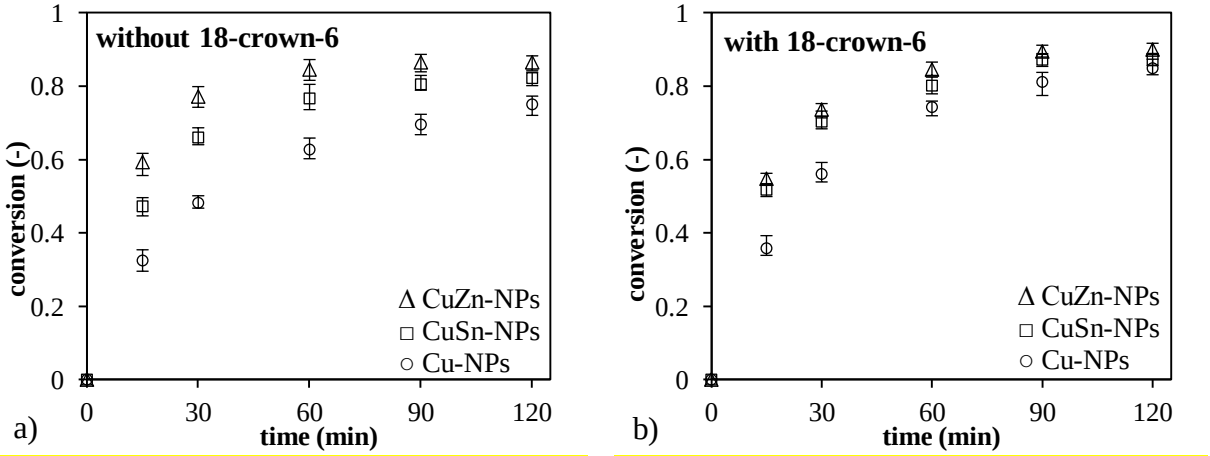

Figure 3.9. Conversion versus time in the liquid-type Ullmann C-O coupling, using Cu, CuSn and CuZn nanoparticles (NPs), both in the absence (a) and the presence (b) of 18-crown-6.

Noting that equilibrium was reached after 2 h (Figure 9a), K^+ was hypothesized to deactivate the catalyst over time. This could occur through complexation by the capping agent, altering the conformation of the polymer and rendering the catalyst surface inaccessible to substrate. Alternatively, it is possible that KCl formed during the reaction could not be retained in the solvent phase. To exclude these effects, crown ether was added as a solubilizing agent for both potassium phenolate as reactant and KCl as product. When nano-Cu was tested in the presence of 18-crown-6 (0.01-0.014 equiv. relative to phenolate) as a kinetic promoter, the yield of 4-phenoxypyridine improved from 75% to 85% (entry 3 in Table 2 and Figure 9b).

Similar enhancements were noted for the use of nano-CuSn (yield increased to 87%, entry 5) and nano-CuZn (yield increased to 90%, entry 7). The performance maximum noted for CuZn can be attributed to a combination of particle ligand-shell effects and intermetallic effects, stemming from interaction of the alloying metals, eventually leading to an increased stability of zero-valent copper. Hence, the coordinative strength of the capping agent (which is dependent on ligand characteristics and particle surface structure) is known to influence the substrate access through variations in polymer density (*e.g.* for Pd colloids [55]).

However, whilst intermetallic effects may be important, it should be noted that the alloy phase effect, discussed in the previous sections, is also known to result in segregation of the metals during the reaction, ultimately leading to catalyst deactivation [29]. This is consistent with our preliminary observations for both bimetallic systems, which, in contrast to monometallic copper, rapidly lost their activity. It seems likely that in either case, the alloying metal underwent sacrificial oxidation with segregation, finally leading to the formation of a zinc/tin oxide shell, as has been noted elsewhere for nano-brass [56]. Detailed studies that seek to compare pre- and post-reaction catalyst surface structures by X-ray spectroscopy (XPS and XAS) are presented in chapter 4.

3.3.3 Activity measurements of the Cu-catalyzed cyclopropanation

In the previous section, the development and utility of various Cu nanoparticles as catalyst in the Ullmann-type C-O coupling reaction for the coupling of aromatic moieties towards a fine-chemical precursor, such as 4-phenoxypyridine, were extensively explored [1-2]. In the next chapter heterogenization of such Cu-based catalyst unto various titania supports will be discussed to establish a sustainable catalyst system for flow chemistry. This section will deal with the CuZn-catalyzed cyclopropanation as a means to prove that the highly active catalyst system is applicable for a wider range of chemical reactions.

C-O coupling reactions are relatively slow as compared to carbene insertion reactions and are accompanied with mild reaction conditions. Therefore, the exploration of the cyclopropanation as an alternative Cu-catalyzed reaction for fine-chemicals synthesis adds the importance of controlled heat release and safe operations of the hazardous diazo-compound. In this study, cyclopropanation of styrene with ethyl diazoacetate (EDA) to *cis*- and *trans*-ethyl-2-phenylcyclopropane-1-carboxylate was used as a model reaction for Drospirenone (see Schemes 3 and 5). According to Long *et al.*, the mechanism behind the original Simmons-Smith cyclopropanation reaction involves CuZn and CH_2I_2 as reactants, where Zn is consumed by the formation of the reactive $Zn(CH_2I)_2$ [37a]. In another report, Fang *et al.* demonstrate via density functional theory investigation that Zn is required to form $IZnCH_2I$ as reactive species for the carbene insertion step. For the reaction described in this section, however, the carbene insertion reaction involves a highly active diazo-compoud, which does not require Zn as activator of the carbene-adduct, but solely catalytic Cu instead. As discussed in the previous chapter, the mechanism of the cyclopropanation using a diazo-compound follows a different pathway as compared to a carbene insertion using

dihalomethanes. Bühl and coworkers reported an extended study, based on experimental evidence and DFT (density functional theory) investigations, on the possible catalytic mechanism of cyclopropane formation from diazo-acetates [57].

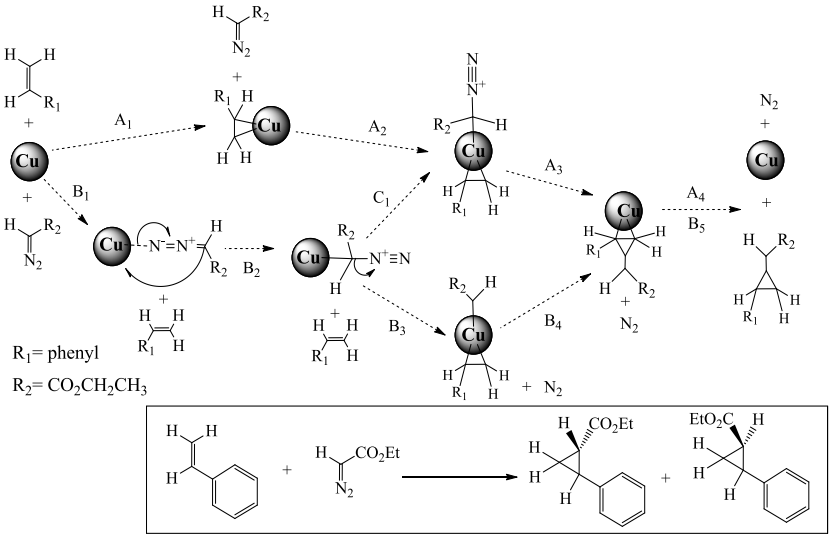

Scheme 3.5. Postulated mechanisms of the Cu-catalyzed cyclopropanation, involving two possible reaction pathways: Cu-insertion of either the diazo-compound or the olefine.

Aligned with their findings, we propose three mechanistic pathways (Scheme 5), where Cu either undergoes interaction with the ethyl diazo-acetate (steps A_1-A_4) or with the styrene (B_1-B_5). In a subsequent step, the cyclopropane ring is formed via a copper-centered addition of either of the two reactants (step C1), which, via a rearrangement and desorption step, yields the cyclopropane functionality.

Following our previous results (Tables 1 and 2), the use of the CuZn-catalyst showed a clear outperformance with respect to the Cu catalyst. Therefore, experiments were intially carried out using a commercially purchased mixture of micron- and nano-powders of Cu and Zn. Figure 10a clearly shows a drastic increase in performance using a nano-powder Cu-Zn (60:40 wt% Cu:Zn with TEM-measured particle sizes of 70 ± 39 nm) over a micron-powder Cu catalyst (3 micron, similar to entry 3 in Table 1). Quantitative yields were attained in less then 10 min at 90 °C with selectivities up to 95%, which, to the best of our knowledge, has not yet been reported employing this type of nano-catalysts. Comparable to the Ullmann C-O coupling, the high reactivity of CuZn nano-colloids is primarily due to the increased surface area of the nanoparticles, but also the oxidative stability of Cu by Zn as preferential oxidizer (see chapter 4 for detailed information) played an important role. In addition, the use of synthesized CuZn nanoparticles in the range of *ca.* 10 nm demonstrated a negative effect at increased Zn-loadings in the CuZn catalyst (see Figure 10b). This effect could be rationalized, based on previous results in the Ullmann-type C-O coupling, by the formation of a ZnO-shell on the Cu-core nanoparticles, which finally limited access of reactants to the Cu surface, thus leading to a decreased catalyst performance.

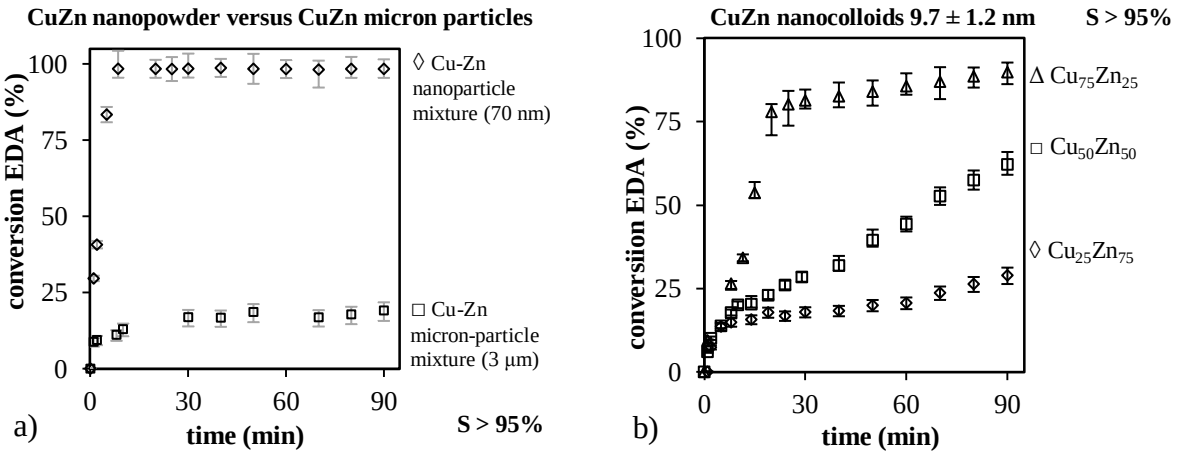

Figure 3.10. The use of nano-powder (70 nm) CuZn, demonstrating a 10-fold performance increase as compared to the use of micron-powder (3 μm) CuZn after 5 min (a). At smaller nanoparticle sizes, an increased zinc fraction appears to deactivate the catalyst due to ZnO formation (b). C_{EDA} = 0.03 M, $C_{styrene}$ = 0.3 M, C_{Cu} = 1.5 mM and T = 90 ºC.

This observation was not made in the case of the 70 nm Cu-Zn nano-alloys since the Cu and Zn particles are present as separated particles. The formed ZnO-particles remain separated from the Cu particles, thus retaining accessibility of the reactants towards the Cu surface.

3.4 Conclusions

In summary, nanoscopic Cu-based catalysts have been used to achieve good-to-excellent yields in the microwave-assisted Ullmann ether synthesis of 4-phenoxypyridine. These yields could be achieved by the use of oxidation-resistant nanoparticle catalysts, stabilized by a protective anti-agglomerant coating of PVP. Moreover, micron-wires have proved excellent yields using oil-bath heated systems. However, their application in microwave-assisted reactions appeared to be impossible due to arcing and, consequently, coke-formation onto the active surface.

In this study, a novel colloid synthesis-route in alcohol using various co-reducing agents was demonstrated. While syntheses using reducing agents, such as $N_2H_4 \cdot H_2O$ and $NaBH_4$, provided only limited success, the deployment of $NaH_2PO_2 \cdot H_2O$ in the presence of PVP (M_{av} 40,000) demonstrated that it is possible to achieve pure Cu(0) nanoparticles. The obtained nanoparticles showed a mean size distribution of 9.6 ± 1.0 nm, which could exhibit oxidative stability (according to PXRD and XPS studies) for several months. The investigation in the field of microwave-assisted etherification with nano-structured Cu(0) was extended by applying copper-based nano-alloys, such as CuSn and CuZn and was based on previous surveys [56]. The development of a liquid-type Ullmann reaction has allowed reductions in both reaction time and temperature with respect to the use of slurry-type Ullmann-type etherifications, using either commercial Cu(0) or stable Cu nanoparticles [1]. Similarly, excellent yields were maintained while improving on previously reported yields for the multimode microwave-assisted synthesis of 4-phenoxypyridine [2].

Targeting the fabrication of continuous-flow devices as a means of overcoming limits of scale traditionally associated with microwave-assisted transformations, the use of heterogeneous Cs_2CO_3 was successfully eliminated without depleting the catalyst efficiency. This step, whilst it introduces the need for using alkali-metal phenolate reagents, avoids the use of a base that otherwise represents an additional cost and source of processing difficulties. Notably, kinetic enhancement of the reaction was demonstrated through the application of 18-crown-6 as an alkali-metal scavenger. In addition, only 1.5 mol% of nano-structured copper catalyst was needed to obtain yields of up to 90%, whereas previous experiments required the use of as much as 10 mol% of commercial copper or copper wires.

These achievements will be combined with previous reports on the fabrication of nano-catalyst supported on fused silica capillary microreactors [58] and presented in the next chapters to develop the reusability of nano-CuM systems in continuous-flow milli-reactors. Although the use of Cu-based nano-catalysts also demonstrated a drastic performance increase in the Cu-catalyzed cyclopropanation, contrary to the Cu-catalyzed C-O coupling, the addition of Zn as co-metal demonstrated a negative effect on the formation of cyclopropanes. This effect is most probably due to ZnO-shell formation in the atomically mixed CuZn nanoparticles, which limited the accessibility of the reactants to the active Cu-core. This effect was not observed in the case of the 70 nm Cu-Zn nano-alloys since the Cu and Zn particles were present as separated particles and, therefore, the formation of ZnO particles would not affect the remaining Cu particles, thus retaining the Cu accessibility for reaction.

References

[1] F. Benaskar, V. Engels, N.G. Patil, E. V. Rebrov, J. Meuldijk, V. Hessel, L. A. Hulshof, D. A. Jefferson, J. C. Schouten and A. E. H. Wheatley, *Tetrahedron Lett.* **2010**, *51*, 248-251.

[2] V. Engels, F. Benaskar, N.G Patil, E. V. Rebrov, V. Hessel, L. A. Hulshof, D. A. Jefferson, J. A. J. M. Vekemans, S. Karwal, J. C. Schouten and A. E. H. Wheatley, *Org. Process Res. Dev.* **2010**, *14*, 644-649.

[3] V. Engels, F. Benaskar, D. A. Jefferson, B. F. G. Johnson and A. E. H. Wheatley, *Dalton Trans.* **2010**, *39*, 6496-6502.

[4] a) F. Ullmann, *Ber. Dtsch. Chem. Ges.* **1903**, *36*, 2382-2384; b) F. Ullmann, *Ber. Dtsch. Chem. Ges.* **1904**, *37*, 853-854; c) F. Ullmann and J. Bielecki, *Ber. Dtsch. Chem. Ges.* **1901**, *34*, 2174-2185; d) F. Ullmann and P. Sponagel, *Ber. Dtsch. Chem. Ges.* **1905**, *38*, 2211-2212; e) I. Goldberg, *Ber. Dtsch. Chem. Ges.* **1906**, *39*, 1691-1692.

[5] a) W. Labadie Jeff, L. Hedrick James and M. Ueda in *Poly(aryl ether) Synthesis, Vol. 624* American Chemical Society, **1996**, pp. 210-225; b) K. C. Nicolaou, X.-J. Chu, J. M. Ramanjulu, S. Natarajan, S. Bräse, F. Rübsam and C. N. C. Boddy, *Angew. Chem., Int. Ed.* **1997**, *36*, 1539-1540; c) D. A. Evans, M. R. Wood, B. W. Trotter, T. I. Richardson, J. C. Barrow and J. L. Katz, *Angew. Chem., Int. Ed.* **1998**, *37*, 2700-2704.

[6] a) J. Hassan, M. Sevignon, C. Gozzi, E. Schulz and M. Lemaire, *Chem. Rev.* **2002**, *102*, 1359-1469; b) F. Monnier and M. Taillefer, *Angew. Chem., Int. Ed.* **2009**, *48*, 6954-6971.

[7] a) M. L. Kantam, S. Laha, J. Yadav, P. R. Likhar, B. Sreedhar and B. M. Choudary, *Adv. Synth. Catal.* **2007**, *349*, 1797-1802; b) B. C. Ranu, K. Chattopadhyay, A. Saha, L. Adak, R. Jana, S. Bhadra, R. Dey and D. Saha, *J. Phys.: Conference Series* **2008**, *106*, 012003; c) S. Roy and M. A. Pericas, *Org. Biomol. Chem.* **2009**, *7*, 2669-2677.

[8] a) G. Mann and J. F. Hartwig, *Tetrahedron Lett.* **1997**, *38*, 8005-8008; b) A. Aranyos, D. W. Old, A. Kiyomori, J. P. Wolfe, J. P. Sadighi and S. L. Buchwald, *J. Am. Chem. Soc.* **1999**, *121*, 4369-4378; c) S. Ding, N. S. Gray, Q. Ding and P. G. Schultz, *Tetrahedron Lett.* **2001**, *42*, 8751-8755; d) N. Kataoka, Q. Shelby, J. P. Stambuli and J. F. Hartwig, *J. Org. Chem.* **2002**, *67*, 5553-5566.

[9] a) Y.-J. Cherng, *Tetrahedron* **2002**, *58*, 4931-4935; b) Y.-J. Cherng, *Tetrahedron* **2002**, *58*, 1125-1129; c) Y.-J. Cherng, *Tetrahedron* **2002**, *58*, 887-890.

[10] S. V. Ley and A. W. Thomas, *Angew. Chem., Int. Ed.* **2003**, *42*, 5400-5449.

[11] K. D. Raner, C. R. Strauss, F. Vyskoc and L. Mokbel, *J. Org. Chem.* **1993**, *58*, 950-953.

[12] N. D. D'Angelo, J. J. Peterson, S. K. Booker, I. Fellows, C. Dominguez, R. Hungate, P. J. Reider and T.-S. Kim, *Tetrahedron Lett.* **2006**, *47*, 5045-5048.

[13] a) A. G. Whittaker and D. M. P. Mingos, *J. Chem. Soc., Dalton Trans.* **1995**, 2073-2079; b) A. G. Whittaker and D. M. P. Mingos, *J. Chem. Soc., Dalton Trans.* **2000**, 1521-1526; c) V. D. Buchelnikov, D. V. Louzguine-Luzgin, G. Xie, S. Li, N. Yoshikawa, M. Sato, A. P. Anzulevich, I. V. Bychkov and A. Inoue, *J. Appl. Phys.* **2008**, *104*, 113505; d) M. Larhed, G. Lindeberg and A. Hallberg, *Tetrahedron Lett.* **1996**, *37*, 8219-8222; e) P. He, S. J. Haswell and P. D. I. Fletcher, *Lab on a Chip* **2004**, *4*, 38-41.

[14] a) A. Biffis, E. Scattolin, N. Ravasio and F. Zaccheria, *Tetrahedron Lett.* **2007**, *48*, 8761-8764; b) J. Niu, H. Zhou, Z. Li, J. Xu and S. Hu, *J. Org. Chem.* **2008**, *73*, 7814-7817; c) M. P. Doyle, R. Duffy, M. Ratnikov and L. Zhou, *Chem. Rev.* **2009**, *110*, 704-724; d) J. Y. Kim, J. C. Park, A. Kim, A. Y. Kim, H. J. Lee, H. Song and K. H. Park, *Eur. J. Inorg. Chem.* **2009**, 4219-4223; e) V. Polshettiwar, A. Decottignies, C. Len and A. Fihri, *ChemSusChem* **2010**, *3*, 502-522; f) G. Shore, W.-J. Yoo, C.-J. Li and M. G. Organ, *Chem. –Eur. J.* **2010**, *16*, 126-133; g) J. I. Garcia, G. Jimenez-Oses, B. Lopez-Sanchez, J. A. Mayoral and A. Velez, *Dalton Trans.* **2010**, *39*, 2098-2107; h) J. J. Mousseau, J. A. Bull and A. B. Charette, *Angew. Chem., Int. Ed.* **2010**, *49*, 1115-1118.

[15] a) A. Sarkar, T. Mukherjee and S. Kapoor, *J. Phys. Chem. C* **2008**, *112*, 3334-3340; b) L. D. Pachón, J. H. van Maarseveen and G. Rothenberg, *Adv. Synth. Catal.* **2005**, *347*, 811-815; c) H. A. Orgueira, D. Fokas, Y. Isome, P. C. M. Chan and C. M. Baldino, *Tetrahedron Lett.* **2005**, *46*, 2911-2914; d) F. Alonso, Y. Moglie, G. Radivoy and M. Yus, *Tetrahedron Lett.* **2009**, *50*, 2358-2362.

[16] a) I. S. Park, M. S. Kwon, Y. Kim, J. S. Lee and J. Park, *Org. Lett.* **2008**, *10*, 497-500; b) G. Molteni, C. L. Bianchi, G. Marinoni, N. Santo and A. Ponti, *New J. Chem.* **2006**, *30*, 1137-1139.

[17] M. L. Kantam, V. S. Jaya, B. Sreedhar, M. M. Rao and B. M. Choudary, *J. Mol. Catal. A* **2006**, *256*, 273-277.

[18] S. F. Vasilevsky, S. V. Klyatskaya, O. L. Korovnikova, D. V. Stass, S. A. Amitina, I. A. Grigir'ev and J. Elguero, *Tetrahedron Lett.* **2004**, *45*, 7741-7743.

[19] K. Sonogashira, Y. Tohda and N. Hagihara, *Tetrahedron Lett.* **1975**, *16*, 4467-4470.

[20] D. M. T. Chan, K. L. Monaco, R.-P. Wang and M. P. Winters, *Tetrahedron Lett.* **1998**, *39*, 2933-2936.

[21] B. C. Ranu, K. Chattopadhyay, A. Saha, L. Adak, S. Bhadra, R. Dey and D. Saha, *Pure App. Chem.* **2009**, *81*, 2337-2354.
[22] S. U. Son, I. K. Park, J. Park and T. Hyeon, *Chem. Commun.* **2004**, *10*, 778-779.
[23] M. Kidwai, N. K. Mishra, V. Bansal, A. Kumar and S. Mozumdar, *Tetrahedron Lett.* **2007**, *48*, 8883-8887.
[24] a) B. Corain, P. Centomo, C. Burato and P. Canton in *Chapter 29 - Gel-Type Cross-Linked Functional Polymers as Template in the Synthesis of Size Controlled Metal Nanoclusters, Vol.* Eds.: B. Corain, G. Schmid, G. S. N. ToshimaA2 - B. Corain and N. Toshima), Elsevier, Amsterdam, **2008**, pp. 413-418; b) B. F. G. Johnson, *Top. Catal.* **2003**, *24*, 147-159; c) C. N. R. Rao, G. U. Kulkarni, P. J. Thomas and P. P. Edwards, *Chem. Soc. Rev.* **2000**, *29*, 27-35; d) N. Toshima, *Macromolecular Symposia* **2008**, *270*, 27-39.
[25] a) P. L. Hansen, J. B. Wagner, S. Helveg, J. R. Rostrup-Nielsen, B. S. Clausen and H. Topsøe, *Science* **2002**, *295*, 2053-2055; b) J. Greeley, A. A. Gokhale, J. Kreuser, J. A. Dumesic, H. Topsøe, N. Y. Topsøe and M. Mavrikakis, *J. Catal.* **2003**, *213*, 63-72.
[26] J. Hambrock, M. K. Schröter, A. Birkner, C. Wöll and R. A. Fischer, *Chem. Mater.* **2003**, *15*, 4217-4222.
[27] R. E. Cable and R. E. Schaak, *Chem. Mater.* **2007**, *19*, 4098-4104.
[28] a) B. Bhushan, *Handbook of Nanotechnology*, Springer, Berlin, **2007**; b) P. V. Kazakevich, A. V. Simakin, G. A. Shafeev, F. Monteverde and M. Wautelet, *Appl. Surf. Sci.* **2007**, *253*, 7724-7728; c) J. Wolfenstine, S. Campos, D. Foster, J. Read and W. K. Behl, *Jour. Pow. Sources* **2002**, *109*, 230-233.
[29] V. Calò, A. Nacci, A. Monopoli, E. Ieva and N. Cioffi, *Org. Lett.* **2005**, *7*, 617-620.
[30] S. Saito and Y. Koizumi, *Tetrahedron Lett.* **2005**, *46*, 4715-4717.
[31] N. A. Dhas, C. P. Raj and A. Gedanken, *Chem. Mater.* **1998**, *10*, 1446-1452.
[32] a) J.-F. Marcoux, S. Doye and S. L. Buchwald, *J. Am. Chem. Soc.* **1997**, *119*, 10539-10540; b) H.-J. Cristau, P. P. Cellier, S. Hamada, J.-F. Spindler and M. Taillefer, *Org. Lett.* **2004**, *6*, 913-916.
[33] a) H. E. Simmons, E. P. Blanchard and R. D. Smith, *J. Am. Chem. Soc.* **1964**, *86*, 1347-1356; b) H. E. Simmons and R. D. Smith, *J. Am. Chem. Soc.* **1958**, *80*, 5323-5324.
[34] M. B. Daniel J. Mack, Alexandra Plichta, Jón T. Njarðarson, *Midas World Review (TM), January 2009-December 2009, IMS Health Incorporated.* .
[35] A. Cornejo, J. M. Fraile, J. I. García, M. J. Gil, S. V. Luis, V. Martínez-Merino and J. A. Mayoral, *J. Org. Chem.* **2005**, *70*, 5536-5544.
[36] D. Bittler, H. Hofmeister, H. Laurent, K. Nickisch, R. Nickolson, K. Petzoldt and R. Wiechert, *Angew. Chem., Int. Ed.* **1982**, *21*, 696-697.
[37] a) J. Long, L. Xu, H. Du, K. Li and Y. Shi, *Org. Lett.* **2009**, *11*, 5226-5229; b) W.-H. Fang, D. L. Phillips, D.-q. Wang and Y.-L. Li, *J. Org. Chem.* **2001**, *67*, 154-160; c) T. Laird, *Proceedings of the 3rd International Conference on the Scale Up of Chemical Processes* **1998**, *Scientific Update*, p 432.
[38] a) E. Nadeau, D. L. Ventura, J. A. Brekan and H. M. L. Davies, *J. Org. Chem.* **2010**, *75*, 1927-1939; b) G. A. Ardizzoia, S. Brenna, F. Castelli, S. Galli, C. Marelli and A. Maspero, *J. Organomet. Chem.* **2008**, *693*, 1870-1876; c) J. M. Fraile, J. I. García, V. Martínez-Merino, J. A. Mayoral and L. Salvatella, *J. Am. Chem. Soc.* **2001**, *123*, 7616-7625; d) J. M. Fraile, J. I. García, C. I. Herrerías, J. A. Mayoral, D. Carrié and M. Vaultier, *Tetrahedron: Asymmetry* **2001**, *12*, 1891-1894; e) J. M. Fraile, J. I. García, J. A. Mayoral, T. Tarnai and M. A. Harmer, *J. Catal.* **1999**, *186*, 214-221; f) M. P. Doyle, C. S. Peterson, Q.-L. Zhou and H. Nishiyama, *Chem. Commun.* **1997**, 211-212; g) M. Doyle, M. Eismont and Q. Zhou, *Russ. Chem. Bull.* **1997**, *46*, 955-958.

[39] a) J. M. Fraile, J. A. Mayoral, N. Ravasio, M. Roldán, L. Sordelli and F. Zaccheria, *J. Catal.* **2011**, *281*, 273-278; b) A. Caballero, M. Sabater, M. E. Morilla, M. C. Nicasio, T. R. Belderraín, M. M. Díaz-Requejo and P. J. Pérez, *Inorg. Chim. Acta* **2009**, *362*, 4599-4602; c) C. Özen and N. S. Tüzün, *Organometallics* **2008**, *27*, 4600-4610.

[40] a) M. Kennedy, M. A. McKervey, A. R. Maguire and G. H. P. Roos, *J. Chem. Soc., Chem. Commun.* **1990**, 361-362; b) S.-i. Hashimoto, N. Watanabe and S. Ikegami, *Tetrahedron Lett.* **1990**, *31*, 5173-5174; c) H. M. L. Davies and D. K. Hutcheson, *Tetrahedron Lett.* **1993**, *34*, 7243-7246; d) M. P. Doyle and M. A. McKervey, *Chem. Commun.* **1997**, 983-990; e) C. G. Espino, K. W. Fiori, M. Kim and J. Du Bois, *J. Am. Chem. Soc.* **2004**, *126*, 15378-15379; f) H. T. Chifotides and K. R. Dunbar in *Rhodium Compounds Multiple Bonds Between Metal Atoms, Vol.* Eds.: F. A. Cotton, C. A. Murillo and R. A. Walton), Springer US, **2005**, pp. 465-589; g) D. Timmons and M. Doyle in *Chiral Dirhodium(II) Catalysts and Their Applications Multiple Bonds Between Metal Atoms, Vol.* Eds.: F. A. Cotton, C. A. Murillo and R. A. Walton), Springer US, **2005**, pp. 591-632; h) C. J. Welch, Q. Tu, T. Wang, C. Raab, P. Wang, X. Jia, X. Bu, D. Bykowski, B. Hohenstaufen and M. P. Doyle, *Adv. Synth. Catal.* **2006**, *348*, 821-825.

[41] O. P. H. Vaughan, G. Kyriakou, N. Macleod, M. Tikhov and R. M. Lambert, *J. Catal.* **2005**, *236*, 401-404.

[42] K. Kunz, U. Scholz and D. Ganzer, *Synlett* **2003**, *2003*, 2428-2439.

[43] M. Aslam, G. Gopakumar, T. L. Shoba, I. S. Mulla, K. Vijayamohanan, S. K. Kulkarni, J. Urban and W. Vogel, *J. Colloid Interface Sci.* **2002**, *255*, 79-90.

[44] P. Y. S. Lam, C. G. Clark, S. Saubern, J. Adams, M. P. Winters, D. M. T. Chan and A. Combs, *Tetrahedron Lett.* **1998**, *39*, 2941-2944.

[45] a) E. D. Cabanillas, E. E. Pasqualini, M. López, D. Cirilo, J. Desimoni and R. C. Mercader, *Hyperfine Interactions* **2001**, *134*, 179-185; b) J. Guo, C. Dong, H. Gao, H. H. Wen, L. H. Yang, F. Zeng and H. Chen, *Chin. Phys. B* **2008**, *17*, 1124-1129.

[46] a) B. H. P. van de Kruijs, M. H. C. L. Dressen, J. Meuldijk, J. A. J. M. Vekemans and L. A. Hulshof, *Org. Biomol. Chem.* **2010**, *8*, 1688-1694; b) W. Chen, B. Gutmann and C. O. Kappe, *ChemistryOpen* **2012**, *1*, 39-48.

[47] A. K. Khanra, L. C. Pathak and M. M. Godkhindi, *J. Mater. Sci.* **2007**, *42*, 872-877.

[48] B. K. Park, S. Jeong, D. Kim, J. Moon, S. Lim and J. S. Kim, *J. Colloid Interface Sci.* **2007**, *311*, 417-424.

[49] E. Díaz, R. B. Valenciano and I. A. Katime, *J. App. Polymer Sci.* **2004**, *93*, 1512-1518.

[50] V. B. Chernogorenko and S. T. Tasybaeva, *Russ. J. Appl. Chem* **1995**, *68*, 461-464.

[51] J. G. Yang, Y. L. Zhou, T. Okamoto, R. Ichino and M. Okido, *Surf. Eng.* **2007**, *23*, 448-452.

[52] T. D. Daff, D. Costa, I. Lisiecki and N. H. de Leeuw, *J. Phys. Chem. C* **2009**, *113*, 15714-15722.

[53] C.-H. Chen, T. Yamaguchi, K.-i. Sugawara and K. Koga, *J. Phys. Chem. B* **2005**, *109*, 20669-20672.

[54] V. Engels, D. A. Jefferson, F. Benaskar, P. C. Thüne, A. Berenguer-Murcia, B. F. G. Johnson and A. E. H. Wheatley, *Nanotechnology* **2011**, *22*, 205701.

[55] Y. Li and M. A. El-Sayed, *J. Phys. Chem. B* **2001**, *105*, 8938-8943.

[56] M. Cokoja, H. Parala, M. K. Schroter, A. Birkner, M. W. E. van den Berg, K. V. Klementiev, W. Grunert and R. A. Fischer, *J. Mater. Chem.* **2006**, *16*, 2420-2428.

[57] M. Bühl, F. Terstegen, F. Löffler, B. Meynhardt, S. Kierse, M. Müller, C. Näther and U. Lüning, *Eur. J. Org. Chem.* **2001**, *2001*, 2151-2160.

[58] E. V. Rebrov, A. Berenguer-Murcia, H. E. Skelton, B. F. G. Johnson, A. E. H. Wheatley and J. C. Schouten, *Lab on a Chip* **2009**, *9*, 503-506.

Chapter 4

Novel Cu-based catalysts supported on TiO_2 films for Ullmann S_NAr-type C-O coupling reactions

This chapter has been submitted as:
F. Benaskar, V. Engels, E.V. Rebrov, N.G. Patil, J. Meuldijk, P.C. Thüne, P.C.M.M. Magusin, B. Mezari, V. Hessel, L.A. Hulshof, E.J.M. Hensen, A.E.H. Wheatley, J.C. Schouten (2012). New Cu-based catalysts supported on TiO_2 films for Ullmann SnAr-type C-O coupling reactions. *Chem. – Eur. J.*, *18*(6), 1800-1810. [1]

F. Benaskar, V. Degirmenci, E.V. Rebrov, P. Abdulkin, N.G. Patil, V. Hessel, L.A. Hulshof, E.J.M. Hensen, A.E.H. Wheatley, J.C. Schouten (2012). X-ray absorption spectroscopy on the role of Zn as co-promoter of a heterogeneous CuZn/TiO_2 catalyst in Ullmann-type C-O coupling reactions. *To be submitted*. [2]

Abstract

Novel routes for the preparation of highly active TiO_2 supported Cu and CuZn catalysts have been developed for C-O coupling reactions. Slurries of a titania precursor were dip-coated onto glass beads to obtain either structured mesoporous or non-porous titania thin films. The Cu and CuZn nanoparticles, synthesized using a reduction by solvent method, were deposited onto calcined films to obtain a Cu-loading of 2 wt%. The catalysts were characterized by inductively coupled plasma (ICP) spectroscopy, temperature-programmed oxidation/reduction (TPO/TPR) techniques, ^{63}Cu nuclear magnetic resonance (NMR) spectroscopy, X-ray diffraction (XRD), scanning and transmission electron microscopy (STEM-EDX) and X-ray photo-electron spectroscopy (XPS). A study based on synchrotron X-ray

absorption spectroscopy (XAS), using various Cu_xZn_y/TiO_2 catalysts provided more detailed information on the Cu and Zn interactions. The fresh and spent catalysts were analyzed in hydrogen from 25 ^oC to 375 ^oC for 12 h and, then, after reoxidation in an air-flow at 140 ^oC using a micro-reactor cell. In this way, the role of Zn as "oxide-scavenger" and, consequently, the retention of the Cu^0 oxidation state were studied. The activity and stability of the catalysts obtained have been studied in the C-O Ullmann coupling of 4-chloropyridine and potassium phenolate. The titania supported catalysts retained catalyst activity for up to 12 h. However, catalyst deactivation was observed for longer operation times due to oxidation of the Cu nanoparticles. The oxidation rate could be significantly reduced over the $CuZn/TiO_2$ catalytic films due to the presence of Zn. The 4-phenoxypyridine yield was 64% on Cu/nonporous TiO_2 at 120 ºC. The highest product yield of 84% was obtained on Cu/mesoporous TiO_2 at 140 °C, corresponding to an initial reaction rate of 104 mmol/g_{cat}/s. The apparent activation energy using the Cu/mesoporous TiO_2 catalyst was found to be 144 ±5 kJ/mol, close to that for unsupported CuZn nanoparticles (123 ±3 kJ/mol) and almost twice the value observed for the catalysts deposited onto the non-porous TiO_2 support (75 ±2 kJ/mol). Moreover, the turnover frequencies provided a clear "Volcano plot" as function of the Cu_x/Zn_y ratio of the mesoporous TiO_2 supported catalyst with a maximum found at $Cu_{0.5}Zn_{0.5}$. X-ray absorption near-edge structure spectra **(**XANES) were used to examine the oxidation state and from extended X-ray absorption fine-structure spectroscopy (EXAFS) analysis the interatomic distances and coordination in the catalyst were studied during operation. These results demonstrated additional evidence of a sacrificial anode effect of Zn-promoted Cu catalysis in the C-O coupling reaction.

4.1 Introduction

Nano-structured metal catalysts in C-O and C-C coupling reactions. The employment of nano-structured metal catalysts for fine-chemicals synthesis has been the subject of increasing research efforts during the past decade [3]. The ultra-high surface area available is a major contributor to the increased reactivity in the particle size range of 5-10 nm. However for nanocluster sizes < 50 nm, these effects are accompanied by a tunable electron band structure [4]. The exploitation of such properties promises the applicability of metals and polymetallic nanoparticles where particle lattice strain [5] and surface energy [6] lead to an entirely changed metal-substrate interaction for both mono- and poly-metallic clusters in comparison to bulk systems [7]. In this vein, we have recently published a novel liquid-type synthetic route to obtain chemically stable Cu^0 nanocatalysts [8]. We have shown that both monometallic Cu and bimetallic CuSn or CuZn catalysts demonstrate excellent yields of up to 90% in 120 min in the C-O cross-coupling of phenoxide and 4-chloropyridine (see Scheme 1) [9].

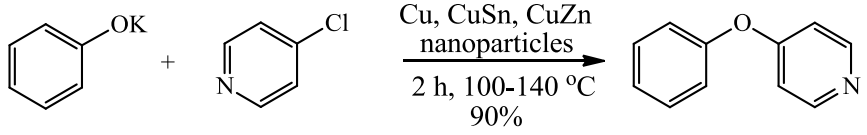

Scheme 4.1. The Cu-catalyzed Ullmann ether synthesis towards phenoxypyridine.

Commonly, substantially more expensive bromo- and iodo-substituted aromatics have hitherto been required for efficient coupling to take place [10].

The synthesis of diphenyl ether from phenol and bromobenzene using a copper catalyst was mainly developed by Ullmann [11], while Goldberg presented initial work on catalytic arylamination using bromobenzene/2-aminobenzoic acid and amidation using bromobenzene/2-phenolamide (see Scheme 2) [12].

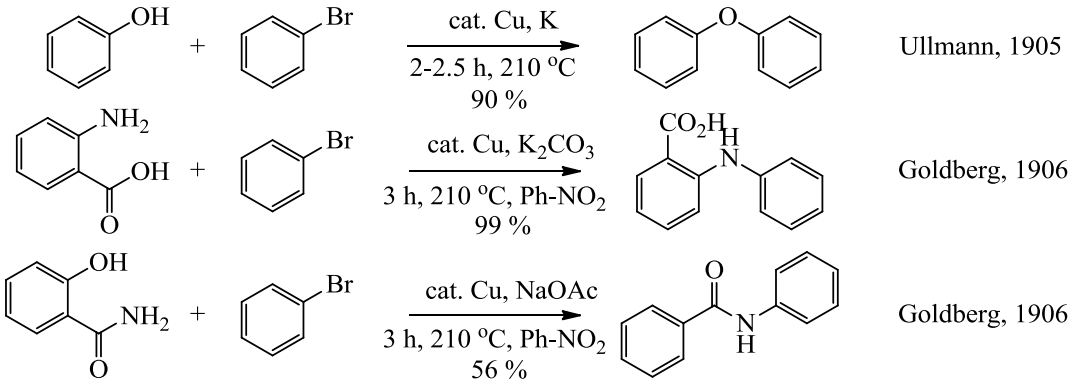

Scheme 4.2. Examples of the Ullmann ether synthesis, Ullmann-Goldberg amination, and Goldberg amidation [22, 26].

Advances in the field of Ullmann and Goldberg chemistry provided various industrial applications, *e.g.* the production of intermediates in pharmaceuticals, agrochemicals, fine-chemicals and polymers [13]. Other industrially interesting applications are the arylation reactions of amines and alcohols under relatively mild reaction conditions, which conventionally were performed in batch-type processes [14]. Coupling reactions in organic chemistry are typically performed using a palladium-based catalyst and since their discovery during the 1970s have received intense attention [15], which led to the Nobel Prize award in 2010.

Nevertheless, the cost related to palladium has driven research towards copper(II) acetate catalyzed coupling reactions involving organometals such as Pb [16], Si [17], Sn [18], but also organoborons and iodonium salts as arylating agents [19]. The very high specific surface area, uniform nano-pore size distribution, chemical stability and precisely adjusted pore morphology, make mesoporous materials very useful as support matrices for metal and metal oxide nanoparticles (NPs) [20]. Moreover, the strong interactions between nano-structured titania and metal NPs, such as Au, Ag and Pt, demonstrated to prevent aggregation and improve the dispersion of NPs [21].

Cu-catalyzed Ullmann coupling reactions. Copper catalysis in organic reactions is mostly known from Ullmann-type homo- and cross-coupling reactions of aromatic compounds. However, hardly any progress has yet been made in terms of rendering these heterogeneous catalysts sustainable in a continuous process. Only a few examples were reported in the literature where Cu nanoparticles have been employed as catalysts in Ullmann reactions. In 2007, Kidwai et al. reported the use of Cu^0 nanoparticles in the coupling of phenol and iodobenzene at 50-60 °C [22].

Following the achievement of a 95% yield in the first run (4 h) catalyst recycling by centrifugation allowed yields of up to 65% to be maintained in the 4th run (12 h), with highest reaction rates being observed for a mean particle size of 20 ± 2 nm. However, inefficient catalyst recycling limited the applicability of this method since a significant drop in catalyst performance was reported after four experimental cycles. Kim *et al.* studied a Cu_2O nanocube catalyst with a mean cube size of 45 ± 3 nm [23]. Catalyst recovery by centrifugation resulted in excellent-to-quantitative yields after 4 runs, with particle morphology remaining largely unchanged. However, the potential of this method was restricted due to high temperatures (T >150 ºC) requiring high boiling point solvents, expensive bases, such as Cs_2CO_3, and complications related to catalyst recovery. To circumvent catalyst separation obstacles, Cu nanoparticles can be deposited either onto a magnetic carrier or a structured support.

Investigations of the Ullmann syntheses of diazodiarylethers on structured supports have been reported by Knepper *et al.*, who used triazene-functionalized poly(styrene) resins to couple various substituted phenols with yields of up to 95% [24]. However, deposition of the active metals onto inorganic supports with a relatively low specific surface area is maintained at low metal loadings to minimize particle sintering. Additionally, loss of active metal due to leaching may occur during operation of the catalytic reactor.

Development of CuZn-based catalyst in chemical synthesis. The methanol synthesis has undoubtedly been pioneering research where a Cu catalyst was supported onto ZnO because of its stabilizing and even activating effects [25]. Since the first commercially operated process in 1923 (BASF) and the Cu-based catalyst establishment by ICI (Imperial Chemical Industries) in the 1960s, the Cu-ZnO based catalyst systems have been intensively investigated in the form of a bulk ZnO support [25a]. However, the understanding on how nano-confinement of catalyst in the support could be used to influence the catalytic reactivity, is still at the start. In the earlier literature, the ZnO component appeared to act as an effective electronic modifier of the Cu activity in steam reforming [26]. The strong metal-support interaction (SMSI) proved to be responsible for this electronic adaptation in CO adsorption as reported by Naumann *et al.* [27], acting as a strong catalysis promoter [28]. The SMSI is mechanistically governed by adjustment of the supporting oxide's vacuum energy levels with respect to the supported metal [29].

The local charge redistribution, responsible for creating the energy barrier, proved to be directly responsible for interfacial reactivity as demonstrated by Brillson [30]. Therefore, shifting the support bandgap through nanodimensional confinement of the short axis, it is theoretically possible to control the realignment of energy levels. Although it is currently well accepted that the methanol synthesis reaction is mainly catalyzed by species of metallic copper supported on a defected ZnO phase [25c-f, 25h-k, 31], also a Cu-C species dissolved in, or supported on, the ZnO phase has been reported as the active site [25b-d, 32]. Reports on Cu/SiO_2 demonstrated catalyst activity, being orders of magnitude lower as compared to generally reported activities over Cu/ZnO catalysts [25g, 33]. It was interpreted that

the zinc component is essential to stabilize the copper oxidation state, retaining its catalytic activity not only in the methanol synthesis, but also for liquid-phase Ullmann-type C-O coupling reactions [1, 13b]. The inseparable and vital interaction of Cu and ZnO as active metal and support oxide, respectively, led to extensive interest in the atomic interface between Cu and ZnO. As a result, nanoparticles are applied as heterogeneous catalysts in the methanol synthesis to acquire atomic structural information of Cu-Zn and Cu-ZnO particles.

Hambrock *et al.* synthesized Cu-Zn (so called "nanobrass") colloidal nanoparticles by a thermal decomposition method from [$Cu(OCH(Me)CH_2$-$NMe_2)_2$] and Et_2Zn in hexadecylamine [34]. Various catalyst characterization techniques have shown that the presence of Cu and Zn at the surface of nanoparticles differs significantly from the chemical precursor's ratio. Also, it was shown that the nanoparticle mean sizes and shapes appear to be strongly dependent on the loading of both Cu and Zn and the Cu to Zn ratio, respectively. Selected Area Electron Diffraction (SAED) measurements provided evidence on the oxidative stability of Cu at already low concentrations of Zn (5% with respect to Cu). At an increased Zn-fraction ($Cu_{0.7}Zn_{0.3}$), it was observed that a Cu-Zn alloy shell is formed around a Cu-core. More recently, it was reported that red-violet Cu-Zn nano-alloys could be synthesized by co-hydrogenolysis of CpCu(PMe3) and Cp*Zn dissolved in mesitylene, which was previously reported only for the synthesis of Cu-Al colloids [35]. Using a combination of TEM, EDX, SAED, EXAFS, powder XRD, and UV-vis spectroscopy, various colloidal nanoparticle structures could be distinguished and characterized. All bimetallic Cu_xZn_y compositions showed preferential oxidation of the Zn atoms while maintaining copper at its metallic state. However, simultaneous formation of core-shell particles (consisting of a ZnO-shell surrounding a gradually Zn-depleting Cu/Zn-core) limited access of the reactants to the active Cu-core atoms.

In this chapter, novel synthesis protocols to obtain supported Cu and CuZn bimetallic catalysts on structured titania supports coated onto glass beads are described. The catalytic activity and stability of the Cu and bimetallic CuZn catalysts supported onto mesoporous and non-porous TiO_2 are compared for the Ullmann-type C-O coupling of potassium phenolate and 4-chloropyridine to give 4-phenoxypyridine. Catalyst activity measurements and catalyst characterization using ^{63}Cu-NMR, (S)TEM, XRD, XPS and XAS techniques are discussed, aimed at establishing the role of zinc and an optimal Cu-Zn ratio in relation to the oxidative stability of copper and at understanding the Cu and Zn atomic interaction. In particular, *in-situ* X-ray absorption spectroscopy (XAS) was used to understand the Cu and Zn atomic interaction. The Zn atoms could serve as oxide-scavengers, maintaining the activity of copper [1, 36], in line with previous results in the Cu/ZnO-catalyzed methanol synthesis [37].

4.2 Experimental

4.2.1 Catalyst preparation

Synthesis of catalyst nanoparticles. A polyvinylpyrrolidone (M_W(average) = 40,000) stabilized suspension of Cu^0 and CuZn (2.5 mg_{Cu}/mL) nanoparticles was prepared as described in chapter 3 [13b].

Synthesis of non-porous titania support. A total of 20 g of glass beads (E&R Chemicals & Equipment B.V., sieved diameter 200-300 μm) was cleaned using acetone and dispersed in 200 mL of dry isopropanol in a rotary evaporator in a nitrogen atmosphere. The dry beads were stirred overnight in aqueous sulfuric acid (2.5 M, Sigma-Aldrich) prior to support coating. A total amount of 0.75 g of titanium(IV) tetra-ethoxide ($Ti(OEt)_4$, 99.99 wt%, Sigma-Aldrich) mixed with an aqueous HNO_3 solution (65 wt%, Fluka) in isopropanol was added to the dry glass beads and vigorously stirred for 1 h. The isopropanol was then removed under reduced pressure at 60 ºC. The resulting coated beads were dried overnight in a stove at 80 ºC and subsequently calcined at 600 ºC for 8 h (10 °C/min).

Mesoporous titania support synthesis. Glass bead preparation was done similarly to that described for the non-porous titania support. A titania-precursor sol with a composition of 1 $Ti(OEt)_4$: 0.006 Pluronic : 40 ethanol : 1.3 H_2O : 0.1 trifluoroacetic acid was prepared as described elsewhere [38]. Pluronic F127, ($EO_{100}PO_{65}EO_{100}$, EO = ethylene oxide, PO = propylene oxide, BASF) was used as surfactant. After dissolution of the surfactant in ethanol, followed by the addition of water and trifluoroacetic acid, the titanium(IV) tetraisopropoxide ($Ti(O^iPr)_4$, 99.99%, Fluka) was added dropwise while stirring. The resulting mixture was left to age for 24 h after a stirring period of 8 h at room temperature. A desired amount of the solution was slowly added to a glass-filter vessel filled with an observable single layer of glass beads. The solution withdrawal rate was set at 2 mm/min using a flow controlled dip-coater. The resulting films were maintained in a glove box at a relative humidity of 80% for 30 h before the residual surfactant was removed by burning at 250 ºC for 4 h. Finally the films were calcined at 380 ºC (heating rate of 1 ºC/min) and a residual pressure of 10 mbar for 8 h.

Catalyst impregnation onto titania support. The titania films were impregnated with a colloidal suspension (metal concentration: 0.25 mg/mL) of Cu or CuZn nanoparticles. The impregnated films were dried at 80 °C. This procedure was repeated twice. Subsequently, the coated beads were calcined for 2 h at 450 °C (unless otherwise mentioned) after a heating rate of 1 °C/min firstly at a residual pressure of 10 mbar and later at atmospheric pressure to remove residual organic compounds. Finally, the catalyst was reduced for 6 h under a hydrogen flow of 1 mL/min (4 vol.% H_2 in N_2) at 350 °C (10 °C/min).

4.2.2 Catalyst characterization

X-ray diffraction measurements (XRD). XRD spectra of PVP-protected copper NPs were recorded on a Röntgen PW3040/60 XPert PRO powder X-ray diffractometer with a high resolution PW3373/00 CuLFF (unmonochromated) tube at λ=1.5404 Å (CuKα) in the range 2Θ = 5-80° and with scanning speed of 0.23°/min (CuZn) and 0.09°/min (Cu). The powder samples were prepared by solvent evaporation from the colloidal suspensions deposited on a glass plate (PW3071/60Bracket).

X-ray photoelectron spectroscopy (XPS). XPS data were obtained with a Kratos AXIS Ultra spectrometer equipped with a monochromatic Al Kα X-ray source and a delay-line detector (DLD). Spectra were obtained using an aluminium anode (Al Kα = 1486.6 eV) operating at 150 W. For survey and region scans, constant pass energies of 160 eV and 40 eV were used, respectively. The background pressure was 2 x 10^{-9} mbar. Samples were prepared in a glovebox (< 10 ppm O_2) and transported in a closed sample holder for oxygen-free XPS analysis.

High-resolution transmission electron microscopy (HR-TEM). HR-TEM images were recorded using a FEI Tecnai G2 Sphera transmission electron microscope at an acceleration voltage of 200 kV. For TEM analyses, 250 mg of the solid catalyst was pulverized and suspended in ethanol. A volume of 30 µL of the suspension was dip-coated onto a 200 mesh molybdenum grid (carbon holey film) and subsequently dried at ambient temperature and pressure. Support surface morphology was analyzed on a FEI Quanta series FEG 3D G2 SEM using an acceleration voltage of 5 kV and magnifications of between 5,000x and 100,000x, providing a maximum lateral resolution of 50 nm^2. Catalyst elemental compositions were elucidated by EDX analysis at a spot size of 50 nm^2 at an interaction-volume of 100 µm.

^{63}Cu nuclear magnetic resonance spectroscopy (NMR). Magic-angle-spinning (MAS) ^{63}Cu-NMR spectra were recorded at room temperature on a Bruker DMX500 spectrometer, operating at a frequency of 132.57 MHz. A 4-mm MAS probe head was used with a sample rotation rate of 6 kHz. To suppress baseline artifacts resulting from probe ringing, ^{63}Cu-NMR spectra were recorded by use of a three-pulse pulse sequence $\theta_{+\square x}$ - $\theta_{\pm x}$-τ- θ_{ψ} - d1 with short pulses of 1-µs pulse length (corresponding to an excitation angle of 18°), an interpulse delay of 0.1 ms and an interscan delay of 100 ms. Typically 8192 scans were recorded. The radio-frequency carrier position was chosen close to the resonance frequency of microcrystalline copper(I) chloride powder. Following the convention in several solid-state ^{63,65}Cu-NMR studies [39], solid CuCl was also used as external reference for the chemical shift 0 ppm. The ^{63}Cu-NMR spectrum of the NMR coil alone (without sample) consisted of a single 90-ppm wide signal (at half height) without MAS sidebands, and was subtracted from the MAS NMR spectra of the catalysts as background correction. The fact that the MAS NMR signal of Cu^0 in the fresh catalyst was narrower and had spinning sidebands, made an unambiguous subtraction possible.

Inductively coupled plasma spectroscopy (ICP). The metal loading was determined by ICP-OES on a SPECTRO CIROS^{CCD} spectrometer.
Temperature programmed reduction/oxidation (TPR/O). For temperature-programmed oxidation a quartz glass tube (outer diameter: 6 mm, inner diameter: 3 mm) was filled with a known amount of supported catalyst, sealed and pre-treated in a convection oven under hydrogen flow for 6 h at 350 °C. After cooling, an oxygen flow (4 vol% in He) was applied at a flow rate of 8 mL/min and heated to 300 °C at a rate of 1 °C/min. During the temperature desorption step, a hydrogen flow (4 vol% in N_2) was passed over the catalyst bed from RT to 400 ºC at a rate of 10 ºC/min. A commercial copper catalyst (BTS-catalyst 30wt% CuO/SiO_2, 125-250 μm, R3-11, lot nr. 0849, BASF) was used as reference standard.

Extended X-ray absorption fine-structure (EXAFS) spectroscopy experiments. X-ray absorption data were collected on beamline DUBBLE (BM26A) at the European Synchrotron Radiation Facility (ESRF, Grenoble, France), using an operating beam of 6 GeV, 200 mA, 2 X 1/3 filling mode. A Si (111) double-crystal monochromator supplemented with a focusing Si mirror to filter off higher harmonics was applied (see Figure 1).

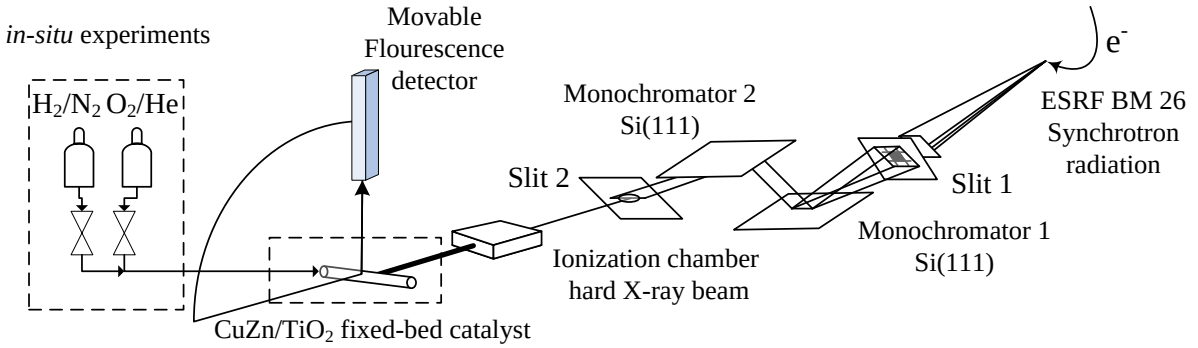

Figure 4.1. XAS cell setup for *in-situ* and *ex-situ* measurements over the $CuZn/TiO_2$ catalyst.

XAS signals could only be measured in the fluorescence mode due to the low Cu and Zn-loadings (with respect to Ti) at 8978 eV and 9658 eV for the Cu K-edge and Zn K-edge, respectively. A copper film (Aldrich, Cu foil thickness 1.0 mm, 99.999% trace metals basis) and a zinc film (Aldrich, Zn foil, thickness 1.0 mm, 99.99% trace metals basis) were used as reference samples. The ionization chambers were filled with an Ar/He gas mixture. XANES data was continuously recorded during the reduction (6 vol% H_2 in N_2) and oxidation (2 vol% O_2 in He) experiments, whereas the EXAFS spectra were recorded only for the fresh catalyst and after treatment. For the spent catalyst samples of the Ullmann reaction, both XANES and EXAFS spectra were recorded. The Cu and Zn K-edges were collected separately, maintaining the reactor cell under inert conditions (sealed and stored in a N_2 box). XANES acquisition times of both Cu and Zn were kept at 40 min whereas EXAFS measurements were done for 120 min at an acquisition frequency of 5 to 25 s/measurement.

The XAS data was initially collected and processed using a VIPER software package [40]. Pre-edge background was subtracted and normalized by fitting a linear polynomial to the pre-edge section and square-spline functions to the post-edge section of the acquired XAS spectrum. Further spectral alterations were done in the EXCURVE package, using Hedin-Lundqvist potentials for phase shifts and backscattering factors by k^3 weighting in the range of 2 to 13 $Å^{-1}$. The refined data was consecutively fitted in IFEFFIT (Athena, Arthemis and Hephaestus) to further obtain the quantitative fitting parameters. XAS measurements were performed in a temperature-controlled micro-reactor cell. The appropriate catalyst amount was mixed, grinded and packed with boron nitride in rectangular pellets (2x4 cm) before being placed in a sample holder. For the XAS oxidation experiments, the reactor cell was heated from 25 ^oC to 300 ^oC and for the reduction experiments, from 25 ^oC to 400 ^oC, in accordance to the TPO/R-experiments). Further XAS samples were done in a CAPTON sealed cell (for detailed information see reference [2]).

4.2.3 Catalytic activity measurements

Potassium phenolate and 4-chloropyridine were separately prepared as described in chapter 3 [13b]. A mixture containing an accurate amount of 4-chloropyridine (0.75 mol), potassium phenolate (0.90 mol) and 18-crown-6 ether as appropriate (*ca.* 0.01 mol equiv. with respect to phenolate), was stirred in a baffled glass reactor (75 mL) loaded with DMA (15-25 mL) at 45 °C until dissolution was complete. After heating the reaction mixture to the desired temperature, an appropriate amount of catalyst was added to the reactor which was mechanically stirred at 500 or 1500 rpm. The procedure was carried out in an argon atmosphere and the resulting slurry was heated. Due to the different synthetic protocols different copper loadings resulted. Therefore the amount of catalyst in the reactor was adjusted for each catalyst type to provide similar Cu metal loadings. The solvent temperature during the reaction was measured using a thermocouple. The yield of 4-phenoxypyridine was determined by recording ^{1}H-NMR spectra of reaction aliquots. The peaks data were compared with literature data and with previously acquired, qualitative GC-MS measurements. Catalyst surface area, pore sizes and metal dispersion were determined by physisorption and chemisorption techniques (see Supporting Information in reference [1]).

The catalytic activity is presented in terms of amount of the reaction product obtained per unit time per catalyst weight (not accounting for the weight of glass beads). The initial reaction rate was determined from the product concentration after a reaction time of 5 min (Equation 1).

$$r_{init} = \frac{C^{\Delta t}{}_P \times V_L}{\Delta t \times w_{cat}} \qquad \textbf{Equation 4.1}$$

$C^{\Delta t}{}_P$ is the concentration of 4-phenoxypyridine after reaction time of 5 min, V_L is the solvent volume, Δt is the time interval (5 min), and w is the catalyst weight. The

catalytic activity was measured for the three catalyst types, *e.g.* the unsupported CuZn nanoparticles (CuZn NPs), Cu supported on non-porous titania (Cu/np-TiO_2) and Cu supported on structured mesoporous titania (Cu/meso-TiO_2). The catalyst deactivation was studied in a fixed-bed reactor at different processing times.

Catalyst pre-treatment. Prior to experiments, the catalysts were pretreated in a flow of *N*,*N*-dimethylacetamide (5 mL/min) for 4, 8 or 12 h (the same duration as the subsequent experiment). In catalyst stability experiments, potassium phenolate was dissolved in the solvent. In the oxidation stability experiments, 4-chloropyridine was added to the solvent at 140 °C. Details on the experimental setup are provided in the Supporting Information of reference [1].

Derivation of kinetic model. Experiments were carried out over the temperature range 110-140 ^{o}C using metallic copper (99%, Aldrich) as described in chapter 2. The catalyst loading (1-10 mol% with respect to 4-chloropyridine), initial reactant concentrations (potassium phenoxide 0.3-0.75 mol/L and 4-chloropyridine 0.2-0.5 mol/L), initial product concentrations (4-phenoxypyridine 0.05-0.25 mol/L) and the crown ether concentration (18-crown-6 ether, 1-10 mol% with respect to potassium phenoxide) were varied. The mole ratios of potassium phenoxide and 4-chloropyridne were varied from 0.5 to 4 [41].

4.3 Results and discussion

4.3.1 Catalyst activity

In this chapter, various highly active Cu-based heterogeneous catalysts, as replacements for common homogeneous catalysts that use expensive ligands for C-O coupling reactions, are discussed. Previous studies utilizing bimetallic Cu^0-based catalysts showed yields, much higher than those obtained using monometallic catalysts [13b]. A list of catalysts, metal loadings and experimental conditions is given in Table 1. Prior to the experiments reported, catalysts were pre-conditioned in a solvent flow for 12 h.

Table 4.1. Metal loadings for different supported systems determined by ICP-OES.

Catalyst	Conditions	Cu-loading (wt%)[b]	Amount support (wt%)[c]	Overall Cu-loading (wt%)[d]	Support pore size (nm)
Cu/ meso-TiO_2	Pre-conditioned	2.0	2.8	0.60	24 ± 4
	Spent[a]	1.8	2.1	0.04	
Cu/ np-TiO_2	Pre-conditioned	11.5	0.21	0.02	4.9 ± 0.8
	Spent[a]	2.0	0.03	0.00	
$Cu_{66}Zn_{34}$/ meso-TiO_2	Pre-conditioned	3.8	2.0	0.08[e]	26 ± 5

[a] 12-h flow experiment as described in the experimental section,
[b] with respect to Ti after pre-conditioning with the reaction mixture,
[c] weight percentage of films on glass beads,
[d] total Cu/bead ratio,
[e] total copper content.

4.3.2 Cu/mesoporous TiO_2

The synthesis of 4-phenoxypyridine starting from potassium phenoxide and 4-chloropyridine (see reaction scheme in Figure 2) using the Cu/meso-TiO_2 catalyst (0.2 mol% Cu with respect to 4-chloropyridine) demonstrated increased yields as compared to previously published results [13b]. A considerable amount of product (60%) was present in the reaction mixture, already after 5 min reaction time at 140 ºC. However, the maximum yield was similar to that recently observed for CuZn NPs. It appears that strong product adsorption on the catalyst surface severely limits the reaction rate at longer reaction times. The Cu-oxidation state was determined by solid-state ^{63}Cu-NMR spectroscopy. However, the amounts of Cu^0 and Cu^{1+} could not be calculated due to a considerable contribution from the background. Nevertheless, a qualitative signal subtraction was made utilizing additional spinning side band signals from the catalyst sample.

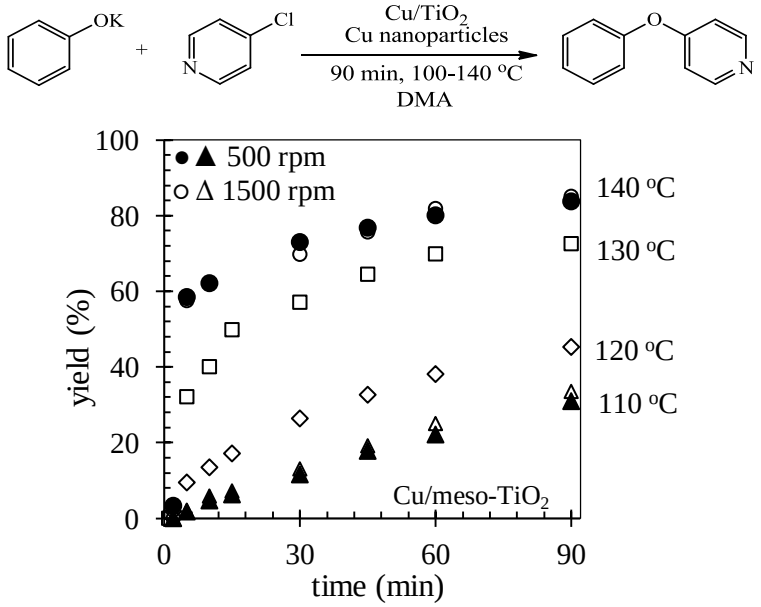

Figure 4.2. The Ullmann C-O coupling as carried out using a heterogeneous Cu/meso-TiO_2 catalyst. Yields obtained from Cu/meso-TiO_2 using C_{cat}=0.2 mol% Cu with respect to 4-chloropyridine at different temperatures and stirring rates. Initial concentrations of potassium phenolate and 4-chloropyridine were 0.36 and 0.3 mol/L, respectively.

Figure 3 shows the magic-angle-spinning (MAS) ^{63}Cu-NMR spectra of fresh and spent catalyst together with the spectra of solid copper(I) chloride, metallic copper (from the NMR coil), and solid sodium sulfate, for comparison. Copper has two NMR-active isotopes ^{63}Cu and ^{65}Cu. ^{63}Cu-NMR was chosen because of the higher natural abundance of ^{63}Cu, and, therefore, higher NMR sensitivity. Like ^{65}Cu, ^{63}Cu nuclei have spin 3/2 and interact strongly with local electric field gradients at the positions of the nuclei arising from their asymmetric coordination in copper(I) compounds. The latter can cause large quadrupolar line broadening, which cannot be averaged out by MAS. This is the reason why there are relatively few solid-state ^{63,65}Cu-NMR studies and most of these have been carried out without sample rotation [39].

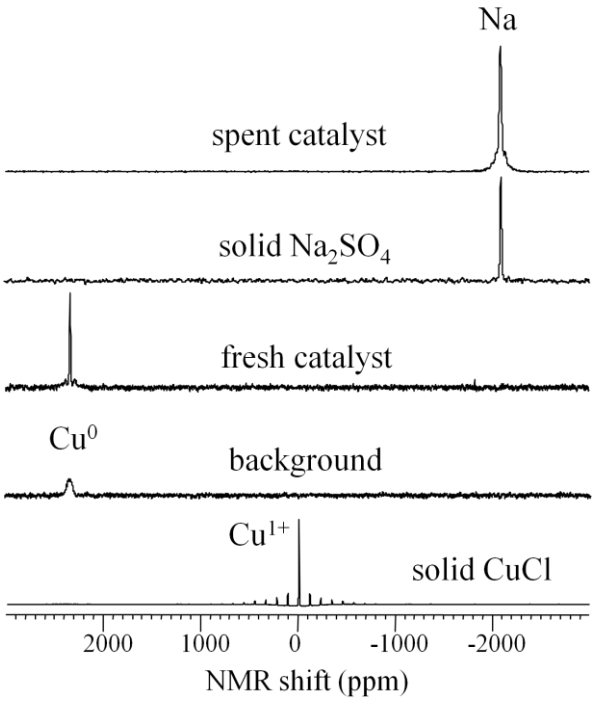

Figure 4.3. MAS ^{63}Cu-NMR spectra of spent and fresh Cu/meso-TiO_2, respectively, before and after the reaction, as well as the the spectra of solid CuCl and Na_2SO_4 and the background spectrum of metallic copper in the NMR coil, for comparison. Except the latter, all spectra are background corrected. ^{23}Na and ^{63}Cu-NMR frequencies differ by only 2×10^3 ppm, which permits ^{23}Na and ^{63}Cu-NMR signals to be recorded in a combined manner.

In contrast to many copper(I) compounds, the MAS ^{63}Cu-NMR signal of Cu^0 in metallic copper is relatively narrow, as a result of the absence of electric field gradients at the copper-atom positions in the fcc crystal structure. In the present study we have, therefore, applied magic-angle-spinning ^{63}Cu-NMR as a facile tool to monitor the fate of metallic copper in the catalyst particles. The spectrum of the fresh catalyst contains a single signal at the same position as the background signal of copper in the NMR coil at 2334 ppm downfield with respect to the NMR frequency of CuCl (Figure 3). This large chemical shift is a so-called Knight shift caused by the interaction with the conduction electrons in copper metal. In the ^{63}Cu-NMR spectrum of the spent catalyst Cu/meso-TiO_2, no metallic copper signal is visible. Since elemental analysis indicates that the spent catalyst still contains copper (see Table 1), Cu^0 has apparently been converted into Cu^{1+} or Cu^{2+} during a 4-h experimental run. Copper(II) compounds are paramagnetic and, hence, ^{63,65}Cu-is NMR invisible.

In principle, copper(I) compounds are NMR visible, but their usually large quadrupolar linewidth generally prevents straightforward detection by use of MAS NMR. The spent Cu/meso-TiO_2 does show a single signal at -2081 ppm. This is actually the ^{23}Na-NMR signal of a sodium containing impurity [42]. The observed ^{23}Na-NMR signal position is -13 ppm with respect to solid NaCl, and coincides with that of solid Na_2SO_4 (Figure 3). The latter is used as a drying agent in the synthesis of 4-chloropyridine (see Experimental Section of reference [13b]), one of the reactants in the catalytic test reaction. Figures 4a and 4b show a porous titania

structure from SEM analysis before and after copper nanoparticle deposition, respectively. Importantly, the porous titania structure remained essentially unaffected, even after a second calcination step subsequent to catalyst deposition.

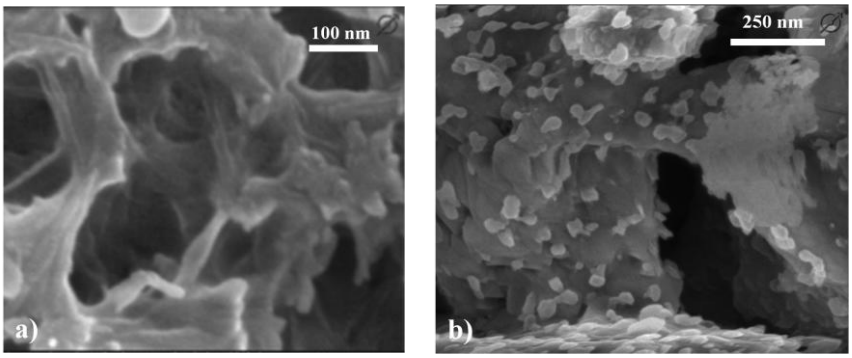

Figure 4.4. SEM image of silica beads coated with mesoporous titania (Cu/meso-TiO_2) a) before and b) after catalyst deposition (magnification 150,000).

EDX spectra were taken from the regions shown in Figures 4a and 4b. Data confirmed the abundant coverage of copper upon catalyst deposition. The increased copper loading on mesoporous titania was concluded to be the case based on the integral ratio of the Cu Kβ1 and Ti Kβ1 emission lines, which were 0.42 and 0.25 for mesoporous (2.1 wt%) and non-porous titania supports (0.2 wt%), respectively (see Supporting Information of reference [1] and Table 1). Figure 5a clearly reveals a highly porous titania matrix with observed pore sizes of 5-50 nm proving a mesoporous support structure for this catalyst. The average pore size was determined to be 24±4 nm for *ca.* 60% of the cross-sectional surface area by HRTEM, whereon the Cu and CuZn nanoparticles were deposited (see Figure 5b). The average particle size, based on a count of 200 particles, was found to be 7.0 ±0.6 nm and the distribution is shown in Figure 5c. The presence of Cu, Zn and Ti in the area shown in the above HRTEM images is confirmed by EDX analysis. The Cu/Zn molar ratio is 2.0. From the analysis of five spectra, over a surface of 500 nm^2 the Cu/Ti molar ratio was 2.7 ± 0.2, which is close to the ratio of 2.5 found from a scan over a larger 250 μm^2 area, confirming a uniform catalyst loading on the support (see Table 1).

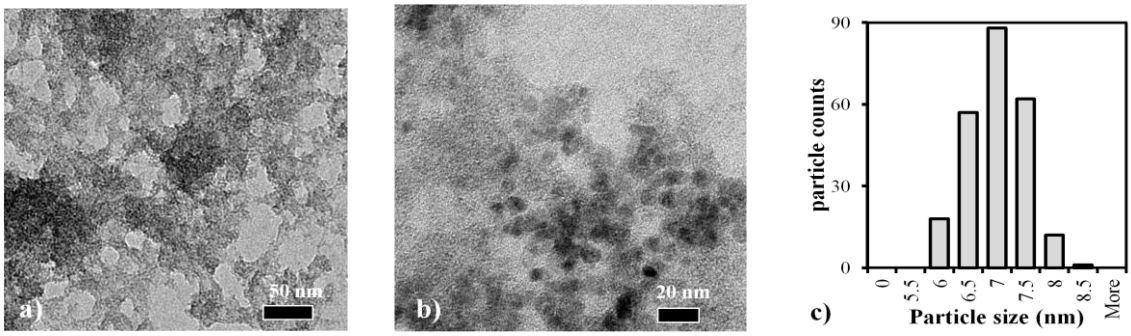

Figure 4.5. HR-TEM images of a) mesoporous structured titania showing the support and b) the deposited CuZn nanoparticles in fresh CuZn/meso-TiO_2. c) Particle size distribution generated by measuring 200 particles (see Supporting Information of reference [1]).

4.3.3 Unsupported CuZn nanoparticles

Recently, higher product yields were reported for bimetallic CuZn NPs as compared to monometallic Cu NPs in the Ullmann etherification reaction [8]. Therefore, the bimetallic CuZn NPs were selected for further investigation in this study. Figure 6a shows 4-phenoxypyridine yield in the temperature range of 110-140 °C and for varying stirring rates for a catalyst concentration of 1.2 mol% with respect to 4-chloropyridine. Yields of 6% and 38% were observed after 300 s for this catalyst at 120 °C and 140 °C, respectively.

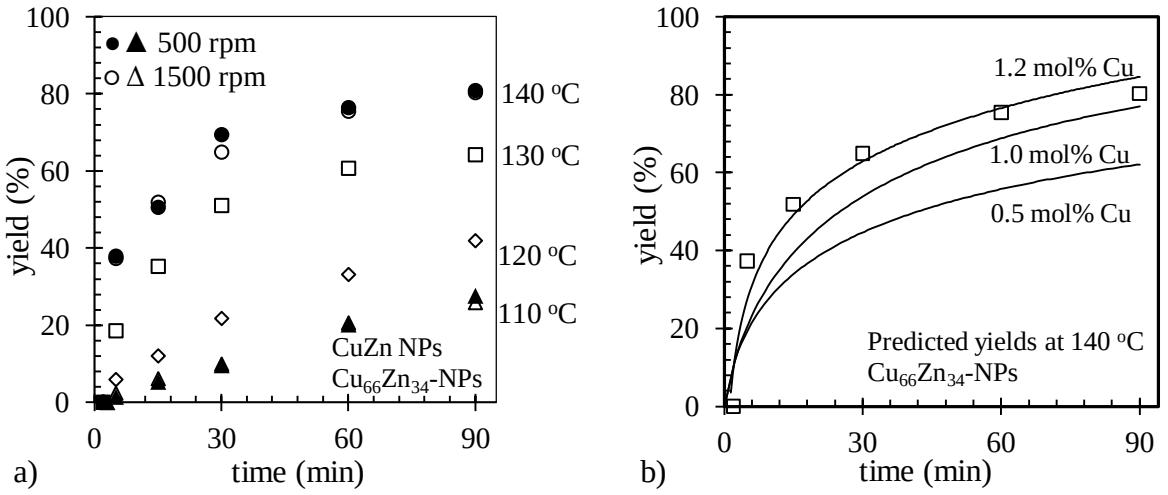

Figure 4.6. Yields of 4-phenoxypyridine using unsupported bimetallic CuZn nanoparticles at different temperatures and stirring rates using C_{cat}=1.2 mol% with respect to 4-chloropyridine (a) and the predicted yields based on a Langmuir-Hinshelwood rate model. Initial concentrations of 0.36 mol/L potassium phenolate and 0.3 mol/L 4-chloropyridine were used.

As described in section 2.4, the experimental results can be accurately described by a Langmuir-Hinshelwood type equation with product inhibition:

$$r = -\frac{kw_{cat}C_N C_E}{(1 + K_N C_N + K_E C_E + K_P C_P)^2} \qquad \textbf{Equation 4.2}$$

Table 4.2. The kinetic parameters of the Cu-catalyzed Ullmann C-O coupling according to a Langmuir-Hinshelwood type rate equation.

k (L^2/g mol·s)	K_N, (L/mol)[a]	K_E, (L/mol)[b]	K_P, (L/mol)
$2.87 \cdot 10^{-3}$	1.26	$2.87 \cdot 10^{-1}$	9.57

[a] N = nucleophile or potassium phenolate.
[b] E = electrophile or 4-chloropyridine.

Subscripts N, E and P in Equation 2 refer to the nucleophile (potassium phenolate), electrophile (4-chloropyridine) and product (4-phenoxypyridine), respectively. The kinetic parameters are listed in Table 2 and the rate-model fit is shown in Figure 6b for different catalyst concentrations.

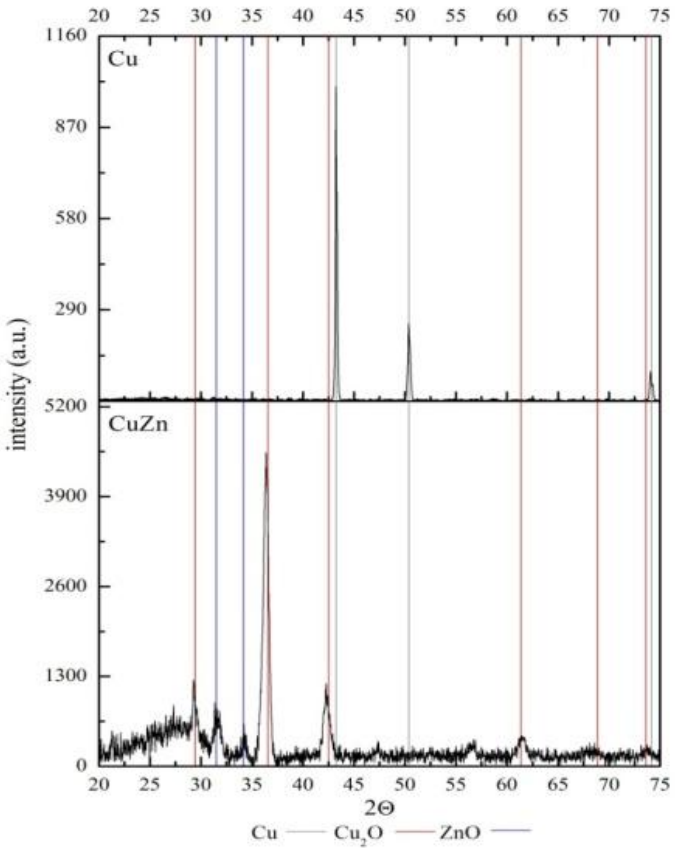

Figure 4.7. XRD spectra of nano-Cu (top) and nano-CuZn (bottom) prior to heterogenization.

At low conversion, a rather constant reaction rate was observed and as a result the product yield was a linear function of the reaction time and the reaction rate, independent of the reactants and product concentration. However, when a substantial amount of 4-phenoxypyridine was formed the adsorption onto the active metal severely limited the reaction rate. Figure 7 shows the XRD spectra of unsupported Cu and CuZn catalysts. The [111], [200] and [220] refractions characteristic of a face-centered cubic metal lattice were observed at 43°, 50.5° and 74.5° [8, 41]. The oxide phases Cu_2O and ZnO were observed only in the bimetallic catalyst [43]. Comparison with our previous results [8] underlined the stability of Cu nanoparticles, while in the case of CuZn nanoparticles, initial alloy formation was followed by the oxidation driven segregation of the elements. This observation is in agreement with DFT and microscopic studies of the alloy system by Greely and Hansen, respectively [44]. This segregation is likely to have been enhanced by the particles' exposure to air in the course of an XRD measurement time of about 5.5 h.

4.3.4 Cu/non-porous TiO_2

The 4-phenoxypyridine yield using the Cu/np-TiO_2 film (0.004 mol% Cu with respect to 4-chloropyridine) was 25% higher at 120 °C as compared to that of using CuZn NPs (Figure 8) and similar to that at 140 °C.

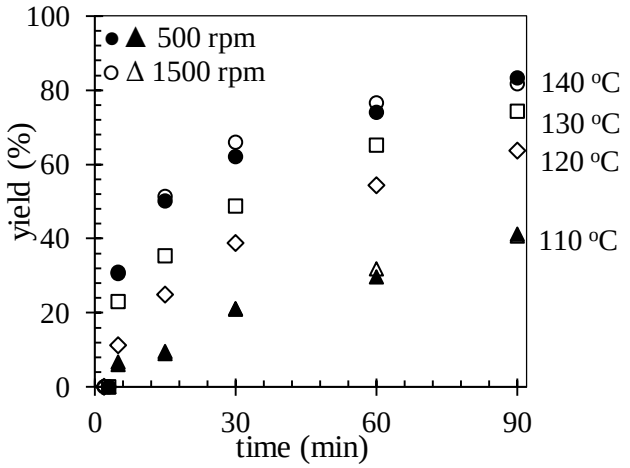

Figure 4.8. Yields obtained from Cu/np-TiO_2 using C_{cat} = 0.004 mol% Cu with respect to 4-chloropyridine at different temperatures and stirring rates. Initial concentrations of potassium phenolate and 4-chloropyridine were 0.36 and 0.3 mol/L, respectively.

A low magnification SEM image of np-TiO_2 films on glass beads is shown in Figure 9a. A smooth surface of np-TiO_2 with a few cracks is seen after calcination at 600 °C in the larger magnification image of Figure 9b. The formation of cracks during calcination demonstrates that adhesion of the titania film to the substrate is rather strong.

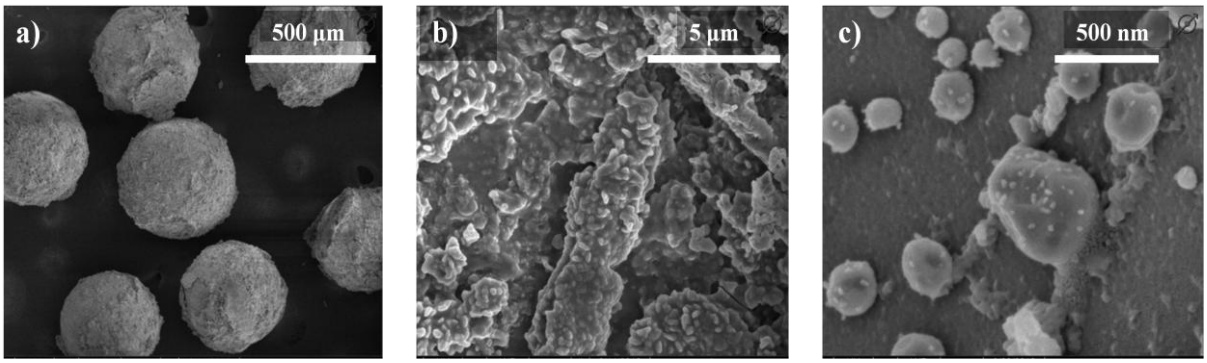

Figure 4.9. SEM images of the single layer TiO_2-coated beads before (a and b) and after copper deposition (c) for Cu/np-TiO_2.

A SEM image of the Cu/np-TiO_2 catalyst after calcination at 400 °C is shown in Figure 9c. One notable feature is that the mean size of Cu NPs in the calcined films (14.3 ± 2.0 nm) was slightly increased as compared to that of the unsupported nanoparticles (9.6 ± 1.0 nm) [8]. However, as was observed from TEM imaging and chemisorption analysis, the catalyst dispersion was maintained unchanged. The thickness of the titania film was estimated between 200 and 500 nm. The supported catalysts showed higher initial rates and product yields than those of the unsupported catalysts (see Figure 2, 6 and 8) and the Cu/np-TiO_2 catalyst demonstrated higher activity at low reaction temperatures. However, the influence of catalyst loading on the reaction rates was most strongly observed for the unsupported CuZn NPs. At a four-fold increase in metal loading, the reaction rate doubled using unsupported CuZn NPs, and this could be attributed to the large

adsorption constant of the product on the copper. Overall, the highest reaction rates were found for the Cu/np-TiO_2 catalyst.

Comparable to recently published results by Engels *et al.*, the lowest reaction rate was found for unsupported CuZn NPs (1.4 s^{-1}), being almost one order of magnitude lower than that for Cu/meso-TiO_2 (22.2 s^{-1}) [13b]. The catalyst activities and apparent activation energies for the different catalysts are shown in Table 3.

Table 4.3. Reaction rates and apparent activation energies for different Cu-based catalysts.

Catalyst	Temperature	Cu-loading		Initial rate	E_A^{App}	TON	Product yield
	(°C)	(wt%)	(mol%)[a]	(mol•g_{cat}^{-1}•s^{-1})	(kJ/mol)	(mol_{prod}•mol_{cat}•s^{-1})	(%)
CuZn NPs[b]	120		$12 \cdot 10^{-1}$	0.002	123 ± 3	0.1	41.9
	140		$12 \cdot 10^{-1}$	0.011		0.6	80.3
Cu/ meso-TiO_2	120	1.8	$2 \cdot 10^{-3}$	0.014	144 ± 5	0.9	47.6
	140		$2 \cdot 10^{-3}$	0.104		6.6	83.8
Cu/ np-TiO_2	120		$4 \cdot 10^{-5}$	1.715	75 ± 2	109	63.7
	140	2.0	$4 \cdot 10^{-5}$	4.55		289	81.7

[a] Relative to 4-chloropyridine.
[b] For experimental data on monometallic CuZn nanoparticles see Engels *et al.* [13b]

The Arrhenius plot (Figure 10) revealed that, at 110 and 140 °C, different stirring rates (of 500 and 1500) appeared to have no effect on the reaction constants for the different catalyst systems. Activation energies were determined from the reaction rate data taken at a reaction time of 120 s, such that the highest conversion was below 8%. The apparent activation energies were found to be 75 ± 2 kJ/mol, 123 ± 3 kJ/mol and 144 ± 5 kJ/mol for Cu/np-TiO_2, CuZn NPs and Cu/meso-TiO_2, respectively. The doubled observed activation energy for meso-porous titania provides evidence for internal diffusion limitations using non-porous titania support in the case of the Cu-catalyzed Ullmann-type C-O coupling reaction.

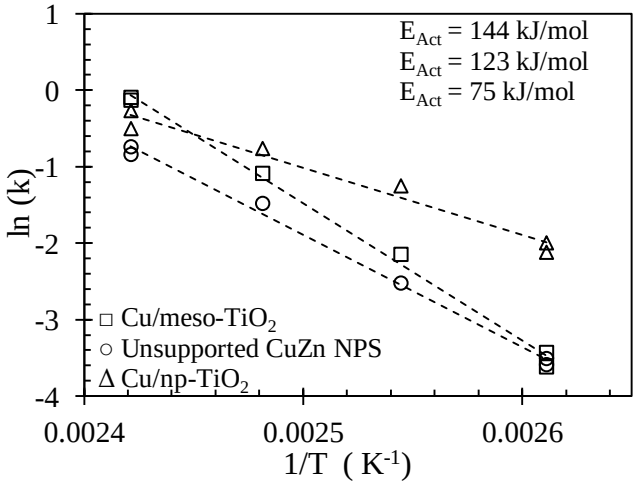

Figure 4.10. Arrhenius plots at a temperature range from 110 to 140 °C using different Cu-based catalysts and stirring rates between 110 and 140 °C.

The Ullmann coupling catalyzed by the porous catalyst obeyed intrinsic kinetics, *i.e.* constants for mass transfer were much smaller than the time constants for reaction. As shown in Figures 2, 6 and 8, decreasing the stirring rate from 1500 to 500 rpm had no effect on the catalyst activity. This confirmed the absence of external mass-transfer limitations, as would be expected in a liquid-solid reaction in which the reactants are completely dissolved in the solvent. The higher product yields achieved over the Cu/meso-TiO_2 are due to an increased surface area, facilitating a higher catalyst loading. The spent Cu/meso-TiO_2 and Cu/np-TiO_2 films were analyzed using SEM-EDX after experiments at 140 °C (Figure 11a and 11b, respectively).

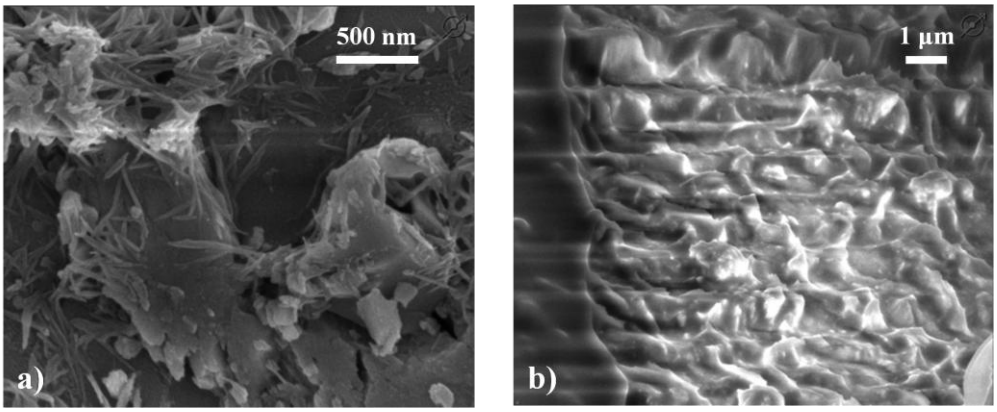

Figure 4.11. SEM image of silica beads coated with mesoporous titania (Cu/meso-TiO_2) a) before and b) after catalyst deposition (magnification 150,000).

The Ti signal remained unchanged which confirmed a good adhesion of the mesoporous titania film. A 10% lower signal for Cu was observed in the spent meso-TiO_2 which indicated only minor Cu losses due to leaching.

4.3.5 Catalyst deactivation and stability study

The catalyst activity experiments demonstrated that the best catalyst support was the mesoporous titania (Cu/meso-TiO_2). For this reason, the following deactivation and stability study was mostly focused on Cu oxidation and Cu/meso-TiO_2 leaching from the glass beads. XPS measurements were performed on unsupported Cu and CuZn NPs, Cu/meso-TiO_2 and CuZn/meso-TiO_2. The supported catalysts were tested for different processing times in a *N*,*N*-dimethylacetamide (DMA) flow of 5 mL/min. The liquid viscosity was increased by dissolving potassium phenolate, while maintaining the temperature at 140 °C. Of particular note, preliminary flow experiments established that the mesoporous titania coating on the glass support appeared to be stable against leaching for 12 h under flow operation. However, ICP measurements demonstrated a 19% titania loss for the non-porous titania film in 4 h. Moreover, when Cu/meso-TiO_2 was tested, copper losses appeared to be ±17% during the first 4 h, while the titania was relatively unaffected. As a result of a relatively stable catalyst support system, activity of the Cu/meso-TiO_2 catalyst could be maintained at tolerably high level for three runs of 4 h each.

X-ray photoelectron spectroscopy. The results of the XPS measurements are shown in Figure 12. Peaks at binding energies of 1021.4 eV (Zn 2p), 932.9 eV (Cu 2p) and 458.7 as well as 465.2 eV (Ti 2p) were observed.

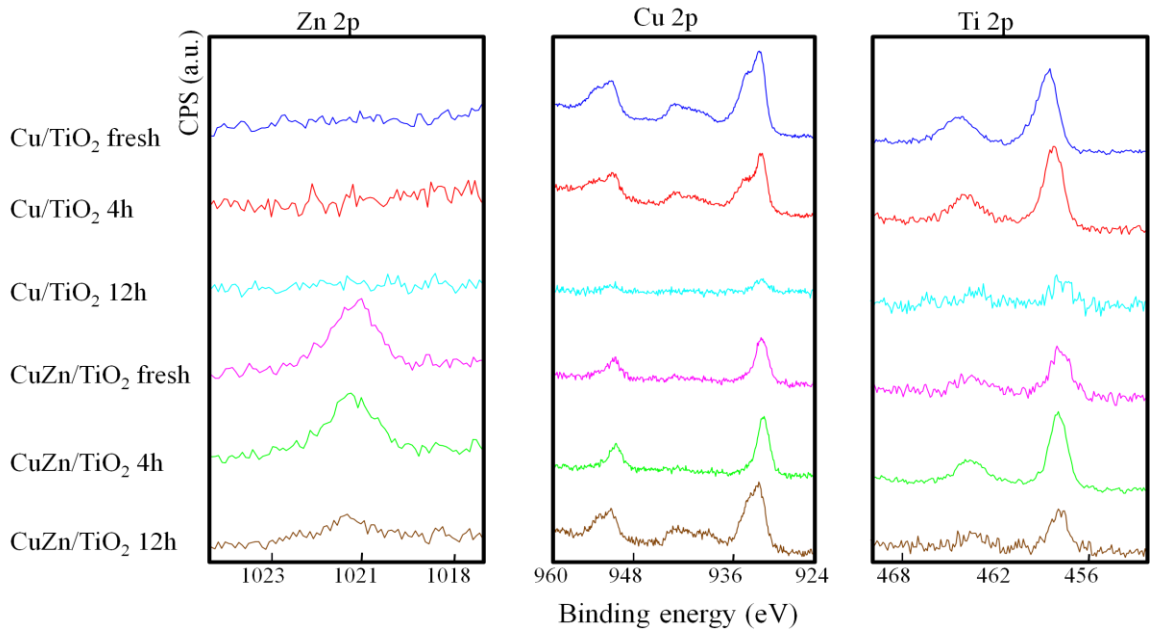

Figure 4.12. XPS analysis of mesoporous titania coated with Cu and CuZn nanoparticles at different reaction times (glass beads loaded into a fixed-bed reactor).

The Cu 2p3/2 peak at 932.9 eV indicated the presence of metallic copper in the bimetallic CuZn catalyst. The appearance of a second Cu 2p3/2 component at 934 eV accompanied by strong shake-up signal between 938 and 945 eV indicates the formation of copper (II) oxide. Comparison of monometallic copper and the bimetallic CuZn catalysts indicated that copper was stabilized against oxidation by the presence of zinc, probably due to alloy formation. The monometallic copper nanoparticles were already partially oxidized after impregnation onto the titania support and were completely oxidized after reaction as was also confirmed by the ^{63}Cu-NMR spectrum. In the presence of zinc, copper remained in the metallic state after impregnation, even after 4 h on-stream. However, no Cu^0 was observed after 12 h reaction time.

For the origins of this effect, both electronic and kinetic mechanisms can be considered [45]. While in the first case, Zn is likely to act as a sacrificial anode through its oxidation to ZnO, the formation of core/shell particles and their consequences for oxygen diffusion also needs to be considered. XPS results for the unsupported CuZn nanoparticles showed the presence of metallic copper, likely through the formation of alloy phases and/or a solid solution. In the course of the catalytic reaction, Zn is likely to segregate to the Cu particle surface. This phenomenon leads to a Cu/ZnO core/shell system by subsequent oxidation of Zn and, eventually, to deactivation. The formation of such a ZnO-shell may lead to a considerable diffusion barrier to oxygen reaching the Cu surface. Consequently, oxidation of copper is inhibited, yet at the same time as the accessibility of the reactants to the active copper surface also decreases,

which is reflected in the conversion plateau. On the other hand, the subsequent complete separation of the shell from the core will lead to the formation of morphologically undefined ZnO agglomerates, distinct from the former Cu-core, which may remain largely intact as a new Cu nanoparticle that is prone to oxide formation. The resulting decrease in the specific surface area of Zn due to the ZnO particle growth and the accompanying decrease in surface-to-volume ratio may then be the cause for the observed reduction in the Zn 2p peak intensity.

However, carbon deposition during the reaction represented a more likely reason for the simultaneous depletion of Cu, Zn and Ti signals. This is best seen from a quantitative XPS analysis based on a constant oxygen content in the carbon holey film substrate (see Experimental Section and Supporting Information of reference [1]). Sodium and nitrogen impurities in the XPS data are attributed to artefact residuals from the copper nanoparticle synthesis.

Temperature-programmed oxidation/reduction (TPO/R). TPO/R experiments were carried out to determine the amount of oxygen and hydrogen uptake by Cu and the temperature at which a spontaneous surface uptake of these gases occurred. This, in turn, allowed the oxidation state and the reduction temperature for the regeneration of spent catalyst to be determined. Figure 13 shows the results for both the temperature-programmed oxidation (dashed lines) and reduction (black lines) of the Cu/meso-TiO_2 and Cu/np-TiO_2 catalysts. Since the first step in these experiments consisted of an oxidative treatment at varying temperatures from 350 to 450 ºC, the dashed lines provided an indication of the original oxidation state of the copper. The oxygen uptake on Cu/meso-TiO_2 showed that copper was predominantly present as Cu^0, consistent with the XPS and ^{63}Cu-NMR spectra. In contrast, Cu in the Cu/np-TiO_2 catalyst appeared to be predominantly in the +2 state, since no oxidation feature appeared in the TPO experiment.

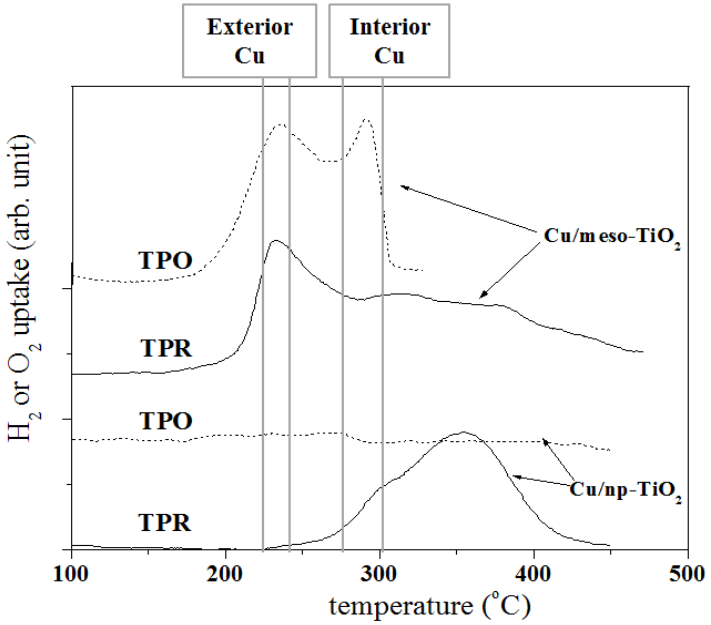

Figure 4.13. TPO signals (dashed line) and TPR signals (solid line) for copper on mesoporous (Cu/meso-TiO_2) and non-porous (Cu/np-TiO_2) titania.

The two peaks in the TPO curve for Cu/meso-TiO_2 signified the occurrence of two separate oxidation steps and provided temperatures at which they occur. The first oxidation peak to CuO occurred at 230-250 °C and was followed by a second peak at 280-290 °C. These data were in good agreement with experiments using a commercial CuO/SiO_2 catalyst (see Supporting Information of reference [1]).

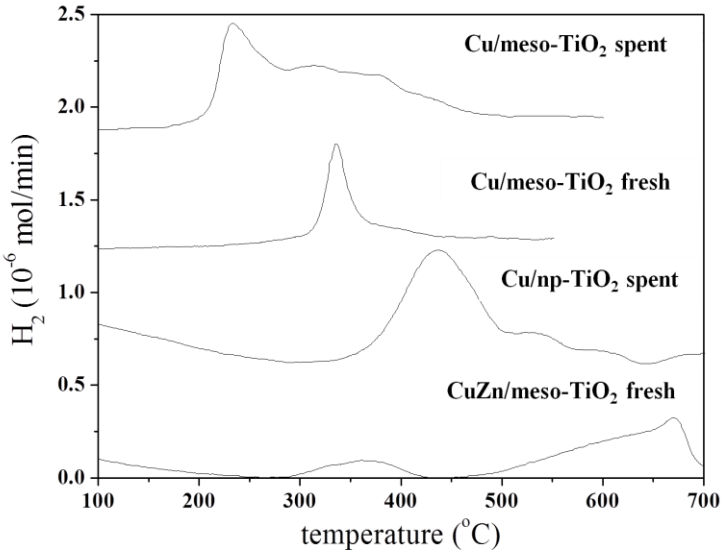

Figure 4.14. TPR results for the determination of copper loading using integrated values of the hydrogen-uptake.

The reduction cycle for Cu in the Cu/meso-TiO_2 catalyst revealed features in three temperature ranges. At 225 °C , all the copper present at the exterior surface of the film was reduced to Cu^0. This was followed by two subsequent reductions in the temperature range 310-370 °C, corresponding to the reduction of CuO species at the interior surface of the porous film. Due to the particle size distribution and dispersion throughout the mesoporous titania film, different reduction processes occurred.

Indeed, it has been postulated [46] that the wide temperature range over which reduction occurred is due to the high dispersion of copper nanoparticles in the mesoporous titania film. The combined results of BET-surface measurements by physisorption and TEM imaging showed a high dispersion of the copper nanoparticles in the mesoporous titania matrix. These findings are supported by the fact that in the case of Cu/np-TiO_2, a single copper reduction peak appeared at a temperature interval around 350 °C [47]. In this latter case, copper was uniformly distributed over the titania film thickness which also explains the low accessibility of copper and, therefore, the considerable mass-transfer limitations and decreased E_A^{App}.

The Cu-loadings of the Cu/np-TiO_2 and Cu/meso-TiO_2 were determined by measuring the total amount of hydrogen consumed after complete oxidation to CuO. The graphical uptake of hydrogen, used to determine the Cu-loadings, is depicted in Figure 14 and is summarized in Table 4. A fresh sample of Cu/meso-

TiO_2 showed a single reduction peak at 321 °C due to the abundant presence of copper inside the porous film, whereas the spent catalyst revealed several reduction peaks, probably due to copper migration to the outer film surface. For Cu/np-TiO_2, a broad reduction peak was observed at (higher) temperatures ranging from 435 °C to 600 °C. For CuZn/meso-TiO_2, two peaks appeared at 352 °C and 671 °C. The first peak clearly originates from the formation of zero-valent copper, while the latter can be attributed to the partial reduction of the zinc oxide species [48].

This latter conclusion is consistent with the observation of sintering of the catalyst due to the melting of metallic Zn at 419.5 ºC. As compared to the metal loadings found from ICP-OES measurements (shown in Table 1), these TPR data (Table 4) afforded corresponding results. The catalyst stability was studied at a reaction time, sufficient for production of 0.1 kg 4-phenoxypyridine. Experiments were carried in a packed-bed reactor at a DMA flow of 5 mL/min in multiple runs of 12 h at 140 °C. A Cu-loading of 2 wt% was observed in both spent Cu/np-TiO_2 and Cu/meso-TiO_2 catalysts, which correspond to active metal losses due to leaching of 82% and 10%, respectively (see Table 1).

Table 4.4. Integrated H_2-uptake values from a TPR study providing the copper loading for the Cu-based heterogeneous catalysts.

Catalyst type	Temperature (°C)				Metal loading (wt%)		
	Oxidation to		Reduction to		Fresh		Spent
	Cu^{1+}	Cu^{2+}	Cu^0	Zn^0	Cu	Zn	Cu
Cu/meso-TiO_2	224	282	321			0.31	0.22
Cu/np-TiO_2[a]	-	-	435			0.38	0.26
CuZn/meso-TiO_2[a]	227	-	352	671[b]	0.12	0.29	-

[a] A single oxidation peak was observed.
[b] Although the reverse process (*i.e.* zinc hydrolysis) requires high temperatures (1900 °C), melting of the catalyst was observed, indicating Zn^0 formation.

The Ti/Si ratio was reduced by 25% in the spent Cu/meso-TiO_2 catalysts, which confirms a rather good adhesion of mesoporous titania films to the glass surface as compared to that of Cu/np-TiO_2 (80% Ti loss). The low Cu/Ti ratio, measured in the spent Cu/np-TiO_2 catalyst after 12 h on-stream, suggests that most of Cu was located uniformly on the film and leached simultaneously with the TiO_2 film.

4.3.6 X-ray absorption spectroscopy to determine the influence of catalyst composition on its activity: a "Volcano-plot"

Activity measurements. Based on the aforementioned results, various Cu:Zn ratios have been supported onto mesoporous titania and applied in the Ullmann-type C-O coupling reaction. The turnover frequencies of the various catalysts were measured and are displayed as function of the Cu and Zn fractions in Figure 15.

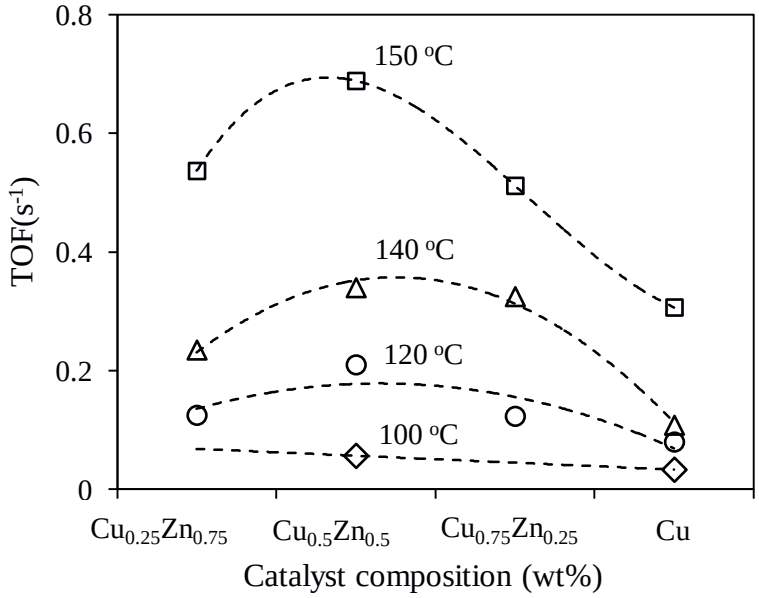

Figure 4.15. Catalyst activity (in TOF) as function of various Cu/Zn ratios.

A clear trend in catalyst activity, as function of the Cu:Zn ratio, was observed over a wide temperature range, demonstrating, in accordance with previous results, that the catalyst activity of various CuZn catalyst composition in the Ullmann-type C-O coupling reaction displays a "Volcano-plot" as described by the Sabatier-principle [49]. The highest catalyst performance appeared to be attained for a $Cu_{0.5}Zn_{0.5}$ catalyst. However, the optimum catalyst would in this case be interpreted as an optimum between the Cu-oxidation state and the accessibility of the active Cu^0. When pure Cu catalyst would be used, the oxidative instability of the active sites would limit the reactivity. Oppositely, at too high Zn-loadings the ZnO-shell on the Cu-core would limit the accessibility of the reactants to the active Cu-sites.

X-ray absorption near-edge spectroscopy (XANES) measurements. The abovementioned conclusions were strengthened by synchrotron X-ray absorption spectroscopy at the near Cu K-edge using various Cu_xZn_y/TiO_2 (x and y in wt%) catalysts. Freshly prepared and spent catalysts were analyzed in a reducing flow (H_2-flow) from 25 °C to 300 °C for 12 h and then re-oxidized in an oxidizing flow (O_2-flow) at the reaction temperature 140 °C, using a micro-reactor cell. In this way, the role of Zn as "oxide-scavenger" and, consequently, retention of the Cu^0-oxidation state were studied. X-ray absorption near-edge structure spectra (XANES) were used to examine the oxidation state (Figures 16a and 16b). Figure 16a shows a decrease in the absorption edge after reduction, which provided the absorption features of both Cu^{2+} and Cu^0 [36b, 50]. The spent catalyst used in the coupling reaction at 140 °C (consisting of Cu, $Cu_{72}Zn_{28}$ and $Cu_{35}Zn_{65}$) were analyzed by XANES (Figure 16b). The corrected edge-absorption intensity demonstrated clearly an increased fraction of Cu^0 for high Zn-loadings in the Cu_XZn_Y catalyst [51]. These results demonstrate a clear evidence of a sacrificial anode effect of Zn-promoted Cu-catalysis in liquid-type coupling reactions.

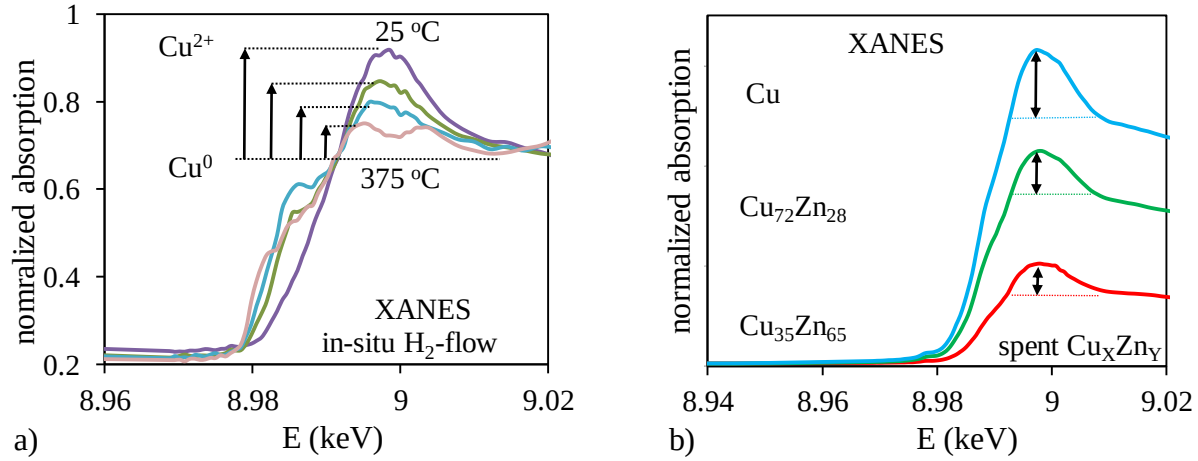

Figure 4.16. In-operando micro-reactor XAS experiments, demonstrating a decreased absorption edge during reduction (a) and Cu^0-oxidation stability at increased Zn fraction after reaction (b).

In another experiment three oxidized catalysts ($Cu_{0.5wt\%}Zn_{0.5wt\%}$, $Cu_{0.35wt\%}Zn_{0.65wt\%}$ and $Cu_{1wt\%}Zn_{1wt\%}$) have been subjected to a reducing flow (6 vol% H_2 in N_2) and simultaneously analyzed for XANES measurements (Figure 17).

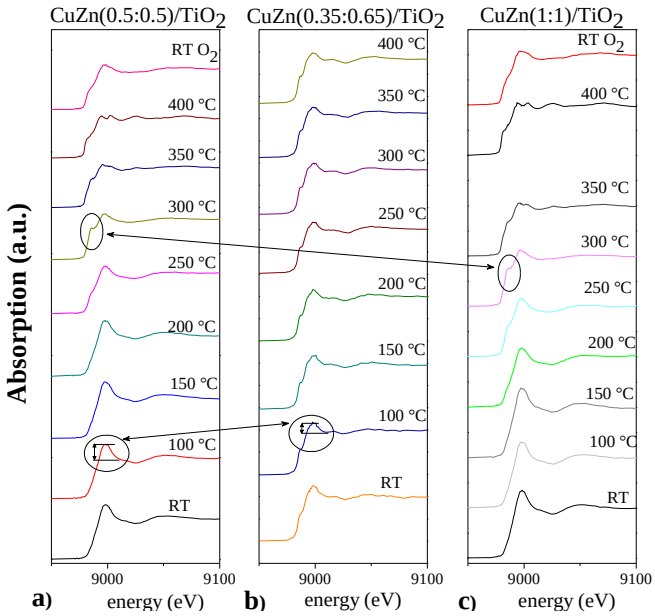

Figure 4.17. In-operando XAS analyses of REDOX cycles using (a) $Cu_{0.5wt\%}Zn_{0.5wt\%}$, (b) $Cu_{0.35wt\%}Zn_{0.65wt\%}$ and (c) $Cu_{1wt\%}Zn_{1wt\%}$ catalysts. A clear decrease of the pre-edge height can be observed for the $Cu_{0.35wt\%}Zn_{0.65wt\%}$, whereas addition of Zn also leads to particle growth

Figure 17 shows the absorbance spectra at the Cu K-edge for two different catalyst compositions and loadings at various temperatures, where the difference in height between the signal from the edge of copper and the signal at higher energies signified the degree of catalyst oxidation [52]. Comparing Figure 17a with 17b demonstrates that the difference in absorbance decreases clearly with an increased Zn fraction (17b). Already at 100 °C the oxidation fraction for $Cu_{0.35}Zn_{0.65}$ clearly

decreased as compared to $Cu_{0.5}Zn_{0.5}$ at a total metal loading of 1 wt% (sum of Cu and Zn). However, the typical pre-edge peak formation for $Cu_{0.5}Zn_{0.5}$ indicated the re-formation of the Cu^0 nanoparticles, which was only limitedly observed for the $Cu_{0.35}Zn_{0.65}$ nanoparticles. This observation demonstrated that formation of larger particles occurs with increased Zn concentration in the nanoparticles, which could be caused by a ZnO-shell growth on the Cu nanoparticles, as reported by Grunwaldt *et al.*[50b] Increasing the overall metal loading to 2 wt% showed for the $Cu_{1wt\%}Zn_{1wt\%}$ catalyst (Figure 17c) similar behavior of the oxidation state. However, the appearance of the pre-edge appeared already at 200 °C indicating that the size of the CuZn nanoparticles could be maintained without either sintering of the particles or ZnO coverage onto the Cu nanoparticles.

X-ray absorption fine-structure spectroscopy (EXAFS) measurements. Figure 18 shows the EXAFS spectra obtained from the fresh, spent and reduced (regenerated) $Cu_{0.5wt\%}Zn_{0.5wt\%}$ catalyst and regenerated $Cu_{1wt\%}Zn_{1wt\%}$ catalyst (similar catalyst as shown for XANES in Figure 17a and 17c).

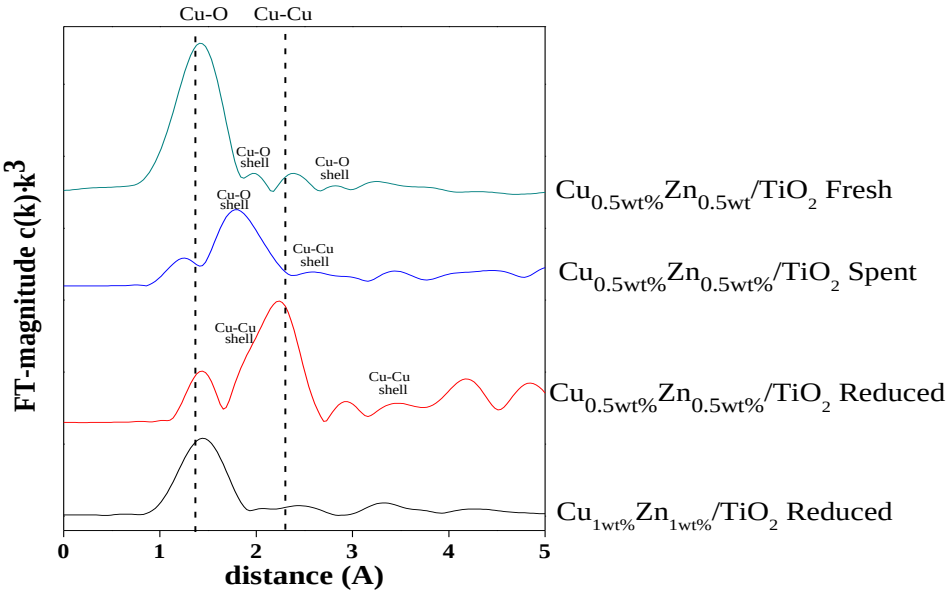

Figure 4.18. EXAFS measurements on the $Cu_{0.5wt\%}Zn_{0.5wt\%}$ catalyst, demonstrating the quantitative regeneration of Cu^0 catalyst using equimolar CuZn.

The fresh $Cu_{0.5wt\%}Zn_{0.5wt\%}$ shows a typical CuO fine-structure, with two Cu-O shells at 1.95 and 2.83 Å, and the Cu-Cu shell at 3.03 Å, indicating that the Cu is predominately present in an oxide state. In the spent $Cu_{0.5wt\%}Zn_{0.5wt\%}$ also metallic Cu-Cu coordination was found for the obtained fine-structure at 2.54 Å. However, also clear Cu-O shells were obtained in the range from 1.85 to 1.95 Å, which could be fitted to the 1st shells of Cu-O in Cu_2O and CuO structures at 1.847 and 1.952 Å, respectively. Based on the fit obtained at a low coordination number of the Cu-O at 1.852 Å, it was concluded that only a negligible amount of Cu_2-O was present. The reduced $Cu_{0.5wt\%}Zn_{0.5wt\%}$ could be fitted with two Cu-Cu shells at 2.54 and 3.58 Å in the fine-structure, in agreement with coordination in the 1st shell and the 2nd shell of metallic Cu, respectively, indicating majorly the presence of metallic Cu.

Surprisingly, at increased catalyst loading $Cu_{1wt\%}Zn_{1wt\%}$ of the reduced catalyst the fine-structure indicated predominately presence of CuO. No apparent signal of Cu-Cu shells could be traced, indicating that the preservation of Cu^0 catalyst is not only dominated by the catalyst composition, yet more severely by the catalyst loading. This indication confirmed that control of the catalyst loading is as important, to avoid sintering of the nanoparticles [36b, 37, 50b, 51b, 52a, 53].

Figure 19 demonstrates the EXAFS spectra and the fitting parameters (*i.e.* N as Cu coordination number, R as bond distance (in Å), σ^2 as mean square displacement and E_0 as energy reference shift) obtained for different Cu_XZn_Y catalysts.

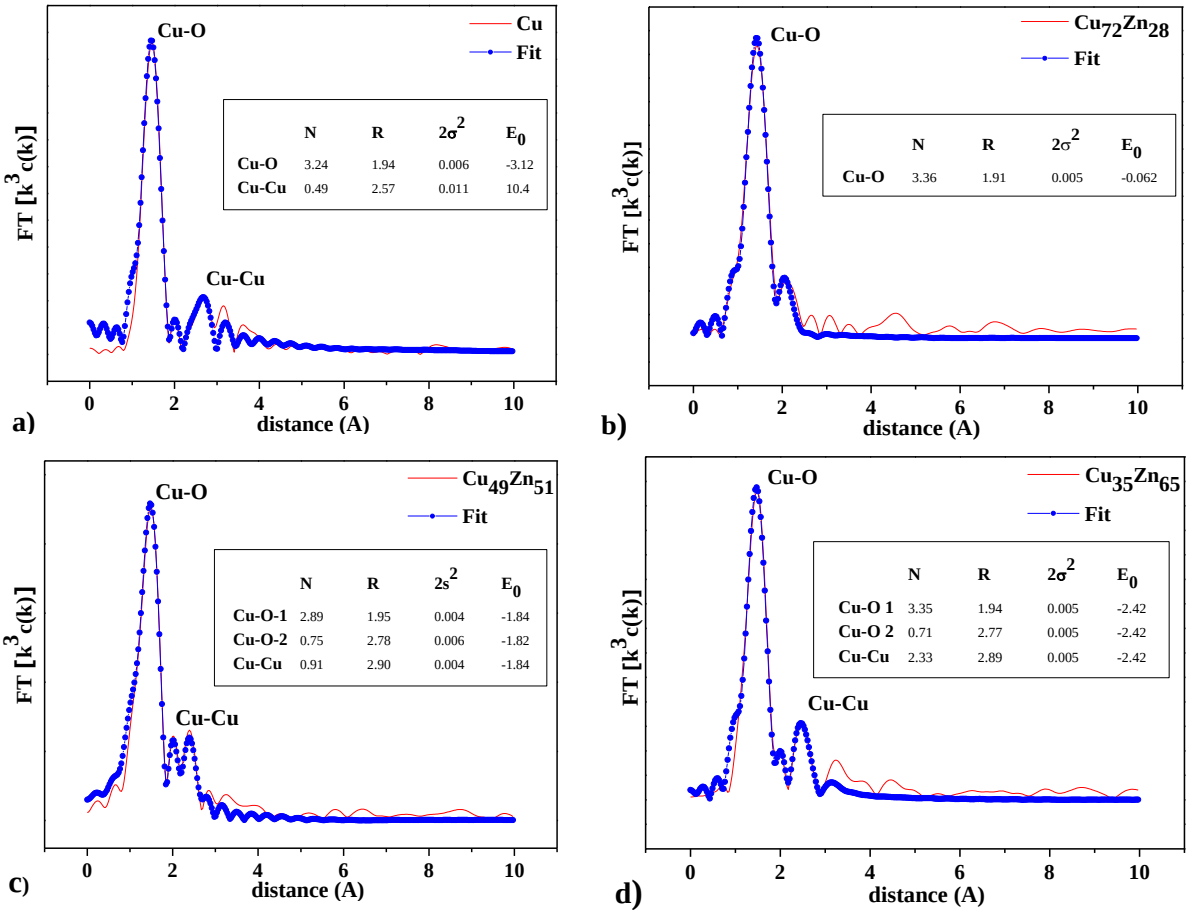

Figure 4.19. EXAFS data and the fitting parameters obtained for various CuZn catalysts.

Clearly, the Cu (Figure 19a) and $Cu_{72}Zn_{28}$ (Figure 19b) catalysts demonstrate the least fit for the coordinated Cu-Cu species as compared to $Cu_{49}Zn_{51}$ (Figure 19c) and $Cu_{35}Zn_{65}$ (Figure 19d). Remarkably, the large differences in Cu-Cu coordination number of 2.33 ± 0.12 and 0.91 ± 0.27 for the bimetallic $Cu_{35}Zn_{65}$ and $Cu_{49}Zn_{51}$, respectively, are not accompanied by large changes in Cu-Cu distances (*i.e.* 2.89 ± 0.04 and 2.90 ± 0.03 Å, respectively). However, compared to the mono-metallic Cu, a significantly changed coordination number of 0.49 ± 0.22, consequently, also led to a considerable decrease of the Cu-Cu bond distance (2.57 ± 0.02 Å). This observation can be explained by the fact that the Cu-Cu distance in

a Cu-Zn nano-alloy are expected to change as compared to the Cu-Cu distance in a monometallic Cu nano-cluster [54].

Following these EXAFS data, Zn in the nanoparticles is predominantly present as a nano-alloy without significant presence of bulk alloying due to the large influence of Zn on the Cu-Cu distance. No major difference in the Cu-Cu coordination at a Cu/Zn-ratio of 35:65 and 49:51 was observed. However, Cu-O coordination was observed at a Cu/Zn-ratio of 72:28. In addition, it should be mentioned that, especially for the $Cu_{35}Zn_{65}$ and $Cu_{72}Zn_{28}$ catalysts, the fits could only accurately be described up to a bond length of 2.5-3 Å, corresponding to neighbouring atoms from the central atom.

4.4 Conclusions

Two novel heterogeneous copper-based, nano-structured catalysts have been synthesized using non-porous TiO_2 and mesoporous TiO_2 films deposited on glass beads as structuring substrate. The catalytic activity of these films, after impregnation with Cu or CuZn nanoparticles, have been studied in the copper-catalyzed Ullmann C-O coupling reaction of 4-chloropyridine and potassium phenolate in a batch-wise operated stirred tank reactor.

The highest product yield of 84% was obtained in 90 min, using catalysts comprising 2 wt% Cu/meso-TiO_2 films with mean pore sizes of 24 ± 4 nm. After 12 h pre-conditioning, the Cu-loading of 1.8 wt% demonstrated that leaching of Cu does not plays a significant role in the case of mesoporous titania support systems. Bimetallic CuZn nanoparticles with a Cu/Zn molar ratio of 2 and a mean size of 4 nm were also deposited onto mesoporous TiO_2 films. The Cu^0-state could be preserved in these catalysts while for the monometallic Cu/meso-TiO_2 films oxidation of Cu was observed. The presence of Zn appeared to be crucial for the stabilization of metallic Cu. Accordingly, XPS, ^{63}Cu-NMR spectroscopy and TPO/TPR data showed the formation of Cu^{2+} in the spent titania-supported catalysts which is in line with the results of Newton and Lai [55]. This finding represents the main source of catalyst deactivation in the Cu/meso-TiO_2 films.

Support leaching was found to be the main reason for catalyst deactivation in the case of the non-porous TiO_2 films. Based on the Cu-EXAFS study, the Cu coordination could be fitted up to inter-atomic distances of 3 Å. Moreover, the supported CuZn nanoparticles clearly showed that the presence of Cu and Zn atoms are predominately present as a nano-alloy without significant presence of bulk alloying. A maximum in activity as function of Zn fraction was found in a "Volcano-plot" for the $Cu_{0.5}Zn_{0.5}/TiO_2$ catalyst. This observation could be explained by the retardation of Cu oxidation due to the sacrificial oxidation of Zn. After catalyst reduction, the CuZn nanoparticles could be reversible regenerated without significant changes in the coordination number of Cu.

This observation, however, underlines the significant potential for further catalyst developments, exploiting tailored metal-support interactions between copper and the nanoscopic oxide after improving adhesion of the TiO_2 support to a structured substrate.

References

[1] F. Benaskar, V. Engels, E. V. Rebrov, N. G. Patil, J. Meuldijk, P. C. Thüne, P. C. M. M. Magusin, B. Mezari, V. Hessel, L. A. Hulshof, E. J. M. Hensen, A. E. H. Wheatley and J. C. Schouten, *Chem.– Eur. J.* **2012**, *18*, 1800-1810.

[2] F. Benaskar, V. Degirmenci, E. V. Rebrov, N. G. Patil, P. Abulkin, J. Meuldijk, V. Hessel, L. A. Hulshof, E. J. M. Hensen, A. E. H. Wheatley and J. C. Schouten, *unpublished results* **2012**.

[3] a) R. Ferrando, J. Jellinek and R. L. Johnston, *Chem. Rev.* **2008**, *108*, 845-910; b) J. M. Campelo, D. Luna, R. Luque, J. M. Marinas and A. A. Romero, *ChemSusChem* **2009**, *2*, 18-45.

[4] C. N. R. Rao, G. U. Kulkarni, P. J. Thomas and P. P. Edwards, *Chem. Soc. Rev.* **2000**, *29*, 27-35.

[5] R. Ferrando, A. Fortunelli and R. L. Johnston, *Phys. Chem. Chem. Phys.* **2008**, *10*, 640-649.

[6] W. Zhang, Y. Liu, R. Cao, Z. Li, Y. Zhang, Y. Tang and K. Fan, *J. Am. Chem. Soc.* **2008**, *130*, 15581-15588.

[7] a) E. V. Rebrov, A. Berenguer-Murcia, H. E. Skelton, B. F. G. Johnson, A. E. H. Wheatley and J. C. Schouten, *Lab Chip* **2009**, *9*, 503-506; b) M. Mavrikakis, B. Hammer and J. K. Nørskov, *Phys. Rev. Lett.* **1998**, *81*, 2819-2822.

[8] V. Engels, F. Benaskar, D. A. Jefferson, B. F. G. Johnson and A. E. H. Wheatley, *Dalton Trans.* **2010**, *39*, 6496-6502.

[9] a) J. K. Nørskov, T. Bligaard, J. Rossmeisl and C. H. Christensen, *Nature Chem.* **2009**, *1*, 37-46; b) G. Somorjai and C. Kliewer, *React. Kinet. Catal. Lett.* **2009**, *96*, 191-208.

[10] E. Sperotto, G. P. M. van Klink, G. van Koten and J. G. de Vries, *Dalton Trans.* **2010**, *39*, 10338-10351.

[11] F. Ullmann and P. Sponagel, *Ber. Dtsch. Chem. Ges.* **1905**, *38*, 2211-2212.

[12] I. Goldberg, *Ber. Dtsch. Chem. Ges.* **1906**, *39*, 1691-1692.

[13] a) F. Benaskar, V. Engels, N.G. Patil, E. V. Rebrov, J. Meuldijk, V. Hessel, L. A. Hulshof, D. A. Jefferson, J. C. Schouten and A. E. H. Wheatley, *Tetrahedron Lett.* **2010**, *51*, 248-251; b) V. Engels, F. Benaskar, N.G. Patil, E. V. Rebrov, V. Hessel, L. A. Hulshof, D. A. Jefferson, J. A. J. M. Vekemans, S. Karwal, J. C. Schouten and A. E. H. Wheatley, *Org. Process Res. Dev.* **2010**, *14*, 644-649.

[14] a) E. Negishi and A. de Meijere, *Handbook of Organopalladium Chemistry for Organic Synthesis*, Wiley-Interscience, New York, **2002**; b) D. Prim, J. M. Campagne, D. Joseph and B. Andrioletti, *Tetrahedron* **2002**, *58*, 2041-2075; c) J. F. Hartwig, *Angew. Chem., Int. Ed.* **1998**, *37*, 2047-2067; d) J. F. Hartwig, *Acc. Chem. Res.* **1998**, *31*, 852-860; e) A. F. Littke and G. C. Fu, *Angew. Chem., Int. Ed.* **2002**, *41*, 4176-4211; f) B. H. Yang and S. L. Buchwald, *J. Organomet. Chem.* **1999**, *576*, 125-146; g) J. P. Wolfe, S. Wagaw, J.-F. Marcoux and S. L. Buchwald, *Acc. Chem. Res.* **1998**, *31*, 805-818; h) A. Muci and S. Buchwald in *Practical Palladium Catalysts for C-N and C-O Bond Formation Cross-Coupling Reactions, Vol. 219* (Ed. N. Miyaura), Springer Berlin / Heidelberg, **2002**, pp. 131-209.

[15] J. F. Hartwig, M. S. Driver, F. E. Goodson, B. C. Hamann, J. Louie and G. Mann, *Abstr. Pap. Am. Chem. Soc.* **1998**, *216*, U449-U449.

[16] a) P. Lopez-Alvarado, C. Avendano and J. C. Menendez, *J. Org. Chem.* **1995**, *60*, 5678-5682; b) D. H. R. Barton and J. P. Finet, *Pure Appl. Chem.* **1987**, *59*, 937-946.

[17] P. Y. S. Lam, S. Deudon, K. M. Averill, R. Li, M. Y. He, P. DeShong and C. G. Clark, *J. Am. Chem. Soc.* **2000** *122*, 7600 – 7601.

[18] a) P. Y. S. Lam, V. Guillaume; D. Bonne, C. G. Charles, *Tetrahedron Lett.* **2002**, *43*, 3091-3094; b) P. Y. S. Lam, C. G. Clark, S. Saubern, J. Adams, K. M. Averill, D. M. T. Chan and A. Combs, *Synlett* **2000**, *5*, 674-676.

[19] a) D. M. T. Chan, K. L. Monaco, R.-P. Wang and M. P. Winters, *Tetrahedron Lett.* **1998**, *39*, 2933-2936; b) D. A. Evans, J. L. Katz and T. R. West, *Tetrahedron Lett.* **1998**, *39*, 2937-2940; c) P. Y. S. Lam, C. G. Clark, S. Saubern, J. Adams, M. P. Winters, D. M. T. Chan and A. Combs, *Tetrahedron Lett.* **1998**, *39*, 2941-2944.

[20] a) J. Hassan, M. Sevignon, C. Gozzi, E. Schulz and M. Lemaire, *Chem. Rev.* **2002**, *102*, 1359-1469; b) S. V. Ley and A. W. Thomas, *Angew. Chem., Int. Ed.* **2003**, *42*, 5400-5449; c) F. Monnier and M. Taillefer, *Angew. Chem., Int. Ed.* **2009**, *48*, 6954-6971.

[21] a) M. S. Chen and D. W. Goodman, *Science* **2004**, *306*, 252-255; b) M. Jakob, H. Levanon and P. V. Kamat, *Nano Lett.* **2003**, *3*, 353-358; c) Z. R. Ismagilov, E. V. Matus, A. M. Yakutova, L. N. Protasova, I. Z. Ismagilov, M. A. Kerzhentsev, E. V. Rebrov and J. C. Schouten, *Catal. Today* **2009**, *147*, S81-S86.

[22] M. Kidwai, N. K. Mishra, V. Bansal, A. Kumar and S. Mozumdar, *Tetrahedron Lett.* **2007**, *48*, 8883-8887.

[23] J. Y. Kim, J. C. Park, A. Kim, A. Y. Kim, H. J. Lee, H. Song and K. H. Park, *Eur. J. Inorg. Chem.* **2009**, 4219-4223.

[24] K. Knepper, M. E. P. Lormann and S. Brase, *J. Comb. Chem.* **2004**, *6*, 460-463.

[25] a) A. Y. Rozovskii and G. I. Lin, *Top. Catal.* **2003**, *22*, 137-150; b) T. Fujitani, M. Saito, Y. Kanai, T. Kakumoto, T. Watanabe, J. Nakamura and T. Uchijima, *Catal. Lett.* **1994**, *25*, 271-276; c) J. Szanyi and D. W. Goodman, *Catal. Lett.* **1991**, *10*, 383-390; d) V. Ponec, *Catal. Lett.* **1991**, *11*, 249-250; e) G. C. Chinchen, P. J. Denny, J. R. Jennings, M. S. Spencer and K. C. Waugh, *Appl. Catal.* **1988**, *36*, 1-65; f) G. C. Chinchen, M. S. Spencer, K. C. Waugh and D. A. Whan, *J. Chem. Soc., Faraday Trans. 1* **1987**, *83*, 2193-2212; g) G. C. Chinchen, K. C. Waugh and D. A. Whan, *Appl. Catal.* **1986**, *25*, 101-107; h) F. Boccuzzi, G. Ghiotti and A. Chiorino, *Surf. Sci.* **1985**, *162*, 361-367; i) K. Klier, *Appl. Surf. Sci.* **1984**, *19*, 267-297; j) J. B. Friedrich, D. J. Young and M. S. Wainwright, *J. Catal.* **1983**, *80*, 14-24; k) J. M. Dominquez E, G. W. Simmons and K. Klier, *J. Mol. Catal.* **1983**, *20*, 369-385; l) X. Wang, J. Zhuang, Q. Peng and Y. Li, *Nature* **2005**, *437*, 121-124.

[26] J. Agrell, M. Boutonnet and J. L. G. Fierro, *Appl. Catal., A* **2003**, *253*, 213-223.

[27] R. Naumann d'Alnoncourt, X. Xia, J. Strunk, E. Loffler, O. Hinrichsen and M. Muhler, *Phys. Chem. Chem. Phys.* **2006**, *8*, 1525-1538.

[28] Y.-G. Lin, Y.-K. Hsu, S.-Y. Chen, L.-C. Chen and K.-H. Chen, *J. Mater. Chem.* **2011**, *21*, 324-326.

[29] W. Monch, *Rep. Prog. Phys.* **1990**, *53*, 221-278.

[30] L. J. Brillson, *Phys. Rev. Lett.* **1978**, *40*, 260-263.

[31] a) B. S. Clausen, G. Steffensen, B. Fabius, J. Villadsen, R. Feidenhans'l and H. Topsøe, *J. Catal.* **1991**, *132*, 524-535; b) L. S. Kau, K. O. Hodgson and E. I. Solomon, *J. Am. Chem. Soc.* **1989**, *111*, 7103-7109; c) M. Muhler, L. P. Nielsen, E. Törnqvist, B. S. Clausen and H. Topsøe, *Catal. Lett.* **1992**, *14*, 241-249; d) L. E. Y. Nonneman and V. Ponec, *Catal. Lett.* **1990**, *7*, 213-217.

[32] G. Apai, J. R. Monnier and D. R. Preuss, *J. Catal.* **1986**, *98*, 563-567.

[33] a) C. A. Leon y Leon and M. Albert Vannice*, *Appl. Catal.* **1991**, *69*, 269-290; b) R. Burch and R. J. Chappell, *Appl. Catal.* **1988**, *45*, 131-150; c) R. Burch, S. E. Golunski and M. S. Spencer, *Catal. Lett.* **1990**, *5*, 55-60; d) B. Denise, R. P. A. Sneeden, B. Beguin and O. Cherifi, *Appl. Catal.* **1987**, *30*, 353-363.

[34] J. Hambrock, M. K. Schröter, A. Birkner, C. Wöll and R. A. Fischer, *Chem. Mater.* **2003**, *15*, 4217-4222.

[35] M. Cokoja, H. Parala, M.-K. Schröter, A. Birkner, M. W. E. van den Berg, W. Grünert and R. A. Fischer, *Chem. Mater.* **2006**, *18*, 1634-1642.

[36] a) M. Cokoja, H. Parala, M. K. Schroter, A. Birkner, M. W. E. van den Berg, K. V. Klementiev, W. Grunert and R. A. Fischer, *J. Mater. Chem.* **2006**, *16*, 2420-2428; b) D. Grandjean, V. Pelipenko, E. D. Batyrev, J. C. van den Heuvel, A. A. Khassin, T. M. Yurieva and B. M. Weckhuysen, *J. Phys. Chem. C* **2011**, *115*, 20175-20191.

[37] A. I. Frenkel, Q. Wang, N. Marinkovic, J. G. Chen, L. Barrio, R. Si, A. L. p. Cámara, A. M. Estrella, J. A. Rodriguez and J. C. Hanson, *J. Phys. Chem. C* **2011**, *115*, 17884-17890.

[38] L. N. Protasova, E. V. Rebrov, T. S. Glazneva, A. Berenguer-Murcia, Z. R. Ismagilov and J. C. Schouten, *J. Catal.* **2010**, *271*, 161-169.

[39] a) B. E. G. Lucier, J. A. Tang, R. W. Schurko, G. A. Bowmaker, P. C. Healy and J. V. Hanna, *J. Phys. Chem. C* **2010**, *114*, 7949-7962; b) J. A. Tang, B. D. Ellis, T. H. Warren, J. V. Hanna, C. L. B. Macdonald and R. W. Schurko, *J. Am. Chem. Soc.* **2007**, *129*, 13049-13065; c) D. Rusanova, K. J. Pike, R. Dupree, J. V. Hanna, O. N. Antzutkin, I. Persson and W. Forsling, *Inorg. Chim. Acta* **2006**, *359*, 3903-3910.

[40] http://feff.phys.washington.edu/~ravel/

[41] F. Benaskar, N. G. Patil, V. Engels, E. V. Rebrov, J. Meuldijk, V. Hessel, L. A. Hulshof, A. E. H. Wheatley and J. C. Schouten, *Dalton Trans.* **2012**, *Revision/Accepted*.

[42] Indeed the NMR frequencies of ^{63}Cu and ^{23}Na differ by 2 × 103 ppm only, so that ^{63}Cu and ^{23}Na NMR signals can be recorded within a single NMR spectrum.

[43] The International Centre for Diffraction Data (ICDD), 2010, Newtown Square, PA, http://www.icdd.com/

[44] a) J. Greeley, A. A. Gokhale, J. Kreuser, J. A. Dumesic, H. Topsøe, N. Y. Topsøe and M. Mavrikakis, *J. Catal.* **2003**, *213*, 63-72; b) P. L. Hansen, J. B. Wagner, S. Helveg, J. R. Rostrup-Nielsen, B. S. Clausen and H. Topsøe, *Science* **2002**, *295*, 2053-2055.

[45] N. S. McIntyre, S. Sunder, D. W. Shoesmith and F. W. Stanchell, *J. Vac. Sci. Technol.* **1981**, *18*, 714-721.

[46] a) K. V. R. Chary, G. V. Sagar, C. S. Srikanth and V. V. Rao, *J. Phys. Chem. B* **2007**, *111*, 543-550; b) M.-F. Luo, P. Fang, M. He and Y.-L. Xie, *J. Mol. Catal. A: Chem.* **2005**, *239*, 243–248.

[47] J. W. Evans, M. S. Wainwright, A. J. Bridgewater and D. J. Young, *Appl. Catal., A* **1983**, *7*, 75-83.

[48] A. Steinfeld, *Int. J. Hydrogen Energy* **2002**, *27*, 611-619.

[49] J. Cheng and P. Hu, *J. Am. Chem. Soc.* **2008**, *130*, 10868-10869.

[50] a) B. S. Clausen, L. Gråbæk, G. Steffensen, P. L. Hansen and H. Topsøe, *Catal. Lett.* **1993**, *20*, 23-36; b) J. D. Grunwaldt, A. M. Molenbroek, N. Y. Topsøe, H. Topsøe and B. S. Clausen, *J. Catal.* **2000**, *194*, 452-460.

[51] a) B. S. Clausen and H. Topsøe, *Catal. Today* **1991**, *9*, 189-196; b) H. Y. Chen, S. P. Lau, L. Chen, J. Lin, C. H. A. Huan, K. L. Tan and J. S. Pan, *Appl. Surf. Sci.* **1999**, *152*, 193-199.

[52] a) Y. Choi, K. Futagami, T. Fujitani and J. Nakamura, *Appl. Catal., A* **2001**, *208*, 163-167; b) E. Groppo, M. J. Uddin, S. Bordiga, A. Zecchina and C. Lamberti, *Angew. Chem., Int. Ed.* **2008**, *47*, 9269-9273.

[53] a) J. M. Fraile, J. A. Mayoral, N. Ravasio, M. Roldán, L. Sordelli and F. Zaccheria, *J. Catal.* **2011**, *281*, 273-278; b) M. Yu, W. Chu and Z. Wu, *Nucl. Instrum. Methods Phys. Res., Sect. A* **2010**, *619*, 408-410; c) B. Singh, M. Gräfe, N. Kaur and A. Liese in *Applications of Synchrotron-Based X-Ray Diffraction and X-Ray Absorption Spectroscopy to the Understanding of Poorly Crystalline and Metal-Substituted Iron Oxides, Vol. Volume 34* (Ed. S. Balwant), Elsevier, **2010**, pp. 199-254; d) M. Tada, R.

Bal, S. Namba and Y. Iwasawa, *Appl. Catal., A* **2006**, *307*, 78-84; e) J. Yoshihara and C. T. Campbell, *J. Catal.* **1996**, *161*, 776-782.

[54] a) W. B. Pearson, *A Handbook of Lattice Spacings and Structures of Metals and Alloys*, Pergamon, London, **1958**; b) J. P. Wilcoxon in *Nanoparticles - Preparation, Charaterization and Physical Properties Vol. 3* (Ed. R. L. Johnston), Elsevier, Oxford, **2012**, pp. 48-52.

[55] a) F.-J. Lai, W.-N. Su, L. S. Sarma, D.-G. Liu, C.-A. Hsieh, J.-F. Lee and B.-J. Hwang, *Chem.– Eur. J.* **2010**, *16*, 4602-4611; b) M. A. Newton, *Chem. Soc. Rev.* **2008**, *37*, 2644-2657.

Chapter 5

Microwave-heating effects in Cu-catalyzed Ullmann synthesis using a continuous-flow milli-plant

This chapter has been submitted as:
F. Benaskar, N.G. Patil, V. Engels, E.V. Rebrov, J. Meuldijk, L.A. Hulshof, V. Hessel, A.E.H. Wheatley, J.C. Schouten, (2012). Microwave-assisted Cu-catalyzed Ullmann synthesis in a continuous-flow milli-plant. *Chem. Eng. J.*, DOI: 10.1016/j.cej.2012.06.147. [1]

Abstract

The combination of milli-scale process technology and microwave heating has been investigated for a liquid-solid Ullmann-type coupling reaction as an example in fine-chemicals synthesis, leading to an improved catalytic activity and selective catalyst heating. Continuous wall-coated and fixed-bed milli-reactors were designed and applied in the Cu-catalyzed Ullmann-type C-O coupling of potassium phenolate and 4-chloropyridine. The added value of using microwaves as a heat source for heterogeneously catalyzed Ullmann synthesis was demonstrated in a batch reactor. The results show clearly increased yields for the microwave-heated process at low microwave powers, whereas at high powers and catalyst loadings arcing reduced the benefits of microwave heating. Activity measurements of the Cu catalyst were undertaken, using a Cu wall-coated (ZnO support) and a Cu fixed-bed (TiO_2 support) tubular reactor, showing somewhat higher yields for the wall-coated reactor. Catalyst deactivation was mainly caused by Cu-oxidation and coke formation. At longer process times, however, significant leaching occurred, which caused permanent deactivation. Catalyst activity could partially be recovered by removal of by-product that had deposited onto the catalyst surface by means of calcination. After 6 h on-stream, the volumetric reactor productivities were found to be 28.3 and 55.1 $kg_{prod}/(m_R^3 \cdot h)$ for the fresh Cu/ZnO wall-coated and Cu/TiO_2

fixed-bed reactor, respectively. After catalyst regeneration, productivities of 20.1 and 55.1 $kg_{prod}/(m_R^3 \cdot h)$ were obtained. Comparison of single- and multimode microwave heating showed a three-fold yield increase when single-mode microwaves with high field density were used instead of multimode microwaves. However, the catalyst stability appeared to be more important and provided a two-fold yield increase for the $CuZn/TiO_2$ catalyst as compared to the Cu/TiO_2 catalyst. This was primarily due to the stability of copper against oxidation by virtue of the preferential oxidation of zinc. In the case of the highly stable $CuZn/TiO_2$ catalyst, a three-fold yield increase was observed using a single-mode microwave cavity which, to the best of our knowledge, led to a not yet reported productivity of 172 $kg_{prod}/(m_R^3 \cdot h)$ for the microwave-heated Ullmann C-O coupling under flow conditions.

5.1 Introduction

Microwave and micro processing in flow systems. Flow chemistry in organic synthesis using micro processing is now well-established as a technology for continuous production of complex organic molecules [2]. Pd and Cu-catalyzed C-C, C-N, C-S and C-O coupling reactions and Cu-catalyzed Simmons-Smith cyclopropanation reactions have been widely developed and applied in flow processes [3]. Moreover, combining milli-reactor operation and microwave-heating, as an alternative energy source, allows the accurate control of residence times as compared to large-scale batch processes and temperatures regarding the microwave penetration depth. This consequently enhances the control of reactor performance in terms of conversion and product selectivity [4]. In particular, regarding the twelve principles of green chemistry, process intensification and novel process windows provide many options by which to meet sustainable processing criteria [5]. The concept of combining microwave and flow chemistry to conduct novel process operations in organic synthesis has recently attracted interest from a wide spectrum of research disciplines in both industry and academia [6].

Kappe and co-workers reported work on combined microwaves and flow systems using meso-scale reactors and microwave heating [7]. The authors employed the concepts of "Novel Process Windows", as introduced by Hessel *et al.*, and discussed the multiple opportunities for operating and controlling organic reactions at elevated temperatures and pressures [8]. Organ and co-workers also contributed to state-of-art microwave-assisted capillary-type flow reactors for metal-catalyzed organic reactions [9]. Many examples of dedicated flow systems, being used in combination with microwave heating for large-scale synthesis and industrial applications, have been reported [10]. AstraZeneca studied various examples of microwave-assisted flow synthesis for pharmaceuticals, leading to rather high productivities [11]. Earlier, Moseley *et al.* developed automated microwave "stop-flow" reactors that provided competitive productivities as compared to typical batch-scale reactions [12].

The current successes in combining microwave heating and flow systems, however, have mainly been achieved using multimode microwave cavities. These suffer from a non-uniform microwave field and a limited microwave penetration

depth, resulting in an inhomogeneous temperature distribution. The use of single-mode microwave cavities in flow chemistry, which provide a highly uniform microwave field, is currently an emerging field of investigation for efficient reaction operation [13]. Since for most organic solvents the penetration depth of microwaves is of the order of centimeters, the optimum microwave-assisted reactor for organic reactions is characterized by reactors with the same or smaller dimensions [14].

At these reactor sizes microwaves, acting as a volumetric heating source, do not suffer from heat-transfer resistance and, combined with a proper reaction medium, provide opportunities to heat the reaction mixture rapidly and efficiently (Figure 1a). Meanwhile, micro- and milli-reactors themselves are characterized by their low resistance to heat transfer. Taken together, these observations suggest the potential for highly efficient microwave-assisted reactions using combined microwave milli-reactors that are optimized with respect to heat supply and release (Figure 1b).

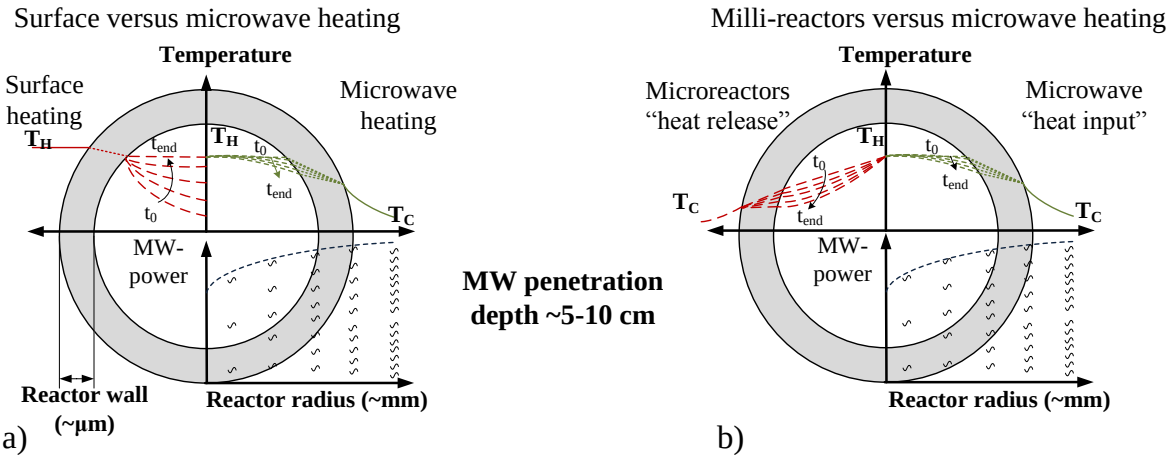

Figure 5.1. Temperature profiles for conventional (surface) and microwave (volumetric) heating (a), showing major benefits at mm-to-cm scale reactors. Nevertheless, an important balance must be struck between fast energy supply by the microwaves and fast heat release owing to the micro- and milli-reactor dimensions (b). T_H,T_C is hot and cold temperature, resp.

Recently, Patil *et al.* have demonstrated the effect of shape and dimensions of a milli-reactor setup on controlled and efficient microwave heating in a single-mode cavity [13b]. The results provided experimental evidence of a complete microwave penetration in a milli-sized tubular reactor in the direction perpendicular to the fluid flow. This resulted in rapid and controlled heating without the development of significant radial temperature gradients in the milli-sized flow reactors used.

Nevertheless, applications in industrial practice still hamper unresolved drawbacks, such as (a) limited microwave penetration depth, (b) high equipment costs, (c) difficult temperature measurement and control and (d) restriction to the use of polar solvents/reactants specific to each process. The penetration depth limitations and the restriction to the use of only polar solvents can be circumvented in metal-catalyzed reactions where microwave heating occurs via interaction of the electric/magnetic components of microwaves with metals. This resultant selective

metal heating provides a unique opportunity to address these limitations in microwave-heated reactors [15].

Cu-catalyzed coupling reactions in flow processing. In 2010 the Nobel Prize for Chemistry was awarded to the pioneers of Pd-catalyzed cross-coupling reactions that have been key to organic synthesis during the last half century [16]. However, the Cu-catalyzed Ullmann-type coupling reaction provides significant advantages regarding the cost aspects (Scheme 1) [17].

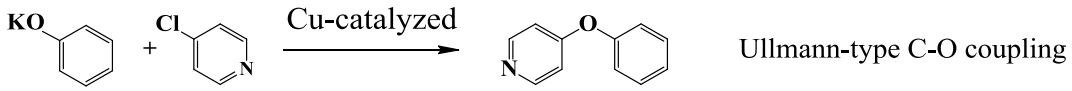

Scheme 5.1. The Cu-catalyzed Ullmann-type coupling reaction towards 4-phenoxypyridine.

The Ullmann-type C-C, C-O and C-N coupling reactions, discovered more than a century ago by Ullmann and Goldberg, have recently encountered a renaissance, mainly as a result of the exploitation of highly efficient copper-based catalysts [18]. However, these Ullmann-type coupling reactions still suffer from the need for harsh reaction conditions, the use of high levels of catalyst (50-100 mol%) and also the need to use relatively reactive and expensive aryl halides. Reaction intensification, improvement of selectivity and development of more stable catalysts represent the current challenges, and catalytic milli-reactors promise to address these challenges. In flow processing, the major issue is to avoid the use of catalyst slurries by supporting catalysts on the reactor wall or by employing micro-structured fixed-beds [19]. Moreover, stable catalyst performance in terms of activity and selectivity in a heterogeneously catalyzed flow process brings a major cost benefit in comparison to the use of homogeneous or slurry catalysts, which require expensive catalyst recovery procedures [17].

When providing a catalyst for reaction, it is also necessary to consider how energy is supplied to the catalyst surface, in particular because the efficiency of this process is governed by classical heat-transfer limitations. However, metal catalysts are known to absorb energy rapidly under microwave irradiation and, as a result, to couple the microwave energy selectively to the catalyst particles, leaving the surrounding environment less or even unheated [20]. In this way, microwaves selectively heat the reaction system at the locus of the reaction and so enhance efficiency as well as activity and conversion. A fast rise in the temperature of the nano-catalyst combined with a relatively low solvent bulk temperature, leads to highly advantageous reaction conditions. This is especially true when the active copper catalyst, *e.g.* in an Ullmann coupling, is supported by a non-magnetic matrix, such as TiO_2, SiO_2 or ZnO, as described by Walton *et al*. [21]. In metals with magnetic character, rapid microwave absorption results from so-called eddy currents and magnetic reversal loss mechanisms when micron-sized particles are present [22].

In addition, the strong coupling of these metals with the microwave field has been reported, providing very fast heating but, dependent on particle size, unfortunately also arcing [22b, 23]. As a result, it is of importance, not only for sustainable use of the catalyst, but also for selective microwave absorption, to synthesize active copper particles of the desired nano-size and with a uniform size distribution. We have recently reported on the development of monometallic and bimetallic Cu-based nanoparticles with a narrow size-distribution and a high resistance to oxidation during Ullmann-type reaction [24]. Additionally, the use of microwave energy in this type of reaction was reported for these nano-catalysts [25]. These results have now been developed in terms of flow chemistry.

In this chapter, an integrated system is proposed, synergizing the benefits of microwave systems (as a novel heating technology) and milli-processing (as a novel reactor technology) in flow synthesis. A tubular milli-reactor was designed, where the catalyst and support were coated either onto the reactor wall or onto a packing material composed of spherical glass beads, leading to a wall-coated or a fixed-bed milli-reactor, respectively. More important, however, was the use of heterogeneous copper which, as a "metallic microwave-absorber", permitted selective heating of the catalyst surface and thus provided improved activity.

5.2 Experimental

5.2.1 Chemical protocol of flow process

Ullmann C-O coupling reactions. 4-Chloropyridine and potassium phenolate were prepared from 4-chloropyridine HCl salt and phenol as described in chapter 3. For the activity experiments 20 g (0.15 mol) of potassium phenolate and 0.40 g (0.0015 mol) of 18-crown-6 ether (Aldrich > 99.0%) were dissolved in 80 mL *N,N*-dimethylacetamide (DMA, Sigma-Aldrich, CHROMASOLV® Plus, for HPLC, ≥99.9%) in a continuously stirred vessel at 50-60 ºC. After a solution was obtained, 11.4 g (0.1 mol) of 4-chloropyridine and 1.9 g (0.01 mol) of tetradecane as internal standard (Fluka, analytical standard) were mixed separately with 20 mL DMA and slowly fed to the storage vessel. The reactants were pumped into the flow-through reactor (see Supporting Information in reference [1]). For batch experiments, the reactants were mechanically mixed at 500 rpm in the abovementioned concentrations, heated until the reaction temperature was reached and then the copper powder (99 wt%, Aldrich) was added as the catalyst (10 mol% with respect to 4-chloropyridine).

5.2.2 Catalyst synthesis

Copper nanoparticles. Cu nanoparticles were synthesized as previously reported from copper(II) sulfate pentahydrate, sodium hypophosphite monohydrate and PVP (M(average) = 40,000) [24-25]. The synthesis of bimetallic CuZn nanoparticles was based on the use of copper sulphate pentahydrate and zinc(II) chloride following our previous work [18i]. (More detailed protocol see chapter 3)

TiO_2 based fixed-bed catalyst. Support synthesis employed titanium(IV) ethoxide (99.99%), isopropanol (anhydrous, 99.5%), hexamethylenetetramine (HMTA, puriss. p.a., ≥99.5%). 250 ± 12 μm spherical SiO_2-beads (E&R Chemicals & Equipment B.V.) were used as support carriers [26]. These beads were first coated with TiO_2 by dip-coating, after which the Cu nanoparticles were coated by wet impregnation. A total of 0.75 g (3.29 mmol) titanium(IV) ethoxide ($Ti(OEt)_4$,) was added to 20 g of glass beads, followed by vacuum solvent removal at 60 ºC, overnight drying at 80 ºC and calcination at 120-350 °C for 12 h (heating/cooling rate: 10 °C/min). See Supporting Information in reference [1].

ZnO based wall-coated catalyst. For the growth of ZnO-nanowires on the internal reactor wall, a seed layer of ZnO nanoparticles (mean size ~100 nm) was deposited by circulation of a nanoparticle suspension in ^{i}PrOH for 48h (flow speed 1.5 mL/min). Subsequently, the system was flushed with pure ^{i}PrOH for 30 min. After drying, an equimolar aqueous solution of HMTA and $Zn(NO_3)_2$ (0.025 M) was pre-heated to 90 °C and circulated through the system for 5 h, followed by flushing with ^{i}PrOH for 1 h (0.5 mL/min). The tube was pre-dried and heated in a muffle furnace (80 °C) for 1 h. The reactor was coated with copper nanoparticles by flowing 50 mL of a Cu nanoparticle suspension in anhydrous methanol (metal mass concentration: 0.25 mg/mL) through the reactor tube at a flow speed of 1 mL/min. After solvent evaporation, the reactor was calcined at 350 °C for 12 h (heating/cooling rate: 10 °C/min).

5.2.3 Wall-coated and fixed-bed tubular reactors in oil-bath and microwave heating experiments

Quartz-glass tubular milli-reactors (L = 1.2-1.5 m, d_{in} = 1-3 mm and d_{out} = 5 mm) were either packed with catalyst coated glass beads or wall-coated with the catalyst.

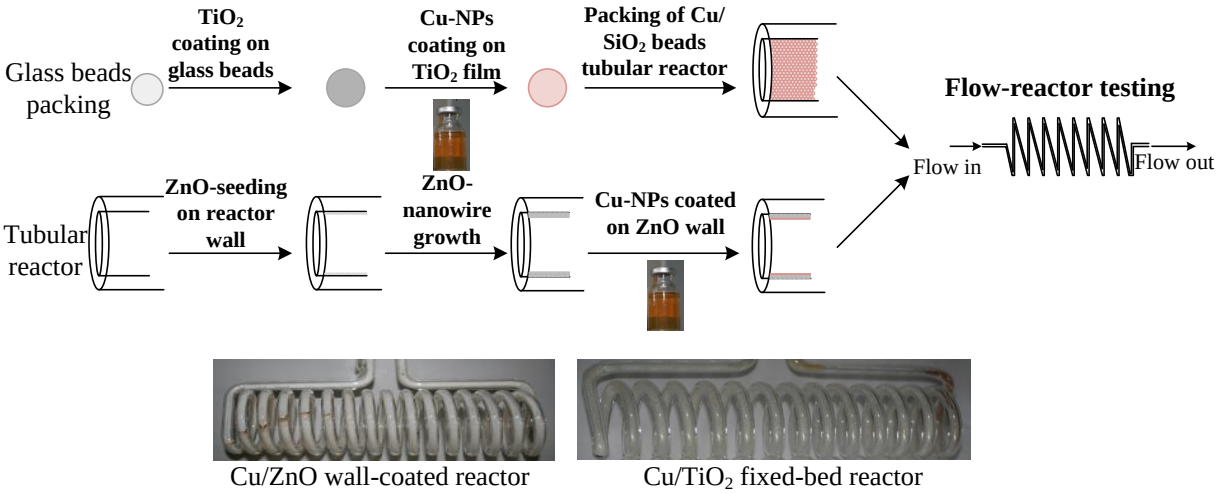

Figure 5.2. The catalyst coating procedure for fixed-bed and wall-coated catalytic reactors. Cu nanoparticles (Cu-NPs) were deposited on a ZnO nanowire support in a wall-coated reactor, and on a TiO_2 support in a fixed-bed reactor.

Figure 2 shows the design procedure for both (wall-coated and fixed) reactor configurations. Reactor inlet and outlet were extended to enable an easy connection

and disconnection to the pump head, sampler and outlet valve. The flowrate was varied (Fv = 5-80 mL/h) to obtain desired residence times. Fixed-bed systems were prepared by packing the coated beads into the tube (V_{total} = 10.10 mL) to mimic a micro fixed-bed reactor with a bead interstitial spacing in the range 10-50 µm. The resulting bed void provided an experimentally determined liquid volume of V_{liq} = 3.34 mL with a catalyst loading of 2.5 mg/mL_{liq}, which was comparable to a batch reactor catalyst loading of 2.7 mg/mL_{liq}.

As shown in Figure 3, the reactor was placed either vertically in an oil-bath (Lauda Ecoline Staredition 012, type E312, 2.3 kW with a half-synthetic oil medium) or horizontally in a multimode microwave cavity (Milestone Multimode Microwave, type ETHOS 2.45 GHz, 2.5 kW). The pre-mixed (mechanical) and pre-heated (50 °C) reactant solution was fed into the reactor through a syringe pump (1000D; Teledyne ISCO Inc., Lincoln, NE/USA), which could be operated at pressures from 1 to 40 bar (see Figure 2, left). An argon injector was placed in the supply vessel to maintain inert atmosphere. At the reactor outlet, a T-splitter (T-junction, Swagelok, 1/8 in.) was connected to the sampler.

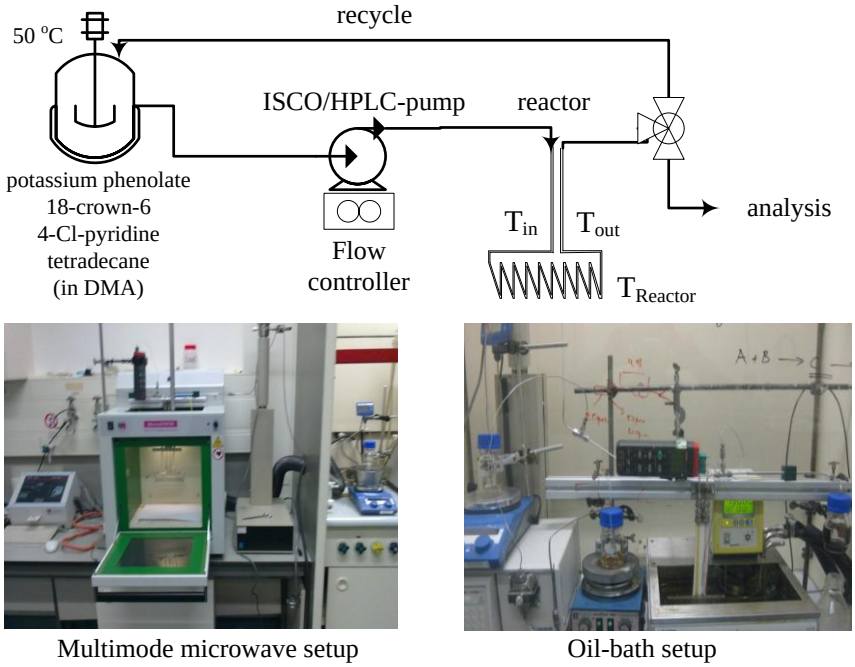

Figure 5.3. A schematic process flow diagram of the oil-bath heated and multimode heated microwave setups.

For the oil-bath reactions, temperatures were measured using K-type thermocouples (Voltcraft K204 data logger) placed inside the oil-bath and at the outlet of the catalyst bed. For the microwave experiments, a fiber-optic probe (ATC-FO sensor, Milestones) was inserted at the inlet and outlet of the reactor inside the microwave oven. To avoid bead floating, the catalyst (coated glass beads) bed was fixed to the lower reactor part by glass filters. Constant pressure was maintained in the reactor using a syringe valve to avoid solvent boiling and bubble formation in the catalyst bed. The inlet and outlet of the quartz-glass reactor

were connected using Swagelok Ultra-Torr (stainless steel, SS 316; inner diameter 1.6 mm) connections with chemically resistant sealing rings.

For the single-mode microwave experiments, a microwave (Fricke und Mallah GmbH) setup consisting of a single-mode microwave cavity and operating at a frequency of 2.45 GHz with adjustable power settings up to 2 kW was utilized. Maximum microwave absorption was assured through focusing the resonant microwaves in the cavity by using stub-tuners and short-circuits. The reflected power was measured, using a detector diode over the isolator. A LABVIEW interface program was used to control the temperature and power input in the reactor, using OPSENS fiber-optic sensors in the center of the fixed-bed. The reference case batch experiments were carried out in a mechanically stirred (500 rpm) 100-mL jacketed batch reactor. Identical setups were used for the batch experiments with oil-bath and microwave heating (see Supporting Information in reference [1]). All reactions were carried out in an argon atmosphere.

5.2.4 Product analysis and catalyst characterization

Product yield analyses. Samples were taken at the outlet of the reactor and diluted with dimethyl sulfoxide-d^6 (DMSO-d^6, Cambridge Isotope Laboratories Inc., D 99.9%) for ^{1}H-NMR spectroscopic analyses. ^{1}H-NMR data were collected using a Varian 400 NMR spectrometer (400 MHz). The chemical shifts (in δ ppm) were based on TMS (tetramethylsilane) at 27 ºC as internal reference and peak integrations were converted to concentrations by using tetradecane ($C_{14}H_{30}$) as internal standard. The productivity and product yield were obtained by comparing the reactants (phenoxide and 4-chloropyridine) and the product (4-phenoxypyridine) signals corrected for the internal standard. The ^{1}H-NMR of the spectra ($CDCl_3$; 8.4-8.6 ppm) of the reactants and product after full conversion are shown in the Supporting Information in reference [1]. The ^{1}H-NMR assignments for the product in δ (ppm, $CDCl_3$) are: 8.48 (d, J = 4.0 Hz, 2H), 7.44 (t, J = 8.0 Hz, 2H), 7.29–7.25 (m, 1H), 7.11 (d, J = 8.0 Hz, 2H), 6.85 (d, J = 8.0 Hz, 2H). The ^{1}H-NMR data was additionally compared with GC-MS data to confirm product formation.

Inductively coupled plasma (ICP) measurements. The losses of catalyst and support were analyzed using inductively coupled plasma measurements, combined with optical emission spectroscopy. A Spectro Ciros^{CCD} spectrometer was used to determine the amounts of copper catalyst and titania and zinc-oxide supports at 1400 W. Sample injection used a nebulizer in a double-pass spray chamber with a sample uptake frequency of 2 mL/min. For the fixed-bed reactor, the catalyst packing was used as sample material and for the wall-coated reactor, the reactor was dried and *ca.* 2 mm of the reactor was cut off for analysis. The samples were treated in H_2SO_4 (5 M) for 24 h before being taken for analysis. In addition, reactions were sampled by collecting an accurate amount of reaction mixture and dissolving it in H_2SO_4 (10 mL, 5 M). The resulting aqueous layer was diluted with 10 mL milli-pore water and separated off by milli-extraction. To avoid an abundance of protonated amide signals, the sample was diluted using an additional

20 mL volume of milli-pore water. Calibration lines were freshly prepared and inserted prior to the catalyst samples.

X-Ray Photoelectron Spectroscopy (XPS) analyses. XPS was used to analyze the catalyst surface and establish the oxidation state of the copper. Various XPS samples were analyzed either using known amounts (in mg) of the wall-coated tubular reactor or by measuring exact quantities of catalyst beads deposited on a carbon holey film in a glove-box (< 10 ppm O_2). The samples were transported in a closed holder for oxygen-free analysis. XPS data was obtained with a Kratos AXIS Ultra spectrometer equipped with a monochromatic Al Kα X-ray source (1486.6 eV at 150 W) using a delay-line detector (DLD). Constant pass energies of 160 eV and 40 eV were applied for survey and region scans, respectively, at a background pressure of 2×10^{-9} mbar. Based on the spectral intensities of Cu, conclusions were drawn with respect to losses observed by ICP analysis and the drops in activity.

Scanning Electron Microscopy (SEM) analyses. SEM images were obtained using a FEI Quanta series (FEG 3D G2 SEM) with an acceleration voltage of 5 kV and magnifications in the range 5-100 x 10^3. The images were used to determine the surface morphology and coating thickness of the wall-coating and the catalyst support beads at a lateral resolution of 50 nm^2. Simultaneously, surface elemental composition analysis was carried out using Energy-Dispersive X-ray (EDX) spectroscopy at an image spot size of 50 nm^2 and an interaction-volume of 100 µm (all EDX spectra are provided in the Supporting Information in reference [1]). Leaching of the catalytic layer was surveyed by comparing the coating thickness and the Cu, Ti and Zn signals in the EDX spectra. Both the fresh and spent catalysts were analyzed using SEM. The surface structure of spent samples was also investigated to probe the effects of microwave irradiation. The same samples as used for XPS analyses were surveyed and the acquired SEM-EDX results were then compared with the XPS data. In particular, the presence of an oxidized or graphitized surface-covering upper layer was compared to either oxidation or deposition of carbon due to degradation of the solvent as a result of arcing.

High Resolution Transmission Electron Microscopy (HR-TEM). HR-TEM images, obtained with a FEI Tecnai G2 Sphera electron microscope operating at 200 kV acceleration voltage, were used to examine the particle size and structure of the pre-synthesized Cu nanoparticles. Nanoparticles supported on the reactor wall and the glass beads were also examined. Samples of fresh and spent catalysts were analyzed. The samples were prepared by scratching the catalyst coating from the reactor wall or by crushing glass beads, respectively, and by suspending the resulting powders in 2 mL ethanol before coating and drying the solvent onto a 200 mesh molybdenum grid (30 µL of the suspension). The obtained images provided information on the dispersion of particles on the supports.

5.3 Results and discussion

In this study, two catalytic flow reactors were investigated, *i.e.* a fixed-bed reactor based on a TiO_2 coating as copper catalyst support and a wall-coated reactor where ZnO was used as copper catalyst support. Initially, both reactors were tested in a conventionally heated (*i.e.* oil-bath) setup, wherein the catalyst stability and activity were optimized. At process times of up to 12 h by-product coverage of the surface, oxidation of the catalyst and particle agglomeration were found to be the main causes for catalyst deactivation. The catalyst could partially be regenerated by thermal treatment. At higher on-stream times, leaching played a major role, in leading to permanent deactivation of the catalyst.

5.3.1 Catalyst design and stability measurements for flow chemistry

Zinc-oxide wall-coating as Cu-support. Figure 4 shows selected SEM images of as-grown ZnO-nanowires on the glass reactor surface. Figures 4a and 4b show monodisperse, rod-like crystals (l_{av} = 500 nm, d_{av} = 20 nm) with a high surface dispersion. However, after 12 h on-stream (Figure 4c) the catalytic wall appeared to be covered with a substance, which, after EDX analysis, was confirmed to be KCl formed as by-product during the reaction.

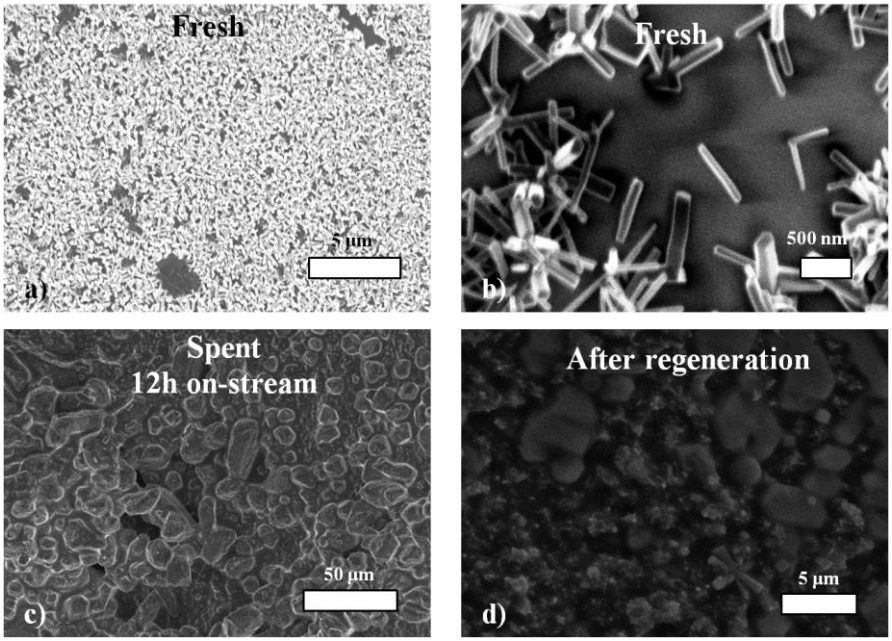

Figure 5.4. ZnO-nanowires grown on the SiO_2 reactor wall, showing a highly disperse nanowire film in SEM-images at low (a) and high (b) magnification. The reactor wall become covered with by-product KCl (c), which could be partially removed (d) by thermal treatment and reduction with hydrogen.

Treatment with DMA, drying, calcination (at 350 ^{o}C) and reduction with a hydrogen flow at 200 ^{o}C removed most of this salt from the surface, as can be seen in Figure 4d (EDX spectra are provided in the Supporting Information in reference [1]). At higher processing times (> 24 h), ICP analysis confirmed a considerable decrease in the levels of both Cu catalyst and ZnO support due to irreversible

leaching. ZnO-nanowires, grown on the internal wall of a tubular glass reactor, provided catalyst loadings similar to those for TiO_2 on the glass-bead packing, *i.e.* 1.26 and 1.38 $mg_{Cu}/mL_{reactor}$ for the wall-coated and the fixed-bed reactors, respectively. Although for the wall-coated reactor the overall available reaction surface was much lower than for the fixed-bed reactor, similar Cu-loadings on ZnO and TiO_2 were achieved during catalyst deposition onto the supports.

Titania bead-coating as Cu-support. Relatively low absolute amounts of both support (TiO_2) and catalyst (Cu nanoparticles) were deposited on the titania-coated glass beads ($d_P \sim 250$ μm). As described in Section 5.2.2, the catalyst was prepared using a TiO_2 support matrix and the metallic nanoparticles were impregnated after the support was deposited onto silica beads. In this way, the catalyst loading (1.38 ± 0.15 $mg_{Cu}/mL_{reactor}$) could be accurately controlled in order to obtain a loading that approximated to that of the wall-coated reactor. Figures 5a, 5b and 5c show the coated beads before and after reaction. The effect of by-product formation, *i.e* surface coverage by KCl, is clearly visible, also in this case. SEM-EDX analysis further confirmed the abundant presence of KCl-salt crystals.

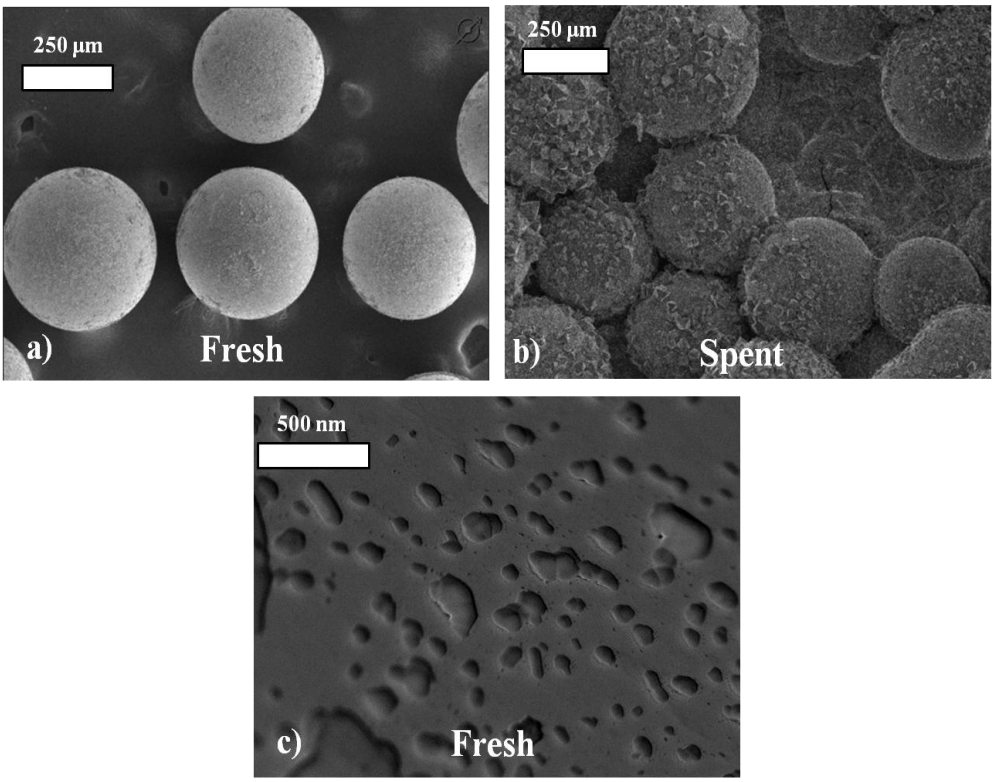

Figure 5.5. SEM images of the fresh (a) and spent (b) Cu/TiO_2-coated glass beads, demonstrating considerable deposition of KCl by-product. Catalyst deposition (c) also shows relatively low catalyst density for the Cu/TiO_2 when compared to that of the Cu/ZnO system.

Copper nanoparticle deposition and stability. In Figure 6, representative TEM images of the nanoparticles are shown for both the fresh and spent Cu catalysts. Figures 6a and 6c show the fresh and spent catalyst of the fixed-bed Cu/TiO_2 system, respectively. The fresh catalyst clearly demonstrates uniformly dispersed

Cu nanoparticles in the titania matrix. The particle size was found to be 7.6 ± 0.8 nm based on measurements for 200 particles in various TEM images.

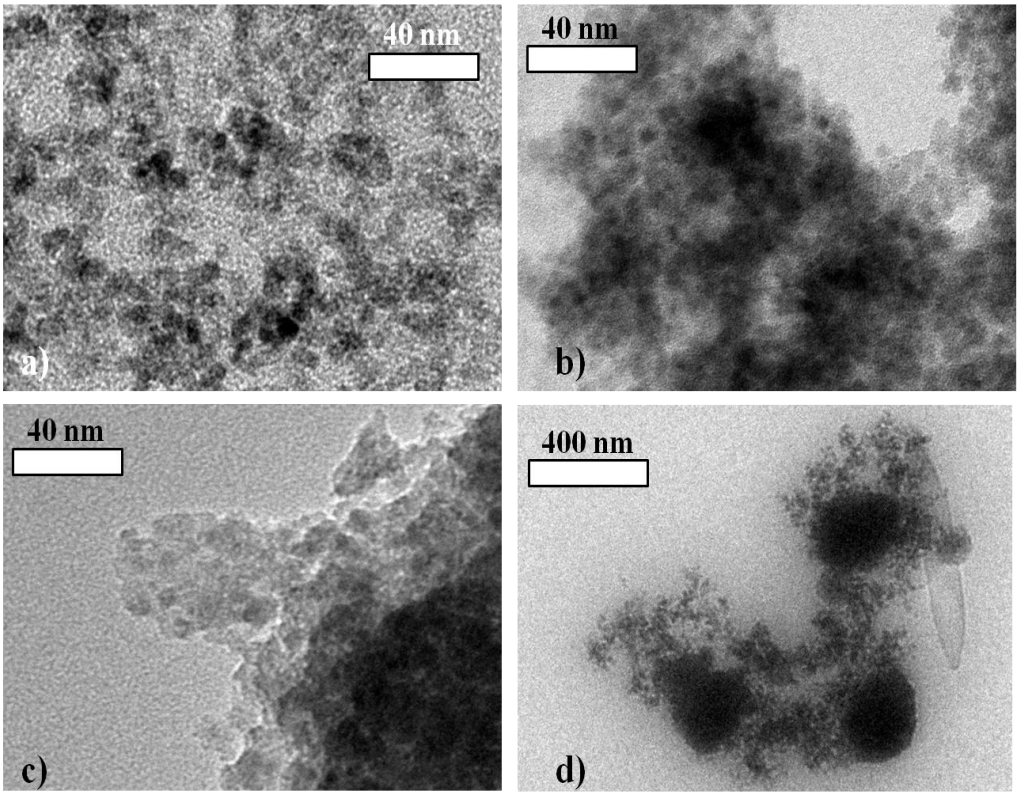

Figure 5.6. Representative TEM images of fresh (a) and spent (c) catalysts used in the Cu/TiO_2 fixed-bed reactor and the fresh (b) and spent (d) catalyst used in the Cu/ZnO wall-coated reactor.

However, after 12 h on-stream in the fixed-bed reactor, the catalyst particles have significantly agglomerated. Figures 6b and 6d show TEM images of the fresh and spent wall-coated Cu/ZnO catalyst. Clearly, the fresh Cu/ZnO wall-coated coated catalyst demonstrated a much higher particle density than the fresh Cu/TiO_2 catalyst (Figure 6a and 6b) did. The higher copper loading in the wall-coated reactor was prepared in order to compensate for the lower macroscopic reaction surface in that system. Figure 6b shows, however, partial nanoparticle agglomeration, already occurring in the fresh catalyst. After 12 h on-stream the Cu/ZnO wall-coated catalyst showed higher nanoparticle agglomerates up to sizes of *ca.* 150 nm (see Figure 6d).

Catalyst and support leaching. The catalyst and support losses are shown in Figure 7. ICP measurements provided the amounts of Cu, Zn (from ZnO) and Ti (from TiO_2) for samples taken during the total process time. For the ICP analyses, multiple catalyst samples were taken from the fixed-bed reactor or from the wall-coated reactor, as described in Section 5.2.4. Neither Cu/TiO_2 nor Cu/ZnO catalysts leached more than 10% after a run of 12 h. Figure 7a shows a significant drop of *ca.* 30 wt% of the Cu signal in the Cu/TiO_2 system after only 24 h on-stream, whereas *ca.* 10 wt% of the TiO_2 support was lost. After 48 h on-stream, however,

roughly 60 wt% of the copper was lost while only 20 wt% of the Ti had leached. After 72 h on-stream, both catalyst and support had completely leached from the glass beads. Generally, however, for the TiO_2-based fixed-bed reactor, the Cu nanoparticles appeared to leach prior to the TiO_2 support.

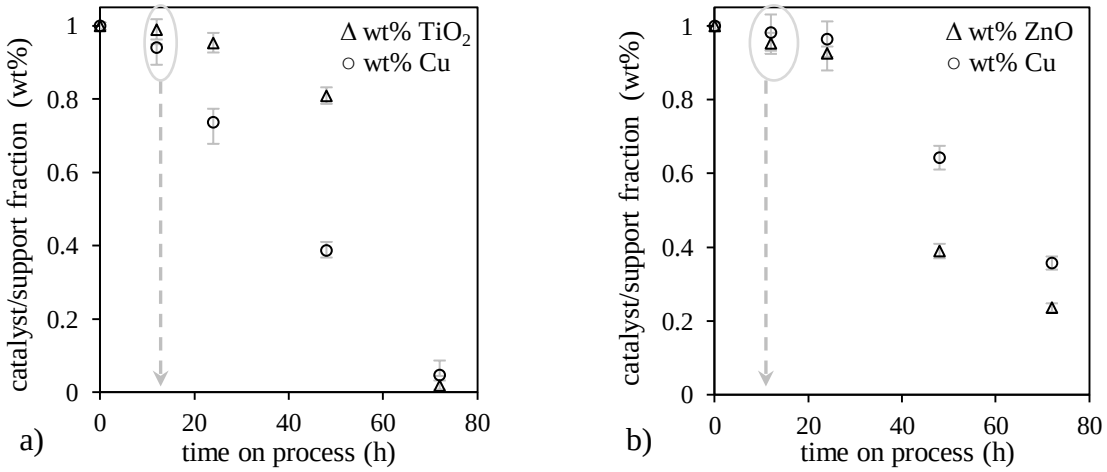

Figure 5.7. Losses of Cu catalyst and TiO_2 support for the fixed-bed reactor (a) and of Cu catalyst and ZnO support for the wall-coated reactor (b) during time-on processing.

The opposite was observed for the ZnO-supported system (Figure 7b), where after 48 h *ca.* 60 wt% of the ZnO-nanowires were removed while only 40 wt% of the Cu nano-catalyst was lost. This observation could only be explained by the fact that, although the ZnO layer was uniformly distributed, the Cu nanoparticles formed islands which stabilized the ZnO-glass interface. As a result, a much higher ZnO fraction leached. After 72 h, about 22 wt% of ZnO and 36 wt% of Cu remained, showing that much less shearing occurred in the wall-coated reactor as compared to the fixed-bed reactor. Overall, at longer process times, adhesion appears to be weak at the Cu/TiO_2-glass interface for the fixed-bed catalyst system and at the ZnO-glass surface for the wall-coated catalyst system. As a result, the subsequent activity experiments were only done using processing times shorter than 12 h, after which a fresh batch of catalyst was used.

5.3.2 Activity experiments

Initially, the effect of multimode microwave heating and conventional oil-bath heating on the catalyst productivity was compared, using a continuously stirred batch reactor and a commercial copper catalyst. In the next step, activity measurements on a supported Cu catalyst were done in an oil-bath using a fixed-bed reactor and a wall-coated reactor as examples of flow-type reactors based on titania and zinc-oxide support materials, respectively. Finally, microwave flow-experiments were carried out in both a multimode and a single-mode microwave cavity.

Batch experiments using conventional and microwave heating. The effects of microwave heating and conductive heating were investigated at three different reaction temperatures. Figure 8 shows the results of experiments conducted at 110,

120 and 140 °C for both heating methods, where a clear trend can be observed in yields with respect to time. Figure 8a demonstrates that the use of microwave irradiation instead of oil-bath heating gives an average yield increase of 20% at 110 °C. At 120 °C (Figure 8b), the difference in yield between microwave and oil-bath heating is far less than at 110 °C, and disappears completely at 140 °C (Figure 8c).

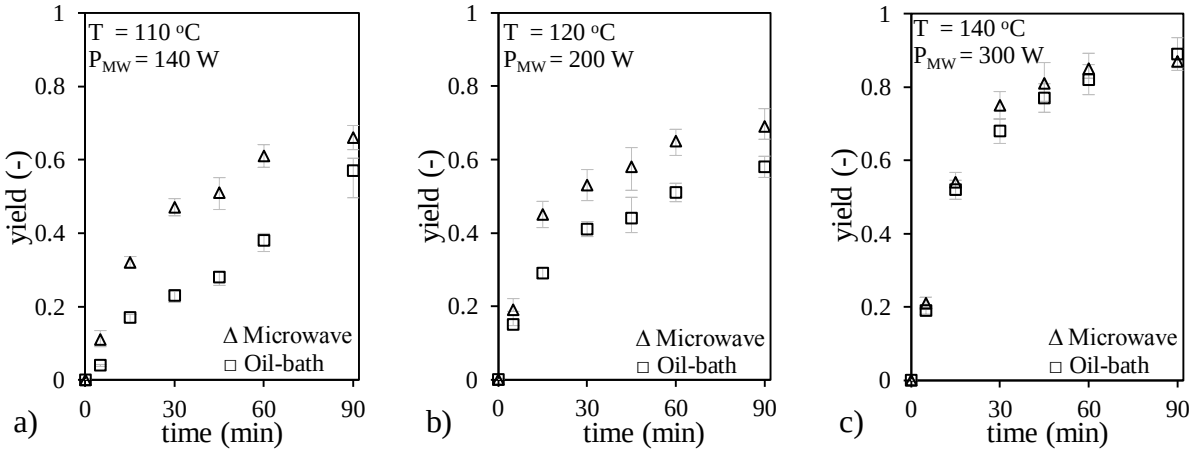

Figure 5.8. Yield versus time plots for batch-type experiments using microwave heating and oil-bath heating at (a) 110 °C, (b) 120 °C and (c) 140 °C. At lower microwave powers, microwaves have the benefit of selectively heating the metal catalyst. At higher powers, microwave absorption by the solvent eliminates this advantage.

The difference in yield between microwave and conductive heating experiments can be attributed to the differential absorption of energy by the catalyst and liquid reaction mixture [20a]. Thus, better yields are recorded for the microwave-heated experiments because higher temperatures are obtained at the locus of the reaction (*i.e.* catalyst surface) due to selective heating of the catalyst [21b, c, 22a, 27]. This effect vanishes at higher reaction temperature, probably on account of a low temperature difference between the catalyst surface and the bulk liquid [28]. Figure 9a shows the temperature-time histories for a microwave power of 120 W and various Cu catalyst loadings in a batch reactor. The initial heating rates (in °C/min) obtained from microwave irradiation appeared to be strongly dependent on the amount of copper catalyst used in a 30-mL batch reactor, demonstrating an optimum heating rate for low amounts of metallic copper. The decay in heating rate at increased Cu-loadings, shown in Figure 9b, is mostly due to arcing effects.

Although it is difficult, if not impossible, to quantify the energy absorption by copper, the heating rates of the liquid in the presence and absence of the catalyst provide an insight into the thermal contribution of microwave absorption by the metal [29]. Based on the heating profiles, the microwave-heating efficiency [30] has been determined according to the work of Stankiewicz *et al* [31]. For these experiments a jacketed and insulated mechanically stirred batch reactor was used (see Supporting Information in reference [1]), allowing energy losses to the environment to be neglected. Additionally, the microwave-heating calculations were based on a cavity-to-reactor power input that ignored losses from the grid to the magnetron.

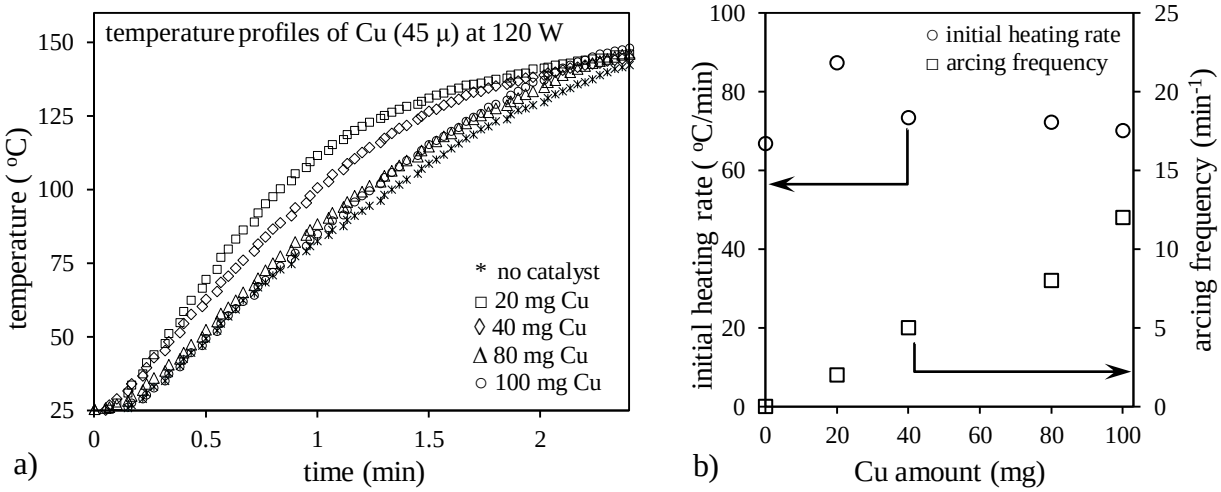

Figure 5.9. Temperature profiles (a) and initial heating rates/arcing frequencies (b) at various powdered Cu-loadings, demonstrating increased initial heating rates (for one minute) at low Cu-levels. Decay in heating rates is mainly due to arcing effects at increased Cu-loadings.

Figure 9b shows the heating rate as a function of the amount of catalyst in the reactor and indicates that the use of 20 mg Cu catalyst increased the heating rate from 67 to 87 ^{o}C/min relative to the heating rate obtained in the absence of catalyst. However, the heating rate stabilizes at higher catalyst loadings, reaching *ca*. 71 ^{o}C/min for 100 mg catalyst. While the heating efficiency decayed, an almost linear increase in the frequency of arcing was observed, indicating a breakdown in microwave-energy accumulation in the catalyst particles, but not necessarily an increase in thermal energy or conversion [20c]. This also explains why in Figure 8 better yields were observed for microwave heating at lower powers than for oil-bath heating. Obviously, microwave energy heated the catalyst surface at lower powers (without arcing), leading to higher yields than expected from the measured temperatures in the bulk liquid.

Batch versus continuous reactors with oil-bath heating. Heterogeneously catalyzed flow reactors have been developed with the intention both of increasing process productivity and ease of catalyst regeneration in comparison to what is achievable with conventional batch-type reactors. For this reason, different flow parameters have received special attention in this study. Firstly, the performance of the catalyst carrier (ZnO wall coating versus TiO_2 fixed-bed coating) in a tubular reactor was investigated to improve the productivity per unit catalyst mass as compared to traditional batch reactors for fine-chemical operations. Secondly, the influence of mixing was investigated by comparing a fixed-bed (disturbed-flow) with a wall-coated (laminar-flow) continuous reactor. The results for these continuous systems were also compared with those obtained using a mechanically stirred and jacket-heated batch reactor, as described in the previous section. Figure 10 shows the product yields as a function of residence time at 130 ^{o}C for a continuous fixed-bed, wall-coated and slurry-type continuous reactor in comparison with those of a slurry-type batch reactor, containing metallic copper powder as catalyst.

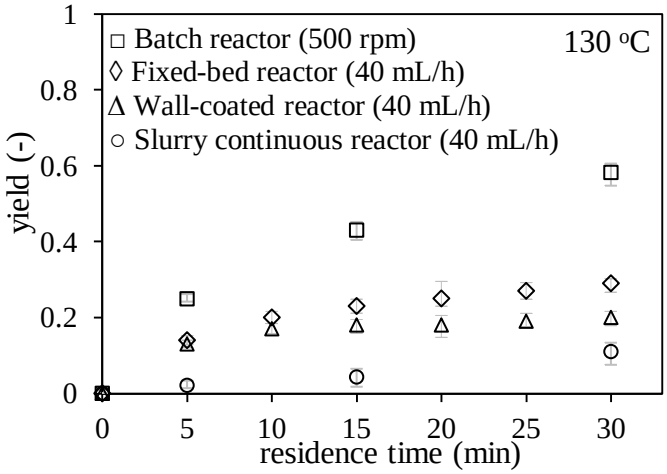

Figure 5.10. Performance as a function of residence time for continuous fixed-bed (◊), wall-coated (Δ) and slurry-type continuous reactors (○) shown with reference to the slurry-type batch reactor (□). The 4-chloropyridine and potassium phenolate concentrations were kept at 1.0 and 1.5 mol/L at 130 °C for all experiments. For batch operation, the catalyst loading was 2.5 mg/mL$_{reactor}$ and the stirring rate was 500 rpm. For continuous operations, a catalyst loading of 1.2 mg/mL$_{reactor}$ and a flow rate of 10-40 mL/h were applied.

Compared to 58% yield obtained after 30 min using the batch reactor, the yield stagnated at *ca.* 18% after 10 min (at flowrates of 5-80 mL/h) for both the fixed-bed and the wall-coated batch-loop flow reactors. In these cases, the highest turnovers were achieved in the first two cycles, while further recycling of the reaction mixture did not lead to a significant yield increase. This flattening of the yield, after only the second cycle, was clearly caused by catalyst deactivation due to oxidation and coke deposition. For these reactor types, catalyst deactivation and regeneration were evaluated through variation of the pre-treatment and post-treatment methods.

Fixed-bed and wall-coated continuous reactors with oil-bath heating.

Cu/TiO$_2$ fixed-bed flow reactor. In most heterogeneous catalyst systems, the conversion drops noticeably when the catalyst surface is subjected to a fluid flow that leads to catalyst oxidation or deactivation due to coke deposition. Catalyst leaching also results from the high shear forces applied to the catalyst surface by the flow. Moreover, catalyst deactivation by surface oxidation occurs when the chemical components possess oxidative properties. This causes physicochemical changes to the active metal and leads to Cu^{I} or Cu^{II} species which have an increased solubility in the amide-containing solvent, facilitating catalyst leaching from the support. To avoid leaching, catalyst regeneration is usually performed by slow heating (to >200 °C) until all surface contaminants have been removed through evaporation and, finally, by combustion of adsorbed organic compounds. Parameters, such as calcinations temperature and time, have to be optimized for regeneration of the deactivated catalyst. The effect of a calcination procedure (at 350 °C for 12 h) on the product yield was investigated for a fresh-catalyst with reference to a non-calcined fresh catalyst sample. Figure 11 shows enhanced yields and the necessity of catalyst calcination at 350 °C, following that procedure.

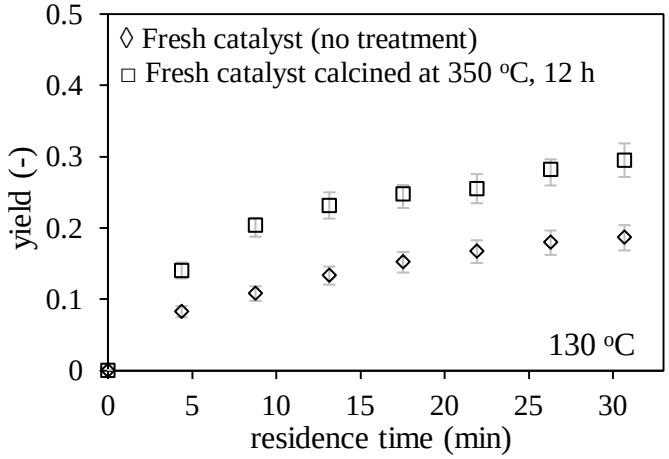

Figure 5.11. Cu/TiO_2 fixed-bed catalytic performance for a fresh catalyst (non-calcined (□) and calcined (◊) at 350 °C for 12 h).

These results show clearly that catalyst stability was improved by an optimized calcination during catalyst synthesis. Enhanced catalyst activity was found to result in a yield increase of roughly 10% after 30 min on-stream (see Figure 11). Lastly, spent catalyst (on-stream for *ca.* 8 h) was regenerated at 350 ºC and its performance was compared with that of fresh catalyst calcined at 350 ºC (Figure 12).

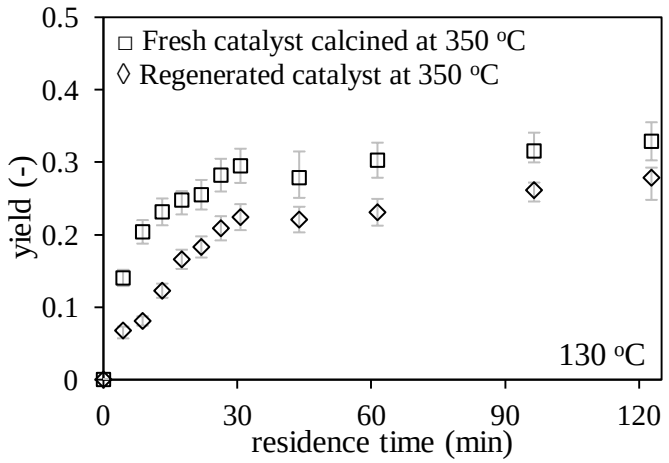

Figure 5.12. Catalytic performance of fresh Cu/TiO_2 fixed-bed catalyst calcined at 350 ºC (□) and regenerated catalyst calcined at 350 °C (◊) for 12 h.

The regenerated catalyst now showed a yield drop of *ca.* 8% in comparison with the fresh catalyst. This shows that the high-temperature calcination was necessary to retain catalyst activity in the flow-through reactor. However, at longer reaction times catalyst regeneration by calcination permitted only the partial retention of activity. Therefore, the main limitation in processing this fixed-bed reactor would be catalyst deactivation and leaching.

Cu/ZnO wall-coated flow reactor. Yields obtained using the ZnO wall-coated reactor were comparable to those observed with the fixed-bed type reactor up to 60-min operation (Figure 13). More importantly, the ZnO-supported catalyst appeared

to retain its activity for operation times longer than those for the TiO_2-supported fixed-bed systems, leading to yields up to 40% (± 2%) after *ca*. 90 min on-stream.

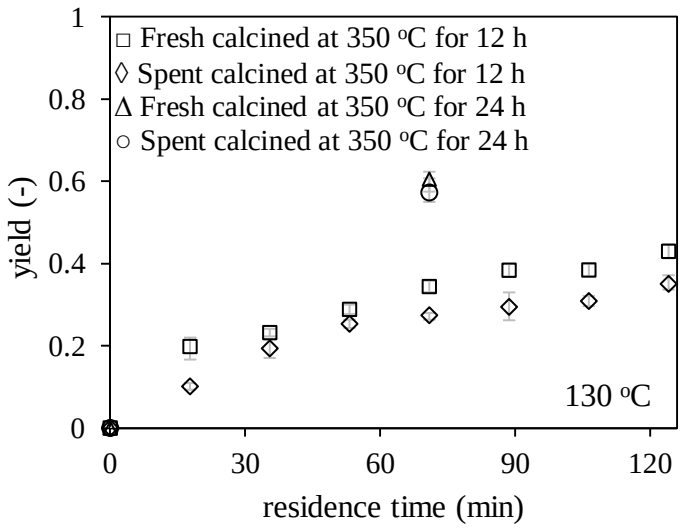

Figure 5.13. Performance of the Cu/ZnO wall-coated reactor after calcination of fresh catalyst (□) and regeneration of spent catalyst (◊) at 350 °C for 12 h. Calcination of fresh catalyst for 24 h at 350 °C showed an impressive yield increase to 61% (Δ) and regeneration of spent catalyst under similar conditions provided a yield of 57% (○), demonstrating the importance of the calcination time.

Similar to the fixed-bed system (Figure 12), the regenerated wall-coated catalyst demonstrated a slight drop in activity comparable to the analogous fresh catalyst. A steady state product yield of 30% (± 3%) instead of 39% (± 2%) was maintained until 124 min (Figure 13). Catalyst regeneration could also be improved by extending the 350 °C calcination step to 24 h. This led to a yield of 61% (± 1%) after 71 min using a fresh catalyst (Figure 13, Δ) and of 57% (±1%) after a further 71 min if the spent catalyst was regenerated by calcination at 350 °C for 24 h (Figure 13, ○). These values represent yield increases of *ca*. 50% with respect to those obtained when fresh and spent catalysts were calcined for only 12 h. Table 1 compares the productivities of fresh and regenerated catalysts for both reactors.

Table 5.1. Reactor productivity for catalysts calcined at 350 °C for 12 h.

	Average productivity ($kg_{prod}/(m_R^3 \cdot h)$)[b]	
	Cu/ZnO wall-coated reactor	Cu/TiO_2 fixed-bed reactor
Fresh[a]	28.3 ± 1.9	55.1 ± 2.4
Regenerated[a]	20.1 ± 2.2	37.3 ± 1.2

a) 6 h time-on-process for both fresh and regenerated catalyst.

b) M_R^3 refers to the volume of empty tubes for both reactors.

Although the yields obtained from the Cu/ZnO wall-coated catalyst were slightly higher than those of the Cu/TiO_2 fixed-bed catalyst, the reactor productivities, however, showed a better performance for the latter. While the catalyst loading per volume reactor was comparable for both reactors, unequal liquid to reactor volume

fractions (V_L/V_R) led to different overall reactor productivities. However, a productivity decrease around 30% was observed for both reactors during a total time on process of 12 h. Calcination of both the Cu/TiO_2 fixed-bed and the Cu/ZnO wall-coated reactors at 200 °C resulted in an obvious drop in yield, although a 24-h calcination treatment at 200 °C led to stable catalyst activities for four consecutive runs with a residence time of 70 min. However, Figure 14 shows higher yields for the latter.

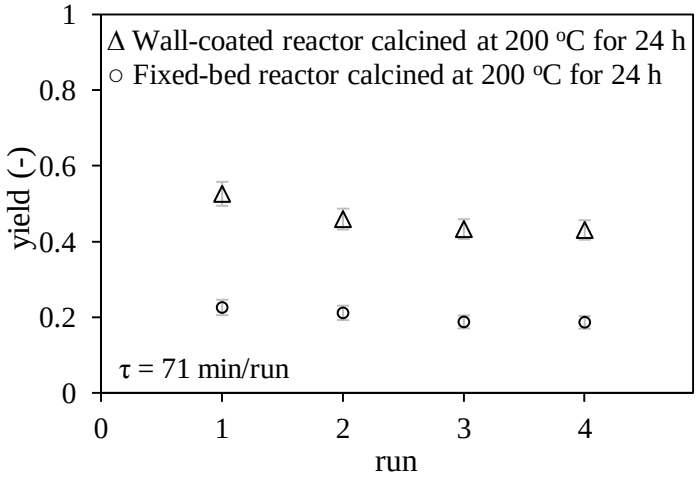

Figure 5.14. Catalytic performance of the Cu/TiO_2 fixed-bed (○) and the Cu/ZnO wall-coated (Δ) reactors for four consecutive runs with a residence time (□) of 71 min (calcination: 24 h, 200 °C).

Figures 12, 13 and 14 show that the sustainability of both Cu/ZnO and Cu/TiO_2 catalysts are mainly governed by the duration of the process, rather than the temperature of the calcination procedure. The first part of the regeneration process (80 °C, 10 mbar) was mainly done to evaporate all components of the reaction mixture. In a second step, residual coke was burned (at 350 °C) in an air-flow (22% O_2 in N_2). In the final step, a stable catalyst-support matrix was achieved by a slow cooling trajectory (for details see Supporting Information of reference [1]).

5.3.3 Effect of Cu-loading

Although the Cu/ZnO-based wall-coated reactor showed a better catalyst performance in terms of yields, its application in microwave heating may still be limited due to large temperature gradients between the center of the reactor and the wall. In such a case, a fixed-bed reactor would provide a more uniform heating profile due to internal mixing and the presence of highly dispersed copper microwave absorber. Therefore, a fixed-bed reactor was tested in both a single-mode and in a multimode cavity microwave-heated flow system. The reactor inlet and outlet were slightly modified to fit the microwave cavity dimensions. Figure 15a shows the temperature-time and power-time histories for the use of multimode microwave cavity. In Figure 15b, the temperature-time and power-time histories for the single-mode microwave cavity setup are given.

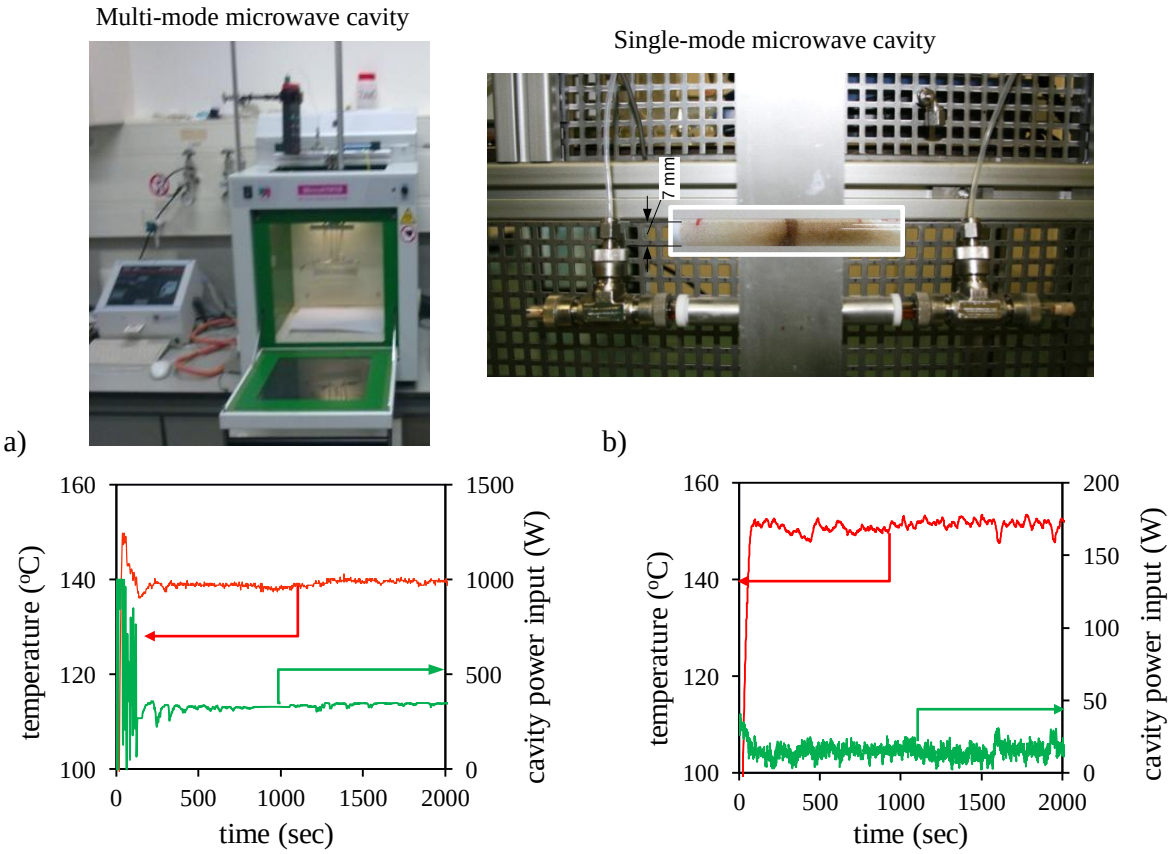

Figure 5.15. Reactor designs for microwave-assisted flow chemistry. A coiled fixed-bed reactor was used in a multimode microwave system (a) and a tubular fixed-bed reactor was applied in a single-mode microwave system (b). Input powers are given in green and temperature profiles inside the catalyst beds are in red.

The microwave power requirements for a multimode microwave experiment were found to be 10 times more (300 W) due to the non-uniform and low-density microwave irradiation in comparison to the single-mode microwave experiment (30 W). Although the single-mode microwaves showed slightly larger temperature and power fluctuations, these equated to less than 5 °C.

Figure 16a shows that for the $Cu/TiO_2/SiO_2$ fixed-bed catalyst a three-fold yield increase resulted when single-mode microwave irradiation was utilized. This could be explained by the fact that in a multimode cavity the microwaves are non-uniformly distributed, leading to reduced production rates due to the existence of strong axial temperature gradients and cold-spots, especially in the absence of forced mixing [32]. The use of lower powers in the case of multimode microwaves could not attain the desired reaction temperatures, whilst at higher powers (> 300 W) arcing was observed. This arcing effect resulted in a decreased product yield due to burning of the catalyst. Also clearly visible is the yield flattening at around 35% yield, which, as discussed in section 5.3.2, was mainly due to oxidation and poisoning of the catalyst. Previously, it has been reported that the Cu catalyst could be protected against oxidation and that leaching could be minimized by adding 50 wt% of Zn to the catalyst as a sacrificial reducing agent [19, 33]. Consistent with this view, Figure 16b shows that a considerable yield increase was achieved when a CuZn-based heterogeneous catalyst was used in the fixed-bed reactor.

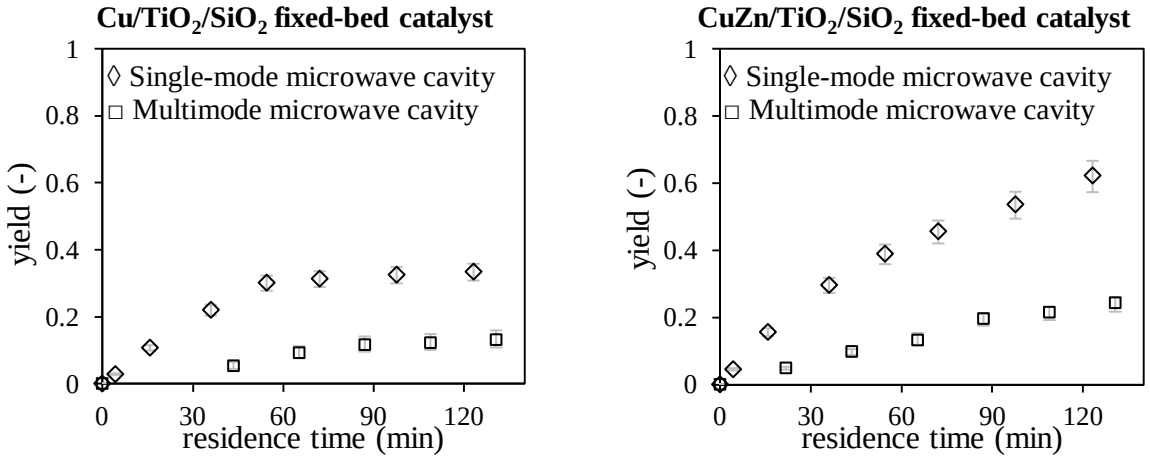

Figure 5.16. A comparison of single-mode and multimode microwave cavities for a conventional Cu/TiO_2 fixed-bed catalyst (a), showing almost a three-fold yield increase for the single-mode microwave cavity due the high and uniform field density achieved. However, these yields were almost doubled (b) using a CuZn catalyst.

Although for low residence times (< 60 min) no major improvement was obtained, at longer residence times two-fold yield increases were achieved for both single-mode and multimode systems. Comparing Figure 16b with Figure 11 signifies that the main reason for this improvement is indeed that, regardless of the heating method, catalyst deactivation is retarded when a CuZn catalyst is used. Figure 15 demonstrates that the energy efficiency achieved using the single-mode microwave cavity of the Fricke-Mallah instrument reached 82% (± 4%) with an average power input of 16 W, while the multimode cavity system could at best be operated with an energy efficiency of only 8.2% (± 0.8%) (following notes [30] and [31]). Use of the single-mode microwave cavity for a Cu-based heterogeneous catalyst gave a yield of 33% (± 1%) for a residence time of *ca.* 120 min with a productivity of 130 $kg_{prod}/(m_R^3.h)$. Only 37 $kg_{prod}/(m_R^3.h)$ was obtained in the case of using the multimode cavity system. However, a highest yield of 62% (± 3%) and a productivity of 172 $kg_{prod}/(m_R^3.h)$ could be achieved using a CuZn-based catalyst in combination with single-mode microwave heating. These high space-time yields have, to the best of our knowledge, not yet been reported for Ullmann-type coupling reactions using flow processing.

5.4 Conclusions

In this chapter, two flow milli-reactors for a microwave-assisted Ullmann-type C-O coupling reaction were discussed. A wall-coated (ZnO support) and a fixed-bed (TiO_2 support) milli-reactor were developed and impregnated with Cu nanoparticles as active catalyst. Copper catalysts leaching from both reactors appeared to be only significant after 24 h on-stream, whcih could partially be avoided by thermal treatment of the reactor after each cycle. Using the Cu/ZnO wall-coated reactor for two consecutive runs, up to 60% yield could be obtained without a significant activity drop if a thermal pre-treatment of the reactor (350 ^oC for 24 h) was undertaken prior to testing. The Cu/TiO_2 fixed-bed reactor showed lower yields due to catalyst leaching. However, reactor productivities of up to 55

$kg_{prod}/(m_R^3 \cdot h)$ suggested a better performance than that of the Cu/ZnO wall-coated reactor.

Microwaves as an alternative energy source for liquid and selective catalyst heating were, therefore, applied for the Cu/TiO_2 fixed-bed reactor. The use of high-density single-mode microwaves showed a three-fold yield increase of the C-O coupling product in the Cu/TiO_2 fixed-bed reactor as compared to multimode microwaves. Furthermore, the use of metallic copper in the microwave cavities appeared to be only advantageous at low microwave powers and catalyst loadings, since at higher powers and catalyst loadings arcing was observed. This arcing led to rapid catalyst deactivation and inefficient heating. A linear relation between the arcing frequency and the catalyst loading was found. It was demonstrated that yields obtained using microwave heating at 140 W were almost 30% higher than those achieved using oil-bath heating, whereas no significant yield increase was observed at 300 W. More important was the use of a $CuZn/TiO_2$ based catalyst, where Zn acted as a sacrificial anode against Cu-oxidation. In this case, a three-fold yield increase could be demonstrated in a highly dense single-mode microwave cavity which, to the best of our knowledge, resulted into a not yet reported productivity of up to 172 $kg_{prod}/(m_R^3 \cdot h)$ for the microwave-assisted flow synthesis of the Ullmann C-O coupling product.

References

[1] F. Benaskar, N. G. Patil, V. Engels, E. V. Rebrov, J. Meuldijk, L. A. Hulshof, V. Hessel, A. E. H. Wheatley and J. C. Schouten, *Chem. Eng. J.* **2012**, *Accepted/in press*.

[2] a) T. Brodmann, P. Koos, A. Metzger, P. Knochel and S. V. Ley, *Org. Process Res. Dev.* **2011**; b) T. Fukuyama, M. T. Rahman, I. Ryu, I. R. Baxendale, J. J. Hayward, S. Lanners, S. V. Ley, C. D. Smith, B. Ahmed-Omer, T. Wirth, V. Hessel, P. Löb, H. Löwe, K. Koch, F. P. J. T. Rutjes and J. C. M. van Hest in *Organic Chemistry in Microreactors*, Wiley-VCH Verlag GmbH & Co. KGaA, **2008**, pp. 59-209; c) T. Illg, P. Loeb and V. Hessel, *Bioorg. Med. Chem.* **2010**, *18*, 3707-3719; d) K. Jähnisch, V. Hessel, H. Löwe and M. Baerns, *Angew. Chem., Int. Ed.* **2004**, *43*, 406-446; e) G. S. Kumar, B. Pieber, K. R. Reddy and C. O. Kappe, *Chem.– Eur. J.* **2012**, *18*, 6124-6128; f) N. G. Anderson, *Org. Process Res. Dev.* **2012**, *5*, 852-869.

[3] V. Hessel, P. Löb and H. Löwe in *Industrial Microreactor Process Development up to Production*, Wiley-VCH Verlag GmbH & Co. KGaA, **2008**, p. 240.

[4] a) C. O. Kappe, D. Dallinger and S. S. Murphree in *Practical Microwave Synthesis for Organic Chemists*, Wiley-VCH Verlag GmbH & Co. KGaA, **2009**; b) T. Wirth in *Microreactors in Organic Synthesis and Catalysis*, Wiley-VCH Verlag GmbH & Co. KGaA, **2008**; c) V. Hessel, A. Renken, J. C. Schouten and J. Yoshida in *Micro Process Engineering: A Comprehensive Handbook*, Wiley-VCH Verlag GmbH & Co. KGaA, **2009**.

[5] a) J. D. Moseley and C. O. Kappe, *Green Chem.* **2011**, *13*, 794-806; b) V. Hessel, *Chem. Eng. Technol.* **2009**, *32*, 1655-1681; c) M. Hempel, *Chem. Eng. Technol.* **2009**, *32*, 1651-1654; d) V. Hessel, D. Kralisch and U. Krtschil, *Energy Environ. Sci.* **2008**, *1*, 467-478; e) A. Stankiewicz, *Ind. Eng. Chem. Res.* **2007**, *46*, 4232-4235.

[6] a) C. O. Kappe, *ChemSusChem* **2010**, *3*, 1085-1085; b) M. H. C. L. Dressen, B. H. P. van de Kruijs, J. Meuldijk, J. A. J. M. Vekemans and L. A. Hulshof, *Org. Process Res. Dev.* **2010**, *14*, 351-361; c) J. D. Moseley, *Chim. Oggi* **2009**, *27*, 6-10; d) T. N.

Glasnov and C. O. Kappe, *Macromol. Rapid Commun.* **2007**, *28*, 395-410; e) G. Shore, S. Morin and M. G. Organ, *Angew. Chem., Int. Ed.* **2006**, *45*, 2761-2766.

[7] M. Damm, T. N. Glasnov and C. O. Kappe, *Org. Process Res. Dev.* **2009**, *14*, 215-224.

[8] a) V. Hessel, B. Cortese and M. H. J. M. de Croon, *Chem. Eng. Sci.* **2011**, *66*, 1426-1448; b) F. Benaskar, V. Hessel, U. Krtschil, P. Löb and A. Stark, *Org. Process Res. Dev.* **2009**, *13*, 970-982.

[9] a) G. Shore, W.-J. Yoo, C.-J. Li and M. G. Organ, *Chem.– Eur. J.* **2010**, *16*, 126-133; b) E. Comer and M. G. Organ, *J. Am. Chem. Soc.* **2005**, *127*, 8160-8167.

[10] G. Cravotto, M. Beggiato, A. Penoni, G. Palmisano, S. Tollari, J.-M. Lévêque and W. Bonrath, *Tetrahedron Lett.* **2005**, *46*, 2267-2271.

[11] F. Bergamelli, M. Iannelli, J. A. Marafie and J. D. A. Moseley, *Org. Process Res. Dev.* **2010**, *14*, 926-930.

[12] a) J. D. Moseley and E. K. Woodman, *Org. Process Res. Dev.* **2008**, *12*, 967-981; b) J. D. Moseley, P. Lenden, M. Lockwood, K. Ruda, J.-P. Sherlock, A. D. Thomson and J. P. Gilday, *Org. Process Res. Dev.* **2007**, *12*, 30-40.

[13] a) P. Öhrngren, A. Fardost, F. Russo, J.-S. Schanche, M. Fagrell and M. Larhed, *Org. Process Res. Dev.* **2012**, *5*, 1053-1063; b) N. G. Patil, A. I. G. Hermans, F. Benaskar, J. Meuldijk, L. A. Hulshof, V. Hessel, J. C. Schouten and E. V. Rebrov, *AIChE Journal* **2011**, online; c) U. Schön, J. Messinger, S. Eichner and A. Kirschning, *Tetrahedron Lett.* **2008**, *49*, 3204-3207.

[14] a) C. O. Kappe and A. Stadler in *Microwave Theory*, *Vol.* Wiley-VCH Verlag GmbH & Co. KGaA, **2006**, pp. 9-28; b) C. O. Kappe and A. Stadler in *Introduction: Microwave Synthesis in Perspective*, *Vol.* Wiley-VCH Verlag GmbH & Co. KGaA, **2006**, pp. 1-7.

[15] M. Gupta and E. W. Wai Leong in *Front Matter*, *Vol.* John Wiley & Sons (Asia) Pte Ltd, **2007**.

[16] a) K. Olofsson, A. Hallberg and M. Larhed in *Transition Metal Catalysis and Microwave Flash Heating in Organic Chemistry*, *Vol.* Wiley-VCH Verlag GmbH & Co. KGaA, **2004**, pp. 379-403; b) A. F. Littke and G. C. Fu, *Angew. Chem., Int. Ed.* **2002**, *41*, 4176-4211; c) J. Hassan, M. Sevignon, C. Gozzi, E. Schulz and M. Lemaire, *Chem. Rev.* **2002**, *102*, 1359-1469; d) J. P. Finet, A. Y. Fedorov, S. Combes and G. Boyer, *Curr. Org. Chem.* **2002**, *6*, 597-626; e) B. H. Yang and S. L. Buchwald, *J. Organomet. Chem.* **1999**, *576*, 125-146; f) J. F. Hartwig, *Angew. Chem., Int. Ed.* **1998**, *37*, 2047-2067; g) A. Muci and S. Buchwald in *Practical Palladium Catalysts for C-N and C-O Bond Formation Cross-Coupling Reactions, Vol. 219* (Ed. N. Miyaura), Springer Berlin / Heidelberg, **2002**, pp. 131-209.

[17] F. Benaskar, A. Ben-Abdelmoumen, N. G. Patil, E. V. Rebrov, J. Meuldijk, L. A. Hulshof, V. Hessel, U. Krtschil and J. C. Schouten, *J. Flow Chem.* **2011**, *1*, 74-89.

[18] a) F. Monnier and M. Taillefer, *Angew. Chem., Int. Ed.* **2009**, *48*, 6954-6971; b) J. Y. Kim, J. C. Park, A. Kim, A. Y. Kim, H. J. Lee, H. Song and K. H. Park, *Eur. J. Inorg. Chem.* **2009**, 4219-4223; c) J. Niu, H. Zhou, Z. Li, J. Xu and S. Hu, *J. Org. Chem.* **2008**, *73*, 7814-7817; d) F. Monnier and M. Taillefer, *Angew. Chem., Int. Ed.* **2008**, *47*, 3096-3099; e) G. Evano, N. Blanchard and M. Toumi, *Chem. Rev.* **2008**, *108*, 3054-3131; f) M. Kidwai, N. K. Mishra, V. Bansal, A. Kumar and S. Mozumdar, *Tetrahedron Lett.* **2007**, *48*, 8883-8887; g) K. Kunz, U. Scholz and D. Ganzer, *Synlett* **2003**, *2003*, 2428-2439; h) M. Taillefer, H.-J. Cristau, P. P. Cellier, J.-F. Spindler and A. Ouali, *Fr 2840303-WO 03101966 (Pr. Nb. Fr 2002 06717)* **2002**; i) V. Engels, F. Benaskar, N. Patil, E. V. Rebrov, V. Hessel, L. A. Hulshof, D. A. Jefferson, J. A. J. M. Vekemans, S. Karwal, J. C. Schouten and A. E. H. Wheatley, *Org. Process Res. Dev.* **2010**, *14*, 644-649.

[19] F. Benaskar, V. Engels, E. V. Rebrov, N. G. Patil, J. Meuldijk, P. C. Thüne, P. C. M. M. Magusin, B. Mezari, V. Hessel, L. A. Hulshof, E. J. M. Hensen, A. E. H. Wheatley and J. C. Schouten, *Chem.– Eur. J.* **2012**, *18*, 1800-1810.

[20] a) A. Mondal, D. Agrawal and A. Upadhyaya, *J. Microwave Power Electromagnetic Energy* **2009**, *43*, 5-10; b) X. Zhang, D. O. Hayward and D. M. P. Mingos, *Catal. Lett.* **2003**, *88*, 33-38; c) A. G. Whittaker and D. M. P. Mingos, *J. Chem. Soc., Dalton Trans.* **2002**, 3967-3970; d) G. Bond, R. B. Moyes and D. A. Whan, *Catal. Today* **1993**, *17*, 427-437.

[21] a) W. L. Perry, D. W. Cooke, J. D. Katz and A. K. Datye, *Catal. Lett.* **1997**, *47*, 1-4; b) D. Walton, H. Boehnel and D. J. Dunlop, *Appl. Phys. Lett.* **2004**, *85*, 5367-5369; c) D. Walton, *J. Appl. Phys.* **2004**, *95*, 5247-5248.

[22] a) V. D. Buchelnikov, D. V. Louzguine-Luzgin, G. Xie, S. Li, N. Yoshikawa, M. Sato, A. P. Anzulevich, I. V. Bychkov and A. Inoue, *J. Appl. Phys.* **2008**, *104*, 113505; b) A. G. Whittaker and D. M. P. Mingos, *J. Chem. Soc., Dalton Trans.* **2000**, 1521-1526.

[23] J. R. Thomas, *Catal. Lett.* **1997**, *49*, 137-141.

[24] V. Engels, F. Benaskar, D. A. Jefferson, B. F. G. Johnson and A. E. H. Wheatley, *Dalton Trans.* **2010**, *39*, 6496-6502.

[25] F. Benaskar, V. Engels, N. Patil, E. V. Rebrov, J. Meuldijk, V. Hessel, L. A. Hulshof, D. A. Jefferson, J. C. Schouten and A. E. H. Wheatley, *Tetrahedron Lett.* **2010**, *51*, 248-251.

[26] G. Piperata, J. M. Meichtry and M. I. Litter in *Photocatalytic reactions over TiO2 supported on porcelain spheres, Vol. 128* Springer, Berlin, **2004**, pp. 303-308.

[27] V. F. Meshcheryakov, Y. K. Fetisov, A. A. Stashkevich and G. Viau, *J. Appl. Phys.* **2008**, *104*, 063910.

[28] a) D. Stuerga and M. Delmotte in *Wave–Material Interactions, Microwave Technology and Equipment*, Wiley-VCH Verlag GmbH & Co. KGaA, **2004**, pp. 1-33; b) W. Chen, B. Gutmann and C. O. Kappe, *ChemistryOpen* **2012**, *1*, 39-48; c) A. G. Whittaker and D. M. P. Mingos, *J. Chem. Soc., Dalton Trans.* **1995**, 2073-2079; d) N. G. Patil, E. V. Rebrov, K. Eränen, F. Benaskar, J. Meuldijk, J.-P. Mikkola, V. Hessel, L. A. Hulshof, D. Y. Murzin and J. C. Schouten, *J. Microwave Power Electromagnetic Energy* **2012**, *46*, 83-92.

[29] The presence of copper also shows heating rates higher compared to those in the absence of copper, which indicates an additional solids absorption term in the overall microwave energy absorption. The following equation has been applied to demonstrate a global energy balance: Q(MW)= Q(liquid) + Q(solid) = {m*Cp*(ΔT/Δt)}(DMA) + Q(Cu). Where Q(MW) is the microwave power input (120 W), m the total liquid mass (0.025-0.035 kg), Cp(DMA) the specific heat capacity of the solvent, dimethylacetamide, (2.01 kJ/kg/K), ΔT/Δt the temperature increase over the heating time (in K/s) and Q(Cu) the microwave energy absorption by the copper.

[30] η_MW=(Q_thermal, sample)/(Q_MW, cavity). Where "Q_thermal, sample" is the overall energy gained by the sample (contributed by liquid and solid absorption) and "Q_MW, cavity" is the total microwave power input to the cavity.

[31] M. Komorowska, G. D. Stefanidis, T. Van Gerven and A. I. Stankiewicz, *Chem. Eng. J.* **2009**, *155*, 859-866.

[32] A. C. Metaxas and R. J. Meredith in *Industrial Microwave Heating*, P. Peregrinus LTD., **1993**, pp 296.

[33] a) D. Grandjean, V. Pelipenko, E. D. Batyrev, J. C. van den Heuvel, A. A. Khassin, T. M. Yurieva and B. M. Weckhuysen, *J. Phys. Chem. C* **2011**, *115*, 20175-20191; b) J. D. Grunwaldt, A. M. Molenbroek, N. Y. Topsøe, H. Topsøe and B. S. Clausen, *J. Catal.* **2000**, *194*, 452-460.

Chapter 6

Micro/Milli-Flow Processing Combined with Selective Catalyst Microwave Heating in the Cu-Catalyzed Ullmann Ether Synthesis: a μ^2-Process

This chapter has been submitted as:
F. Benaskar, N.G Patil, E.V. Rebrov, A. Ben-Abdelmoumen, J. Meuldijk, L. A. Hulshof, V. Hessel, J.C. Schouten (2012). Micro/milli-flow processing combined with selective catalyst microwave heating in the Cu-catalyzed Ullmann etherification reactions: a μ^2-process, *ChemSusChem*, submitted [1].

Abstract

A so-called μ^2-process of the Ullmann-type C-O coupling of potassium phenolate and 4-chloropyridine was successfully performed in a combined microwave (MW) and micro-flow process. Selective MW-absorption in a micro fixed-bed reactor (μ-FBR) using a supported Cu nanoparticle catalyst resulted in a catalyst activity increase up to two orders of magnitude (23 $g_{prod} \cdot m^2_{cat} \cdot h^{-1}$) as compared to that of a conventionally heated process (0.18 $g_{prod} \cdot m^2_{cat} \cdot h^{-1}$). Yields up to 80 % were attained in 75 min using a multi-segmented μ-FBR without significant catalyst deactivation for 12 h. The μ-FBR, packed with beads coated with Cu/TiO_2 and $CuZn/TiO_2$, was used for the catalyst activity study. Temperature measurements along axial positions of the reactor were done using a fiber-optic probe in the catalyst bed. Applying simultaneously MW-power and temperature sensors resulted in an isothermal reactor and a MW-power as low as 20 W. Temperature fluctuations along the axial position of the reactor were controlled at a set temperature of 140 ± 2 °C. Initially, only solvent was used to adjust the MW-field density in the cavity

and to optimize the power utility in an empty milli-reactor. Subsequently, the reaction mixture was added to ensure a maximum MW-power transfer by adjusting the waveguide stub tuners to steady-state operations. This was mainly done to account for the changed reaction mixture composition and, as a result, for changed dielectric properties. Finally, the beneficial effect of the Cu/TiO_2 and $CuZn/TiO_2$ coated glass beads (200 μm) on the MW-absorption, due to an additional absorbing effect of the metallic Cu nanoparticles, was optimized in a fine-tuning step. For the catalyst synthesis various sol-gel, deposition and impregnation methods provided Cu catalyst loadings around 1 wt%. Addition of Zn to the Cu-nanocatalyst, which fulfilled as promoter the role of a preferential oxidizer according to X-ray absorption spectroscopy, revealed an increased catalyst activity, due to a stable Cu-oxidation state. The effect of in-line mixing in the milli-reactor on the productivity was studied, demonstrating that sufficient multi-laminar mixing rather than instantaneous contact mixing in either a T- or Y-mixer was needed as a result of a large difference in fluid viscosities. To the best of our knowledge, the study described in this chapter presents the first extended experimental survey of decisive parameters associated with combining micro process and single-mode MW technologies (a so-called μ^2-process), culminating in concepts for novel process windows in organic syntheses.

6.1 Introduction

Copper-catalyzed Ullmann-type C-O coupling reactions for fine-chemicals synthesis. The Cu-catalyzed coupling of nucleophiles and halo-aromates is extensively applied in the production of active molecules since it was discovered by Ullmann *et al*. more than a century ago [2]. As a result, a variety of industrial applications were reported in pharma-active compounds such as antivirals, herbicides and antibiotics (*e.g.* antibiotic Vancomycin), and also in the synthesis of functional polymers and herbicides [3]. This type of coupling reactions usually required harsh and inefficient reaction conditions for realistic implementation in process chemistry, such as high reaction temperatures (up to 250 °C), activated aryl halides and excesses of copper catalyst [4]. It was already proven in the 1960s that the effect of solvent impurities increased the copper activity and reaction rate [5], only later the role of these organic "additives" demonstrated an increase in copper solubility and stability using specific solvents [6].

It took almost half a century (*i.e.* in 2001) before a copper/ligand system was introduced as an efficient catalyst where sub-stoichiometric catalyst loadings and acceptable temperatures could be applied.[7] This innovation intensified the progress in the field of copper catalysis for coupling reactions considerably, resulting in a remarkable renaissance of copper catalyzed Ullmann coupling reactions [8]. An increasing number, particularly of homogeneous copper complexes as catalysts, provided opportunities to study the reaction mechanism. However, this research field still suffers from many uncertainties related to the active Cu-oxidation state which takes part in the C-O coupling reaction [5b, 9]. Consequently, homogeneous copper-catalyzed coupling processes have been studied intensively and many novel copper/ligand systems with activities comparable to Pd-catalysts

were reported [10], yet very little is done to explore supported heterogeneous catalysts [11]. Despite all these successes with the development of homogeneous Cu catalysts in the last decade, sustainable catalysis can only be achieved using supported heterogeneous catalysts, thus avoiding expensive catalyst separation techniques and unsatisfactory catalyst recovery. Therefore, continuously operated processes can only be realized efficiently when the catalyst is supported on a solid substrate, *e.g.* either as a wall-coating or as a fixed-bed in a flow reactor.

Many examples of catalyst supports exist for various noble metals, such as Pt[12], Au[13] and Pd[14]. However, hardly any examples of heterogenized Cu onto a ceramic support (*e.g.* SiO_2, Al_2O_3 or TiO_2) can be found in the literature. Especially due to a limited catalyst activity and oxidative instability, copper catalysts in organic synthesis have not been extensively applied when compared to Pt and Pd based catalysts. Nevertheless, the low cost and abundant availability make copper an attractive replacement for traditional and expensive noble metals [15]. Coupling reactions in organic chemistry are traditionally achieved with palladium catalysts and have received intense attention since their discovery in the 1970s[16] which even led to a Nobel Prize in 2010. However, driven by high cost and scarcity of palladium, research initiatives were directed towards copper(II) acetate catalyzed coupling reactions, involving highly active organometallic reagents, such as Pb,[17] Si[18], Sn[19] as well as organoboron reagents, organocuprates [20] and iodonium salts as arylating agents [21].

Supported copper catalysts for sustainable catalysis. There are only few reports on the use of Cu nanoparticles as catalyst in the Ullmann reactions. In 2007, Kidwai *et al*. reported on the use of Cu^0 nanoparticles in the coupling of phenol with iodobenzene at moderate temperatures (50-60 °C) [22]. Yields up to 95% could be attained in a 4-h run which after four consecutive catalyst recycles dropped to 65% due to catalyst losses. Another example of Cu_2O colloidal nanocube catalysts was reported by Kim *et al*. who studied the same cross-coupling reaction using cubic nanoparticles of 45 ± 3 nm [23]. Although excellent catalyst recovery yields were attained after recycling by centrifugation, high temperatures and the use of highly reactive iodobenzenes would not necessarily show a productivity drop due to catalyst losses. Additionally, the use of solid bases for nucleophile deprotonation (*e.g.* Cs_2CO_3) complicates the catalyst recovery process, rendering limited prospect for the applications beyond the lab-scale. Therefore, applying heterogeneous nanoparticle catalysts would only be cost-feasible if the necessity of catalyst recovery is avoided by using a catalyst support.

A major drawback, however, for flow-through catalytic reactors with supported catalysts is the loss of active metal due to leaching. Therefore, catalyst synthetic procedures and support deposition methods require a clear understanding of the metal to support interactions. Analytical techniques, such as ^{63}Cu-NMR, XAS, XPS, XRD and TPO/TPR, are crucial and have shown to cope with most of these phenomena [24]. With very high specific surface area, chemical stability, uniform pore size distribution and pore morphology, the mesoporous materials are promising catalyst support matrices for colloidal nanoparticles [2e, 4a, 9b]. Moreover,

due to chemical interactions with metal nanoparticles, such as Au, Ag and Pt, nano-structured titania has long been considered as a supporting matrix to avoid colloidal aggregation which stabilizes the dispersity of nanoparticles [25].

Microwave-assisted metal-catalyzed organic syntheses. Besides catalyzing a reaction, the energy supply towards the catalyst surface is of crucial importance which in classical chemical reactors is governed by conduction and convection limitations. Therefore, the use of microwaves as a replacement of conventional heating in organic reactions attracted a broad spectrum of disciplines in the current academic and industrial research laboratories [26]. Not being limited by thermal barriers like those existing in conventionally heated systems (as a result of energy transport from the heat source, through the reactor wall and, finally, through convection), microwaves render the unique characteristics of direct heating via molecular rotations without any classical heating medium [26a, b, 27]. Patil *et al.* recently showed that microwaves can be used in rapid and very controlled heating with negligible heat losses in capillary-type flow reactors [28]. Consequently, reduced heating times, negligible inner gradients and increased energy efficiencies are often reported in microwave-assisted processes [29].

However, unresolved drawbacks, such as (1) MW-penetration depths limitations, (2) relatively capital-intensive investments, (3) complex temperature measurements and MW-power control, (4) risk of operation and (5) the restriction to use only polar solvent/reactants, still hinder significant applications of this technology in the chemical industry [30]. The latter drawback can sometimes be circumvented or even used for heat integration/extraction, *e.g.* when solvents with different dielectric properties are applied [28]. In this case, microwaves selectively couple with the absorbing (reactive) components, leaving other substances unheated and allowing selective energy input and bulk quenching, hence increased conversion and selectivity. Multimode type MW-cavities (operating at 2.45 GHz) are typically used for laboratory applications, whereas for more dedicated processes single-mode cavities are applied, thus enabling a focused MW-field and optimal utilization efficiency at uniform energy densities on the load (reactor) [31].

The use of MW-energy in Ullmann-type reactions has recently been an intensive topic of research [32]. Utilizing MW-energy by amide-containing organic solvents is very attractive in combination with copper catalysis due to the strong MW-absorption and the chemical interaction of copper and the amide, respectively [33]. Moreover, local heating of the metallic copper catalyst[34], as used in the original Ullmann reaction, provides an additional benefit as a "metallic MW-absorber" [35]. Buchelnikov *et al.* studied the heating mechanisms of various metallic powders using a 2.45-GHz multimode MW-cavity [36]. They showed that ferromagnetic materials (*e.g.* Fe) resulted in rapid MW-absorption via eddy-currents and magnetic-reversal loss mechanisms. In this study, the authors also demonstrated that diamagnetic metals (Sn and Cu) demonstrated significant MW-absorption (contrary to paramagnetic metals, such as Ti and Au), which resulted in a thermal energy supply to the metal surfaces [37]. Further investigations on micron-size powdered catalysts showed a strong coupling of these metals with the MW-

field providing very fast heating and, depending on their particle size [38], even electric discharges [39]. The effect of direct heating of a metal deposited onto a MW-transparent support could be used efficiently to heat the catalyst at the nano-scale while maintaining the bulk of the reaction mixture unheated [40]. The high energy density at the surface of magnetic nanoparticles, in combination with a thermal energy barrier of a MW-transparent support, leads to an increased catalyst activity and selectivity as a consequence of direct reaction [41]. This benefit of selective catalyst heating is enhanced when also the bulk fluid of the reaction mixture has limited or no MW-absorption [42].

Milli and micro process technology as a means to perform process intensification. Micro process technology is currently recognized as a well-established and advanced technology in fine-chemicals synthesis [43]. The advances in micro process technology have led to novel routes with intensified process windows to replace conventional batch processes by continuous flow processing, both at lab and industrial scales [44]. Metal-catalyzed liquid-phase organic reactions in fine chemicals synthesis require different operational windows in micro process technology as compared to gas-phase reactions. A major issue in liquid type reactions is the presence of solids (*e.g.* base and catalyst suspensions), which could be prevented by adding pre-treatment steps [45] or depositing catalysts onto structured supports, *e.g.* by dip-coating or employing milli/micro-reactors [46].

Milli and micro processing facilitates operation at high pressures and temperatures due to the small internal volumes [47], allowing safer operation in regimes that are otherwise risky or difficult without a high degree of technical investment. Moreover, micro processing [48] and green process technologies [49] provide the options to produce chemicals at flexible scales and for local production to directly meet consumer's demands. In this chapter, a process-intensification strategy based on the so-called "Novel Process Window" approach[50] is presented by combining selective energy supply and miniaturized structured reactors, *i.e.* MW-energy and micro fixed-bed reactors, respectively.

Combined microwave and flow chemistry technologies for industrial applications. The combination of MW-heating and flow chemistry has recently emerged as a highly attractive opportunity in novel processing [27a, 28, 31b, 51]. Kappe and co-workers have recently presented an overview on the "Microwave-to-Flow" paradigm, where they demonstrated extremely high temperature and pressure windows to conduct organic reactions, enabled by the combination of meso-scale reactors and MW-irradiation [51e, 52]. Leadbeater *et al.* have demonstrated new temperature monitoring techniques which facilitate highly reliable and reproducible results for synthetic and mechanistic studies [53]. Recent work from Organ and co-workers has considerably contributed to the current developments in microwave-assisted capillary-type flow reactors for metal-catalyzed organic reactions [51c, 51f, 54]. More examples on dedicated flow systems in combination with MW-heating have been reported for large-scale synthesis and industrial applications [32f].

AstraZeneca studied various examples of microwave-assisted organic reactions for flow synthesis of pharmaceuticals, yielding productivities up to 6 L/h [55]. Earlier, Moseley *et al.* developed automated microwave stop-flow reactors which provided competitive productivities as compared to batch-scale reactions [56]. However, the current successes in combining microwave and flow systems have mainly been achieved in multimode MW-cavities which generally suffer from MW-field non-homogeneities and non-uniform temperature distributions due to a limited MW-penetration depth. In this chapter, the first process integration of single-mode MW-technology (as an alternative energy source) and micro process technology (as an alternative method for a pilot-type setup using a numbering-up concept) for the heterogeneously Cu-catalyzed Ullmann-type coupling reaction will be discussed (see Scheme 1).

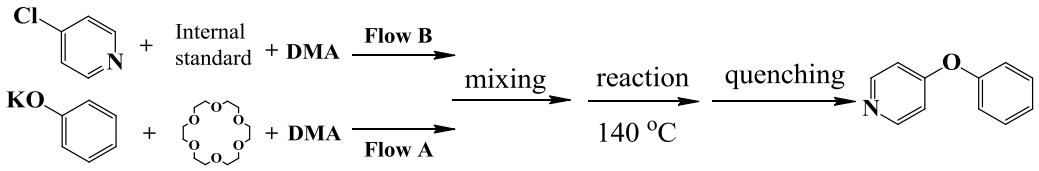

Scheme 6.1. Cu-catalyzed Ullmann etherification towards 4-phenoxypyridine in *N*,*N*-dimethylacetamide (DMA) from a 4-chloropyridine (B) and potassium phenolate (A) flow.

A design has been proposed where catalytic reactors are irradiated with highly focused single-mode microwaves for selective MW-absorption by a metallic copper catalyst. The combination resulted in an intensively heated catalytic flow reactor at MW-powers as low as 20 W which gave comparable if not better catalyst activities as compared to previously reported batch-reactor results [46]. Selective MW-absorption by segmenting the catalyst over the entire reactor volume in catalytic parts (consisting of $CuZn/TiO_2/SiO_2$) and inert parts (consisting of glass beads) and by measuring the temperature at different parts in the axial direction of the reactor was demonstrated. Figure 1 shows the inlet probe at Z_0 (inlet cat-bed) whereas the outlet probe was moved along the cat-bed (outlet cat-bed) from Z_L.

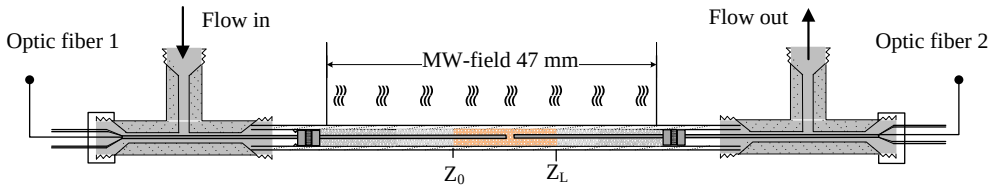

Figure 6.1. MW-setup for determining axial heating profiles.

Finally, a highly efficient $CuZn/TiO_2$ catalyst which was coated onto 200 µm spherical beads and packed in a cylindrical milli-reactor was synthesized. Due to the void between the particles, the interstitial volumes provided a catalytic micro-structured reactor. The small quantities and the size of the nanoparticulate catalyst, employed in this system, prevented the formation of electric discharges or arcing which avoided hazardous conditions.

6.2 Experimental

In the following section the experimental setups and chemical protocols are addressed. Also the different analytical and catalyst characterization techniques are described in detail.

6.2.1 Microwave and reactor setup

A single-mode MW-generator manufactured by Fricke und Mallah GmbH operating at a frequency of 2.45 GHz (λ = 12.24 cm) has been applied. The MW-setup consisted of one main waveguide coaxially coupled with four MW-cavity applicators (see Figure 2).

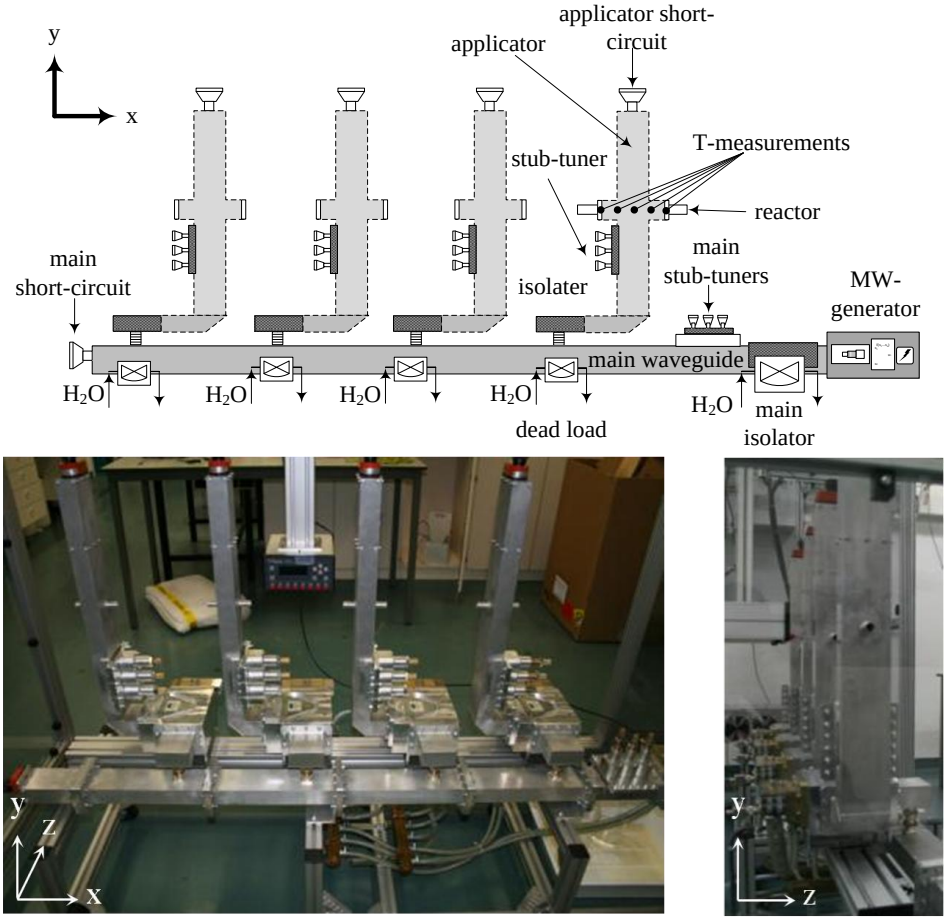

Figure 6.2. Multi-cavity single-mode MW-setup using four cavities in parallel. The reactor is placed at the center of the waveguide to ensure maximal energy density.

The MW-power input in each separate cavity was optimized by tuning both the MW- input (from the main waveguide) and MW-release (to dead load and water flow). The position of the microwaves from the magnetron was tuned in the main waveguide, using a main short-circuit and stub-tuners. In this way, the maxima of the standing waves could be located at the center of the applicator cavities in the main waveguide. After obtaining a resonant wave in the main waveguide, a subsequent fine-tuning (using the applicator short-circuits and stub-tuners) was done to position the wave maxima at the center of the applicator, where the reactor

was placed. The wave tuning of both the main waveguide and the applicators was based on a minimum loss of MW-energy to the dead load and water flow and on a maximum field density at the reactor. As a result, optimum use of magnetron power could be attained, assuring maximum field density at the desired locations of the applicators.

MW-power - temperature calibration. After tuning the waves in the main waveguide and the applicators, the data of the cavity power input and output and temperature was collected. This data was converted by an analog data acquisition system and digitalized using Labview© software. In this way, the MW-radiation, prior to experimental applications, was calibrated from 10 to 1000 Watt, which was satisfactory for accurate efficiency measurements. To ensure isothermal operations, the power input was used as a main input parameter. Due to unstable start-up conditions, the power response sensitivity was also varied until a steady-state temperature was attained. Therefore, the PID-controlling (proportional-integral-derivative controller) system consisted of two sensitivity levels, *i.e.* at dynamic power input and at steady-state power input. The PID-controller was designed to attain desired steady-state temperatures at the first 5 mm of the flow reactor by setting the temperature output and power input as boundary conditions. Initially, the temperature/power calibrations were carried out using only a solvent flow and, subsequently, the chemical components were added to include the perturbation of changing chemical composition on the power response factor.

For the calibration experiments an empty tubular reactor with an inner diameter of 7 mm was placed in the applicator and the solvent was pumped in cycles (HPLC-pump Gilson Model 305, F_v^{max} ~100 mL/min). To avoid precipitation of salts, a conditioned (LaudaM3 water bath at 50.0 ± 0.2 °C) and insulated vessel of 50 mL was applied during the calibration of the reaction mixture flow. Calibration was done in a glass tube (L = 165 mm, ID = 7 mm) packed with $Cu/TiO_2/SiO_2$-beads and placed in the MW-cavity (see Supporting Information in reference [1]). Temperature control inside the MW-cavity was done using fiber-optic probes, placed in a thin (d_{in} = 1 mm, d_{out} = 1.5 mm) protection tube (quartz glass) both at the inlet and outlet of the reactor, as shown in Figures 1 and 3.

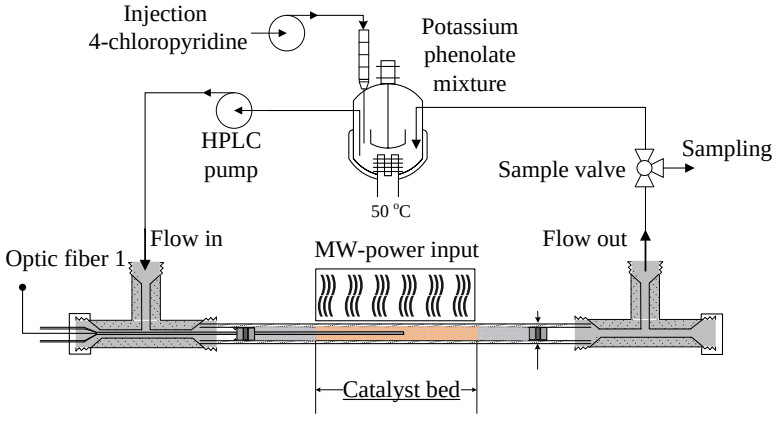

Figure 6.3. Recycle loop reactor setup for a stable flow system and MW-field.

Process setup for the determination of the axial temperature profiles. Axial temperature profiles were obtained using the setup shown in Figure 3, both for the milli-reactor and the micro fixed-bed reactor. The temperature probe holder was designed in such a way that the sensor could be moved freely along the entire axial direction of the reactor. Two probes could be placed simultaneously, one as a controlling probe and the other to measure the axial temperature profiles in the reactor. The probe holder length assured that the fiber-optic tip could cover the complete axial length of the reactor, thus allowing measurements of the longitudinal reactor temperature. The power-controlling sensor was placed at T_1 (the inlet of the reactor positioned at C_0 = 11.4 mm) whereas the second sensor (T_2) was manually moved along the catalyst bed at discrete distances of 2.5 mm from the outlet (position D_0 = 45.5 mm) using an aligned ruler (see Figure 6 in section 6.3.1for the exact positions). In this way, the axial temperatures along the axis of the reactor could be screened.

Process setup for MW-heating without in-line mixing. The reaction mixture composition for the Ullmann C-O coupling reaction has been prepared as reported below. In a recycle loop system the mixture of potassium phenolate (1.25 M) and 18-crown-6 ether (in DMA) was circulated in the tubular reactor at a flowrate of 20 mL/min under an argon atmosphere. After acquiring a stable liquid flow system, a constant microwave-power input was obtained (via PID controlled power input), thus providing a steady reaction temperature (see also in Figure 11 in section 6.3.2). At constant reaction temperatures an appropriate mixture of 4-chloropyridine (1 M) and tetradecane (in DMA) was injected in the buffer vessel using an HPLC pump at similar flowrates as the main stream (see Figure 3). Modification of the flowrate (> 10%) required a manual adjustment of the PID parameters and MW-power input.

Process setup for MW-heating with premixing. In this setup, two separate flows, pre-mixed in buffer vessels were supplied to the reactor using micro-mixers. Storage vessel A contained a pre-stirred mixture of potassium phenolate and crown ether and storage vessel B contained a mixture of 4-chloropyridine and tetradecane, both purged with argon in DMA (see procedure below). A micro-quencher (IMM cross-flow micro-structured heat exchanger, CRMH; see Supporting Information in reference [1]) was integrated at the outlet of the reactor. The heat-exchange unit was used to quench the reaction mixture and to supply heat to the buffer vessel A (containing salts in an organic solvent) and to the micro-mixer as shown in Figure 4 (see also Supporting Information in reference [1]). Buffer vessel A was conditioned to avoid precipitation of the salts in the vessel and clogging in the tubes and process units (pumps, mixer, reactor and quencher). A minimum temperature of 40 °C was required to avoid precipitation of the potassium phenolate. At the following micro-mixing step the temperature was maintained between 45 and 60 °C to avoid precipitation and reaction in the mixer. At the outlet of the reactor, a cross-flow water stream absorbed the heat in the micro heat-exchanger and was fed primarily to the storage vessel A.

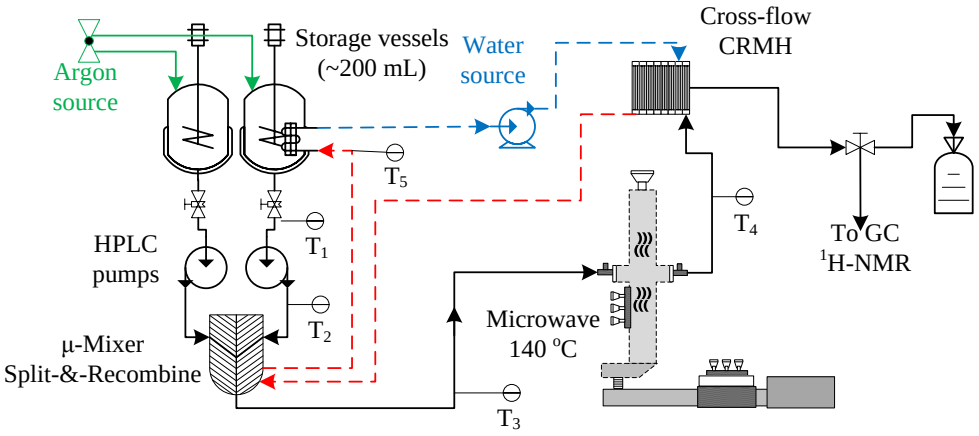

Figure 6.4. Process flow setup for the MW-heated Ullmann reaction using a micro fixed-bed reactor. Oil-bath heating was used to optimize the process conditions, which was the basis of a microwave heat-integrated micro process.

To ensure sufficient energy transfer from the source to the sinks, the coolant flowrate was adjusted to the reactor flowrate.

Process setup for oil-bath heating. As a reference case for MW-heated Ullmann C-O coupling reactions, an oil-bath heated setup (Lauda E100) was used. A copper wall-coated capillary (ID 1.05 mm) reactor with a total volume of 1 mL was used. Both reactants streams were separately pumped from the mechanically stirred buffer vessels A and B (similar to the MW-setup) to the wall-coated capillary reactor, using HPLC-pumps (Gilson Model 305) This setup was used as a reference case, but also to provide preliminary data, which operation-wise would be too complex and a risky start using the MW-setup (see Supporting Information in reference [1]).

Dielectric property measurements. A high temperature dielectric probe kit (85070D, Agilent) and a network analyzer (NWA E5062A, Agilent) were used for the measurements of the dielectric constant (ε') and the dielectric loss (ε'') of ethylene glycol at a frequency of 2.45 GHz. The measurements were repeatedly done in a batch sample at different temperatures and averaged over three runs. An oil-bath was used to maintain the temperature.

6.2.2 Chemicals and procedure

Materials

Potassium phenolate was prepared from phenol and potassium *tert*-butoxide (purum, ≥97.0%, Aldrich) as described in chapter 4. 4-Chloropyridine hydrochloride salt (99%, Aldrich) was used to synthesize 4-chloropyridine. Copper powder (99%, Aldrich) was used as the catalyst and 18-crown-6 (99%, Sigma-Aldrich) as a potassium ion scavenger. Concentrations were determined using tetradecane (purum. p.a., ≥99.5% (GC), Fluka) and 18-crown-6 ether as internal standards for ^{1}H-NMR analysis.

Preparation of the chemicals

4-Chloropyridine. 4-Chloropyridine hydrochloride was pre-treated with potassium carbonate (K_2CO_3 ≥99.5%, Sigma-Aldrich) to obtain 4-chloropyridine as liquid. The preparation was done in four steps (see Supporting Information in reference [1]). A calculated amount of potassium carbonate solution was prepared under argon in an Erlenmeyer. A calculated amount of 4-chloropyridine hydrochloride (0.9 mol equiv. with respect to the base) was slowly added. An aqueous layer on top and a heavier organic layer were formed. Extraction was done with diethyl ether. A yellowish organic phase was obtained containing 93% 4-chloropyridine (^{1}H-NMR) in an overall extraction efficiency of 75%. The organic phase was dried with sodium sulphate. After filtration, diethyl ether was removed in a rotary evaporator (200 mbar, RT) affording 4-chloropyridine in 72% yield at 98% purity.

Potassium phenolate. Deprotonation of phenol required a strong base and was done in four steps (see Supporting Information in reference [1]). A known amount of potassium *tert*-butoxide was dissolved in tetrahydrofuran (THF) under vigorous stirring. A calculated amount of phenol (1.1 mol equiv. to potassium *tert*-butoxide) was slowly added to the reaction mixture resulting in a gel. THF was removed by evaporation (200 mbar, 40 °C) giving a reddish powder. The powder was dried under vacuum (residual pressure *ca.* 10 mbar) at 120 °C to remove excess phenol.

Procedure. The buffer vessels were loaded with the reactants dissolved in *N*,*N*-dimethylacetamide (DMA). Vessel A was loaded with potassium phenolate (0.25 mol, $C_{phenolate}$ = 1.25 M) and crown ether (0.0025 mol) in DMA (0.2 L). Vessel B contained 4-chloropyridine (0.20 mol, $C_{pyridine}$ = 1.0 M) and tetradecane (0.02 mol) dissolved in DMA (0.2 L). Vessel A was maintained at 45 °C using a coiled heat-exchanger heated by a hot water flow from the micro heat-exchanger. The buffer vessels were mechanically stirred at 500 rpm and a continuous argon flow ensured oxygen-free reaction conditions. The flowrate of both reactant streams could be regulated separately using HPLC pumps and were fed to a multi-laminar micro mixer. At the outlet of the mixer, samples were taken to analyse the mixing performance using crown ether and tetradecane as tracers in flows A and B, respectively. Temperatures outside and inside the MW-heated section were measured using thermocouples and fiber-optic probes, respectively. The yield of 4-phenoxypyridine was determined by sampling at the outlet of the reactor and recording ^{1}H-NMR spectra of the samples in DMSO-d^6 (dimethyl sulfoxide-d_6, Cambridge Isotope Laboratories). Data was compared with literature and previously acquired GC-MS measurements.

6.2.3 Catalyst preparation

Synthesis of Cu and CuZn nanoparticulate catalysts. The monometallic Cu and bimetallic CuZn nanoparticles were prepared according to previously reported routes [32b, 45]. For the bimetallic colloids, copper(II) sulfate pentahydrate (1 mmol) and zinc(I) chloride (1 mmol) were mixed with poly[*N*-vinylpyrrolidone] (PVP, 0.8 g, Mw = 24,000 g/mol) in anhydrous ethylene glycol (120 mL). After ageing,

sodium hypophosphite monohydrate (2 mmol in 5 mL millipore water) was added promptly as reductant. Purification was done by extraction using excess of acetone. After sedimentation, decantation and centrifugation the catalyst nanoparticles were re-suspended in ethanol (50 mL).

Synthesis of non-porous powdered titania support. A known amount of titanium(IV) tetra-ethoxide ($Ti(OEt)_4$, 99.99 wt%, Sigma-Aldrich) was mixed for 1 h with aqueous HNO_3 (65 wt%, Fluka) in isopropanol. After evaporation of isopropanol, the obtained powder was dried using a stove at 80 ºC for 12 h and, subsequently, calcined at 600 ºC for 8 h at a heating rate of 10 °C/min.

Synthesis of glass beads coated with a non-porous titania support. Glass beads (E&R Chemicals & Equipment B.V., sieved diameter 200-300 μm) were pre-treated with acetone and isopropanol in an inert atmosphere and overnight stirred in aqueous sulfuric acid (2.5 M, Sigma-Aldrich) before the coating procedure. The titania precursor slurry (as described above) was added to the glass beads and stirred for 1 h. The obtained slurry was dried and calcined, similar to the procedure for powdered titania.

Synthesis of a mesoporous titania support. A titania-precursor sol, consisting of $Ti(OEt)_4$, Pluronic F127, ethanol, H_2O and trifluoroacetic acid, was prepared as described previously [57]. $Ti(OEt)_4$ was added dropwise to a clear solution containing a mixture of Pluronic surfactant in ethanol and trifluoroacetic acid in water. After stirring for 8 h and ageing for 24 h at room temperature, the resulting slurry was maintained for 30 h in a glove box at a humidity of 80%. The residual surfactant was removed by evaporation at 250 ºC for 4 h (heating rate of 5 ºC/min at 10 mbar) and, subsequently, calcined at 380 ºC (heating rate of 1 ºC/min at 1000 mbar) for 8 h to afford white powdered mesoporous titania. For the glass-bead coated titania support a known amount of the titania-precursor solution was slowly added to a filter filled with a single layer of glass beads. The solution withdrawal was monitored using a flow-controlled dip-coater. Similarly, the ageing, drying and calcination steps were performed as described in the procedure for the powdered mesoporous titania.

Deposition of Cu and CuZn catalyst on non-porous titania support. The deposition of the Cu and CuZn catalyst onto the titania support was done by addition of a known amount of pre-synthesized metal nanoparticles in ethanol to the support followed by overnight stirring. The ethanol was evaporated under nitrogen atmosphere at 80 °C prior to calcination at 450 °C for 8 h.

In-situ preparation of mesoporous titania supported Cu and CuZn catalysts. Pluronic F127 ($PEO_{99}PPO_{65}PEO_{99}$, BASF) was dissolved in ethanol under vigorous stirring and under an argon atmosphere for 1 h CuZn nanoparticles (in EtOH) were added under stirring for 30 min. Nitric acid (HNO_3, 65%) was added dropwise until a pH of 1–1.5 of the resulting mixture was attained. Then, $Ti(OEt)_4$ (99.99 wt%,

Sigma-Aldrich) was added until a transparent mixture was acquired. The resulting mixture was stirred for 25 h at 25 ºC and aged at a relative humidity of 80% for 48 h. An excess of Pluronic F127 was used to ensure that micelles were formed before the reaction initiated, which afterwards could easily be removed at 80 °C using a vacuum stove at 10 mbar. After removal of the major fraction of free Pluronic F127, the mesoporous titania structure could be obtained by combusting reacted Pluronic F127 in an air stove at 600 ºC for 8 h (at a heating rate of 10 °C/min). In this way, Cu/TiO_2, $Cu_{35}Zn_{65}/TiO_2$ and $Cu_{51}Zn_{49}/TiO_2$ were obtained with Cu and Zn loadings of 1 ± 0.07 wt% and 1-1.3 ± 0.09 wt%, respectively, determined by ICP analysis.

Drying and calcinations methodology. Removal of trace amounts of excess Pluronic F127 required moderate temperatures and vacuum conditions, whereas reacted Pluronic F127 was removed by combustion at high temperatures and in an oxygen-rich environment. Five steps were required in the calcination procedure, *i.e.* (1) evaporative removal of excess Pluronic F127 in a vacuum oven at 90-110 °C, (2) combustion of reacted Pluronic F127 in air at high temperatures, (3) the "after-burning" of deposited coke using an oxygen flow (10% O_2 in He), (4) controlled cooling to avoid collapse of the mesoporous structure, and (5) reduction at 300 °C (6% H_2 in N_2).

6.2.4 Catalyst analysis

X-ray diffraction spectroscopy. Supported copper nanocatalysts were measured by powder X-ray diffraction (PXRD). Diffractograms were recorded on a Röntgen PW3040/60 XPert PRO powder X-ray diffractometer with a high resolution PW3373/00 Cu LFF (unmonochromated) tube at $\lambda = 1.5404$ Å (Cu Kα) in the range $5° \leq \Theta \leq 80°$ and scanning rates of 0.23 °/min (CuZn) and 0.09 °/min (Cu). The powder samples were prepared by solvent evaporation from the colloidal suspensions deposited on a glass plate sample holder. Powder X-ray diffraction spectroscopy was mainly used to identify crystal phases of the titania support whereon the Cu nanoparticles were deposited. Since the total metal loading of copper on titania was around 2 wt%, simultaneous detection and measurement of the element-specific copper and titanium peaks were not possible due to the large difference in concentration. Therefore, the nanoparticles were measured separately, dispersed in ethanol (Supporting Information in reference [1]).

X-ray photoelectron spectroscopy (XPS). XPS was used to analyze the catalyst surface and detect the metals, their oxidation state and the dispersion of one metal phase over another. XPS signal sensitivity proved highly dependent on the metal dispersion and for supported catalyst the obtained signal for the supported catalyst also depended on the surface dispersion and the metal/support signal ratio. XPS samples were analyzed for several CuZn catalysts with emphasis on the Cu/Zn ratio in the fresh and spent catalyst. XPS data was obtained with a Kratos AXIS Ultra spectrometer equipped with a monochromatic Al Kα X-ray source and a delay-line detector (DLD). Spectra were obtained from an aluminium anode (Al Kα = 1486.6

eV) operating at 150 W. For survey and region scans, constant pass energies of 160 eV and 40 eV were used, respectively. The background pressure was 2 x 10^{-9} mbar (the XPS spectra can be seen in the Supporting Information of reference [1]). The spectral intensities of the Cu and Zn signals demonstrated good correspondence with the ICP data and confirmed quantitative deposition of the CuZn nanoparticles. However, after a run of 48 h the signals of the catalyst (CuZn) and the support clearly dropped, indicating significant leaching from the glass beads. This was also the case for the best $Cu_{50}Zn_{50}/TiO_2$ catalyst (see Supporting Information in reference [1]).

Scanning electron microscopy. SEM images were recorded to determine the size and morphology of the catalyst. A FEI Quanta series FEG 3D G2 SEM with an acceleration voltage of 5 kV and magnifications between 5,000 and 100,000 were used, providing a lateral resolution of 50 nm^2. Surface elemental composition analysis was done by energy-dispersive X-ray spectroscopy at a spot size of 50 nm^2. Both the fresh and spent catalysts were analyzed using SEM. At higher magnification, the film coating appeared to consist of nanosize particles which formed the porous structure of the support. The spent catalyst surface appeared to be affected by MW-irradiation leading to surface cracking and a highly inhomogeneous catalyst film (see Supporting Information in reference [1]). However, the porous character of the support at nano-scale was still intact.

High resolution transmission electron microscopy (HR-TEM). HR-TEM images were made using a FEI Tecnai G2 Sphera transmission electron microscope at 200 kV acceleration voltage. The solid catalyst (250 mg) was crushed in ethanol (2 mL) and coated onto a 200 mesh molybdenum grid (30 µL of the suspension) and dried at atmospheric pressure. The images provided the presence of a mesoporous matrix wherein the nanoparticles were impregnated (see reference [1]). The average particle size for 250 particles and 10 images was found to be 6.0 ± 1.2 nm.

6.2.5 Analytical techniques and methods

Nuclear magnetic resonance spectroscopy. ^{1}H-NMR data was collected on a Varian 400 Magnet NMR spectrometer (400 MHz). Spectra were obtained at 27 ºC and the chemical shifts (in δ ppm) were internally referenced to tetramethylsilane and peak integration externally referenced by tetradecane ($C_{14}H_{30}$). The ^{1}H-NMR spectra ($CDCl_3$; 8.4-8.6 ppm) of the reactants and product after full conversion are shown in the Supporting Information of reference [1]. The ^{1}H-NMR assignments for 4-phenoxypyridine are: δ 8.48 (d, *J* = 4.0 Hz, 2H), 7.44 (t, *J* = 8.0 Hz, 2H), 7.29–7.25 (m, 1H), 7.11 (d, *J* = 8.0 Hz, 2H), 6.85 (d, *J* = 8.0 Hz, 2H).

High performance liquid chromatography (HPLC). A Grace Smart^{TM} RP-18 5 µm apolar column with an internal diameter of 4.6 mm and a length of 150 mm was used. A mixture of methanol and water (40:60 vol%) as a polar solvent was used. A pH-buffer agent was used to maintain the pH-value (0.1% phosphoric acid, H_3PO_4) at the desired level and to protonate phenolate before entering the column. A

gradient eluent of methanol-water provided optimum separation, starting with 10:90 (v/v) and linearly increasing to 70:30 during seven minutes. Two UV-VIS absorption wavelengths (for aromatic systems) were simultaneously applied as an in-line detection method at 210 nm and 245 nm respectively. All four compounds (potassium phenolate, 4-chloropyridine, DMA and 4-phenoxypyridine) were calibrated using methanol and injected with a volume of 10 µl at a flowrate of 1 mL/min, at 47.3 bar column pressure and at 25 °C. The UV-detection range has been set at the typical absorption wavelengths (205-265 nm).

Inductive coupled plasma measurements and optical emission spectroscopy (ICP-OES). ICP-OES was used for the determination of copper, zinc and titanium loadings on the glass beads. A SPECTRO CIROS^{CCD} spectrometer was used at 1400 W. The sample injection was performed by a cross-flow nebulizer using a double-pass spray chamber and a sample uptake at a rate of 2 mL/min. Known amounts of various catalyst samples (Cu(Zn)/TiO_2/SiO_2) were dissolved in H_2SO_4 (5 M) and stirred overnight. Calibration lines were freshly prepared and measured prior to the catalyst samples.

6.3 Results and discussion

Prior to the MW-experiments and activity measurements in the catalytic micro fixed-bed reactor (µ-FBR), the temperature profiles have been determined along the length of the catalyst bed. Besides the temperature profiles in the µ-FBR with the catalyst coating, also a µ-FBR with inert beads was used to determine temperature profiles applying different solvents and flowrates. As shown in Figure 5 and demonstrated in the experimental section, two temperature sensors (fiber-optics) were placed in a thin quartz glass protection holder, which was fixed in the cylindrical axis of the reactor, using spacers (see Figure 5).

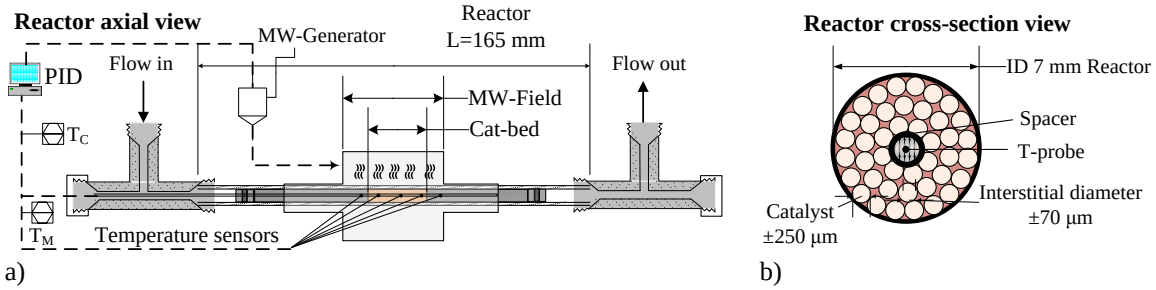

Figure 6.5. Reactor and microwave design (a) with a cross section view of the microporous channels (b).

6.3.1 Axial temperature profiles in a micro fixed-bed milli-reactor

The temperature controller T_1 was used in an auto-controlling (PID) mode at the outlet section of the reactor (position D_0-D_5 in Figure 6) while the T_2 sensor was moved axially along the inlet section of the reactor (30% of the reactor length) at discrete distances of 2.5 mm from the inlet of the reactor (position C_0-C_5 in Figure 6). The temperature graphs (according to the setup in Figure 6) obtained at a flowrate of 5 mL/min in the µ-FBR (with inert beads), using only DMA as the

reaction solvent, are shown in Figure 7 at a constant temperature (~140 °C) and variable powers (with P_{max} = 80 W).

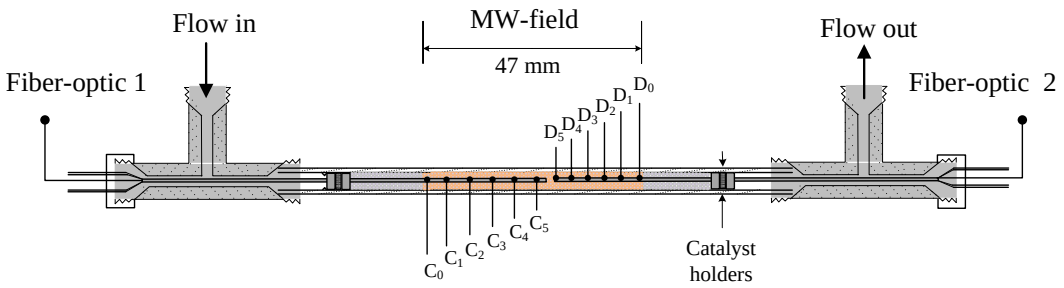

Figure 6.6. Schematic overview of measurements points in the µ-FBR for determination of the axial heating profiles along the length of the reactor.

Figure 7a shows that *ca.* 10 sec was required to reach the set temperature at D_0 starting from ambient temperatures, consecutively reaching the desired steady state temperature. Although the temperature over 12.5 mm of the inlet section of the catalyst bed (position: C_1-C_5) shows hardly any axial gradient, a temperature difference between outlet and inlet of *ca.* 25 °C was still observed (see Figure 7b).

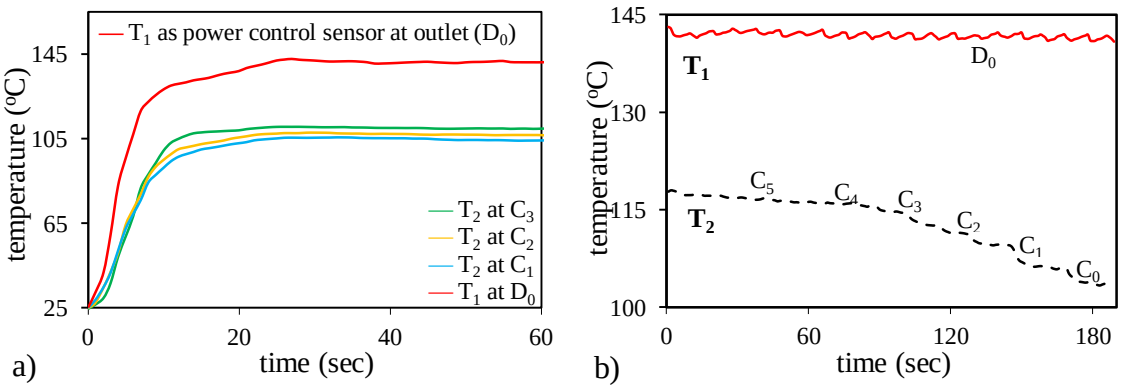

Figure 6.7. a) Temperature profiles obtained at various axial positions in the micro fixed-bed reactor. b) Temperature profiles at various positions at the reactor inlet (solvent: DMA, flowrate: 5mL/min, P_{max}: 65 W).

Similar experiments were carried out using a temperature sensor at the inlet (C_0) of the catalyst coated µ-FBR, using a fixed MW power input of 65 W. Figure 8a shows the temperature profiles at the inlet section of the catalyst bed which demonstrate much higher axial gradients and a strong overshoot at the initial heating rate. At the outlet (Figure 8b) the axial temperature gradients dropped, but the temperature fluctuations increased.

However, at the outlet (Figure 8b) the overshoot appeared to decrease along the length of the catalyst bed due to higher temperatures at the outlet. From these experiments, it can be concluded that controlling the power input by a set temperature condition leads effectively to much more stable conditions and negligible temperature overshoot at the start-up conditions (Figure 7a).

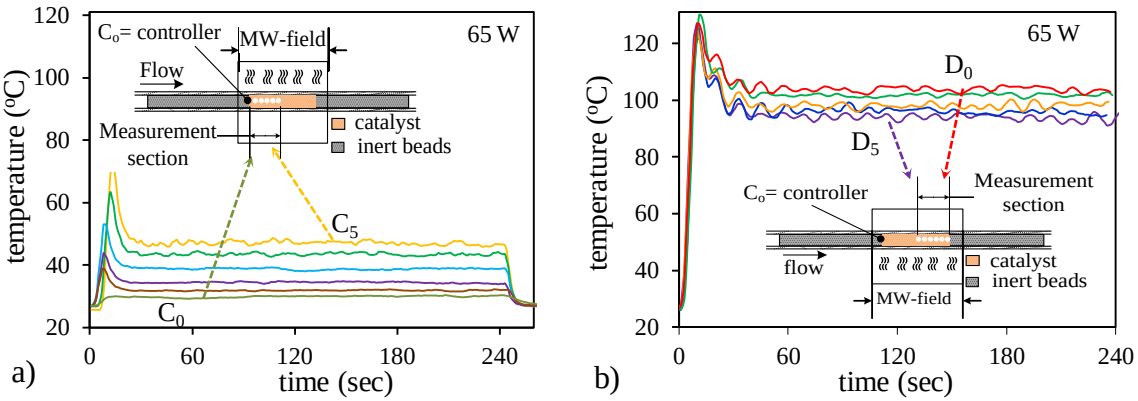

Figure 6.8. Temperature profiles at the inlet section of the reactor (a) and at the outlet section (b) of the reactor at 65 W and a flowrate of 5 mL/min.

Nevertheless, by adjusting the MW-power input to the reactants flowrate, using a PID-control system, the temperature gradients over the length of the reactor could be minimized.

6.3.2 Temperature and microwave-power control in a continuous chemical process

In a consecutive step, the reactants (potassium phenolate, 4-chloropyridine and 18-crown-6 ether) were added to the solvent DMA to envisage their influence on MW-absorption and temperature patterns during flow operations. Figure 9 displays strong temperature fluctuations at the inlet (blue) and outlet (red) of the reactor and regularly safety shut downs of the process. The presence of the reactants demonstrated highly fluctuating temperature conditions.

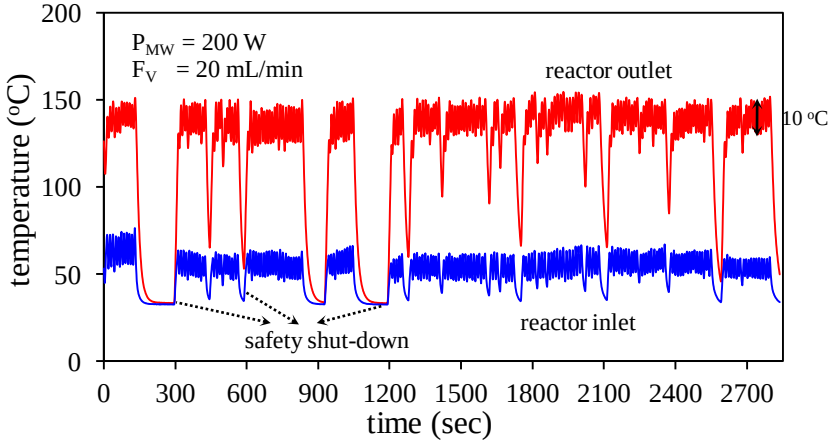

Figure 6.9. Temperature-time histories at the reactor inlet (blue) and outlet (red) demonstrate strong temperature fluctuations up to 10 °C at constant MW-power input as a result of the reactants in the reaction mixture.

The presence of KCl salt, formed as by-product in the reaction of potassium phenolate and 4-chloropyridine, clearly increased the complexity of the temperature control and the PID-response on the power input. Figure 10 depicts the temperature profiles obtained in a batch-loop reactor with auto-PID control for the MW-power input based on the set temperature (T_{out}) at the outlet of the reactor.

The flowrate was maintained constant at 20 mL/min and the temperature was measured at the outlet of the reactor, showing very stable temperatures in Figure 10a. As a result of the changing reaction composition (increasing KCl production) and the related varying dielectric properties, the temperature fluctuations and required power increased during the scope of the reaction process (Figure 10b). The loss tangent (tan δ) is the characteristic parameter to determine the capacity of a substance to convert electromagnetic energy into thermal energy. High absorbing solvents (*e.g.* ethylene glycol, ethanol) typically possess a tan δ value around 0.9, whereas low absorbing solvents have a value below 0.1 (*e.g* toluene, hexane, xylene).

Figure 10c shows the measured tan δ values at the reaction temperature range for the reaction mixture in various compositions (a mixture of solvents, recatnts and product (○), a mixture of DMA and potassium phenolate (Δ), a mixture of DMA and 4-chloropyridine (◊) and a mixture of DMA and KCl (□). Clearly, these measurements proved that the major contributor to the increase of tan δ in the reaction mixture arose from potassium phenolate [58]. Conversely, KCl appeared to have a negative effect on tan δ. This observation was confirmed when the change in tan δ during reaction was monitored (see Figure 10d), demonstrating a clear, yet moderate, decay as the reaction proceeded. From previous work, it was concluded that under MW-irradiation the KCl by-product would deposit onto the catalyst surface, instead of contributing to ionic heating in DMA [58].

This observation reveals an additional and crucial parameter to be considered in controlling MW-energy for changing chemical and dielectric compositions of the flow. An auto-PID control system was programmed to account for the change in reaction mixture composition using both the MW-power supply and additional dead-load as controlling parameters, releasing excessive MW-energy to a water-flow. As a result, the overall magnetron efficiency decreased as more than 80% of the energy was released to the dead-load. However, the cavity efficiency arose far above 90% due to very precise energy input.

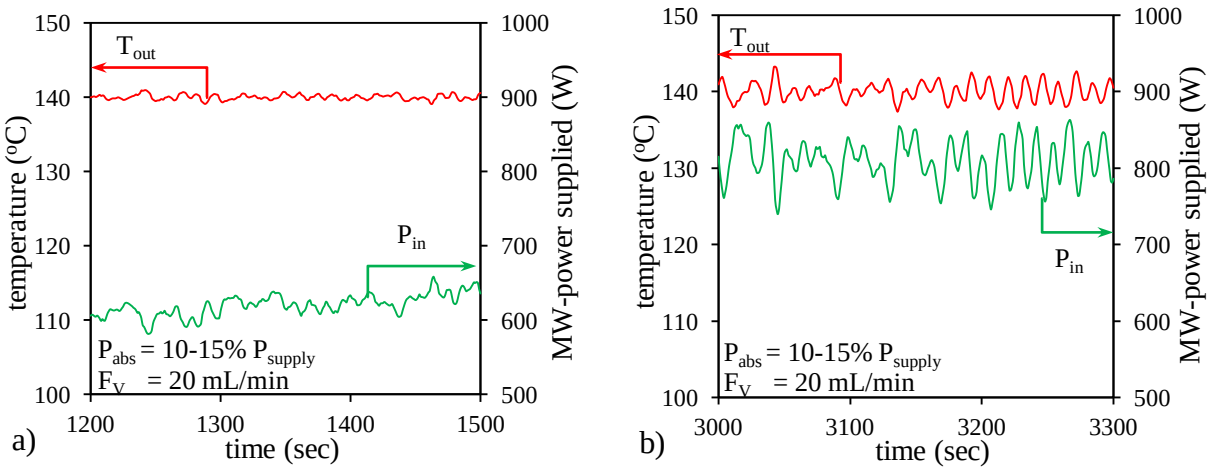

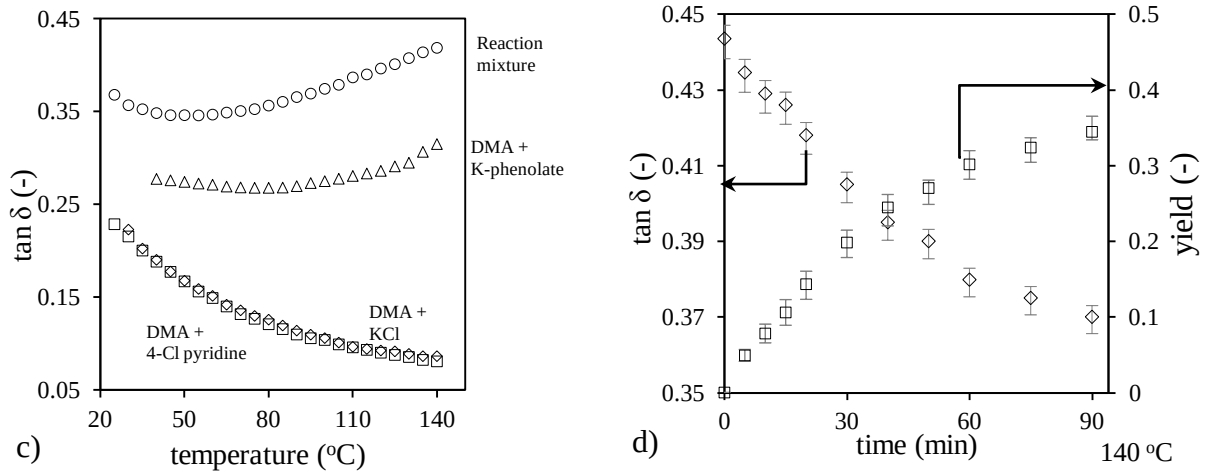

Figure 6.10. Stable temperatures using auto-PID power input at the beginning of the reaction (a). At higher reaction times increased temperature and power fluctuations were observed due to changing reaction mixture compositions in the batch-loop process (b). This effect is shown in (c), showing the major heating effect from potassium phenolate and its consumption (d), leading to drastically changed dielectric properties and loss tangent (tan δ) of the chemical system. It should be noted that < 10% of the supplied MW-power was utilized in the cavity, the remaining part was released to a water flow as a dead-load. In this way, the power inlet to the applicator cavity could be controlled very precisely.

As a result, this approach with a very efficient response of the absorbed MW-power demonstrated highly stable reactor inlet and outlet temperatures, even at 5 mL/min. Also, energy efficiencies (from cavity to reactor) above 90% were achieved with a MW-energy supply of only 10 ± 3 W to the reactor. Figure 11 depicts the temperature-power graphs obtained for the process during 1 h on stream.

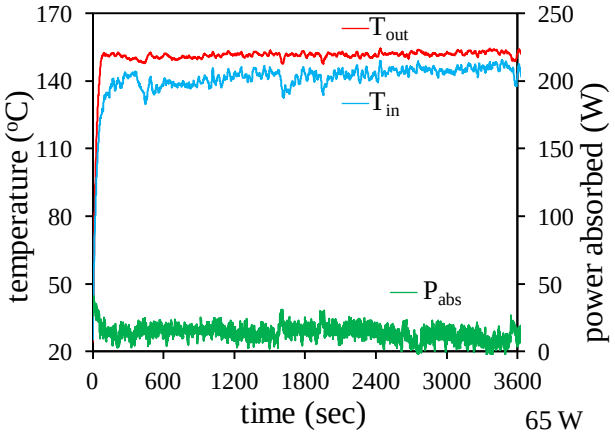

Figure 6.11. Temperature-time history using a MW-power of 65 W resulting in a cavity power of 10 W at a flowrate of 5 mL/min. Highly stable operations could be achieved using adjusted auto-PID control.

6.3.3 Activity experiments using "in-line mixing" in a Cu-capillary flow system

Initial flow experiments have been done using an oil-bath heated Cu-capillary reactor (inner diameter 1.05 mm, see Experimental section) to survey the optimal process conditions and to emphasize only on the in-line mixing properties. In the capillary-based milli-reactor two type of mixing were applied, *e.g.* (1) a "Y-mixer" (250 µm, 316 SS, Valco Instruments Co. Inc.), generating

laminar flow and relatively short contact times, and (2) a "split-and-recombine" mixer (250 µm, DIARC® coated 316 SS channels), generating micron-scale structured mixing and increased contact times, both resulting in enhanced mixing properties (see Figure 12). In the split-and-recombine mixer, multi-lamination was obtained, which created very thin layers by splitting the main streams into many sub-streams, providing an increased contact time and area of the two inlet flows [59]. The main difference between both mixing techniques was the contact times of the fluids and the mixing structure, which was strongly influenced by viscosity differences between both fluids [60].

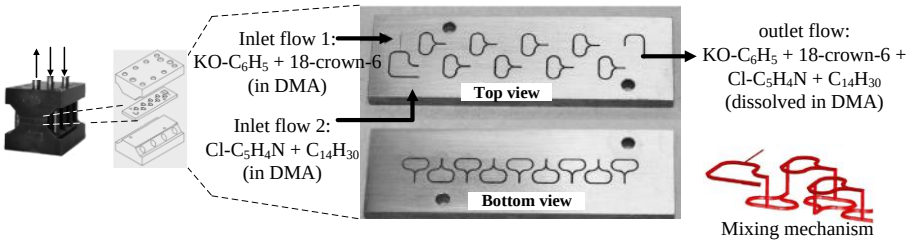

Figure 6.12. Structured mixing by the split-and-recombine mixer showing a schematic view of the mixer and mixing mechanism as described by Zuidhof *et al.* [59]

The residence time was regulated using separate HPLC pumps for each reactant flow. Due to the risk of leakage the flowrates in the split-and-recombine mixer could not exceed 0.2 mL/min which led to mixing times of around 30-60 seconds. To avoid precipitation of potassium phenolate, the mixer was conditioned at 50 °C to maintain a homogeneous solution. Under these conditions, reaction could not occur in the absence of catalyst. The mixer was integrated with a micro heat-exchanger to simultaneously quench the reactor outlet flow (see Supporting Information in reference [1]). Figure 13 depicts the results, comparing the chemical productivities of the Y-mixer (a) and the split-and-recombine mixer (b). The productivity has been defined as the global hourly production term of 4-phenoxypyridine per unit surface catalyst equivalent to the inner capillary surface.

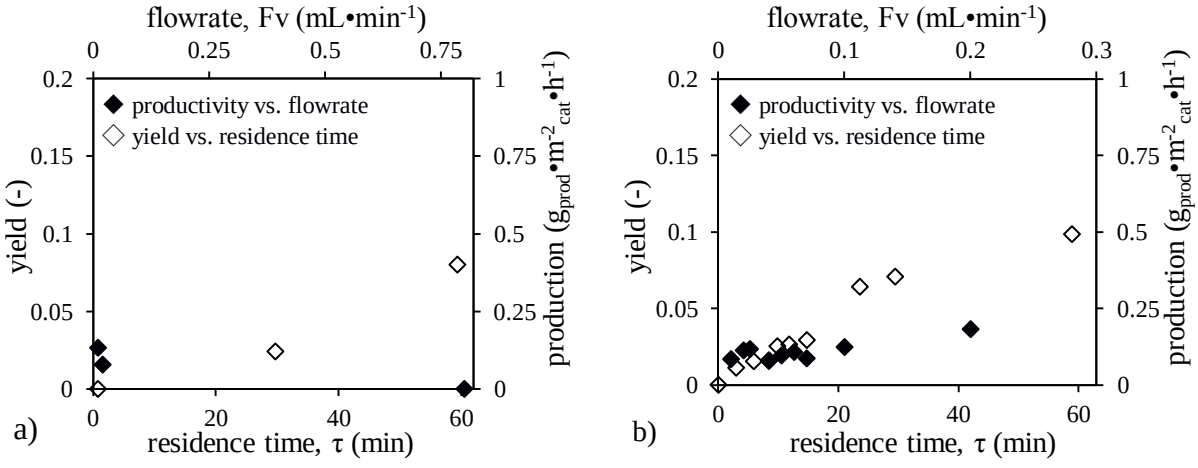

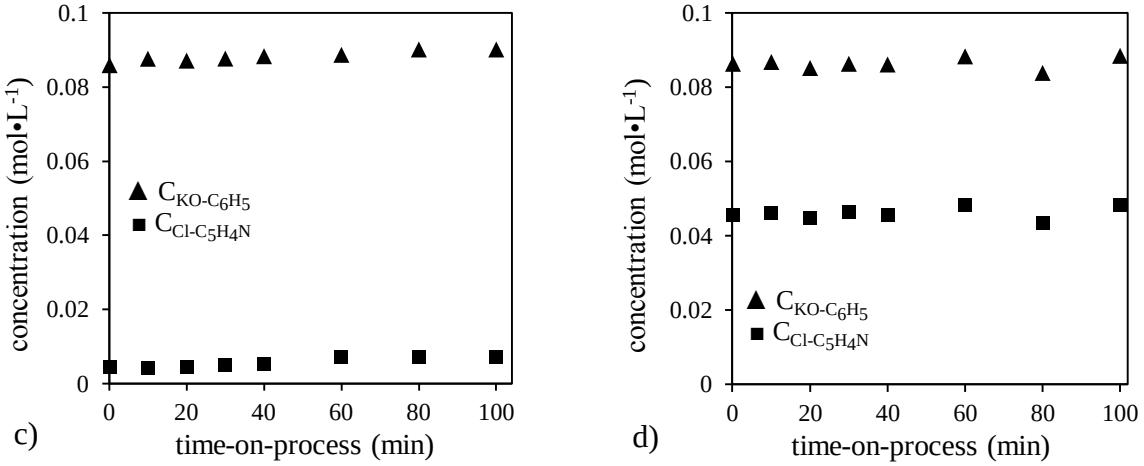

Figure 6.13. The effect of flowrate on productivity using a Y-mixer (a) and the split-and-recombine mixer (b). Yields are shown as a function of residence time in the capillary reactor. Concentration-histories measured at the outlet of both the Y-mixer (c) and split-and-recombine mixer (d). These experiments have been carried out using oil-bath heating.

Although the range of operating flowrates differed for both mixers, a drop in chemical productivity from 0.13 to 0.07 $g_{prod}•m^{-2}_{cat}•h^{-1}$ was observed in the Y-mixer at increasing flowrates from 10 to 20 µl/min (Figure 13a). At flowrates above 100 µl/min, no product was formed even at increased residence times, using a recycle loop reactor in the process. After comparing the reactants composition at the outlet of the Y-mixer, the fluid consisted mostly of potassium phenolate, whereas 4-chloropyridine appeared to be sub-proportional (see Figure 13c). Based on the concentration-time plots, the Y-mixer demonstrated that flow 1 (*i.e.* potassium phenolate) clearly suppressed flow 2 (*i.e.* 4-chloropyridine) due to the large viscosity difference of both flows. The split-and-recombine mixer provided a constant productivity (Figure 13b) as a function of flowrate and, based on the outlet concentration (Figure 13d), also the desired reactant ratio (*ca.* 2:1). From these results, it was clear that a two-flow system with different viscosities and densities required multi-lamination mixing which is applied in the subsequent sections.

6.3.4 Activity experiments in the micro fixed-bed reactor using single-mode MW-heating

Based on the results obtained to determine the axial bed temperature, the fixed-bed setup was applied for single-mode microwave operations in a $CuZn/TiO_2$ based catalytic µ-FBR (see Figure 14). The packing of the catalyst in the tubular reactor is described in the experimental section.

During these experiments, the temperature was controlled using two fiber-optic probes inside the catalyst bed as depicted in Figure 6 (*vide supra*). The micro-cooling / micro-mixing units and connecting tubes were similar to those used in the capillary-based setup (as shown in Figure 4 in the experimental section). However, for the MW-setup a micro fixed-bed was used, aimed at supplying an equivalent amount of catalyst surface and reactor volume and at mimicking micro-channelled hydrodynamics.

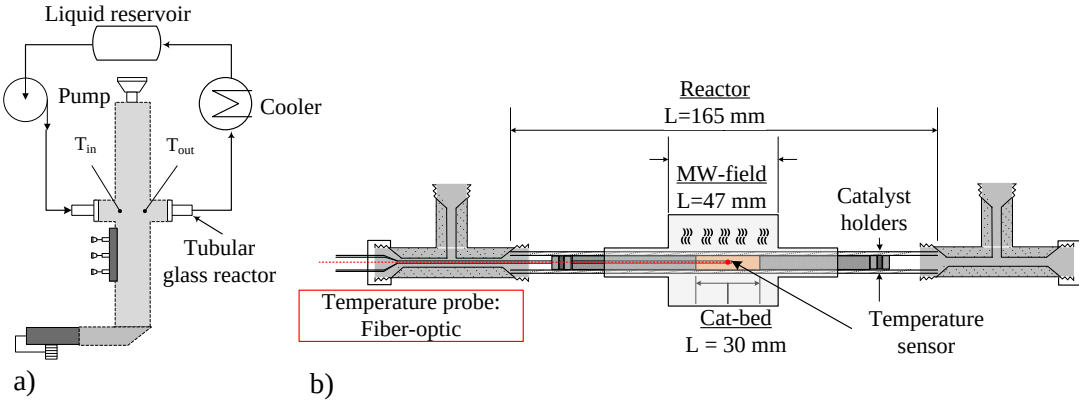

Figure 6.14. Schematic view of the single-mode MW-design (a) and the micro fixed-bed reactor (μ-FBR) design (b).

Influence of catalyst composition. Based on our previous catalyst composition and activity findings [46], the silica beads were coated with various Cu and Zn loadings (onto titania). These silica beads were then packed in the milli-reactor tube to obtain a micro fixed-bed of $Cu_xZn_y/TiO_2/SiO_2$ (x and y in wt%) catalyst. In this way, various Cu and Zn loadings and ratios were examined to propose the most active catalyst composition for maximum productivity (Figure 15).

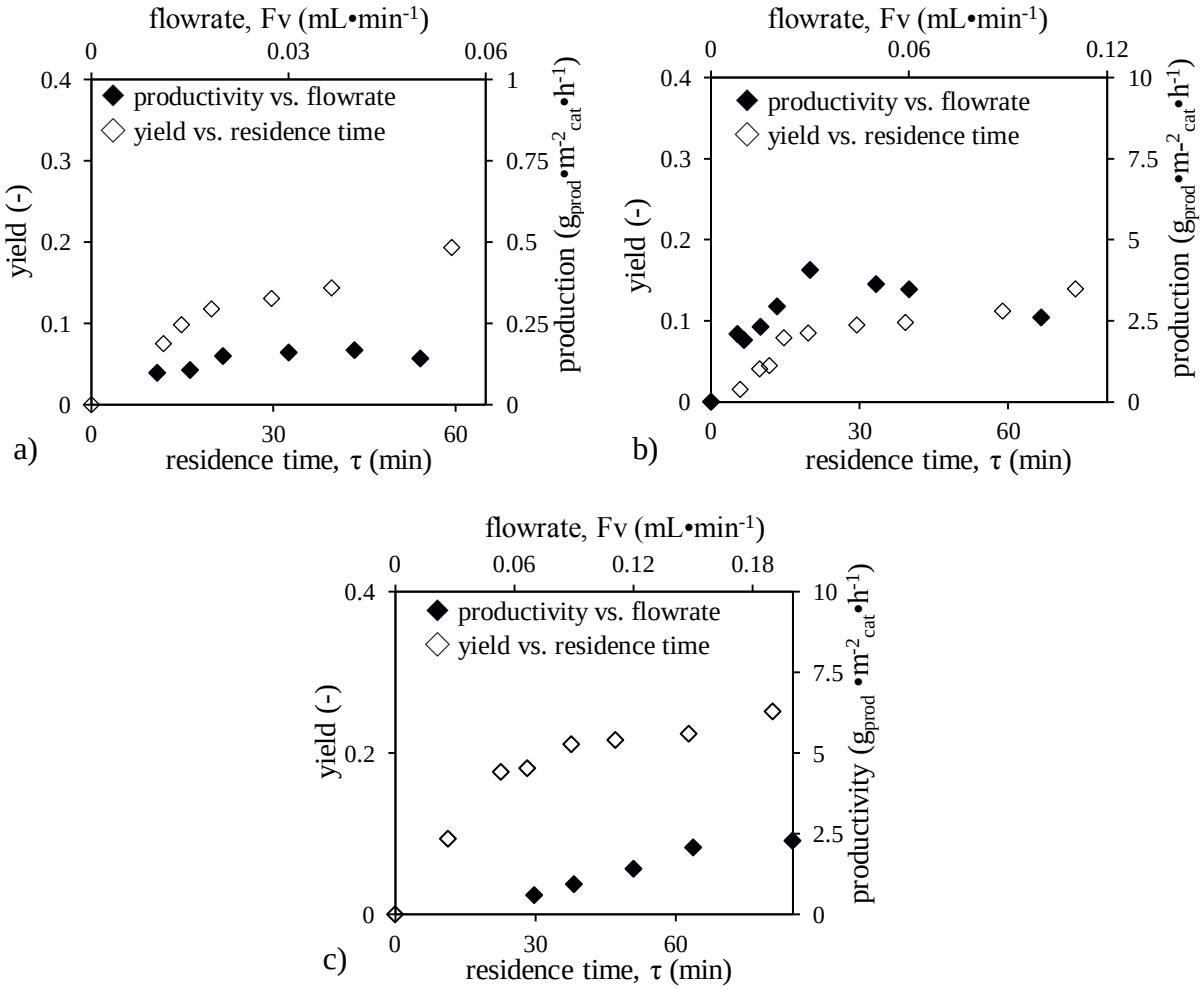

Figure 6.15. Influence of catalyst composition on productivity and yield using different catalyst compositions. Cu/TiO_2 (a) $Cu_{0.3}Zn_{0.7}/TiO_2$ (b) and $Cu_{0.5}Zn_{0.5}/TiO_2$ (c).

Compared to the oil-bath heated Cu-capillary reactor (Figure 13b), the MW-heated $Cu/TiO_2/SiO_2$ catalyst (Figure 15a) showed almost a two-fold yield increase and a three-fold yield increase to 26% for the $Cu_{0.5}Zn_{0.5}/TiO_2$ catalyst (Figure 15c). However, the $Cu_{0.3}Zn_{0.7}/TiO_2$ catalyst showed the lowest yields (around 11%) for residence times around 1 h (Figure 15b), which were found to be even lower than those of the oil-bath heated Cu-capillary reactor. This yield drop could be explained using our previous synchrotron X-ray data for the bimetallic CuZn nano-catalyst where various CuZn compositions were examined as fresh, spent and *in-situ* operated catalysts [61]. From these experiments, it was clear that an excessive use of Zn in a bimetallic supported nano-catalyst led to the formation of a ZnO-shell, thus making the Cu surface less accessible for reactants. Nevertheless, the Zn-promoted catalysts provided generally much higher activities resulting in productivities up to an order of magnitude higher as compared to the pure monometallic Cu catalyst.

Catalyst segmentation for selective and beneficial catalyst MW-absorption. In the previous experiments, the catalyst bed was placed at the center of the reactor and MW-cavity. However, using this way of catalyst packing, the reaction mixture flow would be subjected to high catalyst temperatures, which would lead to local overheating and consequently coke formation and catalyst deactivation. By dividing the fixed-bed, alternatively, in a catalyst segment and an inert segment, the liquid flow would be repetitively exposed to "heating" and "cooling" zones over the entire length of the MW-cavity. In this way, equal amounts of catalyst would be spread over the whole irradiation section which provided equal residence times of the reactants in the catalyst bed. Moreover, this catalyst configuration could also provide advantages due to local and controlled heating by segmentation, resulting from selective MW-absorption of the catalyst. The obtained yields and productivities of a two-fold, three-fold and four-fold segmented catalyst bed are shown in Figure 16a, 16b and 16c respectively.

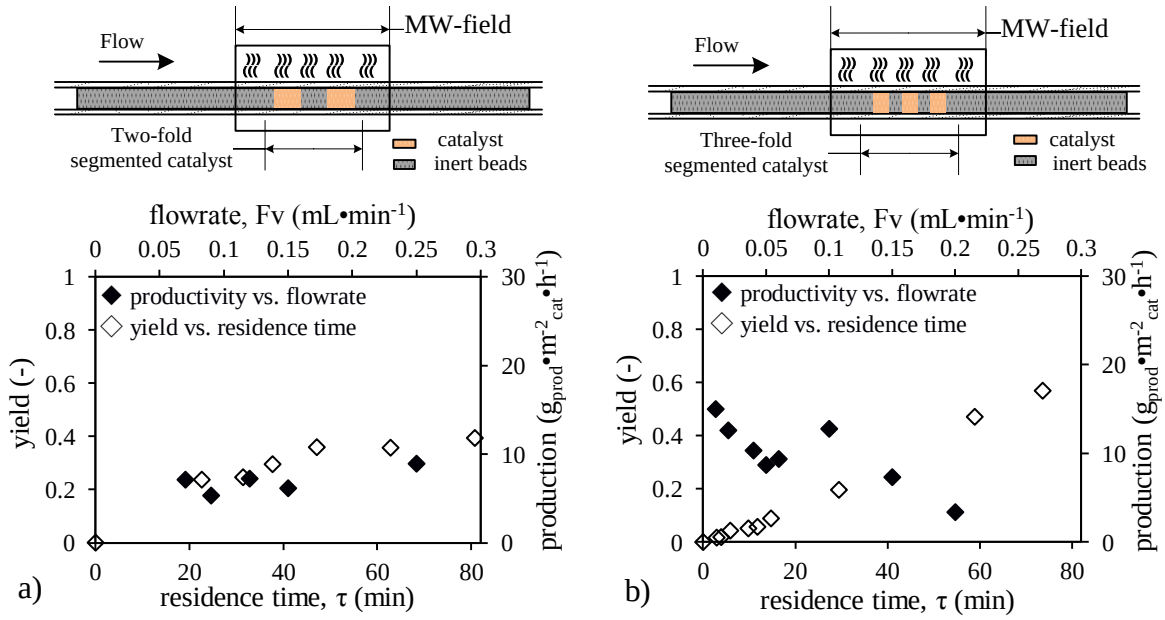

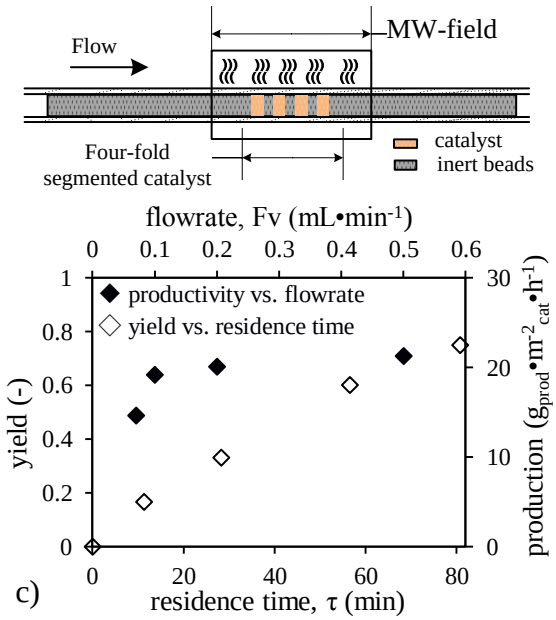

Figure 6.16. Yields and productivities obtained from the two- (a), three- (b) and four-fold (c) segmented catalyst bed. The same catalyst bed was segmented over the entire MW-irradiation section using a $Cu_{0.5}Zn_{0.5}/TiO_2$ catalyst.

Figure 16 also shows the catalyst segmentation structures for all three different reactors, using a $Cu_{0.5}Zn_{0.5}/TiO_2$ catalyst. These experiments showed a linear relation between the number of catalyst segments and the yield increase, *i.e.* up to 75% yield for the four-fold and 57% and 40% yield for the three-fold and two-fold catalyst bed, respectively. These high yields have not yet been reported previously using microwave-assisted flow chemistry in Cu-catalyzed Ullmann C-O coupling reactions.

Furthermore, in the multi-segmented catalyst bed the productivity (as function of the flowrate) increased with an order of magnitude (Figure 16c) as compared to that of the single-segmented catalyst bed (Figure 15c). At best, a productivity of 21 $g_{prod}/m^2_{cat}/h$ could be achieved using a four-fold segmented catalyst bed at a total flowrate of 0.5 mL/min. The fact that the Cu-coated segments do not only catalyze the reaction, but also provide thermal energy to the process, demonstrated that temperature control in metal-catalyzed processes is as important as the actual catalyst activity.

6.3.5 Temperature inside the Cu catalyst bed

The reason behind the increased productivities in a multi-segmented catalyst bed can be attributed to the optimal utilization of the MW-energy by selective catalyst absorption. The Cu nanoparticles played a role as a selective MW-absorbing material and essentially increased the thermal energy "at the spot". This was proved by measuring the temperatures in the single-segmented fixed-bed reactor at the Cu-coated catalyst part and at the MW-inert SiO_2 section for various flowrates, using MW-absorbing (DMA) and non-absorbing (toluene) solvents. Figure 17a shows the experimental setup with the annotated points (a-k) which resulted in an axial temperature gradient, shown in Figure 17b.

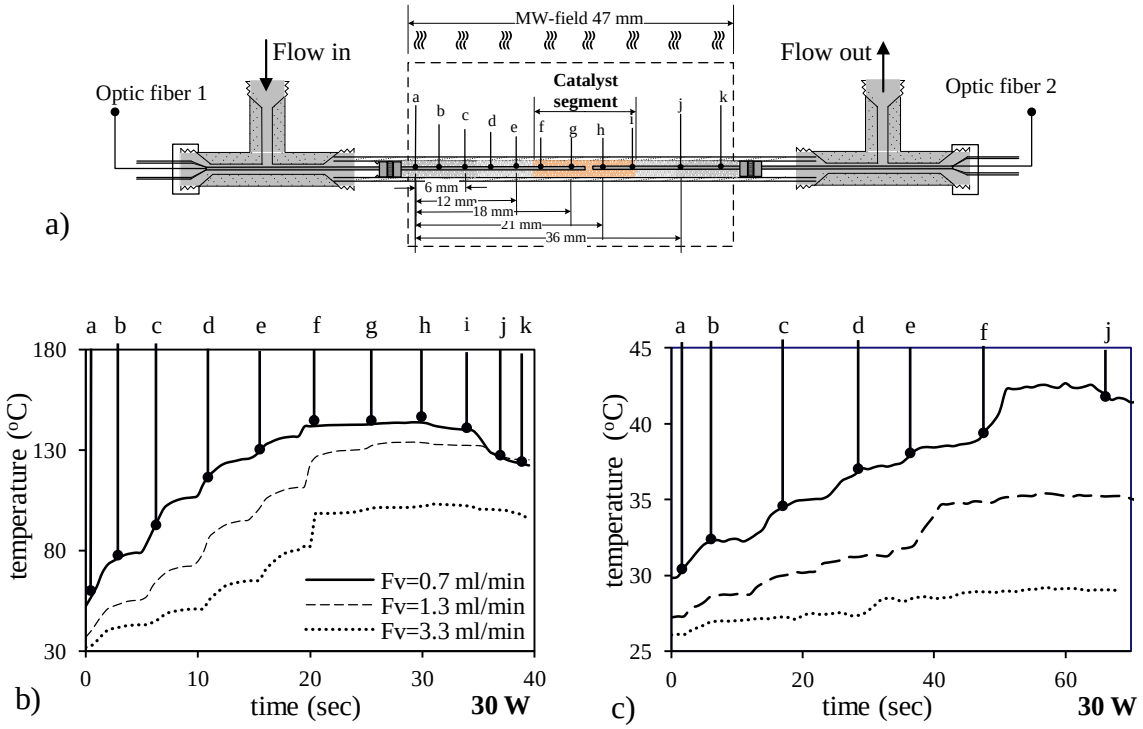

Figure 6.17. Temperature profiles obtained at various axial positions in the $Cu/TiO_2/SiO_2$ micro fixed-bed reactor (a), using DMA (b) and toluene (c) at different flowrates. (─ F_v= 0.7 mL/min; --- Fv= 1.3 mL/min; ••• Fv= 3.3 mL/min).

Since the solvent DMA absorbs microwaves during the measurements, the temperature gradient in the catalyst segment were measured also for toluene, *i.e.* a MW-transparent liquid (Figure 17c). Figure 17 showed that the temperature rise is highest at the catalyst segments (points f, g, h and i), compared to non catalytic segments but rapidly drops outside the catalyst segment (points a - e and j - k). This temperature rise was observed to be proportional at different flowrates of the solvent indicating the selective MW-absorption by catalyst bed. Moreover, using microwave-transparent solvent (*i.e.* toluene) in the fixed-bed reactor resulted in similar temperature profiles albeit at lower overall temperatures, which further confirmed the selective Cu absorption of microwaves.

Also for the multi-segmented reactor (shown in Figure 18a), the axial temperature measurements have been carried out using *p*-xylene as solvent, which has a similar degree of MW-transparency but a higher boiling point than toluene. Figure 18a shows the reactor setup with the catalyst segments and the measurements points.

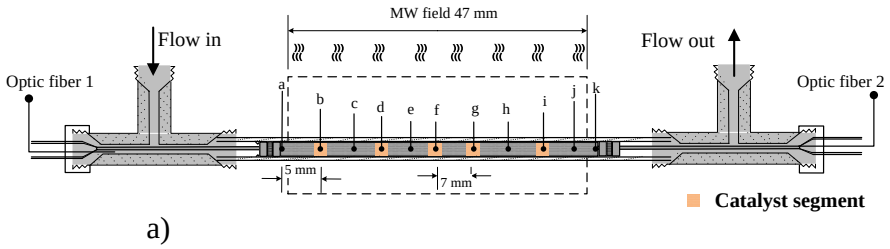

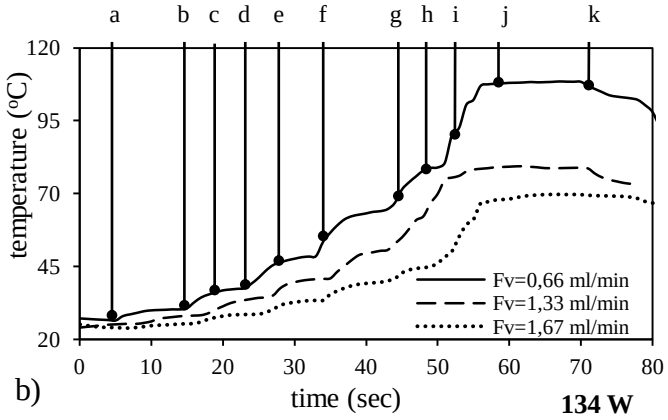

Figure 6.18. Temperature profiles obtained at various axial positions from the multi-segmented $Cu/TiO_2/SiO_2$ micro fixed-bed reactor (using *p*-xylene).

The obtained axial temperature profile is given in Figure 18b, which clearly demonstrates higher temperature gradients at the catalyst segments and more or less stagnant temperature profiles at the inert segments. Figure 18 showed the applicability of MW-heating even for MW-transparent solvents, when a MW-absorbing metal is used, either as catalyst or simply as MW-absorber. However in this study, both characteristics have been utilized and successfully implemented in a MW-heated catalytic flow reactor.

6.4 Conclusions

Very efficient and precise temperature control was achieved in a single-mode MW-cavity, using a power-temperature PID control system. This setup was successfully applied in the Ullmann-type C-O coupling reaction in various fixed-bed catalytic reactors as a means to conduct flow chemistry. It was found that in the case of an empty milli-reactor the axial temperature gradient at the inlet could be maintained lower than 10 °C at low flowrates. However, large temperature gradients appeared at flowrates higher than 10 mL/min. The gradients at the outlet section of the reactor appeared to be minimal and could be maintained below 4 °C. In the case of a micro fixed-bed reactor, it was found that mainly the inlet section was subjected to large temperature gradients and overshooting.

The reactor performance was improved by integrating a temperature conditioned pre-mixer, based on multi-lamination mixing in a split-and-recombine mixer. The mixer unit could be heated by integrating a micro heat-exchanger and utilizing the hot product stream. The mixing performance was demonstrated by measuring the reactants concentration at the outlet of the mixer and the productivity at the outlet of the reactor. The Y-mixer demonstrated very poor mixing, resulting in decreased productivities as function of flowrate. The multi-lamination split-and-recombine mixer, conversely, showed the desired reactants concentration at the mixer outlet which consequently afforded stable productivities.

The temperature fluctuations were minimized to 2 °C with cavity efficiencies above 80% for a flowrate of 10 mL/min by adding a dead-load as variable to control MW-energy into the reactor cavity. This could only be done

when the changing chemical compositions of the flow were taken into account, since liquid heating of the reaction mixture appeared to be predominantly affected by the gradual consumption of the superior MW-absorbing component, *i.e.* potassium phenolate. A yield of 19% in 1 h was achieved in the Ullmann coupling reaction when a Cu/TiO_2 catalyst was used in the fixed-bed reactor applying single-mode MW-heating. This was *ca.* 10% higher as compared to the yield obtained in an oil-bath heated Cu-capillary reactor.

By changing the composition of the catalyst, while adding Zn as co-promoter, a highest yield of 26% was attained in 80 min, using a $Cu_{0.5}Zn_{0.5}$ catalyst. However, increasing the amount of Zn demonstrated a yield drop due to a reduced accessibility of the active Cu-surface. This observation confirms our previous findings, where an optimum composition in Cu:Zn ratio led to much higher activities due to the oxidative stability of Cu [46, 61].

Lastly, catalyst bed segmentation in the MW-field was used to control the liquid temperature by introducing "heating" and "cooling" zones in the fixed-bed reactor. Increasing the number of catalyst segments resulted in enhanced product yields, up to 75% in 80 min for a four-fold segmented catalyst bed. The overall productivity also increased with a factor 5, using a multi-segmented catalyst bed as compared to a single-segmented catalyst bed. An hourly production rate of 22.5 $g_{prod}/m^2_{cat}/h$ was achieved using a four-fold segmented catalyst bed at a flowrate 0.5 mL/min, corresponding to a kg_{prod}/day pilot plant.

Finally, this study also demonstrated that heterogeneously catalyzed processes, involving MW-transparent solvents (*e.g.* toluene and *p*-xylene) and utilizing selective absorption of microwaves by a catalyst, can be successfully performed as a novel approach for microwave-heated flow chemistry.

References

[1] F. Benaskar, N. G. Patil, E. V. Rebrov, A. Ben-Abdelmoumen, J. Meuldijk, L. A. Hulshof, V. Hessel and J. C. Schouten, *ChemSusChem* **2012**, *submitted*.

[2] a) F. Ullmann and P. Sponagel, *Chem. Ber.* **1905**, *36*, 2211-2212; b) F. Ullmann and J. Bielecki, *Chem. Ber.* **1901**, *34*, 2174-2185; c) F. Ullmann, *Chem. Ber.* **1903**, *36*, 2382-2384; d) S. J. Sawyer, *Tetrahedron* **2000**, *56*, 5045-5065; e) F. Monnier and M. Taillefer, *Angew. Chem., Int. Ed.* **2009**, *48*, 6954-6971.

[3] a) M. Taillefer, H.-J. Cristau, P. P. Cellier, J.-F. Spindler and A. Ouali, *Fr 2840303-WO 03101966 (Pr. Nb. Fr 2002 06717)* **2002**; b) S. L. Buchwald, A. Klapars, J. C. Antilla, G. E. Job, M. Wolter, F. Y. Kwong, G. Nordmann and E. J. Hennessy, *WO 02/085838 (Priority number US 2001 0286268)* **2001**; c) V. Balraju and J. Iqbal, *J. Org. Chem.* **2006**, *71*, 8954-8956.

[4] a) S. V. Ley and A. W. Thomas, *Angew. Chem., Int. Ed.* **2003**, *42*, 5400-5449; b) I. P. Beletskaya and A. V. Cheprakov, *Coord. Chem. Rev.* **2004**, *248*, 2337-2364; c) H.-J. Cristau, P. P. Cellier, J.-F. Spindler and M. Taillefer, *Chem. –Eur. J.* **2004**, *10*, 5607-5622.

[5] a) H. Weingarten, *J. Org. Chem.* **1964**, *29*, 977-978; b) Tran-Dinh-Tuong and M. Hida, *Bull. Chem. Soc. Jpn.* **1971**, *44*, 765-771.

[6] a) R. OI, C. Shimakawa and S. Takenaka, *Chem. Lett.* **1988**, *17*, 899-900; b) D. Ma, Y. Zhang, J. Yao, S. Wu and F. Tao, *J. Am. Chem. Soc.* **1998**, *120*, 12459-12467; c) A. Kiyomori, J.-F. Marcoux and S. L. Buchwald, *Tetrahedron Lett.* **1999**, *40*, 2657-2660; d) H. B. Goodbrand and N.-X. Hu, *J. Org. Chem.* **1998**, *64*, 670-674.

[7] M. Taillefer, H.-J. Cristau, P. P. Cellier and J.-F. Spindler in *Fr 2833947-WO 0353225 (Pr. Nb. Fr 2001 16547)*, *Vol.* **2001**.

[8] K. Kunz, U. Scholz and D. Ganzer, *Synlett* **2003**, *2003*, 2428-2439.

[9] a) C. Couture and A. J. Paine, *Can. J. Chem.* **1985**, *63*, 111-120; b) J. Hassan, M. Sevignon, C. Gozzi, E. Schulz and M. Lemaire, *Chem. Rev.* **2002**, *102*, 1359-1469; c) A. J. Paine, *J. Am. Chem. Soc.* **1987**, *109*, 1496-1502; d) E. Sperotto, G. P. M. van Klink, G. van Koten and J. G. de Vries, *Dalton Trans.* **2010**, *39*, 10338-10351; e) R. T. Stibrany, C. Zhang, T. J. Emge, H. J. Schugar, J. A. Potenza and S. Knapp, *Inorg. Chem.* **2006**, *45*, 9713-9720; f) R. W. Turner and E. L. Amma, *J. Am. Chem. Soc.* **1963**, *85*, 4046-4047; g) H. Weingarten, *J. Org. Chem.* **1964**, *29*, 3624-3626; h) F. Benaskar, N. G. Patil, V. Engels, E. V. Rebrov, J. Meuldijk, V. Hessel, L. A. Hulshof, A. E. H. Wheatley and J. C. Schouten, *Dalton Trans.* **2012**, *Revision/Accepted*.

[10] J. P. Finet, A. Y. Fedorov, S. Combes and G. Boyer, *Curr. Org. Chem.* **2002**, *6*, 597-626.

[11] a) S. Benyahya, F. Monnier, M. Taillefer, M. W. C. Man, C. Bied and F. Ouazzani, *Adv. Synth. Catal.* **2008**, *350*, 2205-2208; b) K. Knepper, M. E. P. Lormann and S. Brase, *J. Comb. Chem.* **2004**, *6*, 460-463; c) C. A. Parrish and S. L. Buchwald, *J. Org. Chem.* **2001**, *66*, 3820-3827.

[12] L. N. Protasova, E. V. I. Rebrov, Zinfer R. and J. C. Schouten, *Microporous Mesoporous Mater.* **2009**, *123*, 243-252.

[13] T. A. Nijhuis, T. Visser and B. M. Weckhuysen, *J. Phys. Chem. B* **2005**, *109*, 19309-19319.

[14] E. V. Rebrov, E. A. Klinger, A. Berenguer-Murcia, E. M. Sulman and J. C. Schouten, *Org. Process Res. Dev.* **2009**, *13*, 991-998.

[15] F. Monnier and M. Taillefer, *Angew. Chem., Int. Ed.* **2008**, *47*, 3096-3099.

[16] J. F. Hartwig, M. S. Driver, F. E. Goodson, B. C. Hamann, J. Louie and G. Mann, *Abstr. Pap. Am. Chem. Soc.* **1998**, *216*, U449-U449.

[17] a) P. Lopez-Alvarado, C. Avendano and J. C. Menendez, *J. Org. Chem.* **1995**, *60*, 5678-5682; b) D. H. R. Barton and J. P. Finet, *Pure Appl. Chem.* **1987**, *59*, 937-946.

[18] P. Y. S. Lam, S. Deudon, K. M. Averill, R. Li, M. Y. He, P. DeShong and C. G. Clark, *J. Am. Chem. Soc.* **2000** *122*, 7600 – 7601.

[19] a) P. Y. S. V. Lam, Guillaume; Bonne, Damien; Clark, Charles G. , *Tetrahedron Lett.* **2002**, *43*, 3091-3094; b) P. Y. S. Lam, C. G. Clark, S. Saubern, J. Adams, K. M. Averill, D. M. T. Chan and A. Combs, *Synlett* **2000**, *5*, 674-676.

[20] J. A. Kozlowski in *Organocuprates in the Conjugate Addition Reaction*, *Vol.* Eds.: M. T. Barry and F. Ian), Pergamon, Oxford, **1991**, pp. 169-198.

[21] a) D. M. T. Chan, K. L. Monaco, R.-P. Wang and M. P. Winters, *Tetrahedron Lett.* **1998**, *39*, 2933-2936; b) D. A. Evans, J. L. Katz and T. R. West, *Tetrahedron Lett.* **1998**, *39*, 2937-2940; c) P. Y. S. Lam, C. G. Clark, S. Saubern, J. Adams, M. P. Winters, D. M. T. Chan and A. Combs, *Tetrahedron Lett.* **1998**, *39*, 2941-2944.

[22] M. Kidwai, N. K. Mishra, V. Bansal, A. Kumar and S. Mozumdar, *Tetrahedron Lett.* **2007**, *48*, 8883-8887.

[23] J. Y. Kim, J. C. Park, A. Kim, A. Y. Kim, H. J. Lee, H. Song and K. H. Park, *Eur. J. Inorg. Chem.* **2009**, 4219-4223.

[24] a) A. S. Lipton, R. W. Heck, W. A. de Jong, A. R. Gao, X. Wu, A. Roehrich, G. S. Harbison and P. D. Ellis, *J. Am. Chem. Soc.* **2009**, *131*, 13992-13999; b) D. Rusanova, K. J. Pike, R. Dupree, J. V. Hanna, O. N. Antzutkin, I. Persson and W. Forsling,

Inorg. Chim. Acta **2006**, *359*, 3903-3910; c) J. A. Tang, B. D. Ellis, T. H. Warren, J. V. Hanna, C. L. B. Macdonald and R. W. Schurko, *J. Am. Chem. Soc.* **2007**, *129*, 13049-13065; d) B. Clausen, S., B. Lengeler, B. Rasmussen, S., W. Niemann and H. Topsøe, *J. Phys. Colloques* **1986**, *47*, C8-237-C238-242; e) J. D. Grunwaldt, A. M. Molenbroek, N. Y. Topsøe, H. Topsøe and B. S. Clausen, *J. Catal.* **2000**, *194*, 452-460; f) D. Grandjean, V. Pelipenko, E. D. Batyrev, J. C. van den Heuvel, A. A. Khassin, T. M. Yurieva and B. M. Weckhuysen, *J. Phys. Chem. C* **2011**, *115*, 20175-20191; g) A. I. Frenkel, Q. Wang, N. Marinkovic, J. G. Chen, L. Barrio, R. Si, A. L. p. Cámara, A. M. Estrella, J. A. Rodriguez and J. C. Hanson, *J. Phys. Chem. C* **2011**, *115*, 17884-17890.

[25] a) M. S. Chen and D. W. Goodman, *Science* **2004**, *306*, 252-255; b) M. Jakob, H. Levanon and P. V. Kamat, *Nano Lett.* **2003**, *3*, 353-358; c) Z. R. Ismagilov, E. V. Matus, A. M. Yakutova, L. N. Protasova, I. Z. Ismagilov, M. A. Kerzhentsev, E. V. Rebrov and J. C. Schouten, *Catal. Today* **2009**, *147*, S81-S86.

[26] a) C. O. Kappe, D. Dallinger and S. S. Murphree, *Practical Microwave Synthesis for Organic Chemists*, **2009** b) C. O. Kappe and A. Stadler in *Chapter 2. Microwave Theory*, Wiley-VCH Verlag GmbH & Co. KGaA, **2006**, pp. 9-28; c) D. Stuerga and M. Delmotte in *Wave–Material Interactions, Microwave Technology and Equipment*, Wiley-VCH Verlag GmbH & Co. KGaA, **2004**, pp. 1-33.

[27] C. O. Kappe, *ChemSusChem* **2010**, *3*, 1085-1085; b) C. O. Kappe and A. Stadler in *Microwave Processing Techniques*, Wiley-VCH Verlag GmbH & Co. KGaA, **2006**, pp. 57-90.

[28] N. G. Patil, A. I. G. Hermans, F. Benaskar, J. Meuldijk, L. A. Hulshof, V. Hessel, J. C. Schouten and E. V. Rebrov, *AIChE Journal* **2011**, online.

[29] J. D. W. Moseley, Emily K. Energy Efficiency of Microwave- and Conventionally Heated Reactors Compared at meso Scale for Organic Reactions. Energy & Fuels (2009), 23(11), 5438-5447, *Energy & Fuels* **2009** *23*, 5438-5447.

[30] a) C. O. Kappe and A. Stadler in *Microwave Processing Techniques*, Wiley-VCH Verlag GmbH & Co. KGaA, **2006**, pp. 57-90; b) N. S. Wilson, C. R. Sarko and G. P. Roth, *Org. Process Res. Dev.* **2004**, *8*, 535-538.

[31] a) R. Hoogenboom, T. F. A. Wilms, T. Erdmenger and U. S. Schubert, *Aust. J. Chem.* **2009**, *62*, 236-243; b) U. Schön, J. Messinger, S. Eichner and A. Kirschning, *Tetrahedron Lett.* **2008**, *49*, 3204-3207.

[32] a) F. Benaskar, A. Ben-Abdelmoumen, N. G. Patil, E. V. Rebrov, J. Meuldijk, L. A. Hulshof, V. Hessel, U. Krtschil and J. C. Schouten, *J. Flow Chem.* **2011**, *1*, 74-89; b) F. Benaskar, V. Engels, N. Patil, E. V. Rebrov, J. Meuldijk, V. Hessel, L. A. Hulshof, D. A. Jefferson, J. C. Schouten and A. E. H. Wheatley, *Tetrahedron Lett.* **2010**, *51*, 248-251; c) N. D. D'Angelo, J. J. Peterson, S. K. Booker, I. Fellows, C. Dominguez, R. Hungate, P. J. Reider and T.-S. Kim, *Tetrahedron Lett.* **2006**, *47*, 5045-5048; d) X.-H. Zhu, G. Chen, Y. Ma, H.-C. Song, Z.-L. Xu and Y.-Q. Wan, *Chin. J. Chem.* **2007**, *25*, 546-552; e) Y. Baqi and C. E. Müller, *Org. Lett.* **2007**, *9*, 1271-1274; f) G. Cravotto, M. Beggiato, A. Penoni, G. Palmisano, S. Tollari, J.-M. Lévêque and W. Bonrath, *Tetrahedron Lett.* **2005**, *46*, 2267-2271; g) T. M. Gädda, Y. Kawanishi and A. Miyazawa, *Synth. Commun.* **2011**, *42*, 1259-1267; h) P. Nilsson, K. Olofsson and M. Larhed in *Microwave-Assisted and Metal-Catalyzed Coupling Reactions Microwave Methods in Organic Synthesis, Vol. 266* Eds.: M. Larhed and K. Olofssonq), Springer Berlin / Heidelberg, **2006**, pp. 103-144.

[33] G. Franc, Q. Cacciuttolo, G. Lefèvre, C. Adamo, I. Ciofini and A. Jutand, *ChemCatChem* **2011**, *3*, 305-309.

[34] a) A. G. Whittaker and D. M. P. Mingos, *Journal of the Chemical Society, Dalton Transactions* **2002**, *21*, 3967-3970; b) A. Mondal, D. Agrawal and A. Upadhyaya, *J. Microwave Power Electromagnetic Energy* **2009**, *43*, 5-10.
[35] G. Bond, R. B. Moyes and D. A. Whan, *Catal. Today* **1993**, *17*, 427-437.
[36] V. D. Buchelnikov, D. V. Louzguine-Luzgin, G. Xie, S. Li, N. Yoshikawa, M. Sato, A. P. Anzulevich, I. V. Bychkov and A. Inoue, *J. Appl. Phys.* **2008**, *104*, 113505.
[37] W. Chen, B. Gutmann and C. O. Kappe, *ChemistryOpen* **2012**, *1*, 39-48.
[38] J. R. Thomas, *Catal. Lett.* **1997**, *49*, 137-141.
[39] A. G. Whittaker and D. M. P. Mingos, *J. Chem. Soc., Dalton Trans.* **1995**, 2073-2079.
[40] W. L. Perry, D. W. Cooke, J. D. Katz and A. K. Datye, *Catal. Lett.* **1997**, *47*, 1-4.
[41] X. Zhang, D. O. Hayward and D. M. P. Mingos, *Catal. Lett.* **2003**, *88*, 33-38.
[42] a) D. Walton, *J. Appl. Phys.* **2004**, *95*, 5247-5248; b) J. S. Garitaonandia, M. Insausti, E. Goikolea, M. Suzuki, J. D. Cashion, N. Kawamura, H. Ohsawa, I. Gil de Muro, K. Suzuki, F. Plazaola and T. Rojo, *Nano Lett.* **2008**, *8*, 661-667; c) D. Walton, H. Boehnel and D. J. Dunlop, *Appl. Phys. Lett.* **2004**, *85*, 5367-5369.
[43] T. Wirth in *Microreactors in Organic Synthesis and Catalysis, Vol.* **2008**.
[44] F. Benaskar, V. Hessel, U. Krtschil, P. Löb and A. Stark, *Org. Process Res. Dev.* **2009**, *13*, 970-982.
[45] V. Engels, F. Benaskar, N. G. Patil, E. V. Rebrov, V. Hessel, L. A. Hulshof, D. A. Jefferson, J. A. J. M. Vekemans, S. Karwal, J. C. Schouten and A. E. H. Wheatley, *Org. Process Res. Dev.* **2010**, *14*, 644-649.
[46] F. Benaskar, V. Engels, E. V. Rebrov, N. G. Patil, J. Meuldijk, P. C. Thüne, P. C. M. M. Magusin, B. Mezari, V. Hessel, L. A. Hulshof, E. J. M. Hensen, A. E. H. Wheatley and J. C. Schouten, *Chem.– Eur. J.* **2012**, *18*, 1800-1810.
[47] a) K. Geyer, J. D. C. Codée and P. H. Seeberger, *Chem. –Eur. J.* **2006**, *12*, 8434-8442; b) K. Jähnisch, V. Hessel, H. Löwe and M. Baerns, *Angew. Chem., Int. Ed.* **2004**, *43*, 406-446; c) V. Hessel, P. Lob and H. Lowe, *Curr. Org. Chem. 9*, 765-787; d) V. Hessel, H. Löwe, A. Müller and G. Kolb in *Micro Structured Reactor Plant Concepts, Vol.* Wiley-VCH Verlag GmbH & Co. KGaA, **2005**, pp. 505-638; e) H. Pennemann, P. Watts, S. J. Haswell, V. Hessel and H. Löwe, *Org. Process Res. Dev.* **2004**, *8*, 422-439.
[48] T. Illg, P. Loeb and V. Hessel, *Bioorg. Med. Chem.* **2010**, *18*, 3707-3719.
[49] V. Hessel, D. Kralisch and U. Krtschil, *Energy Environ. Sci.* **2008**, *1*, 467-478.
[50] a) V. Hessel, C. Hofmann, P. Löb, J. Löhndorf, H. Löwe and A. Ziogas, *Org. Process Res. Dev.* **2005**, *9*, 479-489; b) H. Löwe, V. Hessel, P. Löb and S. Hubbard, *Org. Process Res. Dev.* **2006**, *10*, 1144-1152; c) E. R. Murphy, J. R. Martinelli, N. Zaborenko, S. L. Buchwald and K. F. Jensen, *Angew. Chem., Int. Ed.* **2007**, *119*, 1764-1767.
[51] a) P. Öhrngren, A. Fardost, F. Russo, J.-S. Schanche, M. Fagrell and M. Larhed, *Org. Process Res. Dev.* **2012**, *5*, 1053-1063; b) M. H. C. L. Dressen, B. H. P. van de Kruijs, J. Meuldijk, J. A. J. M. Vekemans and L. A. Hulshof, *Org. Process Res. Dev.* **2010**, *14*, 351-361; c) G. Shore, M. Tsimerman and M. G. Organ, *Beilstein J. Org. Chem.* **2009**, *5*, 35; d) J. D. Moseley, *Chim. Oggi* **2009**, *27*, 6-10; e) T. N. Glasnov and C. O. Kappe, *Macromol. Rapid Commun.* **2007**, *28*, 395-410; f) G. Shore, S. Morin and M. G. Organ, *Angew. Chem., Int. Ed.* **2006**, *45*, 2761-2766.
[52] D. Dallinger, H. r. Lehmann, J. D. Moseley, A. Stadler and C. O. Kappe, *Org. Process Res. Dev.* **2011**, *15*, 841-854.
[53] N. E. Leadbeater, *Chem. Commun.* **2010**, *46*, 6693-6695.
[54] a) G. Shore, W.-J. Yoo, C.-J. Li and M. G. Organ, *Chem.– Eur. J.* **2010**, *16*, 126-133; b) E. Comer and M. G. Organ, *J. Am. Chem. Soc.* **2005**, *127*, 8160-8167; c) E. Comer and M. G. Organ, *Chem. –Eur. J.* **2005**, *11*, 7223-7227.

[55] F. Bergamelli, M. Iannelli, J. A. Marafie and J. D. A. Moseley, *Org. Process Res. Dev.* **2010**, *14*, 926-930.
[56] a) J. D. Moseley and E. K. Woodman, *Org. Process Res. Dev.* **2008**, *12*, 967-981; b) J. D. Moseley, P. Lenden, M. Lockwood, K. Ruda, J.-P. Sherlock, A. D. Thomson and J. P. Gilday, *Org. Process Res. Dev.* **2007**, *12*, 30-40.
[57] L. N. Protasova, E. V. Rebrov, T. S. Glazneva, A. Berenguer-Murcia, Z. R. Ismagilov and J. C. Schouten, *J. Catal.* **2010**, *271*, 161-169.
[58] F. Benaskar, N. G. Patil, V. Engels, E. V. Rebrov, J. Meuldijk, L. A. Hulshof, V. Hessel, A. E. H. Wheatley and J. C. Schouten, *Chem. Eng. J.* **2012**, *In press*, DOI:10.1016/j.cej.2012.1006.1147.
[59] K. T. Zuidhof, M. H. J. M. de Croon and J. C. Schouten, *AIChE Journal* **2010**, *56*, 1297-1304.
[60] K. T. Zuidhof, *Eind. Univ. Tech.* **2010**, *PhD thesis*.
[61] F. Benaskar, V. Degirmenci, E. V. Rebrov, N. G. Patil, P. Abulkin, J. Meuldijk, V. Hessel, L. A. Hulshof, E. J. M. Hensen, A. E. H. Wheatley and J. C. Schouten, *unpublished results* **2012**.

Chapter 7

Techno-economic assessment of an integrated microwave and micro process plant for novel processing

This chapter has been published as:
F. Benaskar, A. Ben-Abdelmoumen, N.G. Patil, E.V. Rebrov, J. Meuldijk, V. Hessel, L.A. Hulshof, U. Krtschil, J.C. Schouten (2012). Cost analysis on a continuously operated fine chemicals production plant at 10 kg/day using a combination of micro processing and microwave heating, *J. Flow Chem.*, *1*(2), 74-89. [1]

Abstract

An extended cost study consisting of 14 process scenarios was carried out to envisage the cost-impact of micro processing and microwaves separately or in combination for two liquid-phase model reactions in fine-chemicals synthesis: (I) the Ullmann C-O cross-coupling reaction and (II) the Aspirin synthesis. The former Cu-catalyzed reaction was based on an experimental investigation, whereas the latter, a non-catalyzed aromatic esterification, was based on literature data. The costs of the production of 4-phenoxypyridine, a pharmaceutical intermediate in the synthesis of Vancomycine or Vancocin, were compared with those of the Aspirin synthesis, a key example of a large-scale fine-chemicals production plant. The operating costs in the Ullmann synthesis were found to be a material-based process (reactant excess, pretreatment and catalyst synthesis), whereas the Aspirin synthesis appeared to be a downstream-based process (work-up, waste-treatment). The impact of an integrated microwave heating and micro processing system on profitability was demonstrated with respect to overall costs and productivity. Different modes of microwave heating and catalyst supply were studied and compared with conventional oil-bath heated systems in batch and continuous processes. The overall costs, including profitability breakthrough for a competitive market price of product, were obtained from various combinations of heating and

processing. In the case of the Ullmann synthesis the CAPEX (capital expenditure) was negligible compared to the OPEX (operational expenditure), whereas in the Aspirin synthesis the CAPEX was found to be around 40%, both at a production scale of 1 kg/day. The source of the catalyst strongly determined the profitability of a continuously operated Ullmann process due to its effect on the chemical performance. Higher energy efficiencies could be attained using single-mode microwave irradiation. However, the energy contribution to the overall costs was found to be negligible. Different scenarios provided a costs-feasible and profitable process. Nevertheless, integrated microwave-heating and micro-flow processing lead to a cost-efficient system using a micro packed-bed reactor in comparison to a wall-coated micro-reactor, showing a profit margin of 20%.

7.1. Introduction

Microwave-assisted flow chemistry. Currently, microwave irradiation is mostly applied to small-scale synthesis of complex molecules for pharmaceutical purposes. Nevertheless, microwave-process applications at larger scales are presently gaining more interest in the synthesis of fine-chemical intermediates [2]. Upscaling microwave technology to higher production scales from multi-gram to kilogram scale has become a major topic for industrial chemists [3]. As one of the few industrial examples, Novartis designed and built a microwave work station that is equipped with four single-mode microwave reactors, capping and decapping stations, robotic arm, transport and rack storage system, pipetting robot and feed stations, and drying and gassing stations. Process control is made via an ethernet connection and the throughput is maximized by parallel multi-tasking [4]. In another study, Novartis reports about their scaling attempts and procedures from a 15-mL scale which end with a microwave-assisted batch reactor in their kilo lab, having a reaction volume of approximately 1.1 L. Several reactions were carried out successfully on a 50-g to 100-g scale [5].

Presently, the challenge in this area is to establish a reliable and safe process design, where typical scale-up issues, such as the limited penetration depth, energy efficiency and temperature control are addressed [3b, 6]. Conventional lab-scale organic syntheses, typically below volumes of 100 mL, are conducted in classical batch processes where commercial microwave cavities are designed for these limited volumes. However, due to the limited penetration depth of the microwave field, uniform heating at larger-scales cannot be achieved without internal mixing. Depending on the dielectric properties of the liquid reaction mixture the penetration depth is in the order of 10^{-2} - 10^{-3} m and, therefore, heating is dominated by convective heat-transfer at larger liquid volumes. The maximum size of a batch reactor that can be heated homogeneously using microwave irradiation in standard ovens, thus, is limited to approximately 1 L [7].

As a result, effective and fast heating can only be achieved in combination with a high power input and vigorous mixing, making the use of microwave heating energy-inefficient. Although the power-to-reactor volume ratio can be scaled linearly for most microwave reactors, fast heating and cooling profiles cannot be achieved as effectively as for small-scale reactors. In order to overcome

these problems, stop-flow and continuous-flow reactors [8] have been developed to maintain the productivity in terms of space-time-yield and retain efficient heating by properly fitting the reactor size to the penetration depth [9].

Continuous processing for fine-chemicals synthesis. Similar to most of the continuous operations at micro- and millimeter channel diameter scales, process incompatibilities, such as solids precipitation and capillary clogging accompanied with heterogeneous mixtures, are a major drawback for these microwave systems, especially when heterogeneous catalysts are required. The use of microwave-transparent thin-film coated reactors or packed-bed reactors provides options to conduct continuous chemical processes for heterogeneous systems as described by Organ *et al.*[10] The change from batch towards continuous processing requires dedicated modifications in the process conditions. These modifications also explain the limited number of publications which describe continuous processing exceeding kg-volumes for fine-chemicals. Benaskar *et al.* used glass and Teflon-coiled flow cells which were placed into a multimode microwave cavity to investigate the Kolbe-Schmidt carboxylation reaction as precursors for the Aspirin synthesis [11]. A Suzuki coupling was investigated by Wilson *et al.* on 10-g scale [9a]. However, product crystallization and formation of solid particles resulted in tube-clogging and limited its usability. Similar obstacles were found when Leadbeater *et al.* aimed to scale a series of organic reactions from gram to multi-gram scale using a commercially available continuous-flow microwave reactor [12]. Further studies using stop-flow microwave reactors also revealed the same limitation of clogging and optimal operations could only be attained when converting homogeneous solutions in a batch-loop system [13].

Therefore, the chemical composition of a flow mixture in continuous processes often requires modifications, such as increasing the reactants solubility and use of supported catalyst. Engels *et al.* published the modified Ullmann C-O coupling reaction, substituting a solid base containing reaction mixture by a homogeneous reaction mixture for continuous processing in homo- and cross-coupling reactions [14]. This development, however, has shown that the first step towards continuous processing in slurry systems requires several modifications to the chemistry. Illg *et al.* provided additional examples in organic reactions, showing the benefits of micro processing where guidelines with requirements and restrictions of milli- and micro-structured reactors are proposed regarding safety and energy consumption in process intensification [15]. Similarly, studies on scale-up and multifunctional micro-reactors in real-case applications have been reported, underlining the scale-up strategy for industrial implementation [16]. An increasing number of reviews and reports on the chemical and technological feasibility of micro processing and microwave heating have been published, also by companies such as Merck [17] and Lonza, highlighting the scope and limitations of both novel technologies at small scales [18]. Krtschil *et al.* demonstrated that generally the cost division of process-intensified production plants at 1 kg-scale using micro processing can be visualized as shown in Figure 1. The proposed scenarios were based on an existing process for the production of 4-cyanophenylboronic acid at

AzurChem GmbH, providing general applicability of the best scenario for non-catalyzed single-phase liquid systems [18b].

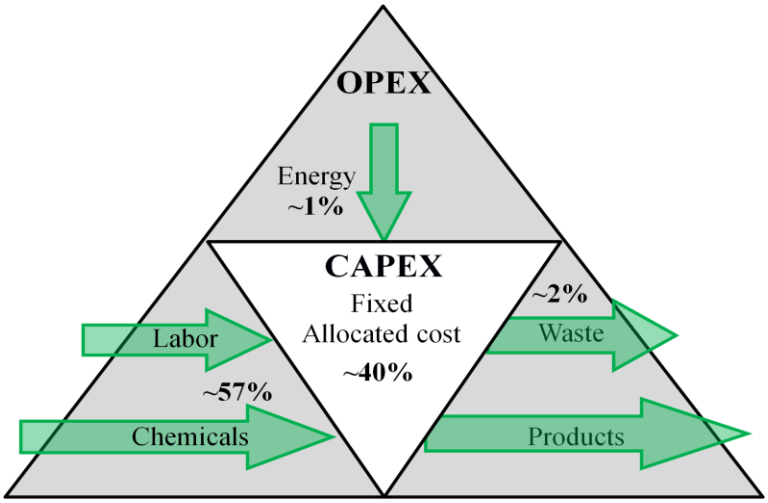

Figure 7.1. Overall cost division in a micro process plant in a non-metal catalyzed homogeneous system.

Although first insights in cost-environmental analysis have been reported [18a], a thorough cost-technological evaluation on an integrated concept of micro processing and microwave heating has not yet been reported and will be explored in this study in a so-called "techno-enviro-economic" analysis. The costs and technological feasibility of implementing microwave heating and micro processing in fine-chemicals processing at 1-kg production scale will be demonstrated. The main aspects, highlighted in this study, concern the costs share of capital investment and operational costs. Microwave equipment and conventional heating systems were compared in both batch and continuous processes. Additionally, a sensitivity analysis for larger production scales was carried out.

7.2. Experimental and methodological approach

The presented cost analysis is based on a fine-chemicals plant for different liquid-phase flow syntheses at a production scale varying from 1 to 10 kg/day. In this case, the plant has been designed for two pharmaceutically relevant processes, *i.e.* heterogeneously Cu-catalyzed homo- and cross-coupling reactions and the homogeneously acid-catalyzed Aspirin synthesis. Wall-coated, micro-packed bed and nano-slurry reactors, operated either in a batch or continuous mode, are compared for the Ullmann-type C-O cross-coupling reaction. The reaction rate constants using the Cu catalyst in this coupling reaction of phenol and 4-chloropyridine•HCl and those of the liquid-phase Aspirin synthesis from salicylic acid and acetic anhydride were taken from the literature ([19] and [20], respectively).

7.2.1. Chemistry

In this case study the heterogeneous reaction was based on the liquid-phase Ullmann-type C-O coupling of phenol and 4-chloropyridine•HCl as shown in Scheme 1.

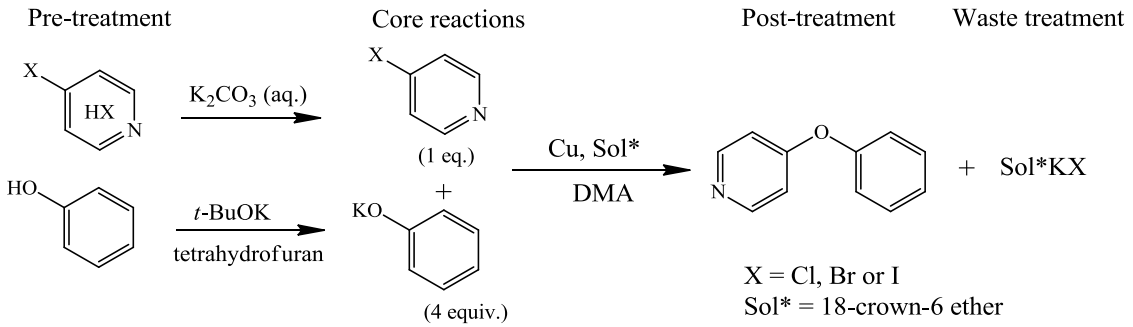

Scheme 7.1. Liquid-phase Cu-catalyzed Ullmann C-O coupling. Starting material was subjected to separate pre-treatment steps to avoid solids in the downstream chemistry. Different Cu-based catalysts were applied in this study.

Since the original Ullmann reaction requires an excess of carbonate to deprotonate phenol and neutralize 4-chloropyridine•HCl, a novel chemical protocol was developed, allowing safe and sustainable continuous processing whilst increasing the productivity [14]. The acid-catalyzed liquid-phase Aspirin synthesis from salicylic acid and acetic anhydride (see Scheme 2) differs from the Ullmann reaction since instead of pre-treatment and catalyst synthesis, a more demanding product workup and waste-treatment are required due to an acidic waste stream. The well-studied chemical protocol has previously been carried out in a microwave-assisted continuous process, allowing reliable use of kinetic data [21].

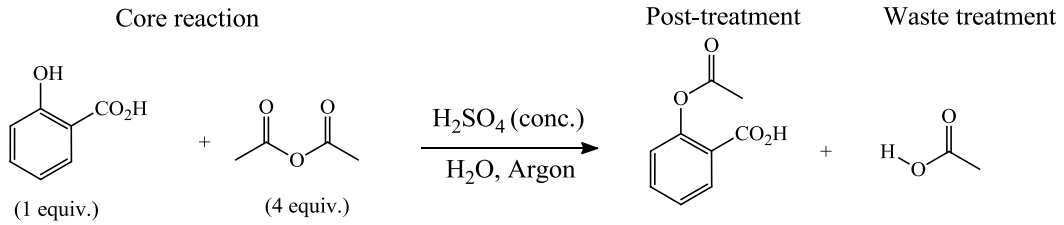

Scheme 7.2. The Aspirin synthesis from salicylic acid and acetic anhydride under highly acidic conditions.

7.2.2. Design criteria and methodology

The studied process scenarios were designed according to process criteria as annotated below:

- A maximum capacity of the production plant of 10 kg/day of isolated Aspirin and 4-phenoxypyridine.
- Production capacity was fixed at 80% of the maximum capacity.
- The microwave-assisted Aspirin synthesis has been proposed for single-mode microwave cavities due to the higher energy efficiency.
- Market prices of products and raw materials were based on existing sources of large-scale suppliers (See Supporting Information of reference [1]).
- The price of raw materials was based on purchases for 50-100 kg product and storage in designated buffer vessels. Purchase at smaller volumes led to unprofitable raw materials prices (Supporting Information of reference [1]).

- Capital investments were based on existing suppliers of equipment or estimated using existing software. Allocated costs related to equipment installations were fixed at 400% (Supporting Information of reference [1]).
- Energy and waste costs were taken from the literature [18b].
- Lifetime, depreciation time and investment rate of return were typically fixed and calculated at 12, 8 and 2 years, respectively [18b].
- Operational load was covered by one man-power at one shift/day, while the production capacity was set at 2000 working hours/year for 8 h/shift.

7.2.3. Process flow diagram

For a consistent approach, a structured design of the overall process has been proposed, comprising of essentially four sections where the equipment was mainly characterized by the size of operations and degree of utilization, being:

1) reactant storage for 100-kg production scale,
2) pre- and post-treatments at 25-kg scale,
3) production site at 10-kg/day scale and
4) catalyst preparation at 1-kg scale.

Sections 1 and 3 are continuously operated at a utilization degree of 100%, whereas sections 2 and 4 are based on a batch-wise production with a utilization degree of 20% (*i.e.* 1 day/week). Therefore, these sections can be utilized by various on-site processes. Scheme 3 provides the areal division of an on-site production plant for fine-chemicals starting from raw material storage to product purification and waste treatment. The Supporting Information of reference [1] provides a more detailed process flow diagram of the site whereupon the various scenarios and the required equipment and utilities are based. It will be clarified throughout this chapter that the capital investment can be minimized by combining several utilities in each section.

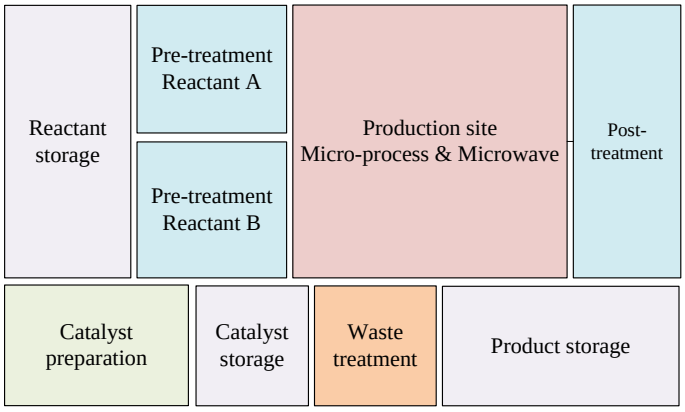

Scheme 7.3. Container-concept of a production plant for the synthesis of fine-chemicals using micro processing and microwave equipment.

The storage (grey), pre-treatment and post-treatment (product work-up and waste treatment) units (blue) are essentially the same for all subsequently presented scenarios and can be utilized in a synchronized manner, whereas the catalyst preparation and the production sites are varied for each scenario. The latter units

also strongly influence the productivity and operational cost and, hence, have the highest impact on cost effectiveness. Therefore, the catalyst and production sections are of major importance and have been explored in much more detail to reveal the most economically feasible scenario for the production of fine-chemicals using either micro processing, microwave heating or a combination thereof.

7.2.4. Scenario studies

In this section, several scenarios are proposed to investigate the economic feasibility of a process-intensified production plant from a combination of various catalysts, heating methods and process operations applied for the Ullmann C-O coupling and the Aspirin synthesis. Figure 2 shows a schematic overview of these combinations resulting in 14 different scenarios, each highlighting a different system for fine-chemicals synthesis. Scenarios 1-12 deal with the Ullmann C-O coupling reaction, whereas the Aspirin synthesis is covered in scenarios 13 and 14. In the Aspirin synthesis, single-mode microwave heating, being highly energy efficient, was compared with oil-bath heating [22]. In this section the separate process units will be explored in more detail.

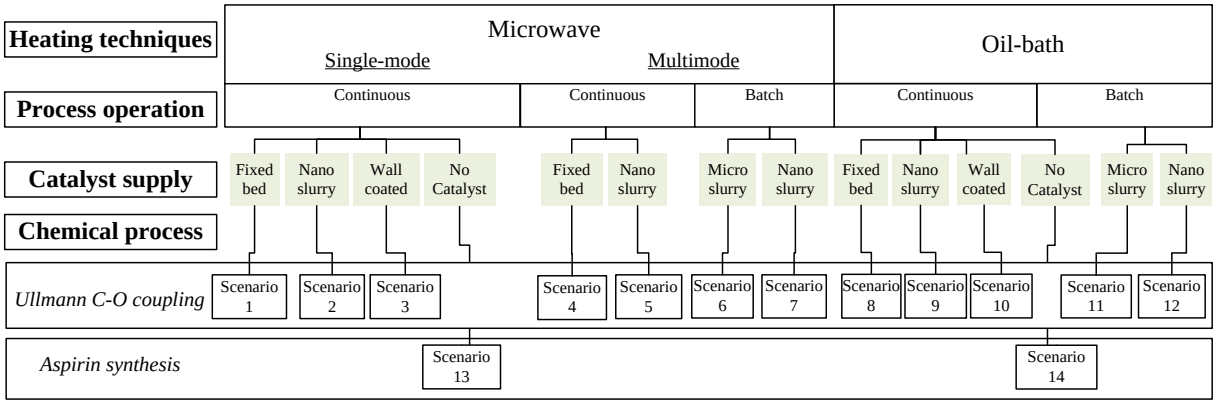

Figure 7.2. Schematic overview of the scenarios divided over various sections applied for the Cu-catalyzed Ullmann C-O coupling and the non-metal catalyzed Aspirin synthesis.

7.2.5. Heating techniques

During this study three types of heating techniques have been applied, *i.e.* oil-bath, multimode microwave and single-mode microwave heating as shown in Figure 3. The oil-bath size was chosen to provide enough capacity for both fine-chemical processes and the related productivity requirements were provided using a LAUDA Proline P 50 C thermostat. For multimode microwave heating two different cavities were considered with a maximum power output of 1 kW, *i.e.* a batch operated Milestones BatchSynth system and a continuously operated Milestones FlowSynth system. These multimode cavities provide enough power capacity for the productivity criteria. The single-mode microwave system consists of four cavities. It was designed and built by Fricke und Mallah GmbH and TU/e. Due to application of single-mode cavities the power output in each cavity was fully utilized without internal losses, thus providing the highest energy efficiency.

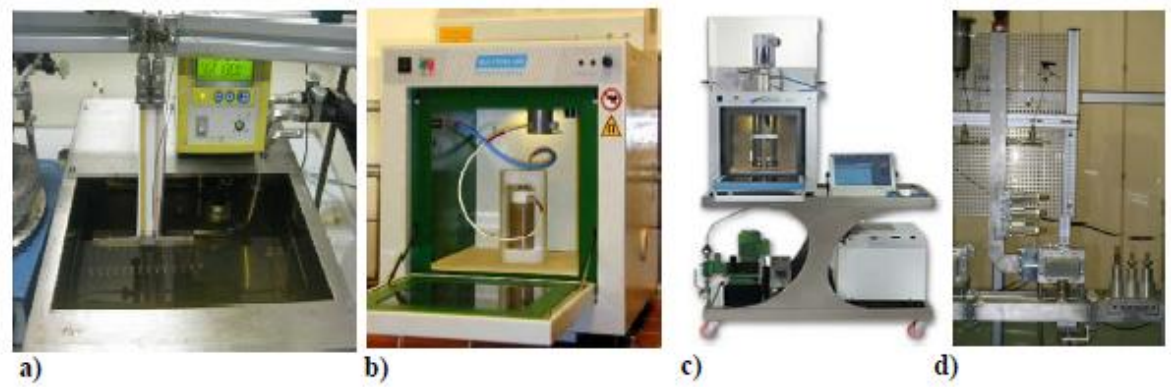

Figure 7.3. Three different heating methods: a) oil-bath setup for batch and continuous processing; b) multimode microwave cavity for batch processes; c) multimode microwave cavity for continuous processes; d) single-mode microwave cavity for continuous processing.

7.2.6. Processes and equipment for chemical syntheses

In view of micro processing and process intensification, all continuously operated systems have been explored in detail after the chemistry was developed in batch systems. The batch reactors were designed and manufactured for 100-mL liquid volumes and could easily be scaled to 1-L processing. The continuously stirred batch reactors were heated using a jacket-heating via either an oil-bath or direct insertion in the microwave cavity. Different tubular reactors (d_i = 1-5 mm) were made to fit the microwave cavity dimensions and the catalyst loading techniques for the continuous processes. For the oil-bath and multimode microwave systems, a tubular glass reactor was coiled to fit the vessel/cavity size, whereas a straight tubular reactor was used in the single-mode microwave cavity (Figure 4).

7.2.7. Cu catalysts used in the Ullmann C-O coupling reaction

Different Cu-based supported and unsupported catalysts were developed for the Ullmann C-O coupling reactions [14].

Micro-slurry catalysts (scenarios 6 and 11). Initially, the Ullmann reaction has been carried out using metallic Cu powder of 30-50 µm and excessive use of solid bases (cesium carbonate) and has, therefore, been referred to the micro-slurry catalyst cases. Obviously, scenarios 6 and 11 could not be carried out in a continuous process due to clogging in the tubular milli-reactors and the pump parts and have, therefore, been considered only in the batch processes.

Nano-slurry catalysts (scenarios 2, 5, 7, and 9). Once the modified Ullmann C-O coupling and the synthesis of copper nano-particles were developed, the difficulties with large solid particles were overcome through the introduction of the nano-slurry catalyst. This catalyst supply method, however, was subjected to highly expensive and inefficient catalyst separation and recovery and was, therefore, the least suitable for continuous operations.

Structured catalytic films (scenarios 1, 3, 4, 8 and 10). The fixed-bed system was further developed to provide titania or zinc-oxide thin film supported Cu catalysts. The films were dip-coated on 200 µm glass beads as shown in Figure 4a and 4b. The wall-coated catalytic films were synthesized using the same protocol as that for the glass beads or via direct impregnation of the wall by a copper precursor [23].

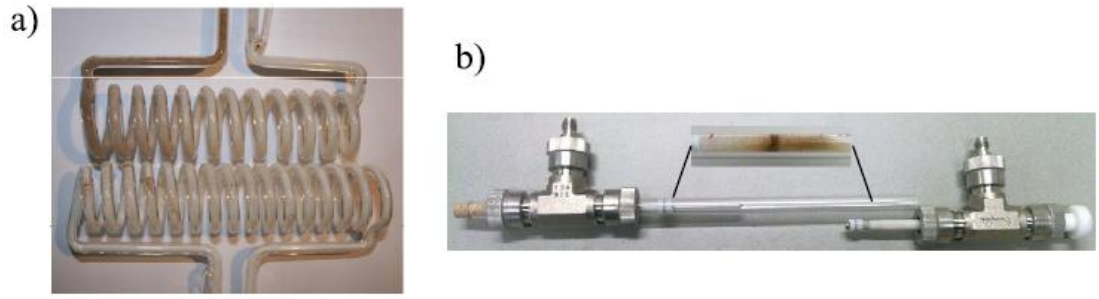

Figure 7.4. Two types of continuously operated tubular reactors were used; a) a coiled tubular reactor for the multimode microwave cavity and b) a straight tubular reactor for the single-mode microwave cavity.

7.2.8. Reaction processing

Since both the unsupported and supported catalysts were studied, a different approach in reaction processing was required for the unsupported catalysts resulting in two additional case studies. In the cases of the micro-slurry Ullmann C-O coupling a one-pot synthesis was performed without separate pre-treatment requirement, but needed an excessive use of 3 molar equivalents of a highly expensive base. Alternatively, separate pre-treatment steps were performed where both reactants were individually treated using less expensive materials, prior to reaction over supported catalysts in a continuous synthesis.

7.2.9. Aspirin synthesis (scenarios 13 and 14)

The Aspirin synthesis did not require a metal catalyst. The pre-mixed reactant mixture was heated using either oil-bath or single-mode microwave heating, representing two alternative scenarios.

7.3. Results and discussion

This cost study has been divided in four major process units which will be presented in this section as a reagents treatment unit, a catalyst preparation unit, a chemical reaction unit and a product work-up unit. Firstly, the capital and operating cost of each unit will be determined reflecting the overall production costs and, secondly, the profitability will be calculated based on the current market price of the target products.

7.3.1. Capital expenditure (CAPEX)

Based on the process flow diagram (see Supporting Information of reference [1]), the required equipment units in each system have been used to determine the CAPEX figures for each scenario as given in Figure 2. Table 1 summarizes the facility- and equipment-related expenses in the CAPEX calculations.

Table 7.1. Fixed-cost assumptions and characteristics related to process equipment and facility.

Capital costs		
Lifetime core process	10	a
Annual output of the product	250	kg/a
Depreciation period core process	8	a
Depreciation period catalyst process	8	a
Annual depreciation	linear	equipment costs/depreciation period
Equipment related fixed-cost	3.8	factor of equipment cost
Facility costs		annual total costs building, including heating, lighting, etc.
Specific facility costs	300	EUR/(m² a)
Storage	300	EUR/(m² a)
Floor space required	10	m²
Storage	15	m²
Maintenance costs	1,000	EUR/ a
Annual facility costs	3,000	EUR/ a
Storage	4,500	EUR/ a
Total	***8,500***	***EUR/ a***

The above given facility- and equipment-related fixed costs are equal for each scenario study and are based on realistic values for container-concept production plants [18b]. The equipment costs related to the production site is given in Figure 5. Cost contributions from chemical processing, catalyst synthesis, heating technique and processing technique are shown separately as proposed for the different scenarios. The process-related units are referred to setup housing, safety sensors, software-related equipment and additional analysis-related equipment (See Supporting Information of reference [1]).

In the chemicals processing part, the catalyst preparation was divided in different catalyst preparation techniques according to the previously presented scenario proposals while the remaining part of the process was left unchanged in each scenario. Figure 5 shows a clear influence of the choice of catalyst and heating technique where especially the production costs of the supported catalyst and the use of multimode microwave heating appeared to be dominant (see Supporting Information of reference [1]). In this section the equipment costs of different heating techniques and catalyst systems are combined with either continuous micro processing or batch processing to obtain the overall equipment costs for a fine-chemicals production site.

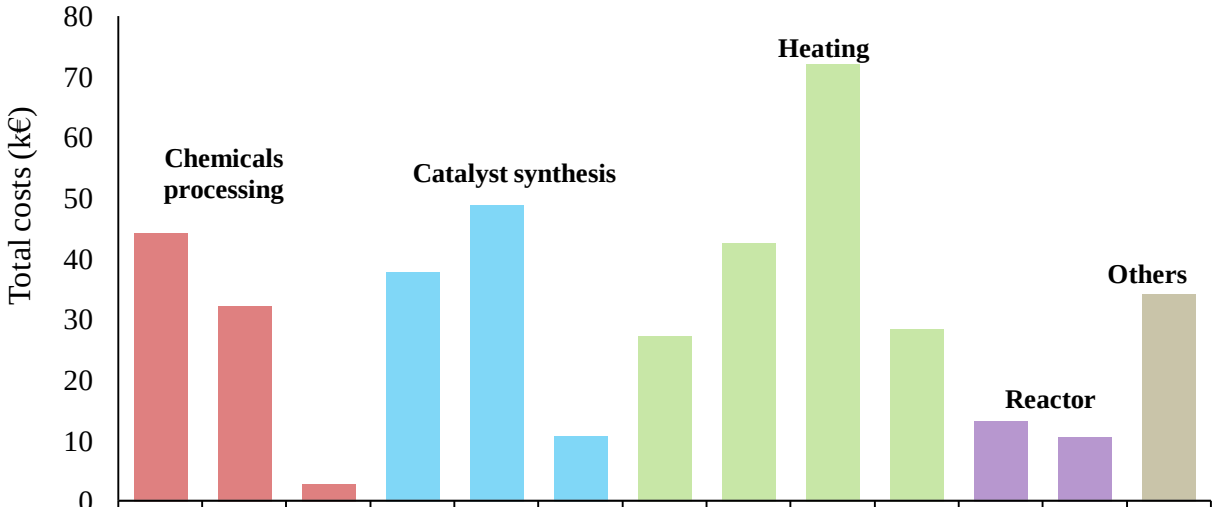

	Pre/post-treatment	Reactant upgrading	Storage	Catalyst synthesis	Support synthesis	Wall-coated catalyst	Single mode MW (flow)	Multi mode MW (batch)	Multi mode MW (flow)	Oil-bath	Micro-reactor	Batch-reactor	Process related
Cost (€)	44155	32150	2850	37750	48750	10700	27160	42506	72108	28370	13150	10420	34100

Figure 7.5. Total costs based on the major process units for chemicals processing, catalyst synthesis, heating and reactor design.

It was concluded that when microwaves were applied a realistic cost-competitive process could be attained using single-mode microwave heating in combination with a fixed-bed catalyst. The costs related to micro processing were found to be slightly higher than those of the conventional batch systems where a profitable micro process plant scenario could, however, only be reached at moderate benefits in the operational costs. Figure 6 shows the equipment-related CAPEX for each operation unit using different catalyst supply methods and heating techniques. The dominating costs using a fixed-bed catalyst are shown once more for all heating methods (orange) with respect to the wall-coated and slurry catalysts scenarios. However, comparison of the CAPEX contributions from the different heating techniques reveals that the multimode microwave cavity for flow systems is more expensive than all other heating techniques. Both the wall-coated continuous and the micro-slurry batch systems appear to be very attractive regarding the equipment-related CAPEX costs. However as will be concluded later, this catalyst does not provide satisfying chemical conversions and results in a non-profitable scenario.

Obviously, for the non-metal catalyzed Aspirin process the catalyst-related costs vanish completely and are, therefore, 33% lower than those of the fixed-bed scenario. In the following sections, case studies of the different scenarios will be discussed, where both the CAPEX and OPEX costs are screened on profitability and cost-feasibility for implementation in a real process. A cost-feasible scenario is defined as a scenario where the profitability (*i.e.* sales price minus production costs) exceeds 5% of the production costs and retains 5% margin with respect to the competitor's sales price. Simultaneously, this criterion must also hold for a CAPEX-ROR (rate of return) of less than two years.

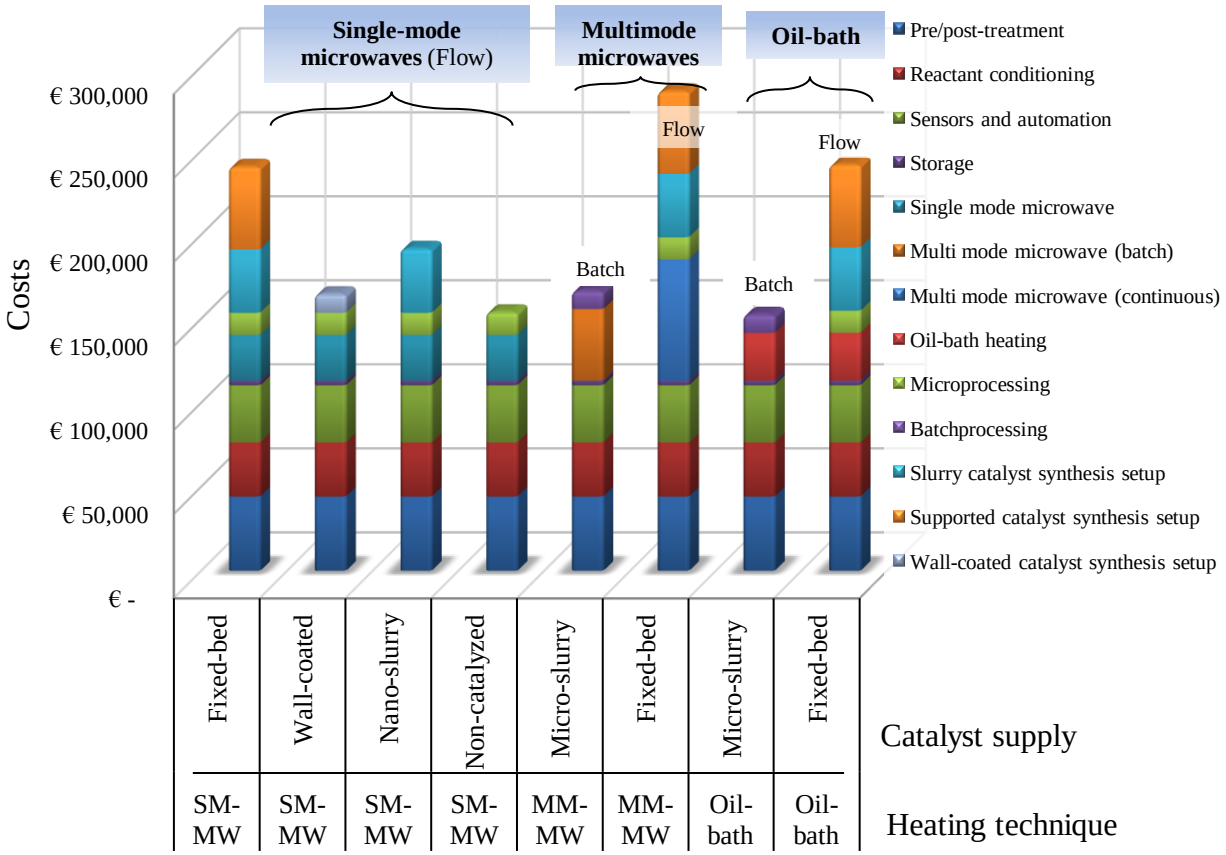

Figure 7.6. Overall cost and the contributions for all different heating systems, reactors and catalyst options. SM-MW and MM-MW correspond to single-mode and multimode microwaves, respectively.

7.3.2. Operating expenditure (OPEX)

In this study the operating costs have been mainly divided in raw and waste materials, energy and personnel (operator) which will be discussed separately in the subsequent section.

Raw materials costs. The raw materials costs are calculated for three different chemical systems, *i.e.* the slurry-type Ullmann C-O coupling reaction (scenarios 6 and 11), the liquid-type Ullmann C-O coupling reaction (scenarios 1-5, 7-10 and 12) and the Aspirin synthesis (scenarios 13 and 14). The raw materials costs can be divided in reagents, solvents and catalysts costs and have been explored as such. As shown in Scheme 1, in the Ullmann reaction halopyridines and phenol were applied as so-called electrophiles and nucleophile, respectively. The reactivity of the halopyridines strongly depends on the halogen used, *i.e.* 4-bromopyridine or 4-iodopyridine show approximately 1.3 and 1.6 times faster reaction kinetics than 4-chloropyridine [24]. However, regarding the atom efficiency, iodo- and bromopyridine are much heavier than chloropyridine (and end up as waste) and regarding storage, iodo- and bromopyridine are relatively unstable. Figure 7

demonstrates the overall reagents costs for both liquid-type (blue) and slurry-type (red) Ullmann C-O coupling reactions using different halopyridines.

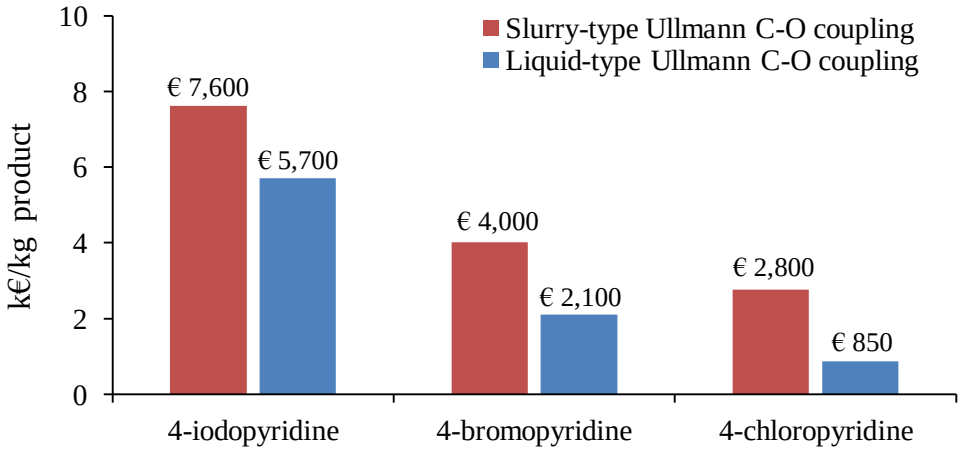

Figure 7.7. Reagents expenses in €/kg product in the traditional slurry-type and the modified liquid-type Ullmann C-O coupling reaction using chloro-, bromo-, or iodopyridine as key reactants.

In general, it can be seen that the reagent expenses for the liquid-type Ullmann C-O coupling are a factor two lower than those of the slurry-type reaction. The two main reasons for this difference can be attributed to the additional costs of raw materials in the one-pot synthesis applied in the slurry-type reaction and, secondly, to the poor chemical performance of this system due to the rate-limiting *in-situ* deprotonation of phenol and neutralization step of the 4-halopyridine salts. Consequently, it was concluded that the use of 4-bromo- or 4-iodopyridine would not lead to profitable production processes and both were, therefore, not considered as potential reactants in this study.

Figure 8 provides an overview and comparison of the chemicals expenses related to the different catalysts used in this study.

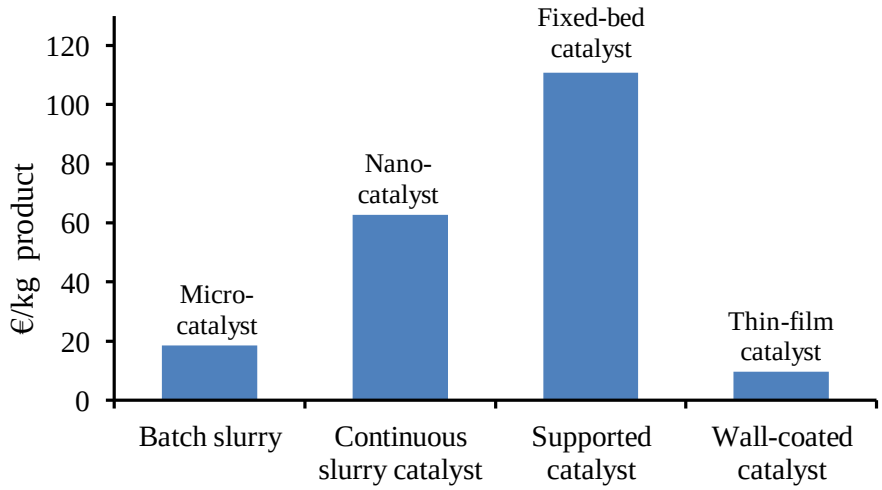

Figure 7.8. Catalyst expenses for the slurry-type Ullmann C-O coupling reaction (micro-slurry catalyst) and three liquid-type Ullmann C-O couplings (wall-coated, nano-slurry and fixed-bed catalyst).

The straightforward way of synthesizing Cu coatings onto the reactor wall results in the lowest manufacture costs related to this catalyst system. Alternatively, the relatively complex fixed-bed system, impregnated with Cu nanoparticles onto a thin-film support [25], led to the highest catalyst expenses and appeared, therefore, economically the least attractive. However, compared to the reagents expenses the catalyst costs are relatively low but still have a strong influence on the effective use of chemicals and on the cost price due to an enhanced conversion. Consequently, the type of applied catalyst is not related to the catalyst expenses, but to the resulting conversion performance.

Figure 9 shows a comparison diagram of chemicals expenses related to the overall raw materials cost of the five different processes.

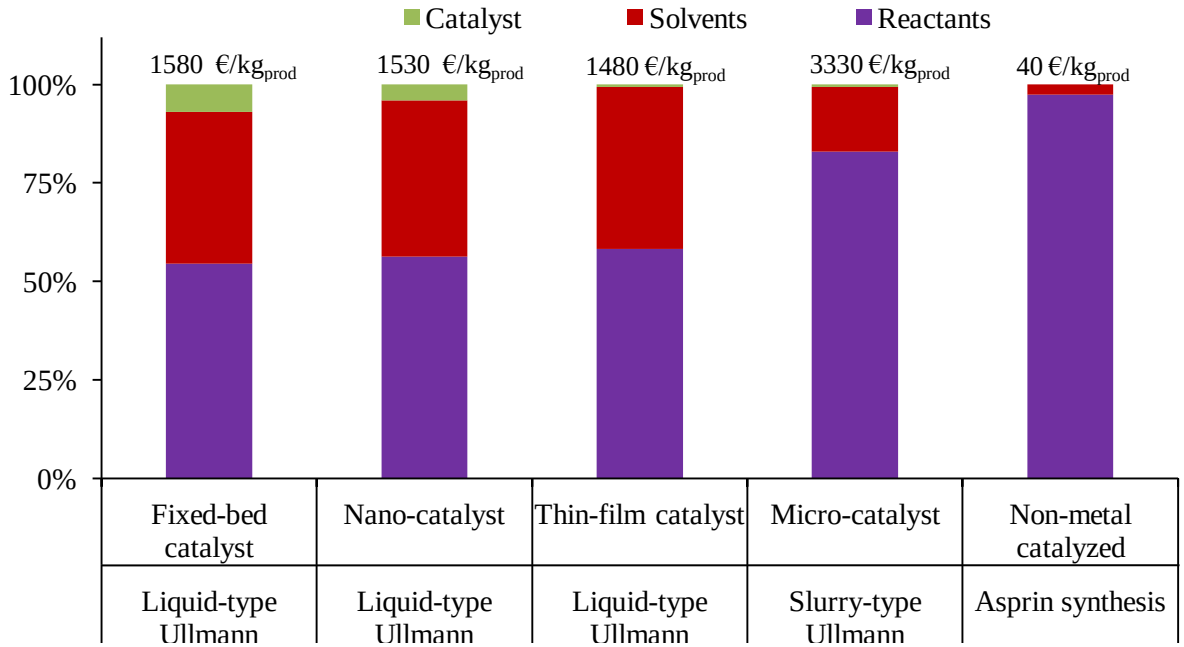

Figure 7.9. Source of the chemicals expenses based on the raw materials cost of the five different chemical systems.

Figure 9 clearly demonstrates a major difference in overall raw materials costd for the non-metal catalyzed Aspirin synthesis and the Cu-catalyzed Ullmann C-O coupling reactions due to the price of raw materials and the origin of solvents, *i.e.* organic versus aqueous conditions. It will be clarified that this difference causes a process to be either OPEX- or CAPEX-dominated and, consequently, determines the sales price and profitability of the target fine-chemical product.

Personnel and disposal costs. As explained in the introductory part, the proposed production plant is operated at a one-shift/day and, therefore, requires a single operator cost-load. It has been assumed that the pre- and post-treatments, stock loading and catalyst preparation can be done simultaneously in a fully automated production plant. However, the time spend based on five shifts/week, at which all different processes are spread, differs for each process unit.

- Pre-/post-treatment 2 times ½ shifts/week, *i.e.* 1 shift/week
- Catalyst synthesis 1 times 1 shift/week, *i.e.* 1 shift/week
- Production plant 5 times ⅓ shift/week, *i.e.* 1⅔ shift/week
- Monthly storage 1 times ⅓ shift/week, *i.e.* ⅓ shift/week
- Reporting and office work 5 times $^1/_5$ shift/week, *i.e.* 1 shift/week

The disposal costs depend on the waste source and have been divided in 2 categories for this study, *e.g.* organic (halogen-rich) for the Ullmann reaction and aqueous (acidic) for the Aspirin synthesis. Figure 10 shows the general costs division for both chemical systems where microwave heating has been applied as heating technique. It is shown that for the catalyzed systems the operational costs are clearly dominated by the raw materials share, whereas in the case of the non-metal catalyzed Aspirin synthesis the personnel costs determine the profitability in operational costs. More interestingly is the fact that energy hardly affects the costs in both cases and, therefore, the heating technique does not influence the operational costs.

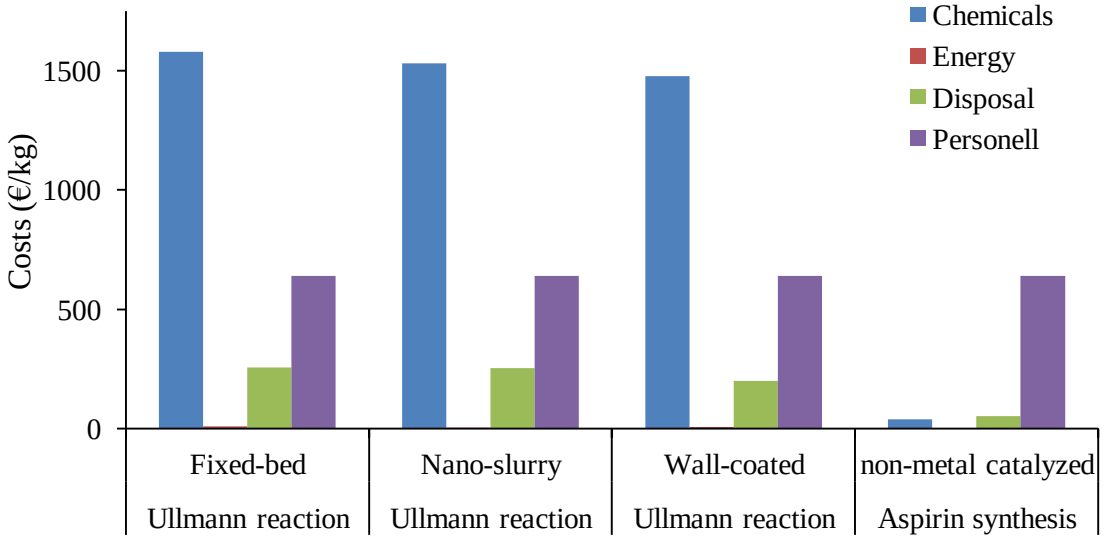

Figure 7.10. Source of the chemicals expenses based on the raw materials cost of the five different chemical systems.

Energy costs. Generally, energy consumption is considered to be of less importance in the synthesis of fine chemicals at the kg-scale production [26]. However, comparing conventional with microwave heating techniques the most important operational costs parameter is energy. The energy efficiency of both technologies will be elucidated in this section, although at the chosen scale its contribution is only 6%. The energy conversion efficiencies in microwave systems are mainly dependent on the internal microwave generator and cavity losses, whereas for electric heating the losses are dominated by losses of the medium to the environment as found in earlier studies [27]. In this section, the energy required to heat the reaction medium was based on the Ullmann reaction conditions and are described in Table 2.

Table 7.2. Energy balance based on the process conditions

Process requirements			
$m_{solvent} = \frac{m_{product}}{C_{product} \cdot Mw_{product}}$ Eq. 1	$m_{product}$ = 1 kg/day $C_{product}$ = 0.75 mol_p/L_{sol} $Mw_{product}$ = 0.172 kg/mol		$m_{RM} \approx m_{solvent}$ = energy absorbing fluid $Cp_{,RM} \approx Cp_{,solvent}$ Solvent: dimethylacetamide
Microwave energy balance			
$Q_{req} = m_{RM} C_{P,RM} * (T_R - T_{Env})$ Eq. 2	$\rho_{solvent}$ = 0.93 kg/L $m_{solvent}$ = 0.25 g/s		T_R= reaction temperature T_{env} = environment temperature
$Q_{MW} = Q_{loss} + Q_{abs}$ Eq. 3	$C_{p,solvent}$ = 2[a] kJ/kg/°C		Q_{MW} = microwave energy
$Q_{loss} = \frac{Q_{abs}}{\eta_{gen}}$ Eq. 4	T_R = 140 °C T_{env} = 25 °C		Q_{req} = energy for fluid heating Q_{loss} = reflected microwaves
$Q_{abs} = \frac{Q_{req}}{\eta_{app}}$ Eq. 5	Q_{req} = 58 W η_{gen} = 55-60 % η_{app} = 35-90 %		Q_{abs} = absorbed microwaves η_{gen}= efficiency MW generator η_{app}= efficiency MW heating
Oil-bath energy balance			
$Q_{RM} = Q_{req} = V_{RM} C_{P,RM} (T_R - T_{Env})$ Eq. 6	V_{RM} = 1-10 L		Q_{HM} = energy for heating medium
$Q_{HM} = V_{HM} C_{P,HM} (T_R - T_{Env})$ Eq. 7	V_{HM} = 4 V_{RM} L		V_{HM} = volume heating medium
$\eta_{app} = \frac{Q_{RM}}{Q_{HM}} = \frac{V_{RM} C_{P,RM}}{V_{HM} C_{P,HM}}$ Eq. 8	$Cp_{,HM}$ = 1.48[a] kJ/kg/°C η_{app} = 30 %		V_{HM} = volume reaction mixture η_{app} = efficiency oil-bath heating

Figure 11 shows the energy flow diagrams of a single-mode microwave system with four cavities, a multimode microwave system and an oil-bath system with the given energy conversion efficiencies for each [18e, 20a]. The thermal efficiency using electrical heating depending on the energy boundaries can be assumed to be 100%.

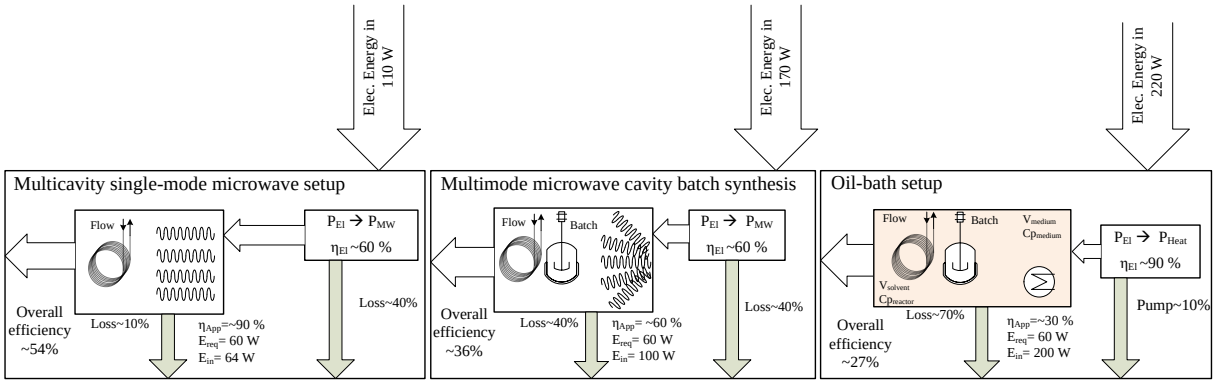

Figure 7.11. Energy flow-diagrams for three heating systems studied, *i.e.* single-mode (left), multimode (middle) microwaves and oil-bath (right) heating.

However, commercially available electric heaters using a liquid medium for this production scale are equipped with internal pumping devices which require roughly 10% of the electric energy [28] . Electric heating requires a higher heating medium volume than the reaction mixture which leads to an additional loss in the overall energy efficiency in addition to heat losses to the environment [29] . Although a fair

comparison of microwave heating with oil-bath heating is not straightforward and can even lead to contradicting results [30], it is mandatory to assign the energy boundaries for deducing the overall energy efficiency and consumption [31]. Similar to comparing the oil-bath and microwave heating efficiencies, the microwaves modes, single-mode or multimode, require a thorough energy comparison study as given by Nüchter *et al.* and for upscaled microwave-heated processes by Strauss *et al.*[18e, 32] However, the given efficiencies clearly show 50% reduction in energy consumption for single-mode microwave systems [33]. Only a fraction of the overall process energy originates from reactor heating in fine-chemical synthesis as shown in Figure 12.

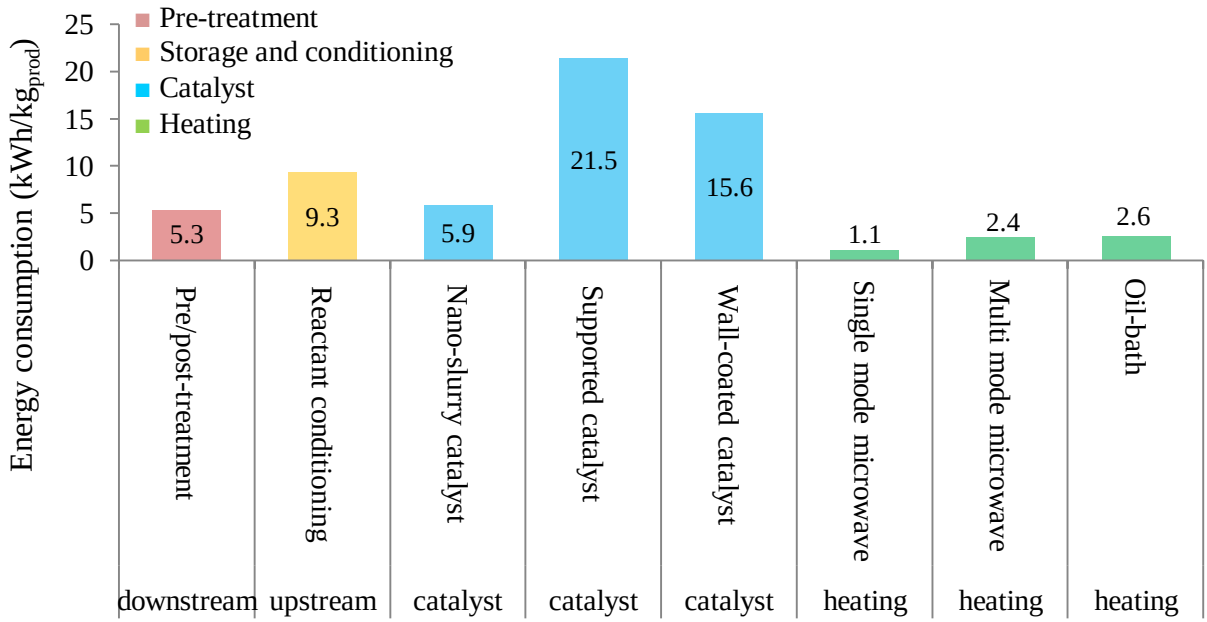

Figure 7.12. Energy consumption in the overall process, showing a major consumption in the catalyst synthesis part with heating as a minor contributor.

Figure 13 shows the cost share related to the overall process energy for the catalyzed and non-catalyzed systems using all different heating techniques. It is clearly shown that a significant cost contribution originates from the catalyst synthesis section for the metal-catalyzed systems. Most studies that refer to energy efficiency in microwave applications are mainly targeting non-catalyzed or homogeneously catalyzed processes where rapid heating is required [34]. Therefore, beneficially applying microwave heating in large-scale continuous processing could only be achieved at relatively short residence times.

In the case of longer residence times, the benefits of microwave heating could be maintained using a loop-reactor with short microwave irradiation times [35]. For catalyzed systems, the preparation and regeneration of the catalyst require energy-intensive processes (vacuum-processing, calcination, centrifugation, etc.) and for the overall-energy consumption these contributions are most dominating (see Supporting Information of reference [1]).

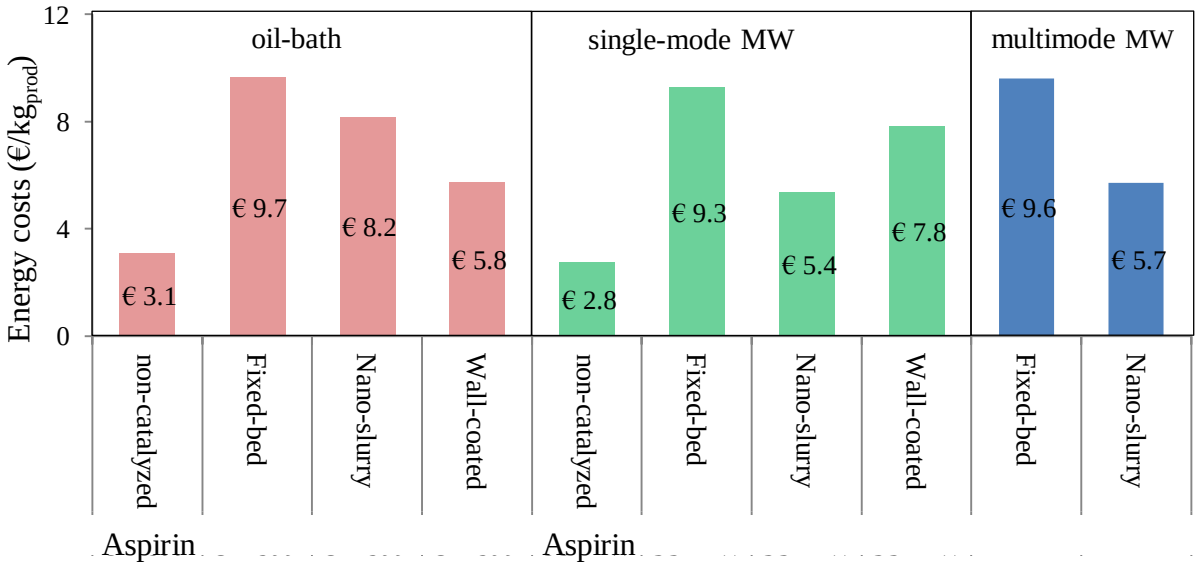

Figure 7.13. Overall energy costs for different scenarios study in the non-catalyzed Aspirin synthesis and the Cu-catalyzed Ullmann C-O coupling using various heating techniques.

7.4. Case studies

In this part the overall costs of the different scenarios as proposed in Figure 2 will be clarified and compared. Finally, an overall evaluation on profitability of each scenario is given providing information on cost-feasible implementation in practice (Supporting Information of reference [1] provides a detailed data-sheet whereupon the scenario studies were based).

Costs effects of the chemical systems. Most interestingly for this study is the type of chemistry performed according to an integrated microwave heating and micro processing concept. Figure 14 shows the overall costs related to the heterogeneously Cu-catalyzed Ullmann C-O coupling and the non-metal catalyzed Aspirin synthesis using the same setup.

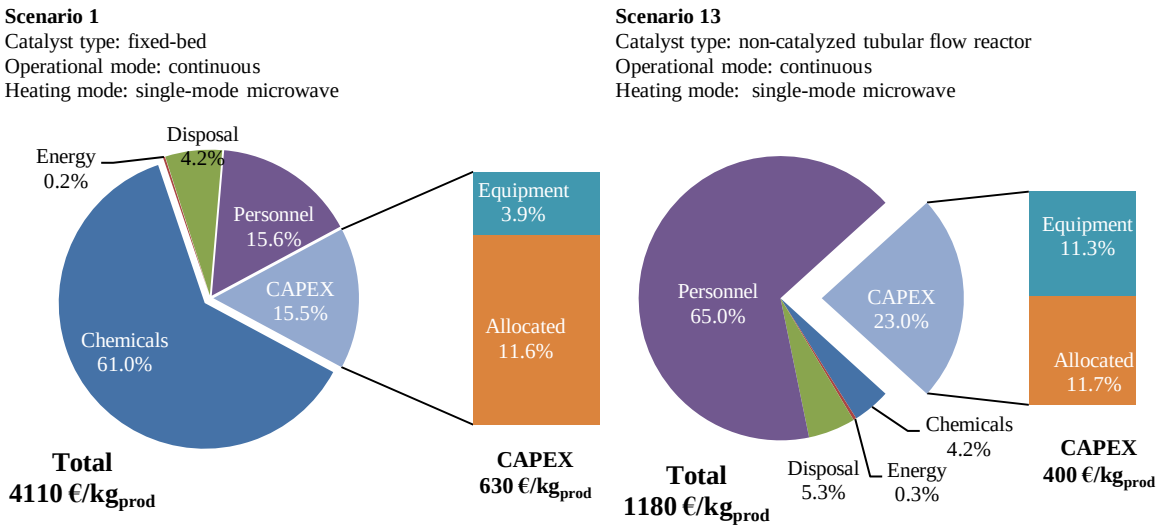

Figure 7.14. Comparison of two chemical systems, *i.e.* the Cu-catalyzed Ullmann C-O coupling (scenario 1) and the non-metal catalyzed Aspirin synthesis (scenario 13).

The main cost-aspects for cost-feasibility in a microwave-assisted catalyzed and non-metal catalyzed system are highlighted from a process and heating point of view. Figure 14 shows that in the case of the Aspirin process the personnel costs become OPEX dominating, whereas the CAPEX/OPEX ratio increases considerably compared to that of the Ullmann process.

However, the comparable cheap synthesis of Aspirin is strongly reflected in the final sales price and, therefore, the profitability (*vide infra)*. For this study it can be concluded that the costs effect between scenarios 1 and 13 are governed to a large extent by the prices of the raw materials. At these scales, the Ullmann process can be defined as a raw materials-priced process, whereas the Aspirin process can be defined as an equipment-priced process. For the former process it should also be noted that, as a result of these much smaller production scales combined with micro process technology, the variable costs, consisting of raw chemicals and energy, are much higher than those in the case of conventional scale fine-chemicals production plants where usually the fixed-to-variable cost ratios is found to be 1.5 (60% CAPEX and 40% OPEX) [36]. Moreover, the sales price of 4-phenoxypyridine was compared with that of Tokyo Chemical Industry (TCI-America), a commercial producer, being 4500 €/kg in 2011 [37].

Costs effects of the catalyst system. As concluded from the earlier CAPEX study in section 7.3.1., a large difference in equipment costs would result when different catalyst synthesis options would be used (see Figure 15). This can be explained by the costs evaluated for the site utilities related to the catalyst preparation, which were found to be much higher than those of any other unit in the production site. The effect on the operational costs due to the catalyst precursors was negligible since the amounts used in the chemical process were at trace level.

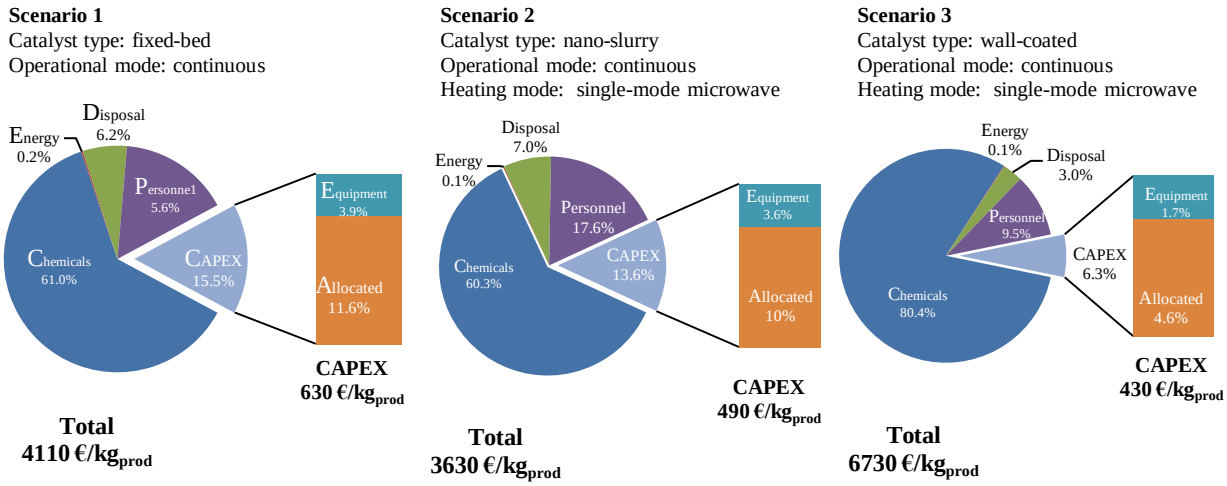

Figure 7.15. Cost comparison of scenarios 1, 2 and 3 of the different supported catalyst systems in the Ullmann C-O coupling, *i.e.* fixed-bed, nano-slurry and wall-coated catalyst.

However, the catalyst preparation section contributed significantly to the overall energy consumption (Figure 12, supported catalyst ca. 60% as 21.5 kWh_{cat} over 36.1 kWh_{tot}), though the overall energy consumption played a minor role in the

operational costs. Figure 15 shows the CAPEX and OPEX contributions to the overall costs related to the different catalyst systems. Major contributions from the CAPEX side are given again for the fixed-bed catalysts system (scenario 1) as compared to the nano-slurry and wall-coated catalysts (scenarios 2 and 3). Regarding the overall costs given per kg product, the wall-coated catalyst appeared to be the least attractive due to a low chemical conversion and, therefore, high operational costs, whereas the fixed-bed and nano-slurry catalysts showed much lower costs. Additionally, it was already shown in Figure 9 that the large difference in chemical costs between nano-catalysts and micro-slurry catalyst resulted from an enhanced chemical performance when using the nano-slurry catalysts.

Costs effects of the operational mode. The costs effects of employing a continuously operated process or a batch operated process are shown in Figure 16, where a micro process plant is compared with a 1-L scale stirred batch reactor in a microwave cavity.

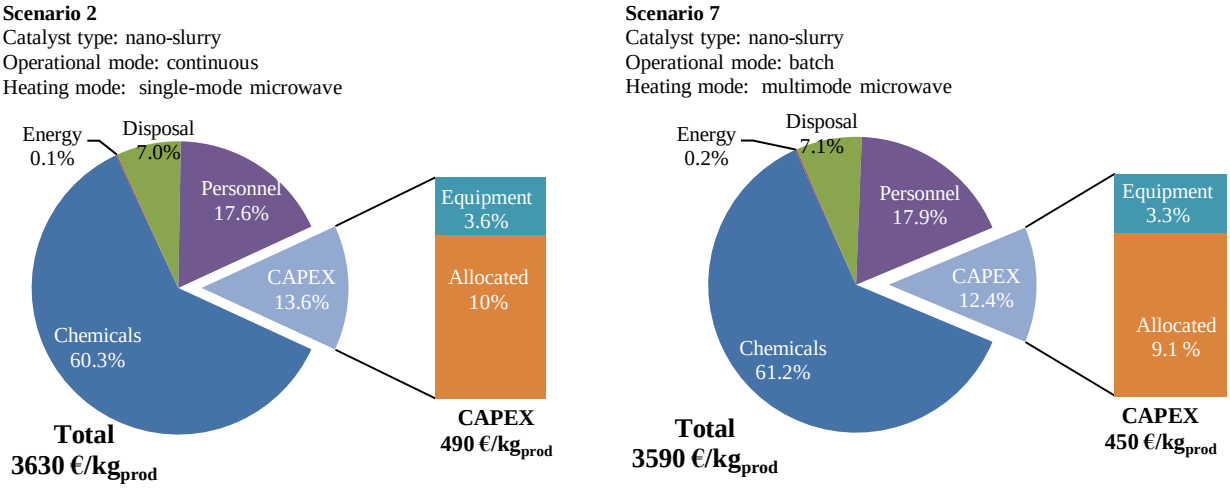

Figure 7.16. Comparison of scenarios 2 and 7, emphasizing the cost-benefits of the continuous processing mode.

To keep reactor dimensions at these space-time-yields within reasonable limits a single-mode cavity was applied in micro processing, while for the batch process a multimode cavity was used. This comparison is justifiable since energy contributes only moderately to the costs and, therefore, the large difference in energy efficiency for the two microwave modes would not be reflected significantly in the overall costs.

Microwave costs effect. Figure 17 shows the overall costs related to the micro-slurry catalyst case using microwave (scenario 6) and oil-bath (scenario 11) heating. It was previously [38] shown that the use of a slurry reaction mixture enhances the heating efficiency and reaction rate due to the presence of salts and their rapid heating effect in combination with microwaves. For this reason, a microwave-assisted process finally turned out to be cheaper and favourable when compared to oil-bath heated systems.

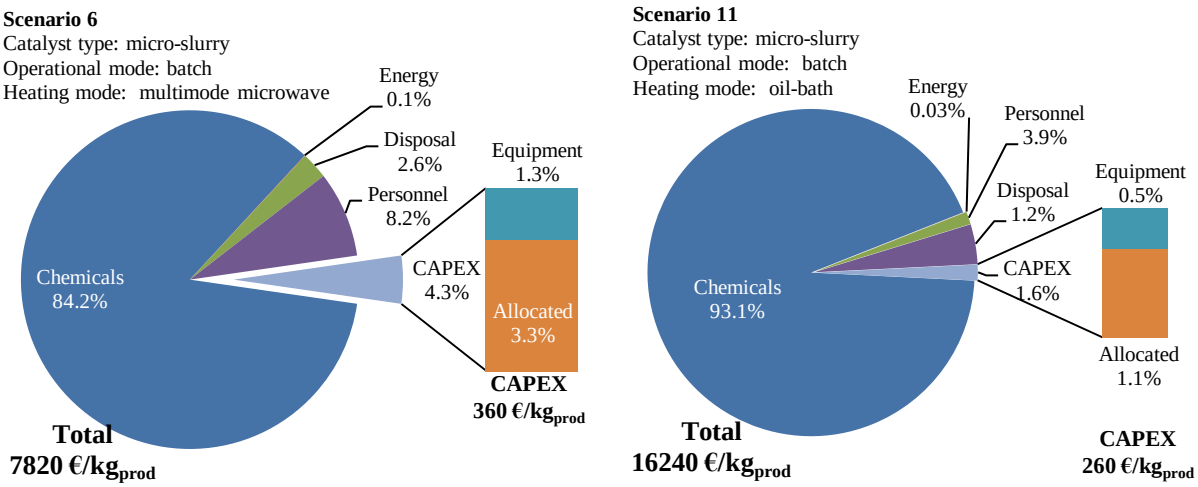

Figure 7.17. Comparison of scenarios 6 and 11, demonstrating the cost-benefits of using microwaves.

Costs effect of single- and multimode microwave cavities. In the previous section it was shown that the use of microwaves provided a beneficial cost-effect compared to oil-bath heating. In this section, two different microwave modes are screened and compared; *i.e.* single-mode and multimode microwaves.

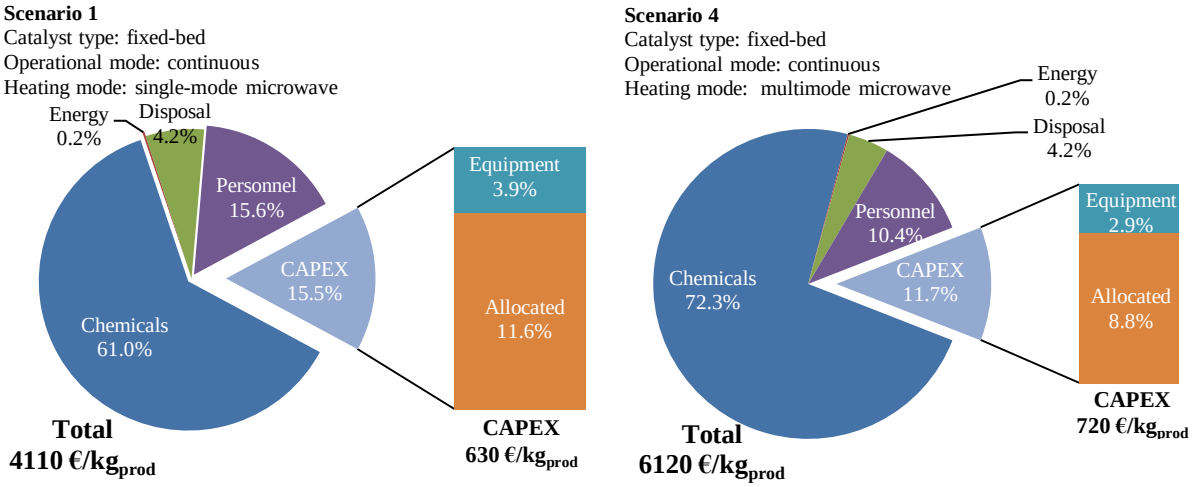

Figure 7.18. Comparison of scenarios 4 and 1, providing the benefits of using single-mode compared to multimode microwave cavities.

Figure 18 shows the costs diagrams related to both multimode (scenario 4) and single-mode microwave cavities (scenario 1) for a fixed-bed micro process system. The total costs of the multimode microwave technique appear to be 30% higher than those in the case of single-mode microwaves applications. However, the costs related to the energy consumption are hardly reflected in the operational costs, even at higher energy efficiencies from the single-mode microwave cavities.

7.5. Sensitivity analysis of scale and catalyst costs contributions

In this section the previously presented case studies will be discussed in more detail using a one-parameter-at-the-time sensitivity analysis. Based on the total permanent investments (C_{TPI}) and the total capital investments (C_{TCI}) of the processes, three parameters on the rate of return (ROR) and the payback period (PBP), both as major indicator of the venture profit (VP), were considered, *i.e.* an increased catalyst activity in terms of turnover frequency and number, an increased chemical process intensification and process scale. Figure 19 shows schematically their influence on techno-economic feasibility, related to the costs and profits of the studied scenarios (see for more details Supporting Information of reference [1]).

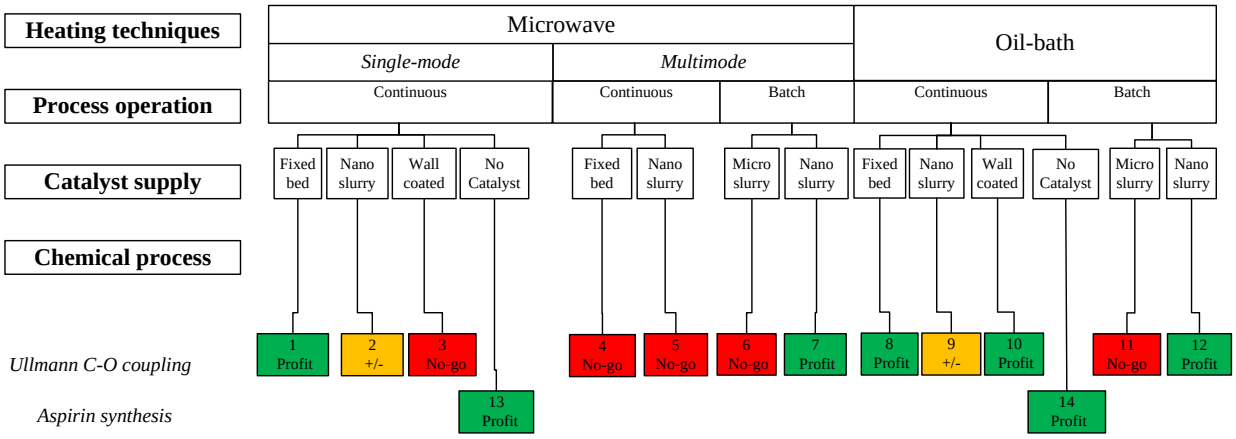

Figure 7.19. Profitability for each scenario proposed in this study. The profitable, potentially profitable and non-profitable scenarios are shown in green, orange and red, respectively.

Based on these results, a sensitivity analysis was carried out to envisage the potential of bringing unprofitable scenarios to profitability by expanding the process window.

Sensitivity of increasing the catalyst activity. The influence and the effects of increased catalysts activity on the overall cost price, the profitability and, eventually, the ROR and PBP have been investigated by comparing increased TOF and TON of the catalysts with the current catalyst activities.

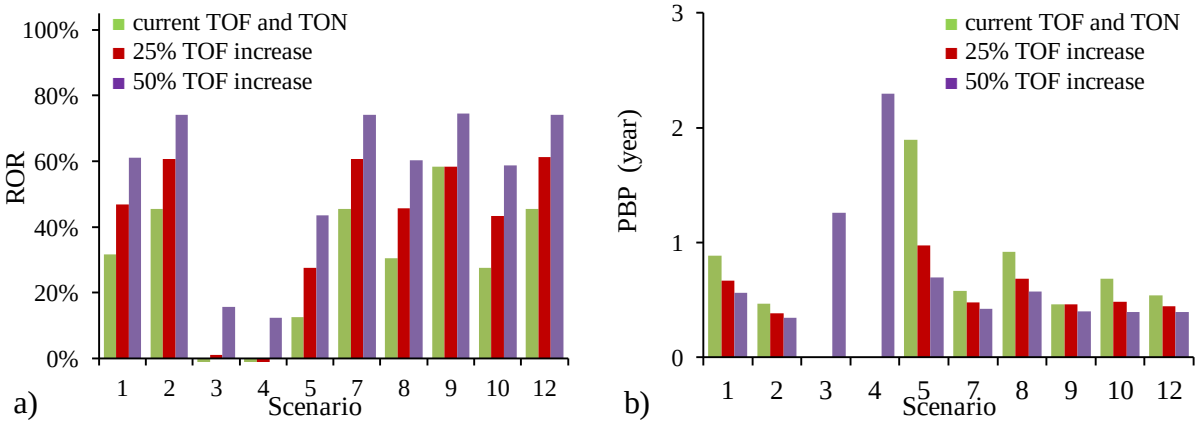

Figure 7.20. Influence of the catalyst activity on the rate on return (a) and payback period (b).

Figure 20 shows the ROR for the different scenarios and the related PBP for different catalyst activities. Most noticeably for the catalyzed systems, the ROR showed the linear dependency on catalyst activity, while a more asymptotic dependence was observed in the case of the PBP (see Figure 20b). The highest impact of an activity increase on the PBP was observed for scenario 5 (nano-slurry catalyzed, multimode microwave setup) due to a relatively low ROR for the current catalyst activities. Moreover, scenarios 3 and 4 (wall-coated, single-mode microwave and fixed-bed, multimode microwave setup) can even reach a positive ROR and feasible PBP by only 50% increase in catalyst activity. Therefore, for these scenarios both microwaves and micro-reactors are clearly not the cost drivers. Scenarios 3 and 4 rather appear to be governed by the catalyst activity.

Sensitivity of chemical process intensification. In addition to an increased catalyst activity, the reactant concentrations in the chemical process could also lead to decreased solvent costs and increased productivity in terms of space-time yield. However, increasing the reactant concentrations might consequently lead to an increased reaction mixture viscosity, risk of crystallization and modified liquid polarity and, accordingly, microwave absorption properties. The pressure drop profiles based on the Ergun equation as a function of increased viscosities are supplied in the Supporting Information of reference [1]. A sensitivity analysis of process intensification by increasing reactant concentrations is required to justifiably assess its effect on both the ROR and PBP. Figure 21a shows the ROR for all the scenarios at doubled and tripled reactant concentrations with respect to the current experimental conditions. In contrast to the linear effect of the catalyst activity on the ROR, the effect of the reactant concentrations appears in most cases to behave logarithmic. This means that an optimum can already be attained by doubled concentrations, whereas a three-fold increase demonstrates less benefit. Besides the benefits of increasing the catalyst activity, the wall-coated micro-reactor in a single-mode microwave system would be economically even more favourable at increased reactant concentrations, resulting in a PBP of even less than two years (see Figure 21b).

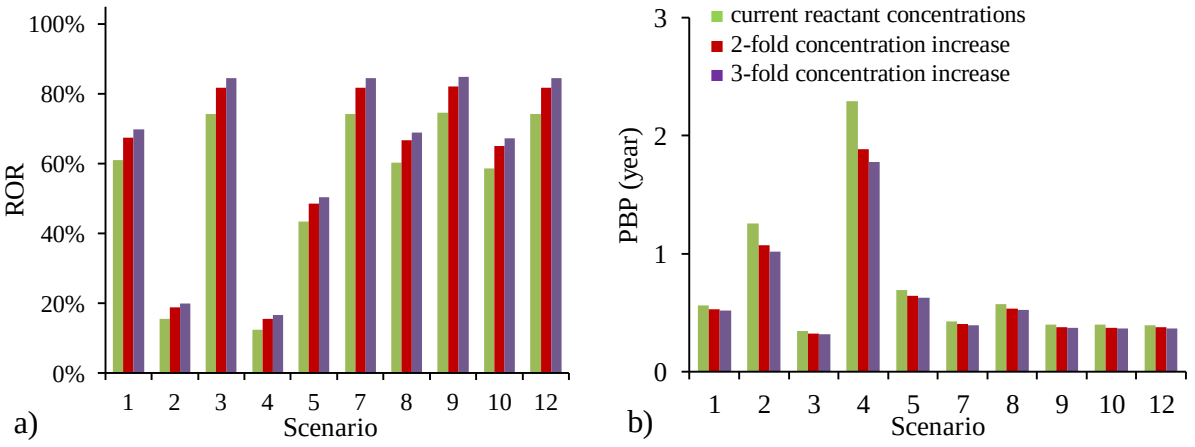

Figure 7.21. Influence of the reactant concentrations on the ROR (a) and PBP (b).

Sensitivity of process-scale: numbering up or numbering out? The scale-up of the given processes has also been surveyed as a method to monitor the profitability window for the different scenarios. The current process was based on 10 kg/day production scale and, as can be expected, expansion of the production capacity will lead to decreased operating costs and, therefore, a decreased PBP for all scenarios. Figure 22a shows the effect of 10, 100 and 500-fold process scale-up on the PBP which demonstrates only a minor decrease in the PBP at 10-fold upscale factor.

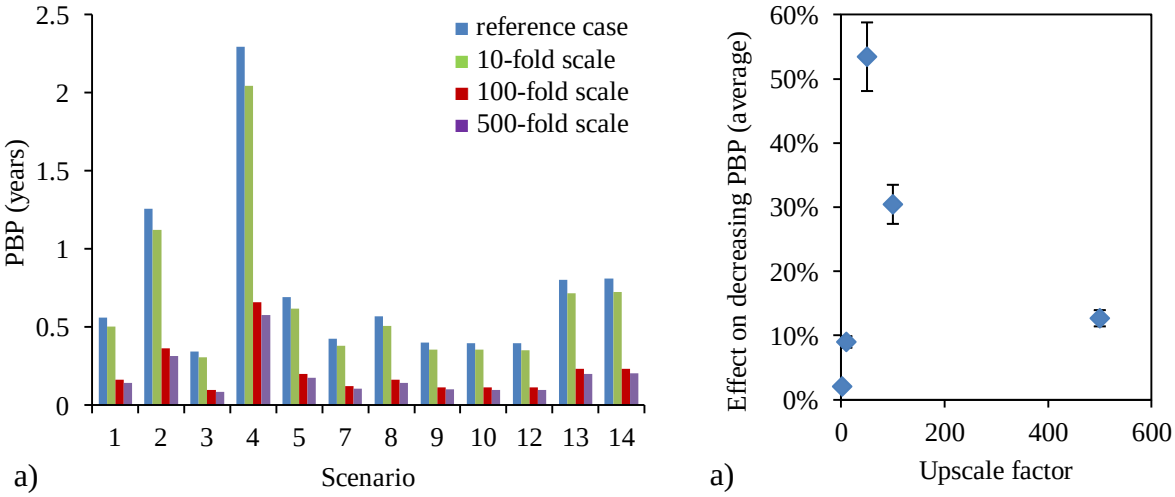

Figure 7.22. Influence of operating scale on PBP (a) and the optimal upscale factor for minimizing the PBP (b).

However, a 100-fold process upscale demonstrated a much larger decrease in the PBP, resulting in a decrease of 58% at best case for the wall-coated micro-reactor in a single-mode microwave cavity. Figure 22 (right) shows that at much larger upscale factor the cost benefits, with respect to decrease in the PBP, reduce and provide no added value. It also shows that the optimal upscale factor of this process is found to be around 50-fold upscale in capacity. However, for higher production capacities it becomes more beneficial to have a number of delocalized production plants at an optimal capacity of 500 kg/day (*i.e.* 10 times 50 kg/day; equivalent to a 50-fold scaled plant) production plant. In this way of scaling by "numbering out" an optimized production facility provides an efficient way for a capacity to 5 tons/day at ten delocalized sites of 500 kg/day (equivalent to a total of 50-fold with respect to the base case) and would lead to an economically more efficient production plant.

7.6. Conclusions

In this study, the impact of various chemical process parameters (such as type of catalyst, heating mode, processing mode and scale) on the overall production costs has been investigated when implementing each of them in a microwave-assisted micro process plant for the synthesis of fine-chemicals. Two existing production lines were considered, *i.e.* 4-phenoxypyridine, a precursor in the production of the antibiotic Vancocin, and for Aspirin. The sales price of these products has been

derived on a 10 kg/day scale, based on recent market values of 4-phenoxypyridine and Aspirin [39].

Figure 19 showed that the use of single-mode microwave heating combined with micro processing, as a replacement for conventional heating and processing, can be beneficially done in a heterogeneously catalyzed process when using a micro-fixed reactor (scenario 1). This combination resulted in an operating profit of 385 €/kg for 4-phenoxypyridine and exceeded the techno-economic benefits for supported systems among all microwave-related scenarios. An alternative method to carry out catalytic reactions can be achieved profitably using catalyst nano-slurries (scenarios 2 and 9). However, due to the large technical risk and catalyst-recovery costs these profit margins are most probably insufficient, making these processes difficult to commercialize.

For non-metal catalyzed homogeneous liquid systems, the use of microwave heating in a micro process plant (scenario 13) can be carried out feasibly in all cases as compared to conventional heating (scenario 14), resulting in a highly profitable process. The use of wall-coated reactors (scenario 3) can provide a profitable scenario. However, this can only be achieved if the chemical performance could be improved, *e.g.* by increasing the catalyst surface either by using small (reactor) channel diameters (<50 µm) or highly porous wall material. This conclusion was confirmed by the performed sensitivity analysis, where the catalyst activity appeared to be more influential on the rate of return and the payback period than the effect of chemical process intensification on the space-time yield. However, the most influential parameter on the profitability (in terms of ROR and PBP) appeared to be the production scale, at an optimal capacity of 500 kg/day. Larger production scales could generate even more profitability at decentralized production sites by means of "numbering-out", thus providing the added-value of flexible and transportable production of fine-chemicals.

7.7. Remarks

The results obtained for the Ullmann ether synthesis allow to derive some general conclusions regarding the profitability of fine-chemical processes when carried out in flow (as compared to batch technology), and regarding the dominating and decisive role of selecting the right choice of heating and catalyst concept. In general, micro processing and microwave-related equipment costs consist of given cost shares comparable to other fixed costs of the selected scenario and are by no means dominant over the alternative, more classical, processing (*e.g.* stirred batch reactors) and heating (*e.g.* electric heating). An economic benefit from these novel technologies is reflected in the operating costs caused by various factors, such as an increased reaction rate, product selectivity, p-T window and improved residence time control, rather than by costs related to the equipment purchase. Thus, when referring to new, innovative, but yet unfamiliar type of processing, the equipment costs are only apparent cost drivers and this processing type requires justified scaling to generate process technological benefits and overall profitability.

Both micro processing and microwave heating change most importantly the process protocol and thus their secondary effects, as derived from a modified protocol, such as for example changes in catalyst supply (microwave-transparent support, such as titania), in reaction mixture homogeneity (addition of solubilizing agents, such as crown ethers) and in a controlled heat input (presence of a metal catalyst in a microwave field). These modifications are much more relevant and are in fact the actual cost drivers when compared to existing fine-chemical technology based on the traditional reactor and related heat input.

The most relevant message from this chapter is that the process design needs to be taken into account in a holistic manner rather than focusing only on the fine-chemical reaction. In deduction, it can be concluded that micro-reactor technology (*i.e.* channel-coated) typically combines preferably with oil-bath heating (compare scenarios 3 and 10), whereas flow chemistry in fixed-bed milli-reactors can also be combined with microwave technology (compare scenarios 8 and 1). This is simply the result of surface heating versus volumetric heating, respectively. In addition, micro processing was found to be most advantageous for non-catalyzed systems, due to the catalyst preparation costs. Catalyzed operations in micro-systems increase the process complexity as most of the technical investments shift to catalyst design rather than to reactor design. Finally, the type of chemistry might well be of major importance in view of the costs as compared to technological issues.

References

[1] F. Benaskar, A. Ben-Abdelmoumen, N. G. Patil, E. V. Rebrov, J. Meuldijk, L. A. Hulshof, V. Hessel, U. Krtschil and J. C. Schouten, *J. Flow Chem.* **2011**, *1*, 74-89.

[2] D. Bogdal and A. Prociak, *Chimica Oggi (Chemistry Today)* **2007**, *25*, 30-33.

[3] a) J. D. Moseley, P. Lenden, M. Lockwood, K. Ruda, J.-P. Sherlock, A. D. Thomson and J. P. Gilday, *Org. Process Res. Dev.* **2007**, *12*, 30-40; b) S. E. Wolkenberg, W. D. Shipe, C. W. Lindsley, J. P. Guare and J. M. Pawluczyk, *ChemInform* **2006**, *37*.

[4] S. Chamoin, *Adv. Microwave-Assisted Org. Synth.: MAOS Conference and Exhibition* **2006**.

[5] H. Lehmann, *Ernst Schering Foundation Symp. Proc.* **2007**, *3*, 133-149.

[6] J. Kremsner, A. Stadler and C. O. Kappe, *Top. Curr. Chem.* **2006**, *266*, 233-278.

[7] Assuming a cylindrical reactor with a diameter twice the penetration depth in a homogeneously irradiated cavity.

[8] S. Arai, A. Tanaka, M. Hida and T. Yamagishi, *Bull. Chem. Soc. Jpn.* **1979**, *53*, 821-825.

[9] a) N. S. Wilson, C. R. Sarko and G. P. Roth, *Org. Process Res. Dev.* **2004**, *8*, 535-538; b) C. B. Kelly, C. Lee and N. E. Leadbeater, *Tetrahedron Lett.* **2011**, *52*, 263-265; c) G. Pipus, I. Plazl and T. Koloini, *Chem. Eng. J.* **2000**, *76*, 239-245.

[10] G. Shore, S. Morin and M. G. Organ, *Angew. Chem., Int. Ed.* **2006**, *45*, 2761-2766.

[11] F. Benaskar, V. Hessel, U. Krtschil, P. Löb and A. Stark, *Org. Process Res. Dev.* **2009**, *13*, 970-982.

[12] M. D. Bowman, J. L. Holcomb, C. M. Kormos, N. E. Leadbeater and V. A. Williams, *Org. Process Res. Dev.* **2007**, *12*, 41-57.

[13] J. D. Moseley and E. K. Woodman, *Org. Process Res. Dev.* **2008**, *12*, 967-981.

[14] V. Engels, F. Benaskar, N.G. Patil, E. V. Rebrov, V. Hessel, L. A. Hulshof, D. A. Jefferson, J. A. J. M. Vekemans, S. Karwal, J. C. Schouten and A. E. H. Wheatley, *Org. Process Res. Dev.* **2010**, *14*, 644-649.

[15] T. Illg, P. Loeb and V. Hessel, *Bioorg. Med. Chem.* **2010**, *18*, 3707-3719.

[16] a) D. M. Roberge, M. Gottsponer, M. Eyholzer and N. Kockmann, *Chimica Oggi (Chemistry Today)* **2009**, *27*, 4; b) R. L. Hartman, J. R. Naber, S. L. Buchwald and K. F. Jensen, *Angew. Chem., Int. Ed.* **2010**, *49*, 899-903.

[17] M. H. D. Schmalz, N. Oldenburg, M. Grund, H. Muntermann, U. Kunz *Chem. Ing. Tech.* **2005**, *77*, 859-866.

[18] a) V. Hessel, D. Kralisch and U. Krtschil, *Energy Environ. Sci.* **2008**, *1*, 467-478; b) U. Krtschil, V. Hessel, D. Kralisch, G. Kreisel, M. Kuepper and R. Schenk, *Chimia* **2006**, *60*, 6; c) T. Nakamura, R. Nagahata, K. Kunii, H. Soga, S. Sugimoto and K. Takeuchi, *Org. Process Res. Dev.* **2010**, *14*, 781-786; d) H. Lehmann and L. LaVecchia, *Org. Process Res. Dev.* **2010**, *14*, 650-656; e) M. Nuchter, B. Ondruschka, W. Bonrath and A. Gum, *Green Chem.* **2004**, *6*, 128-141; f) J. D. Moseley and E. K. Woodman, *Energy Fuels* **2009**, *23*, 5438-5447; g) T. N. Glasnov and C. O. Kappe, *Macromol. Rapid Commun.* **2007**, *28*, 395-410; h) E. Comer and M. G. Organ, *Chem. –Eur. J.* **2005**, *11*, 7223-7227; i) E. Comer and M. G. Organ, *J. Am. Chem. Soc.* **2005**, *127*, 8160-8167; j) D. M. Roberge, L. Ducry, N. Bieler, P. Cretton and B. Zimmermann, *Chem. Eng. Tech.* **2005**, *28*, 318-323; k) J. R. Schmink, C. M. Kormos, W. G. Devine and N. E. Leadbeater, *Org. Process Res. Dev.* **2010**, *14*, 205-214.

[19] F. Benaskar, N. G. Patil, V. Engels, E. V. Rebrov, J. Meuldijk, V. Hessel, L. A. Hulshof, A. E. H. Wheatley and J. C. Schouten, *Dalton Trans.* **2012**, *Revision/Accepted*.

[20] a) M. H. C. L. Dressen, B. H. P. van de Kruijs, J. Meuldijk, J. A. J. M. Vekemans and L. A. Hulshof, *Org. Process Res. Dev.* **2010**, *14*, 351-361; b) V. M. Drevina, L. I. Markitanova and V. M. Nesterov, *Khimiko-Farmatsevticheskii Zhurnal* **1976**, *10*, 53-55; c) V. M. Drevina, V. M. Nesterov and L. I. Markitanova, *Khimiko-Farmatsevticheskii Zhurnal* **1976**, *10*, 120-122; d) L. I. Markitanova, V. M. Drevina and V. M. Nesterov, *Khimiko-Farmatsevticheskii Zhurnal* **1976**, *10*, 85-88.

[21] a) M. H. C. L. Dressen, *PhD-thesis* **2009**, Eindhoven University of Technology; b) L.-D. Wang and P. Cui, *Liaoning Huagong* **2009**, *38*, 623.

[22] N. G. Patil, E. V. Rebrov, F. Benaskar, E. Esveld, J. Meuldijk, V. Hessel, L. A. Hulshof and J. C. Schouten, *European process intensification conference* **2011**, *Manchester, United Kingdom*.

[23] a) G. Shore, M. Tsimerman and M. G. Organ, *Beilstein J. Org. Chem.* **2009**, *5*, 35; b) L. N. Protasova, E. V. Rebrov, T. S. Glazneva, A. Berenguer-Murcia, Z. R. Ismagilov and J. C. Schouten, *J. Catal.* **2010**, *271*, 161-169; c) T. Glazneva, E. Rebrov, J. Schouten, E. Paukshtis and Z. Ismagilov, *Thin Solid Films* **2007**, *515*, 6391-6394.

[24] N. D. D'Angelo, J. J. Peterson, S. K. Booker, I. Fellows, C. Dominguez, R. Hungate, P. J. Reider and T.-S. Kim, *Tetrahedron Lett.* **2006**, *47*, 5045-5048.

[25] F. Benaskar, V. Engels, E. V. Rebrov, N. G. Patil, J. Meuldijk, P. C. Thüne, P. C. M. M. Magusin, B. Mezari, V. Hessel, L. A. Hulshof, E. J. M. Hensen, A. E. H. Wheatley and J. C. Schouten, *Chem.– Eur. J.* **2012**, *18*, 1800-1810.

[26] A. Stankiewicz, *Chem. Eng. Res. Des.* **2006**, *84*, 511-521.

[27] a) R. Hoogenboom, T. F. A. Wilms and U. S. Schubert, *Polymer Preprints* **2008**, *49*, 930-931; b) W. H. J. Graus, M. Voogt and E. Worrell, *Energy Policy* **2007**, *35*, 3936-3951.

[28] After personal discussion with Lauda Company the pump energy for internal circulation of heating medium was determined.

[29] In this study the minimum heating medium volume required for uniform and stable heating was experimentally found to be around four-fold heating medium volume for the reaction mixture. At lower heating medium volumes temperature fluctuations and high temperature gradients result. In conventional lab-scale systems, a much higher volume ratio of medium and reaction mixture is used.

[30] a) M. J. Gronnow, R. J. White, J. H. Clark and D. J. Macquarrie, *Org. Process Res. Dev.* **2005**, *9*, 516-518; b) H. E. Simmons and R. D. Smith, *J. Am. Chem. Soc.* **1958**, *80*, 5323-5324.

[31] M. Nüchter, U. Müller, B. Ondruschka, A. Tied and W. Lautenschläger, *Chem. Eng. Tech.* **2003**, *26*, 1207-1216.

[32] C. R. Strauss, *Org. Process Res. Dev.* **2009**, *13*, 915-923.

[33] R. Hoogenboom, T. F. A. Wilms, T. Erdmenger and U. S. Schubert, *Aust. J. Chem.* **2009**, *62*, 236-243.

[34] T. Razzaq and C. O. Kappe, *ChemSusChem* **2008**, *1*, 123-132.

[35] D. R. Godwin, S. J. Lawton, J. D. Moseley, M. J. Welham and N. P. Weston, *Energy Fuels* **2010**, *24*, 5446-5453.

[36] a) A. Bruggink, *Chimica Oggi (Chemistry Today)* **1998**, *16*, 44-47; b) A. Bruggink, *CphI Conference Proceedings* **1993**, 38 - 47; c) C. E. Berkoff, K. Kamholz, D. E. Rivard, G. Wellman and H. Winicov, *Chemtech* **1986**, 552-559.

[37] The profitability, as defined in section 7.3.1, and the cost-price were based on the existing sales price.

[38] F. Benaskar, V. Engels, N.G. Patil, E. V. Rebrov, J. Meuldijk, V. Hessel, L. A. Hulshof, D. A. Jefferson, J. C. Schouten and A. E. H. Wheatley, *Tetrahedron Lett.* **2010**, *51*, 248-251.

[39] The market prices have been evaluated based on price information provided on "http://www.pharmacychecker.com" for pharma-grade products. Other chemicals providers have not been evaluated in this study.

Chapter 8

Conclusions and Recommendations

Conclusions

As described in this thesis, novel routes to synergistically combine microwave technology and flow processing have been investigated and proposed. Both technologies exist for many years and have established a mature position in academia and more and more in industry. To achieve a successful combination of microwave heating and flow technology, it appeared to be of paramount importance to firstly investigate the scope and more important also their limitations with respect to chemical applications. To the best of my knowledge and as concluded in this study, this would mean to search for suitable chemistry which can realistically be adapted for these technologies. Therefore, an important message is to start with a thorough development of the chemistry and catalysis, prior to any judgment on the technical feasibility and potential of microwave heating, flow-process technology and a combination thereof.

Inspired by the "Factory of the Future concept" the aim was to start thinking out of scratch and to search for solutions on a higher systemic level, knowing that such development is deeply holistic and needing inventions on all individual levels such as the catalyst, the reactor, the heating, and finally the processing system. It was moreover clear that there is an interplay between these innovations which finally would demand a multi-cascaded and multi-criteria decision platform. Although this level of complexity was not aimed for during the early stages of this topic, interactions between innovations appeared to dominate, *i.e.* between the catalyst formulation and its coating ability in a micro-reactor or on a micro-bead and its heating efficiency when entering a microwave field.

Reaction kinetcis and mechanism. Following the abovementioned strategy, this work was instigated with a parametric study to address all the factors that influence the Ullmann-type C-O bond formation and to elucidate the mechanism by which copper mediates the Ullmann-type S_NAr reaction of 4-chloropyridine with

potassium phenolate. Since the project aim was driven by application in flow processing, the use of the conventionally applied solid base Cs_2CO_3 could successfully be eliminated without depleting process efficiency. Therefore, potassium phenolate and liquid-phase 4-chloropyridine were successfully introduced as reactants, avoiding additional chemicals cost as well as processing difficulties. Furthermore, rate enhancement of the reaction through the application of 18-crown-6 as an alkali metal scavenger was demonstrated. Process parameters and chemical conditions, such as temperature, reactant concentrations, catalyst type, catalyst concentration and amounts of solubilizing additives were varied to obtain key kinetic parameters, fit for use in flow systems. It was found that the nucleophile concentration played a more important role than the electrophile concentration. Consequently, increasing the 18-crown-6 ether cation solubilizer concentration demonstrated to be most important at low potassium phenolate conversions. However, at high conversion the excessive by-product potassium chloride limited its functionality. The obtained kinetic data provided an activation energy of 55.4 kJ/mol over a Cu^0 catalyst and could be best described by a Langmuir-Hinshelwood kinetics model with a strong adsorption of 4-phenoxypyridine on copper.

Nano-based catalyst development. Subsequently, these advances were extended by using a nano-Cu(0) catalyst, which eventually led to more efficient copper-based nanoalloys CuSn and CuZn. These nano-alloys allowed reductions in both reaction time and reaction temperature in the copper-catalyzed Ullmann-type etherification reaction as compared to the performance of either commercial Cu(0) or the monometallic Cu(0) nanoparticles. Only 1.5 mol% of nanostructured CuZn catalyst was needed to obtain yields of up to 90%, whereas previous experiments required the use of as much as 10 mol% of commercial copper or copper-wires. The synthesis of these nanoparticles was based on the improvement of the chemical reduction method of the Cu-precursor by adding $NaH_2PO_2 \cdot H_2O$, which led to improved particle morphologies and mean particle sizes and distributions. This alcohol-based procedure, in the presence of *N*-poly(vinylpyrrolidone) (PVP, Mw_{av} 40,000), showed superior results with respect to the procedure of using the conventional $N_2H_4 \cdot H_2O$ and $NaBH_4$ reductants. In this way, oxidative stable Cu nanoparticles were obtained with a mean particle size of 9.6 ± 1.0 nm. These catalysts showed a considerable improvement in the batch-type Ullmann-type etherification and, in conjunction with DFT (Density Functional Theory) and Monte Carlo modeling of copper-support interactions, long-term stability studies were done to immobilize stable nano-copper catalysts and copper-based bimetallic colloids on titania based supports.

Heterogeneous catalyst for flow processing. These findings were utilized to develop two novel heterogeneous copper-based nanostructured catalysts, using non-porous TiO_2 and mesoporous TiO_2 films, deposited on glass beads as substrates for a fixed bed flow reactor. The catalytic films, after impregnation with Cu or CuZn nanoparticles, were used to study the catalytic activity in the same

copper-catalyzed Ullmann C-O coupling reaction towards 4-phenoxypyridine in a batch-wise operated stirred tank reactor. A highest product yield of 84% was obtained in 90 min by using catalysts with 2 wt% Cu onto mesoporous TiO_2 films with mean pore sizes of 24 ± 4 nm. After 12 h preconditioning, the observation of a Cu loading of 1.8 wt% demonstrated that leaching of Cu does not play a significant role for these mesoporous titania support systems. Moreover, bimetallic $Cu_{70}Zn_{30}$ nanoparticles (deposited onto mesoporous TiO_2 films) with a mean size of 4 nm showed a significant preservation of the Cu(0) oxidation state. The presence of Zn appeared to be crucial for the stabilization of metallic Cu, especially in the case of a mesoporous titania support. Conversely, the main reason for catalyst deactivation in the case of the non-porous TiO_2 films was found to be support leaching, more profoundly than the Cu catalyst losses. This observation underlines the significance of metal-support interactions between copper and the nanoscopic support oxide, especially in the mesoporous TiO_2 support.

The effect of microwave heating in flow processing. Further employment of these findings was carried out in two flow milli-reactors for microwave-assisted Ullmann-type C-O coupling reaction. Both a tubular wall-coated (ZnO support) and a fixed bed (TiO_2 support) milli-reactor were designed and loaded with the aforementioned Cu nanoparticles. Copper catalyst deactivation for both reactors appeared to be only significant after 24 h on-stream and this deactivation could partially be avoided by thermal treatment of the reactor after each cycle. Up to 60% yield was attained using the Cu/ZnO wall-coated reactor for two consecutive runs. No significant activity drop was observed if a thermal pre-treatment of the reactor (350 ^{o}C for 24 h) was undertaken prior to each run. The Cu/TiO_2 fixed bed reactor revealed lower yields due to catalyst leaching. However, reactor productivities of up to 55 $kg_{prod}/(m_R^3 \cdot h)$ suggested a better performance than those of using the Cu/ZnO wall-coated reactor. Therefore, experiments were further applied in the Cu/TiO_2 fixed bed reactor using microwaves as an alternative energy source for selective catalyst heating. The use of high-density single-mode microwaves showed a three-fold yield increase in the Cu/TiO_2 fixed bed reactor when compared to the application of multimode microwaves. Nevertheless, the use of metallic copper in the microwave cavities appeared to be only advantageous at low microwave powers and catalyst loadings. At higher powers and catalyst loadings arcing led to rapid catalyst deactivation. A linear relation between the arcing frequency and the catalyst loading was found. It was demonstrated that yields obtained using microwave heating at 140 W were almost 30% higher than those achieved with oil-bath heating, whereas no significant yield increase was observed for microwave powers above 300 W. In the case of a $CuZn/TiO_2$ catalyst, a three-fold yield increase could be demonstrated in a highly dense single-mode microwave cavity which, to the best of our knowledge, resulted to a not yet reported productivity of up to 172 $kg_{prod}/(m_R^3 \cdot h)$ for microwave-assisted flow synthesis in the Ullmann C-O coupling.

Structured fixed bed flow-reactor for microwave heating. Clearly, a single-mode microwave cavity would provide more efficient and precise temperature control as compared to multimode microwave ovens. Therefore, a single-mode microwave cavity was applied in the Ullmann-type C-O coupling reaction in various fixed bed catalytic reactors as a means to perform flow chemistry. In addition, using a multi-lamination split-and-recombine mixer showed the desired reactant concentrations at the mixer outlet which consequently afforded stable productivities. The temperature fluctuations were minimized to 2 °C with cavity energy efficiencies above 80% for a flowrate of 10 ml/min by adding a dead-load as variable to control the microwave energy into the reactor cavity. This step was crucial to account for changing dielectric properties of the reaction mixture composition after reaction. A yield of 19% in 1 h was achieved in the C-O coupling reaction when a Cu/TiO_2 catalyst was used in the fixed bed reactor combined with single-mode microwave heating. This yield was *ca.* 10% higher as compared to that an oil-bath heated Cu-capillary reactor. By changing the composition of the catalyst and adding Zn as co-promoter, a highest yield of 26% was attained over a $Cu_{50}Zn_{50}$ catalyst in 80 min. However, increasing the amount of Zn demonstrated a yield drop due to a reduced accessibility of the active Cu surface. More importantly, catalyst bed segmentation in the microwave field was used to control the liquid temperature by introducing "heating" and "cooling" zones in the fixed bed reactor. Increasing the number of catalyst segments resulted in remarkable yield enhancements, up to 75% after 80 min for a four-fold segmented catalyst bed. Finally in this study, a novel approach to conduct heterogeneously catalyzed microwave chemistry, involving microwave-transparent solvents (*e.g.* toluene) using selective absorption of microwaves by the catalyst, was demonstrated

Techno-economic evaluation of combined microwave and micro processing. In the final part of this thesis, the impact of various chemical process parameters on the overall production costs has been reported when implementing them in a microwave-assisted micro-process plant for the synthesis of fine-chemicals. Two chemical production models were considered, *i.e.* 2-acetoxybenzoic acid as Aspirin and 4-phenoxypyridine as antibiotic precursor in Vancocin production. Single-mode microwave heating and micro processing as replacements for conventional heating and processing can only be beneficially for a heterogeneously catalyzed process when a micro fixed-reactor is used. This combination resulted in an acceptable operating profit and provided the largest techno-economic benefits in all microwave-related scenarios. An alternative method to carry out catalytic reactions can be achieved profitably by using catalyst nano-slurries. However, due to insufficient profit margins balanced over the large technical risk and catalyst recovery limitations, these processes are not advisable. For non-metal catalyzed homogeneous liquid systems, the use of microwave heating in a micro-process as compared to conventional heating plant can generally be carried out feasibly, resulting in profitable scenarios. The use of wall-coated reactors can provide a favorable scenario, but only if the chemical performance could be improved, *e.g.* by increasing the catalyst surface either by using small (reactor) channel diameters

(<50 µm) or highly porous wall materials. This conclusion was confirmed by the sensitivity analysis performed, where the catalyst activity appeared to be more influential on the ROI (rate on investment) and on the PBP (payback period) as compared chemistry intensification. However, far most influential parameter on profitability (in terms of ROI and PBP) appeared to be the production scale, at an optimum capacity of 500 kg/day. Larger production scales could generate even more profitability at decentralized production sites by means of "numbering-out" and by providing the added-value of flexible and transportable production sites.

Recommendations

Our efforts to combine microwave heating with flow processing in micro-structured fixed bed and wall-coated milli-reactors provided various economically feasible strategies to proceed with. However, as discussed in the conclusions summarized in this thesis the type of chemistry and the related need for heterogeneous catalysts appeared to be much larger game-players for establishing cost-competitive processes. Therefore, it is of vital importance to primarily evaluate and separately develop suitable chemistry before considering combinations of novel technologies, such as microwave heating and micro processing, at all.

This evaluation must initially proceed by ensuring that the chemistry can be feasibly operated in a continuous micro- or milli-reactors. At this stage, the reaction kinetics must be investigated in a CSTR (continuously stirred tank reactor) or differentially operated tubular reactor to determine not only the influence of stoichiometry of the reactants and the catalyst loading, but also to foresee the presence of an induction period or catalyst pre-activation. Undoubtedly, also the presence of insoluble components (such as salts and bases) should be avoided to prevent clogging, *e.g.* using liquid bases or different solvents. These results provide the major input to establish the feasibility of a continuous process and to finally correlate reaction kinetics between batch-chemistry and continuous processing.

Simultaneously, batch-type experiments need to be performed to investigate the presence or absence of rate enhancement effects of microwave heating with respect to conventional heating methods. In this step, the influence of microwave heating on chemical transformations must be determined accurately and correctly by investigating the effect of mixing, presence of salts and metallic particles, but, most importantly, adequate conversion of microwave energy into thermal energy by accurate temperature measurements. To meet this latter requirement, it is highly recommended to measure temperatures at various points in the reactor using various probes simultaneously.

Special attention must be paid when microwaves are concurrently applied with metallic particles as their interaction would lead to much faster and usually undetectable heating effects. Metals (and more pronounced magnetic particles) lead to much higher surface temperatures than those measured at the probe and often provide higher "observed" reaction rates which could easily trick the chemist. Many examples in the literature exist where such effects were ignored and results

were wrongly interpreted due to incorrect temperature measurements, especially when a coated (read insulated) probe and inert N_2 or Ar flows (also functioning as coolant) were applied. Therefore, understanding and distinction of very fast microwave-metal interactions and rather slow microwave-liquid interactions must be established by preliminarily investigating the effect of metals in non-absorbing solvents.

If (and only if) a clear understanding of the effect of microwaves on the chemical reaction has been established and correlated to conventional heating, the next step can be taken by combining microwave heating with flow-processes. However, during this step it should be realized that microwave energy is supplied statically while liquid flow is dynamic over the reactor length. Especially in single-mode microwave cavities, the microwave density is equal over the entire length of the reactor, leading to thermal energy accumulation in the reaction mixture. Consequently, the effect of temperature rise on the degree of microwave absorption must be included, noting that microwave absorption might increase at higher temperatures. In addition, increasing product and decreasing reactant concentrations might change the overall dielectric properties which sometimes, but not necessarily, may lead to decreased microwave absorption.

Finally, also the optimum production scale for beneficial use of single-mode microwaves needs to be assessed carefully, especially in view of the equipment cost which enables the highly structured microwave patterns in single-mode cavities. By numbering-up parallel cavities production scale-up can be established, however the cost-competiveness limit is reached much faster as compared to the scale-up in multimode microwaves. This disadvantage of single-mode microwaves can simply be attributed to the non-linear CAPEX increase when the maximum magnetron capacity is exceeded. Cavity size limitations are of less importance in multimode microwaves as, dependent on the magnetron capacity, the dimensions of the cavity do not influence their random microwave distribution significantly. Nevertheless, the drawbacks of multimode microwaves will still be of main concern when uniform microwave distribution and temperature control are required such as for near-bulk-scale and smart-scale-flow applications. Therefore, a thorough consideration of CAPEX and product quality becomes important in deciding for the most suitable mode of microwaves when scale-up issues are addressed.

Undoubtedly, the abovementioned recommendations are crucial to combine both microwave technology and micro processing for a techno-economically feasible process. However, it should be emphasized that the steps to combine these technologies should not be investigated in series. On the contrary, most of the steps recommended above must be performed as parallel steps as the major hurdles are mainly accompanied by marrying the chemistry and each novel technology separately. Keeping this in mind, the investigator will be provided with a “go” or “no-go” scenario, already at a very early stage, which results in efficient use of research resources, but, most importantly, sufficient confidence to combine those technologies.

Curriculum Vitae

Faysal Benaskar was born in Berkane, Morocco in 1984. He obtained his B.Sc. and M.Sc. degrees in chemical engineering and chemistry at the Eindhoven University of Technology, The Netherlands, in 2006 and 2008, respectively. His M.Sc thesis research was carried out at the Shell Research and Technology Centre Amsterdam (currently STC) on the topic of hydrogen manufacturing, logistics and retailing as an alternative fuel for the automotive industry.

In 2007, he also joined the Institut für Mikrotechnik Mainz (Mainz, Germany) for a research project aiming at the combination of microwave and micro-process technology to conduct organic reactions. This work contributed to motivate a follow-up Ph.D. project.

Since 2008 he is working in the Laboratory of Chemical Reactor Engineering to obtain his Ph.D. degree from the Eindhoven University of Technology in the field of microwave-enhanced micro-processing for fine-chemicals synthesis. His work mainly focuses on the development and optimization of catalyzed organic reactions to suit the operational window of microwaves and micro processing.

He has authored and co-authored 15 scientific journal papers and around 25 conference contributions and established a strong collaboration with several highly ranked international research groups.

List of publications

2012

F. Benaskar, N.G. Patil, E.V. Rebrov, A. Ben-Abdelmoumen, J. Meuldijk, L.A. Hulshof, V. Hessel, J.C. Schouten (2012). Micro/milli-flow processing combined with selective catalyst microwave heating in the Cu-catalyzed Ullmann etherification reactions: a μ^2-process. *ChemSusChem,* submitted.

F. Benaskar, N.G Patil, V. Engels, E.V. Rebrov, J. Meuldijk, L.A. Hulshof, V. Hessel, A.E.H. Wheatley, J.C. Schouten (2012). Microwave-assisted Cu-catalyzed Ullmann synthesis in a continuous-flow milli-plant. *Chem Eng. Jour.,* Accepted, DOI: 10.1016/j.cej.2012.06.147.

F. Benaskar, N.G. Patil, V. Engels, E.V. Rebrov, J. Meuldijk, V. Hessel, L.A. Hulshof, A.E.H. Wheatley, J.C Schouten (2012). A kinetic study on the Cu(0)-catalyzed Ullmann SArN-type C-O coupling of potassium phenolate and 4-chloropyridine. *Dalton Trans.*, submitted / in press.

F. Benaskar, A. Ben-Abdelmoumen, N.G Patil, E.V. Rebrov, J. Meuldijk, V. Hessel, L.A. Hulshof, U. Krtschil, J.C. Schouten (2012). Cost analysis on a continuously operated fine chemicals production plant at 10 kg/day using a combination of microprocessing and microwave heating. *J. Flow Chem.*, *1*(2), 74-89.

F. Benaskar, V. Engels, E.V. Rebrov, N.G. Patil, J. Meuldijk, P.C. Thüne, P.C.M.M. Magusin, B. Mezari, V. Hessel, L.A. Hulshof, E.J.M. Hensen, A.E.H. Wheatley, J.C. Schouten (2012). New Cu-based catalysts supported on TiO2 films for Ullmann SnAr-type C-O coupling reactions. *Chem. - A Eur. J.*, *18*(6), 1800-1810.

M.H.C.J. van Houtem, F. Benaskar, C.F.C. Fitie, R. Martin-Rapun, P.E.L.G. Leclère, J.A.J.M. Vekemans, E.W. Meijer (2012). Helical self-assembly and amplification in chirality in fluorinated, preorganized discotic systems (mixing on the molecular level with apolar discs). *Org. Biomol. Chem.*, *10*, 5898-5908.

N.G. Patil, F. Benaskar, E.V. Rebrov, J. Meuldijk, L.A. Hulshof, V. Hessel, J.C. Schouten (2012). Continuous multi-tubular milli-reactor with a Cu thin film for microwave assisted fine-chemical synthesis. *Ind. Eng. Chem. Res.*, submitted / in press.

N.G. Patil, A.I.G. Hermans, F. Benaskar, E.V. Rebrov, J. Meuldijk, L.A. Hulshof, V. Hessel, J.C. Schouten (2012). Energy efficient and controlled flow processing under microwave heating by using a milli reactor-heat exchanger. *AIChE Journal: Chem. Eng. Res. Dev.*, submitted / in press.

N.G. Patil, E.V. Rebrov, E. Esveld, K. Eränen, F. Benaskar, J. Meuldijk, J.-P. Mikkola, V. Hessel, L.A. Hulshof, D.Y. Murzin, J.C. Schouten (2012). Effect of the load size on the efficiency of microwave heating under stop flow and continuous flow conditions. *J. Microwave Power Electromagnetic Energy*, on-line.

2011

V. Engels, D.A. Jefferson, F. Benaskar, P.C. Thüne, A. Berenguer-Murcia, B.F.G. Johnson, A.E.H. Wheatley (2011). Nanoparticulate PdZn – Pathways towards the synthetic control of nanosurface properties. *Nanotechnology*, *22*(20), 205701.

2010

F. Benaskar, V. Engels, N.G. Patil, E.V. Rebrov, J. Meuldijk, V. Hessel, L.A. Hulshof, D.A. Jefferson, J.C. Schouten, A.E.H. Wheatley (2010). Copper(0) in the Ullmann heterocycle-aryl ether synthesis of 4-phenoxypyridine using multimode microwave heating. *Tetrahedron Lett.*, *51*(2), 248-251.

F. Benaskar, V. Engels, N.G. Patil, E.V. Rebrov, J. Meuldijk, V. Hessel, L.A. Hulshof, D.A. Jefferson, J.C. Schouten, A.E.H. Wheatley (2010). Corrigendum to: Copper(0) in the Ullmann heterocycle-aryl ether synthesis of 4-phenoxypyridine using multimode microwave heating. *Tetrahedron Lett.*, *51*(44), 5849-5849.

F. Benaskar, V. Engels, N.G. Patil, E.V. Rebrov, V. Hessel, L.A. Hulshof, D.A. Jefferson, J.A.J.M. Vekemans, S. Karwal, J.C. Schouten, A.E.H. Wheatley (2010). *Org. Process Res. Dev.*, *14*(3), 644-649.

V. Engels, F. Benaskar, D.A. Jefferson, B.F.G. Johnson, A.E.H. Wheatley (2010). Nanoparticulate copper - Routes towards oxidative stability. *Dalton Trans.*, *39*, 6496-6502.

2009

F. Benaskar, V. Hessel, U. Krtschil, P. Löb, A. Stark (2009). Intensification of the capillary-based Kolbe-Schmitt synthesis from resorcinol by reactive ionic liquids, microwave heating or a combination thereof. *Org. Process Res. Dev.*, *13*(5), 970-982.

List of publications to be submitted

F. Benaskar, V. Degirmenci, E.V. Rebrov, P. Abdulkin, N.G. Patil, V. Hessel, L.A. Hulshof, E.J.M. Hensen, A.E.H. Wheatley, J.C. Schouten (2012). X-ray absorption spectroscopy on the role of Zn as co-promoter of a heterogeneous $CuZn/TiO_2$ catalyst in Ullmann-type C-O coupling reactions. *J. Catal.*, to be submitted.

F. Benaskar, P. Abdulkin, E.V. Rebrov, N.G. Patil, L.A. Hulshof, J. Meuldijk, A.E.H. Wheatley, J.C. Schouten, V. Hessel (2012). Cu-based nano-catalysis towards flow-systems in the cyclopropanation from ethyldiazo acetates. *Nanotechnology Rev*., to be submitted.

F. Benaskar, N.G. Patil, G.S.J. Sturm, G. Stefanidis, E.V. Rebrov, L.A. Hulshof, J. Meuldijk, A.I. Stankiewicz, V. Hessel, J.C. Schouten (2012). Microwave-enhanced micro processing for fine-chemicals synthesis. *Chem. Eng. Process.: Process Intensif.*, to be submitted.

List of conference contributions

2012

F. Benaskar, E.V. Rebrov, N.G. Patil, J. Meuldijk, L.A. Hulshof, V. Hessel, J.C. Schouten (2012). Process intensification in a microwave heated fine-chemical milli-plant at large scale operation. *Proceedings of the International Symposium on Chemical Reaction Engineering (ISCRE 22), 2-5 September 2012, Maastricht, the Nederlands.* **Oral**.

F. Benaskar, N.G. Patil, E.V. Rebrov, J. Meuldijk, L.A. Hulshof, V. Hessel, J.C. Schouten (2012). Micro-process technology combined with selective catalyst microwave heating in Cu-catalyzed reactions for fine-chemicals synthesis: a micro2 process. *Proceedings of the 20th International Congress of Chemical and Process Engineering (CHISA 12), 25-29 August 2012, Prague, Czech Republic.* **Oral**.

F. Benaskar, V. Degirmenci, J. Meuldijk, V. Hessel, L.A. Hulshof, E.J.M. Hensen, E.V. Rebrov, J.C. Schouten (2012). In-operando EXAFS study on CuxZny/TiO2 catalyst for C-O coupling. *Proceedings of the 13th Netherlands' Catalysis and Chemistry Conference (NCCC 13), 5-7 March 2012, Noordwijkerhout, the Netherlands.* **Oral**

F. Benaskar, N.G. Patil, E.V. Rebrov, E. Engels, V. Hessel, L.A. Hulshof, J. Meuldijk, A.E.H. Wheatley, J.C. Schouten. (2012). A novel continuous process for copper catalyzed Ullmann-type C-O coupling under microwave heating. *Proceedings of the Microwave & Flow Chemistry Conference (MFCC 12), 28 February – 2 March 2012, Lanzarote, Spain.* **Oral**.

F. Benaskar, A. Ben-Abdelmoumen, N.G. Patil, J. Meuldijk, E.V. Rebrov, V. Hessel, L.A. Hulshof, J.C. Schouten (2012). Process intensification using a microwave heated micro plant in the Ullmann type C-O coupling for production scale operation. *Proceedings of the 12th International Conference on Microreaction Technology (IMRET 12), 20-22 February 2012, Lyon, France.* **Poster**.

N.G. Patil, E. Esveld, F. Benaskar, E.V. Rebrov, L.A. Hulshof, J. Meuldijk, V. Hessel, J.C. Schouten (2012). Microwave assisted flow processing: coupling of electromagnetic and hydrodynamic phenomena. *Proceedings of the 2012 AIChE Annual Meeting, 28 October – 2 November, 2012, Pittsburgh, Pennsylvania.* **Oral**.

N.G. Patil, F. Benaskar, E.V. Rebrov, J. Meuldijk, L.A. Hulshof, V. Hessel, J.C. Schouten (2012). Scale-up of microwave assisted flow processes for fine chemical synthesis. *Proceedings of the 22nd International Symposium on Chemical Reaction and Engineering (ISCRE 2012), 2-5 September 2012, Maastricht, The Netherlands.* **Poster**.

N.G. Patil, F. Benaskar, J. Meuldijk, E.V. Rebrov, L.A. Hulshof, V. Hessel, J.C. Schouten. (2012). Cu thin films for enhanced microwave assisted flow synthesis of fine chemicals at industrial scale. *Proceedings of the 13th Netherlands' Catalysis and Chemistry Conference (NCCC 13), 5-7 March 2012, Noordwijkerhout, The Netherlands.* **Poster**.

N.G. Patil, A.I.G. Hermans, E.V. Rebrov, F. Benaskar, J. Meuldijk, L.A. Hulshof, V. Hessel, J.C. Schouten (2012). Microwave heating in a continuous flow reactor heat exchanger. *Proceedings of the Microwave & Flow Chemistry Conference (MFCC 12), 28 February - 2 March 2012, Lanzarote, Spain.* **Poster**.

N.G. Patil, F. Benaskar, E.V. Rebrov, J. Meuldijk, L.A. Hulshof, V. Hessel, J.C. Schouten (2012). Design of a continuous multi-tubular milli-reactor with a Cu thin film for microwave assisted fine-chemical synthesis at industrial scale. *Proceedings of the 12th International Conference on Microreaction Technology (IMRET 12), 20-22 February 2012, Lyon, France.* **Oral**.

2011

F. Benaskar, A. Ben-Abdelmoumen, J. Meuldijk, N.G. Patil, E.V. Rebrov, L.A. Hulshof, V. Hessel, J.C. Schouten (2011). Process economics and cost analysis of a process-intensified milli-plant for fine-chemicals synthesis. *Proceedings of the Netherlands Process Technology Symposium (NPS 11), 24-26 October 2011, Arnhem, The Netherlands.* **Oral**.

F. Benaskar, A. Ben-Abdelmoumen, J. Meuldijk, E.V. Rebrov, L.A. Hulshof, V. Hessel, J.C. Schouten (2011). Design of mini chemical-plants for local and flexible production of added-value chemicals. *Proceedings of the 2011 STW Annual STW Congress, 6 October 2011, Nieuwegein, the Netherlands.* **Poster**.

F. Benaskar, E.V. Rebrov, V. Engels, N.G. Patil, J. Meuldijk, L.A. Hulshof, V. Hessel, A.E.H. Wheatley, J.C. Schouten (2011). Novel heterogeneous Cu-Zn catalysts for the C-O cross-coupling reaction in micro(wave)-process flow chemistry applications. *Proceedings of the 22nd North American Catalysis Society Meeting, 5-10 July 2011, Detroit, MA, USA.* **Oral.**

F. Benaskar, E.V. Rebrov, V. Engels, N.G. Patil, J. Meuldijk, L.A. Hulshof, V. Hessel, J.C. Schouten (2011). Cu/meso-TiO2 films for C-O coupling reactions. *Proceedings of the Netherlands Catalysis and Chemistry Conference 2011 (NCCC 12), 28 February - 2 March 2011, Noordwijkerhout, The Netherlands.* **Oral.**

V. Engels, F. Benaskar, P. Abdulkin, E.V. Rebrov, D.A. Jefferson, B.F.G. Johnson, J.C. Schouten, A.E.H. Wheatley (2011). Mechanistic study on the base-free Ullmann condensation with copper-based nanocatalyts. *Proceedings of the 22nd North Americal Catalysis Society Meeting, 5-10 June 2011, Detroit, USA.* **Poster.**

2010

F. Benaskar, V. Engels, E.V. Rebrov, J. Meuldijk, L.A. Hulshof, V. Hessel, J.C. Schouten (2010). Cu-based nanoalloys in the liquid-liquid Ullmann C-O coupling for microreactor and microwave applications. *11^{th} Proceedings of the Netherlands Catalysis and Chemistry Conference (NCCC 11), 1 - 2 March 2010, Noordwijkerhout, The Netherlands.* **Oral.**

F. Benaskar, E.V. Rebrov, J. Meuldijk, L.A. Hulshof, V. Hessel, J.C. Schouten (2010). Continuous fixed-bed milli-processing for Cu catalyzed Ullmann-type C-O coupling in conjunction with highly efficient microwave radiation. *Proceedings of the Netherlands Process Technology Symposium (NPS 10), 25-27 October 2010, Veldhoven, The Netherlands.* **Poster.**

F. Benaskar, E.V. Rebrov, J. Meuldijk, L.A. Hulshof, V. Hessel, J.C. Schouten (2010). Development of microwave-assisted copper-catalyzed Ullmann-type CO-coupling chemistry for microreactor applications in an integrated micro^2-concept. *Proceedings of the IMM Young Scientists Workshop, 19-20 November 2009, Mainz, Germany.* **Oral.**

A.E.H. Wheatley, V. Engels, F. Benaskar, J.C. Schouten, E.V. Rebrov, L.A. Hulshof, D.A. Jefferson (2010). On the fabrication and stabilization of copper-based nanoparticles for catalysis. *Proceedings of the 39th International Conference on Coordination Chemistry (ICCC), 25-30 July 2010, Adelaide, Australia*. **Oral.**

2009

F. Benaskar, V. Engels, E.V. Rebrov, J. Meuldijk, L.A. Hulshof, V. Hessel, J.C. Schouten (2009). Development of microwave-assisted Cu-catalyzed Ullmann CO-coupling for microreactor applications. *Proceedings of the Netherlands Process Technology Symposium (NPS 9), 19-22 October 2009, Veldhoven, The Netherlands.* **Poster.**

F. Benaskar, V. Engels, E.V. Rebrov, J. Meuldijk, L.A. Hulshof, V. Hessel, A.E.H. Weathley, J.C. Schouten (2009). Oxidatively stable nanoalloys in the base-free Ullmann heterocyle-aryl ether synthesis for microreactor applications. *10th Proceedings of the Netherlands Catalysis and Chemistry Conference (NCCC 10), 2-4 March 2009, Noordwijkerhout, The Netherlands*. **Poster.**

2008

F. Benaskar, E.V. Rebrov, V. Hessel, J.C. Schouten (2008). Process intensification of the Kolbe-Schmitt synthesis by application of reactive ionic liquids and microwaves. *14e PAC-symposium: KNCV Posterwedstrijd, 2008, Amsterdam, The Netherlands.* **Poster.**

U. Krtschil, F. Benaskar, V. Hessel, P. Löb (2008). Continuous microreactor processing, reactive ionic liquids and microwave heating - approaches towards intensified Kolbe-Schmitt synthesis. *Proceedings of the 2008 AIChE Annual Meeting, 16-21 November 2008, Philadelphia, PA, USA.* **Oral.**

U. Krtschil, F. Benaskar, V. Hessel, P. Löb (2008). Intensified Kolbe-Schmitt synthesis using continuous microreactor processing, reactive ionic liquids and microwave heating. *1st Smart Synthesis and Technologies for Organic Processes Conference (SYNTOP), VDI Berichte Nr. 2039, 2008, Germany, Potsdam.* **Oral.**

2007

F. Benaskar, E.V. Rebrov, U. Krtschil, V. Hessel, P. Löb, G. Wille. (2007). Process intensification for Kolbe-Schmitt synthesis by reactive ionic liquids and microwaves. *Proc. 2nd Symposium on Microwave Accelerated Synthesis*. *Gesellschaft Deutscher Chemiker, 2007, Düsseldorf, Germany*. **Oral.**

Acknowledgements

Many people's support and confidence considerably facilitated the collection of all scientific facts described in the preceding 8 chapters. First of all, I would like to thank my supervisors Prof. Jaap Schouten, Prof. Bert Hulshof, Prof. Volker Hessel, Prof. Evgeny Rebrov and Prof. Jan Meuldijk.

Dear Jaap, I would like to thank you in the first place for allowing me to conduct my PhD project in your group. I have very much appreciated and enjoyed, the way that you have educated me to doctor: analytic, determined and responsible. You have given me the unique opportunity to expand my scientific network, and allowed me to fish in unknown seas. Only now, I realize that I was very lucky and that the outcome of my work would have been different, if I was only allowed to fish at the coast. It is my great honour to have attained my Dr-degree under your supervision and as I said once before in difficult times: *Je maintiendrai!* I am proud to be able to approach you in the future, whenever, wherever.

Dear Bert, most of what is written in this thesis is thanks to you, the chemistry, the collaboration initiatives, the motivation and freedom to diffuse to other scientific fields, etc. Without your experience, dedication for science and your "simply-try-it-strategy", this quantity and quality of data could never have been realized. Your accuracy for reviewing papers is simply amazing: it is unbelievable how you can differentiate between font 8 and 7,5 in a footnote! I have learned a lot from you, also at a personal level, learning from (and dealing with) difficult scenarios in life, and combining them with a tough professional career. You have taught me how to endure difficult moments and you are still doing that...thank you! Chapeau!!! I hope I have given you some of this strength and energy back and I am sure we will keep exchanging this.

I would like to express my sincere gratitude to my friend Volker Hessel. Dear Volker, you were the first to approach me for this topic and provided me this opportunity during a coffee break in a conference. It was easy to convince me, I already knew you and your qualities. During my project I have taken the opportunity to absorb some of these qualities, and you stimulated me to add a bit of my style and flavour. Volker, I am very grateful to you! Not only for the professional part, but also for the unforgettable and indescribable moments we had together (also with Jürgen). Maybe, this is why I won't even make an attempt to describe them here... ;-)

Dear Evgeny, you have been a friend and mentor. Your endless drive and fundamental knowledge of various scientific areas make you a very special scientist.

Your spirit, which shaped a scientist out of me, is simply amazing. I have witnessed you as a great and determined scientific leader in Moscow, but also as a dedicated and detailed lab-researcher in our synchrotron experiments in Grenoble. This infinitely large spectrum of professional qualities has brought you very far and the end is hard to find. I hope that I'll be able to keep learning from you. Also, I am so thankful and am very happy to have had so many leisure activities with you, especially during the jogging sessions when we could always speak about everything.

Dear Jan, I thank you for sharing your widespread knowledge and experience in the academic world with me, during my BSc, MSc and PhD period. You were always a great inspiration and very open to me. You always allowed me a slot to visit you when I got stuck, for all kind of issues. I thank you very much for this, especially regarding your schedule and agenda of the last years. I would also like to thank your wife, Anneke, for her nice words and the great care she is taking.

My special thanks go to Prof. Oliver Kappe for many scientific discussions and his great contributions to this thesis as core-committee member of my PhD-defense.

Denise, you have been of great help during my stay in SCR. I learned the value of a perfect organization. I thank you...for everything!

Jef Vekemans, Anja Palmans, Michel van Houtem and Martin Wolfs: thank you for making me a Synthetic Organic Chemist during the last 6 years. Dear Jef, I have learned Organic Chemistry via your way, the right way! Thank you very much!

For cooperating and hosting us in their labs, I also would like to express my thanks to Prof. Emiel Hensen, Prof. Bert Meijer, Prof. Rene Janssen, Prof. Hans Niemantsverdriet, Prof. Rutger van Santen, Dr. Evgeny Pidko, Dr. Peter Thüne, Dr. Volkan Degirmenci, Tiny Verhoeven, Adelheid Elemans-Mehring and Dr. Volker Engels.

In particular, I would like to thank Dr. Patrick Wenmakers, Dr. Ulrich Krtschil, Dr. Maartje Kemmere, Ir. Henk Leeuwis, Dr. Monique Wiegel/Mrs. Tine Bertrand-Karthaus, Prof. Andrzej Stankiewicz, Dr. Georgios Stefanidis, Ir. Guido Sturm, Dr. Tom van Gerven, Prof. Martin Verweij, DSM, FrieslandCampina, Lionix BV, Milestones MLS, IMM GmbH STW and the Delft University for their contributions in the MEMFiCS project.

For the very fruitful discussions and collaboration I would like to thank Dr. Andrew Wheatley (also for participating in the PhD-committee), Prof. Brian Johnson, Prof. David Jefferson, Prof. Yoshinori Kondo and their co-workers from the Cambridge University and Sendai University.

Aladin, Janine, Saurab, Tim, Mourad, Toufik, Pavel, Ben, Brahim, Sami, Abdulkarim, thank you for helping me in my PhD work.

Ma'moun and Carlos! Guys! What to say...well, let's make it easy: "a man has to do what a man has to do" or rather "*omne bonum pulchre veniens in fine beatum*". We had a marvellous time together and, I think, we have learned to know ourselves better by doing so many things together.

Halabi, Wim, Gregory! Thank you for being such great office mates! With you, Halabi, I have enjoyed all our nice talks and have the greatest admiration for your knowledge and determination: het ga je goed! Much of what I have achieved during my MSc and PhD period was shared with you Narendra. Together, we have suffered difficult times and enjoyed glorious moments. It was my sincere pleasure to work with you for such a long time. Thank you! Erik, Dolf, Anton, Carlo, Marlies, Peter, Martin and Leontien: thank you very much in supporting me during my stay at the SCR-group. Beste Madan, I enjoyed very much to learn from you during my stay. Thanks! John, Xander, Timothy: I would like to thank you for helping me in my scientific mission. Mart, I thank you for teaching me the fundamentals of Reactor Engineering and for allowing me to drop by in your office any time. I also enjoyed very much the moments that you dropped by...and we discussed...discussed...discussed...∞

Patrick, Marco, Stijn, Joost, Maurice, Bianca, Oki: you were my first warm hosts at SCR and allowed me to flow into the SCR spirit. Today, I hope to have conveyed this spirit to my successors.

Ooh guys! Violeta, Qi, Nopi, Dulce, Christine, Katya, Lida, Maria, Fernanda, Lara, Serdar, Jiaqi, Jack, Paola, Emila, Roman, Frans, Shohreh, Michiel, Slavisa, Kevin, Ivana, Stefan: thank you so much for being such nice colleagues and friends. You always allowed me some minutes, just to talk. Thank you!

Las but not least, I thank my family and friends. Mama, my Angel, your unlimited strength and, simultaneously, your care has allowed your son to become what he is today. Papa, my Colonel, your discipline and determination has proudly obliged your son to be what he is today – *Rabi Arham Abi, Wa Ummi, Kama Rabaiani Sageeran* – Hamida, Aissa, Youssef, Mohammed, Khalid...my brothers and sisters...sometimes we play, sometimes we struggle, sometimes we cry, sometimes we have fun, sometimes we laugh, and sometimes we are worried, but we always stay together...for each other, for our parents and for our children. My Rita, my light in darkness, I simply cannot imagine what would have happened to me without you...and I don't want to imagine. Senior Abilio, Donna Mirtes, Tania, Sarah, Senior El-Presidente, obrigado!

Agnesa, Ana-Suares, Ana-Louisa, Branu, Aninia, Elnaz, Dragana, Maria, Roman, thank you for the great times in my PhD-period!